UNIVERSITY OF CANTERBURY
Te Whare Wānanga o Waitaha
CHRISTCHURCH NEW ZEALAND

Lesions of the extended hippocampal system and activation of the anterior thalamus: from impairment to recovery

---

A thesis submitted in partial fulfilment of the requirements for the Degree of Doctor Philosophy in Psychology at the University of Canterbury by Sophie Barnett

---

University of Canterbury

2020

Acknowledgements

Firstly, I would like to thank Prof. John Dalrymple-Alford for his invaluable knowledge and guidance throughout my doctorate, as well as for passing on his passion for research. I will always be incredibly grateful for the opportunities and freedom that he has allowed me. I would also like to extend my heartfelt gratitude to my three co-supervisors: Prof. Neil McNaughton, Assoc. Prof. Louise Parr-Brownlie and Assoc. Prof Stephanie Hughes. A large thank you to Neil for teaching me not only to understand the basics of electrophysiology, but also to enjoy it. I have appreciated all your constructive criticism throughout the writing process; it was not something I expected to enjoy as much as I did. I would like to thank Louise for her expertise, support and guidance throughout the whole process. My sincere thanks to both Louise and Steph for sharing their knowledge of optogenetics with our lab and enabling the set up of optogenetics at the University of Canterbury. Thankyou to Steph for supplying the viral construct used in this thesis.

I would also like to acknowledge all the amazing people I have had the honour of working with over the past four years. In particular, I would like to thank Jenny Hamilton for being a wonderful colleague and friend, providing much needed laughter, memes and vino throughout my PhD. A massive thank you to Brook Perry, who selflessly taught me many of the skills without which I could not have completed this thesis and more importantly, thank you for remaining a great friend even from the other side of the world. My thanks to Calvin Young for his assistance in troubleshooting many of the issues that are inherent to open-source software, as well as his help interpreting the electrophysiology results. I would also like to thank Echo Pei and Tina Yee for the many laughs we have shared both in and out of the lab, and the much-needed Shilling Club outings. Lastly, I would like to express my appreciation to Fraser Doake for his support and fantastic sense of humour throughout the past eight years.

I would also like to thank all the laboratory staff, Neroli Harris, Silvana De Freitas Costa and Anya Armstrong for the excellent care they provided to the animals, their patience concerning the implementation of the new PC2 requirements in the lab and their constant understanding and support. My thanks too, to Ben McGinley for his expertise and for the exceptional quality of all the testing equipment made for us over the years, and especially for helping me fix the Open Ephys set up every time it decided to throw a hissy fit.

I was fortunate enough to be the recipient of a Brain Research New Zealand Doctoral Scholarship and I would like to acknowledge this financial support and express my gratitude for this stipend. This scholarship enabled me to dedicate myself to my research, whilst also making a significant contribution towards the many pieces of equipment required for this thesis.

Lastly, I would like to thank my parents, Steph and Dave, and my partner, Ben, for their unwavering love and support throughout this ordeal. Thank you for believing in me at times when self-belief was at an all-time low. There is absolutely no way I could have done this without you.

I declare that the work described in the current thesis has been done by myself, except where indicated.

Sophie Barnett

This thesis uses *The Journal of Neuroscience* referencing format.

Table of Contents

Contents

List of Figures

Introductory Chapters 1-5

Chapter 6: PCFx and MTT comparison

Chapter 7: Optogenetic stimulation of the ATN following MTT lesions

List of Tables

Abbreviations

AAV adeno-associated virus

Ach acetylcholine

ACC anterior cingulate cortex

AD Alzheimer's disease

AM anteromedial nuclei

ANOVA analysis of variance

Arch/ArchT archeorhodopsin

ATN anterior thalamic nuclei

Aud auditory cortex

AV anteroventral thalamic nucleus

B-L bregma to lambda measurements

CA1-3 cornu ammonis area 1-3

CamKII Calmodulin-dependent protein kinase II

c-AMP cyclic adenosine mono-phosphate

CG cingulate cortex

ChR2 channelrhodopsin-2

Contra Contralateral side

COX cytochrome oxidase

CREB c-AMP response element binding protein

DG dentate gyrus

DREADDs designer receptors exclusively activated by designer drugs

DTg dorsal tegmental nuclei of Gudden

DV dorsal to ventral measurement

dHPC dorsal hippocampus

EEG electroencephalogram

ENR environmental enrichment

Fx fornix

GAD-67 Glutamic acid decarboxylase 67

GAP-43 growth associated protein 43

GFAP Glial fibrillary acidic protein

HIV human immunodeficiency virus

HPC hippocampal formation

IEG immediate early gene

IL infralimbic cortex

ILN intralaminar nuclei

Ipsi ipsilateral side

KS Korsakoff's syndrome

LED light-emitting diode

LFP local field potential

LV lentivirus

MB mammillary bodies

MCI mild cognitive impairment

MD mediodorsal nucleus

mPFC medial prefrontal cortex

MRI magnetic resonance imaging

MS medial septum

MS/DB medial septum/ diagonal band

MTT mammillothalamic tract

MTG mammillotegmental tract

NMDA N-Methyl-D-Aspartate

pCreb phosphorylated c-AMP response element binding protein

PD Parkinson's disease

Prl prelimbic cortex

PFC prefrontal cortex

PCFx post commissural fornix (descending limb)

post-sub post subiculum

PSD power spectral density

RAM radial arm maze

Rb rabies

Rdg dysgranular retrosplenial cortex

Rga granular a retrosplenial cortex

Rgb granular b retrosplenial cortex

RSC retrosplenial cortex

SEM standard error of the mean

SSFO stabilized step-function opsin

Sub subiculum

SUM supramammillary nucleus

Sup superficial layers

TBS theta burst stimulation

WE Wernicke's encephalopathy

VHPC ventral hippocampus

VSV vesicular stomatitis virus

VTNg ventral tegmental nuclei of Gudden

Abstract

The mammillothalamic tract (MTT) and descending arm of the post-commissural fornix (PCFx) are key fibre tracts within an extended hippocampal system for episodic memory. Evidence from both clinical and animal model studies supports the involvement of the MTT in memory function. The role of the PCFx is less certain. Some MRI evidence suggests that the integrity of the PCFx is associated with memory in humans. However, PCFx transection in rats has produced negligible memory impairments. In rats, localised damage to the MTT, but not the PCFx, profoundly reduces the expression of immediate early gene proteins in distal structures in the extended hippocampal system. Experiment 1, however, found that both MTT and PCFx lesions *equally* impaired spatial working memory in the 12-arm radial arm maze (RAM). Both lesions also reduced Zif268 activity in the hippocampus (HPC) and retrosplenial cortex (RSC), albeit more extensively after MTT lesions. MTT and PCFx lesions also reduced spectral power and coherence across the ATN-HPC-prefrontal axis, although only MTT lesions attenuated HPC peak theta power. This evidence suggests that the descending PCFx has a more significant impact on memory than was anticipated by previous research in rats. This new evidence may lead to a revised account of the influence of subicular outputs from the hippocampal formation. Experiment 2 showed that the spatial working memory deficits produced by MTT lesions can be ameliorated through selective stimulation of glutamatergic neurons in the anterior thalamic nuclei (ATN). The ATN occupy a nodal position in the extended hippocampal system and are recipients of MTT efferents from the MB. Regular optogenetic theta burst stimulation (TBS) of the ATN led to a striking improvement in spatial working memory in rats with MTT lesions. This ATN stimulation also increased Zif268 expression in the RSC, HPC, prelimbic cortex and cingulate cortex and increased global spectral power and coherence within and across the ATN, HPC and PFC in the 2-14Hz frequency band. The lack of mnemonic effect found using closed-loop TBS, which was driven by each rat's own hippocampal theta, suggests that the regularity of stimulation was critical for the recovery of memory function. This is the first study to show that long-lasting functional deficits after MTT lesions can be ameliorated. This latter evidence encourages developments to understand and treat clinical memory impairments in people with diencephalic brain injury.

Chapter 1
Introduction

This Chapter provides an initial overview of the more detailed information presented in the experimental Chapters. In this first section, “General Introduction”, the background information chapters (Chapters 2-5) will be summarized, and an impetus for the current study will be provided. In the subsequent section, “aims of the current study”, the main aims of the thesis will be stated.

1.1 General Introduction

This chapter presents a brief overview of the thesis. The thesis focuses on (1) the comparative mnemonic role of the postcommissural fornix (PCFx) and the mammillothalamic tract (MTT), two brain pathways in the extended hippocampal memory system, and (2) the prospect that failing memory, due to injury to the MTT, is amenable to intervention through optogenetic stimulation of the intact anterior thalamic nuclei (ATN), a key structure in the extended hippocampal memory system.

Memory is a crucial component of cognition. It refers to the ability to encode, store and retrieve information, in order to use it for adaptive purposes (Fuster, 1995). Severe memory dysfunction in the presence of otherwise intact cognition is known as amnesia; it can have a profoundly negative impact on a person’s quality of life (Corkin, 2013). Anterograde amnesia is the most common type of amnesia. This represents a substantially marked inability to form new episodic memories following brain injury, which is most easily defined by a traumatic event causing brain injury. Episodic memory or ‘episodic-autobiographical memory’ allows individuals to remember past experiences, including their temporal and spatial context. At least in humans, it may include facets such emotion, sensory input and autonoetic consciousness (Tulving, 2002).

The current field of memory research often appears “hippocampocentric”. This focus is a natural development after the influential description of the striking memory impairments reported in patient HM (Corkin, 2002; Squire, 2009; Postle, 2016). Patient HM presented with severe anterograde amnesia following bilateral medial temporal lobectomy. However, the association between damage or degeneration in the diencephalon with

anterograde amnesia predates the occurrence of HM, at least in the context of the alcoholic Korsakoff's syndrome (Aggleton, 2014; Kopelman, 2015). Anterograde amnesia, therefore, has been consistently associated with neuropathology in both the medial diencephalon and the medial temporal lobe. The considerable overlap in memory impairments following damage to these two distinct regions suggests that they work in concert to support episodic memory (Aggleton & Brown, 1999; Spiers, Maguire, & Burgess, 2001; Kopelman, 2002; Vann & Aggleton, 2004; Aggleton et al., 2010; Corkin, 2013; Vann, 2013). Although not the first, the most influential proposal that these two regions function in concert was that of Aggleton and Brown in 1999, who formally developed the concept of an "extended hippocampal system" responsible for episodic recollection. This system included the hippocampus (HPC), anterior thalamic nuclei (ATN), mammillary bodies (MB), retrosplenial cortex (RSC), and prefrontal cortex (PFC). Of relevance to the current thesis, the system includes key fibre pathways, in particular the MTT and different components of the fornix (Fx). More recently, the circuit has been further extended to include a unique brainstem input via the tegmental nuclei of Gudden (Dillingham et al., 2015; Vann & Nelson, 2015). Chapter 2 will expand upon the extended hippocampal system, providing further detail about the structural components, fibre tracts and connectivity of the circuit.

Evidence supporting the role of the extended hippocampal circuit stems from neuroanatomical work, its primary impetus derives from clinical research on human cases of amnesia. This clinical evidence is discussed in Chapter 3. Instances of diencephalic stroke, in particular, have provided insight on the relative contributions of individual structures or fibre tracts. Lacunar stroke can produce a relatively localised area of damage; this has provided strong evidence to support a key role for the MTT in normal memory function (Carlesimo et al., 2011). The MTT provides a fibre pathway from the MB to the ATN and is unique to the extended system by virtue of the unidirectional flow of information from the former to the latter structure. Experimental studies creating localised MTT lesions in rodents have consistently reported spatial working memory deficits (Sziklas & Petrides, 1999; Vann & Aggleton, 2003; Vann, 2013; Dalrymple-Alford et al., 2015; Perry et al., 2018; Dillingham et al., 2019). The descending arm of the post-commissural fornix (PCFx) provides direct hippocampal subicular input into the MB. It is therefore to be expected that the PCFx is also critical to memory function. Some human evidence has suggested that the integrity

of PCFx fibers may contribute to the mnemonic deficits associated with MCI and normal ageing (Christiansen et al., 2016; Coad et al., 2020). However, two rat lesion studies that focused on the descending arm of the post-commissural fornix, surprisingly, have produced negative evidence that the PCFx pathway to the MB has a strong influence on spatial working memory (Vann et al., 2011; Vann, 2013). The current thesis revisited this issue by comparing the effects of MTT and PCFx lesions in rats with a view to examine their relative impact on electrophysiological parameters during working memory performance.

The ATN constitute a prominent node within the extended memory system. There are strong direct and indirect reciprocal connections between the ATN and other major structures in the extended memory system, in particular the cingulate cortex, retrosplenial cortex and subicular cortex. It is therefore unsurprising that the ATN also play a critical role in mnemonic functioning. Cell loss in the ATN is a crucial factor underlying the dense amnesia observed in patients with the alcoholic Korsakoff's syndrome (Harding et al., 2000; Arts et al., 2017; Segobin et al., 2019). Similarly, ATN lesions in rodents are associated with severe and persistent memory impairments (Aggleton et al., 2010; Aggleton & Nelson, 2015; Dalrymple-Alford et al., 2015).

An interesting feature of damage to components of the extended hippocampal system is evidence of covert pathology in distal structures in the network beyond the site of injury. Covert pathology is where a structure appears normal by standard histology, but shows the presence of a 'functional lesion' (Aggleton, 2008). For example, immediate early genes (IEGs) are markers of neuronal activation. A decrease in IEG activity can indicate loss of normal neuronal function. A substantial loss of IEG markers has been reported in structures such as the RSC in the extended system following localised lesions to the MTT and ATN (Aggleton, 2008; Vann & Albasser, 2009; Vann, 2013; Perry et al., 2018). Although there is little direct evidence, these 'functional lesions' may contribute to the mnemonic deficits produced by ATN and MTT lesions (Aggleton, 2008; Aggleton & Nelson, 2015; Dillingham et al., 2015). Conversely, IEG activity across structures of the extended circuit was reported to be unaffected by PCFx lesions (Vann, 2013).

Another means of exploring whether diencephalic damage impacts other structures within the system is to examine functional interactions using electrophysiology. Rhythmic oscillatory activity is generated by the cumulative electrical currents produced by excitable

membranes, and this in turn typically produces oscillatory waves of varying amplitude and frequency (Buzsaki et al., 2012). The oscillatory bands, delta, theta, and gamma have received considerable attention in memory research (Buzsaki, 2002; Nyhus & Curran, 2010; Colgin, 2013). However, theta rhythmicity has been consistently shown to be critically involved in memory, and the slow theta wave is capable of synchronizing distally located neural ensembles (Colgin, 2013). In humans, a distinction is made between theta (4-7 Hz) and alpha (8-12 Hz). In rats, 'theta' frequency typically ranges from 5-14 Hz, also referred to as rhythmic slow activity (Mitchell et al., 2008). Therefore, a frequency range encompassing rat 'theta'/ RSA (2-14 Hz) was used in the current study. Electrophysiological aberrations within the extended hippocampal system have been documented in neurological conditions and may contribute to the cognitive dysfunction that arises in these cases (Nimmrich et al., 2015; Basar et al., 2016; Palop & Mucke, 2016). Recently, MTT lesions have been shown to alter hippocampocortical oscillatory activity (Dillingham et al., 2019).

Lesion injury to either the MTT or PCFx is permanent, but the 'functional lesions' may be reversable. For example, it has been reported that enriched housing conditions or treatment with cerebrolysin (neurotrophic factor) can improve spatial memory in rats following permanent lesions of the ATN (Wolff et al., 2008; Loukavenko et al., 2016). These effects are likely to be mediated by increased activation of multiple structures within the extended memory system (Dalrymple-Alford et al., 2015). In order to target the distributed network, one potential avenue for intervention might be selective stimulation of a nodal structure in the circuit, such as the ATN. The ATN has extensive reciprocal connections with the prefrontal cortex and retrosplenial cortex, as well as the subicular regions of the hippocampal formation (Jankowski et al., 2013; Bubb et al., 2017; Mathaisen et al., 2017). Electrical stimulation of the ATN has been shown to improve cognitive performance in both humans and rats (Hamani et al., 2011; Oh et al., 2012). Optogenetic stimulation, however, affords much greater cellular specificity and spatial and temporal precision for neural control than electrical or pharmacological techniques. Therefore, the second aim of the thesis was to test the hypothesis that optogenetic stimulation of the ATN would ameliorate memory function following damage to the MTT.

1.2 Aims of the current study

The current thesis had two key aims. The first aim was to directly compare the impact of MTT and PCFx lesions on spatial working memory and their effects on function across the wider memory system. Functional changes in the memory system were examined using measures of IEG activity and theta electrical activity. The second aim was to test whether impaired spatial working memory in rats with MTT lesions was ameliorated by optogenetic stimulation of the ATN. The effect of optogenetic stimulation was measured by changes in spatial memory, IEG activation and theta rhythmicity. As establishing optogenetic techniques at the University of Canterbury required an extensive amount of time, the effect of optogenetic intervention was not examined in PCFx lesions, which is part of the discussion in the final chapter.

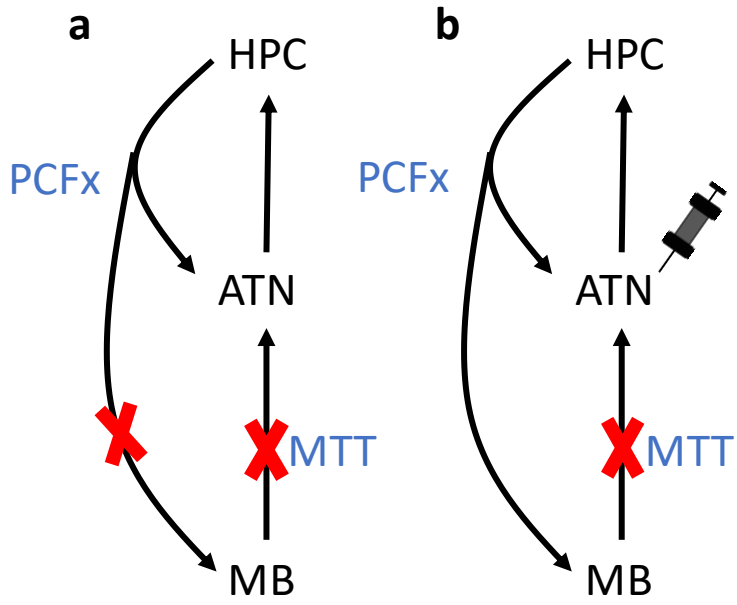

Figure 1.1. A diagrammatic representation of the connectivity between the HPC, ATN and MB. a, To address the first aim comparisons were made between lesions of the MTT, thus removing the MB input to the ATN, or the descending arm of the post-commissural fornix, thus removing the HPC input to the MB.Note that the post-commissural fornix provides HPC input to both the ATN and MB, but the descending limb innervates only the MB. b, To address the second aim rats received MTT lesions and lentiviral infusion into the ATN. Optogenetic stimulation was then made in the ATN. Abbreviations: ATN= anterior thalamic nuclei; HPC= hippocampus; MB= mammillary bodies; MTT= mammillothalamic tract; PCFx= post-commissural fornix.

Chapter 2:
Neuroanatomy of the extended hippocampal system

This chapter summarises the anatomy of key structures and fibre pathways comprising the extended hippocampal memory system (or hippocampal-diecephalic memory system). A general overview is provided before a more detailed description of the anatomy of key structures and their neural connections in the system. Following this chapter, an overview of the human literature implicating structures of the extended circuit in diencephalic amnesia will be given.

2.1 The extended hippocampal memory system

As indicated earlier, both the medial temporal lobe and medial diencephalon have been implicated in episodic memory for over one hundred years. Initially, James Papez (1937) proposed a neuroanatomical circuit for emotion that "built up in the hippocampal formation and…transferred to the mammillary body and thence through the anterior thalamic nuclei to the cortex of the gyrus cinguli" (Vann & Nelson, 2015). It is, however, now clear that this circuit is critically involved in memory, initially described as the Delay and Brion memory circuit (1969). Aggleton and Brown (1999) extended this idea and brought together both clinical and experimental animal studies to coin the term, extended hippocampal system. This reformulation combined both key temporal lobe and diencephalic structures in the shape of a unified hippocampal-diencephalic system that was critical for the encoding of information for episodic recollection. They also described a "familiarity-based" system that proposed key links between the perirhinal cortex and the mediodorsal nucleus. While this latter concept remains contentious, their primary focus on an extended hippocampal system for recollection has been supported by both clinical and experimental lesion studies (Aggleton & Brown, 1999; Brown & Aggleton, 2001; Aggleton et al., 2010). Naturally, the primary extended system centres on the hippocampal formation (HPC), but it also draws on the importance and interdependence of connections with the thalamus, in particular the anterior thalamic nuclei (ATN), as well as the mammillary bodies (MB), prefrontal cortex (PFC) and, more so in recent elaborations, the retrosplenial cortex (RSC) (see figure 2.1 for a diagrammatic representation of the extended hippocampal system in the human and rat brain).

Of relevance for the current thesis, the recollection memory system highlights two major neural tracts. These are the fornix and the mammillothalamic tract (MTT) (Aggleton & Brown, 1999; Vann & Nelson, 2015). It is also important that the fornix diverges at the level of the anterior commissure, forming two unique tracts. One of these forms the pre-commissural fornix, which continues forward to innervate the basal forebrain, ventral striatum and the prefrontal cortex (providing a direct HPC-mPFC connection) (Nauta, 1956; Poletti & Creswell, 1977; Vann et al., 2011). The second branch forms the post-commissural columns; it is particularly relevant for the current thesis that these columns split once more to yield a major bidirectional connection directly between the HPC and the ATN, plus the unidirectional connection from the HPC to the MB. This last tract is known as the descending post-commissural fornix (PCFx), which is a focus for the current thesis. The MTT is also of particular relevance to this thesis. The MTT provides only a unidirectional pathway from the MB to ATN, thus facilitating an indirect connection from the HPC to the ATN. In addition, there are reciprocal connections between the MB and the tegmental nuclei of Gudden (via the mammillary peduncle and mammillotegmental tract) (Kocsis et al., 2001), which enable the MB to contribute a unique brainstem input to the wider circuit via these MTT efferents (Vann, 2013; Vann & Nelson, 2015).

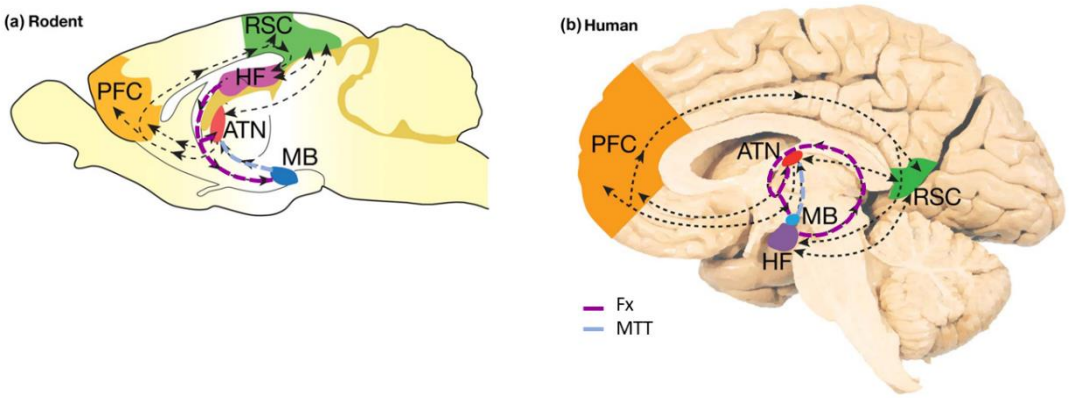

Figure 2.1. Schematic diagrams representing the major components of the extended hippocampal memory system in a rat (a) and human (b) brain. The fornix connections are shown here in purple dashed lines and the mammillothalamic tract is shown in light blue. Abbreviations: HF, hippocampal formation including the subicular and entorhinal cortices; RSC, retrosplenial cortex; PFC, prefrontal cortex; MB, mammillary bodies; ATN, anterior thalamic nuclei. Adapted from Barnett et al. (2018).

2.2 The hippocampal formation

The hippocampus has been consistently shown to be critical for the acquisition of episodic memory and, in particular, spatial navigation (Scoville & Milner, 1957; Morris et al., 1983; Eichenbaum, 2017a, 2017b). The hippocampal formation (HPC) is an archicortical, medial temporal lobe structure, which is composed of multiple subregions: the hippocampus proper (areas CA1, CA2, CA3, CA4 and the dentate gyrus) and the subicular cortex (here referring to the combination of the subiculum, presubiculum and parasubiculum; Aggleton, 2012; Squire et al., 2004). The major sources of extrinsic projections from the hippocampal formation are the CA1 and subicular cortex, with the subiculum exclusively projecting to the RSC, entorhinal cortex, ATN, and MB; a relatively even combination of CA1 and subicular outputs terminate in the PFC. It is worth noting that area CA3 also contributes to HPC projections to the septum and nucleus accumbens alongside the subicular cortex and area CA1. Projections originating in the subiculum have been shown to exhibit lamina separation in both rodents and primates. For example, the ATN receives projections originating in the deepest subicular cell layer, whilst the MB receives inputs from more superficial cells (Aggleton, 2012). Moreover, most subicular outputs terminate in specific parts of the RSC, ATN and MB demonstrating the degree of intrinsic separation found within components of the HPC. The HPC also receives return connections from both the RSC and ATN (see figure 2.1 above). There is, therefore, a complex circuit of direct and indirect connections within the extended hippocampal system.

2.3 The mammillary bodies (MB)

The mammillary bodies are located on the ventral surface of the brain, posterior to the hypothalamus. As mentioned above, the HPC projects directly to the MB, and for many years these connections were seen as key HPC outputs. More recently, however, it is has become apparent that the MTT, that is, the ascending projection from the MB, influence normal memory function.

The MB are different to other components of the extended hippocampal system as they appear to have fewer connections, namely with the HPC, ATN and tegmental nuclei of Gudden. The bilateral MB consist of two major nuclei groups: the lateral and medial nuclei. The medial group is notably larger in size compared to the lateral nuclei. Both nuclei contain a narrow array of cell types, with the largest cells located in the lateral nuclei (Vann &

Aggleton, 2004). The two primary inputs to the MB are from the HPC (via the descending post-commissural fornix) and from the tegmental nuclei of Gudden via the mammillary peduncle (Dillingham, 2015). Thus, the HPC input to the MB provides an indirect HPC input to the ATN via the MTT in addition to direct subicular ATN afferents. The MB seem to project almost exclusively to the ATN via the MTT (unidirectional), as well as sending a reciprocal projection to the tegmental nuclei of Gudden via the mammillotegmental tract.

The lateral and medial MB project to different subregions of both the ATN and the tegmental nuclei of Gudden, which has led to the proposal that they form two parallel systems (see Figure 2.2 for a diagrammatic representation of the two parallel MB circuits). The medial mammillary nucleus projects ipsilaterally to the anteromedial (AM) and anteroventral (AV) thalamic nuclei and reciprocally connects with the ventral tegmental nuclei of Gudden (VTNg), forming the medial 'theta' system. Conversely, the lateral mammillary nuclei project bilaterally to the anterodorsal (AD) thalamus and have reciprocal connections with the dorsal tegmental nuclei of Gudden (DTg), forming the lateral 'head direction' system (Cruce, 1977; Hayakawa & Zyo, 1984; Allen & Hopkins, 1989; Vann & Aggleton, 2004). Therefore, the MB may not only provide an indirect hippocampal connection into the ATN but also a unique brainstem input from the DTg and VTNg into the ATN, HPC and the wider circuit.

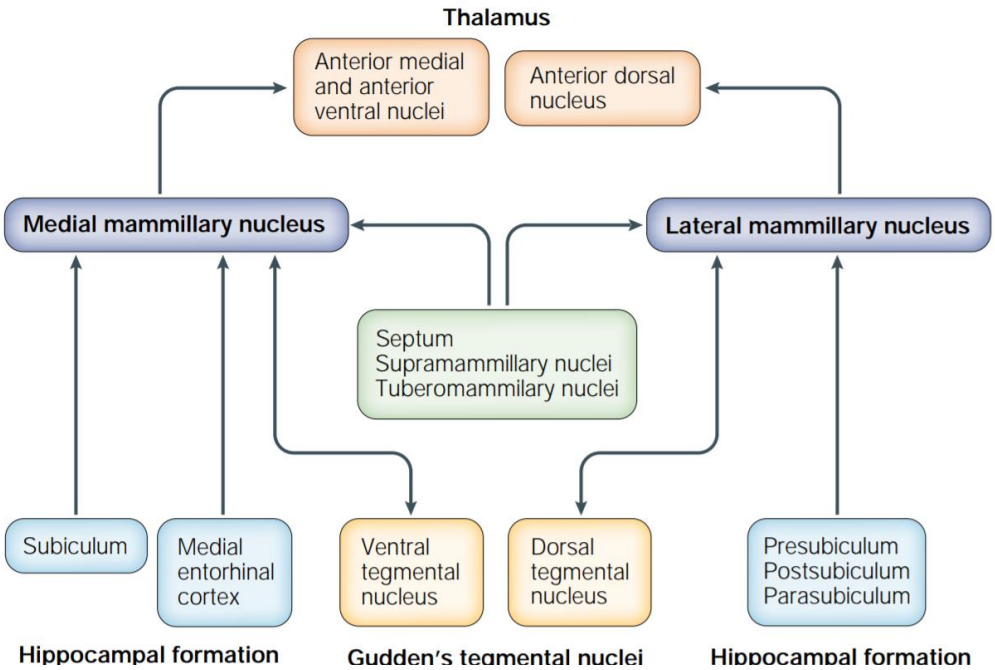

Figure 2.2. Schematic representation of the main direct connections of the lateral and medial mammillary nuclei. Diagram from Vann and Aggleton (2004).

2.4 The mammillothalamic tract (MTT)

As previously mentioned, the MTT provide the sole MB input to the ATN, and thus may provide distinctive insight into the role of this circuit (Vann & Aggleton, 2003). Unlike the fornix, the fibres of the MTT are contained entirely within the extended hippocampal system (Vann, 2010), and thus may provide critical insight into how the constituent structures interact to support episodic memory. Transection of the MTT has been considered a means of assessing MB contribution to mnemonic functioning through the elimination of their inputs into the ATN (Dillingham et al., 2015). Removal of MTT MB inputs not only removes the indirect input from the HPC (via the PCFx), but it also removes input from the tegmental nuclei of Gudden (via the mammillotegmental tract) (Vann & Nelson, 2015). As a result, transection of the MTT eliminates key brainstem input implicated in both head direction and theta function (Vann & Aggleton, 2004; Vann & Nelson, 2015).

2.5 The anterior thalamic nuclei (ATN)

The ATN are a nodal structure in the circuitry of the extended hippocampal memory system. The ATN receive numerous projections from both cortical and subcortical structures including the RSC, prelimbic cortex, anterior cingulate cortex, as well as the HPC (subiculum), MB and laterodorsal tegmental nucleus (Sikes and Vogt, 1987; Mitchell, Dalrymple-Alford and Christie, 2002). Of these, the connections from the prelimbic, anterior cingulate and retrosplenial cortex appear reciprocal, whilst the subicular and brainstem inputs are unidirectional (Sikes and Vogt, 1987; Mitchell, Dalrymple-Alford and Christie, 2002; Shibata & Naito, 2005; Aggleton et al., 2010). Furthermore, recent evidence from Mathiasen et al. (2017) suggests that different nuclei within the ATN may exhibit asymmetric connectivity with cortical structures. That is, anteromedial thalamic nuclei (AM) efferents to the cortex and subiculum appear ipsilateral, whilst those target sites provide reciprocal bilateral connections back to the AM. Conversely the AV demonstrated a similar level of ipsilateral projections to the cortex, but these reciprocal connections were also relatively ipsilateral. This was most marked in the case of the projections from the anterior cingulate to the AV (Mathiasen et al., 2017).

As mentioned above, the difference in connectivity between the AV, AM and AD has been suggested to hold functional significance for these nuclei within the memory circuit. The AD is proposed to play a key role in spatial navigation by virtue of its involvement in the

head direction circuit, together with the lateral MB and the DTg (Vann & Aggelton, 2004; Aggleton, 2010; Jankowski et al., 2013). These structures contain head direction cells, which selectively discharge when the animal points its head in a given direction irrespective of the rat's position in the environment. That is, these cells appear to encode information for spatial orientation within an environment much like a compass (Jankowski et al., 2013). Evidence suggests that the AD forms part of a hierarchical network responsible for the propagation of head direction information from lower brainstem structures (DTg, MB) up to the higher components such as the post- and para-subiculum via the AD (Jankowski et al., 2013; Dillingham et al., 2015). The AV and AM parallel the head direction circuit but in what is referred to as the 'theta circuit', a collection of nuclei including the medial MB and VTNg that mediate theta rhythmicity. 'Theta' activity, in awake behaving rats, is categorised as a slow-wave rhythmic oscillation between 5-14Hz, also known as rhythmic slow activity (Mitchell et al., 2008). Theta rhythmicity is thought to enable synchronisation across distally located populations of neurons to facilitate inter-structural communication and is strongly associated with memory function (Buzsaki, 2002, 2005; Kirk & Mackay, 2003; Colgin, 2011). Although the AV contains some head direction cells, approximately 75% of AV cells discharge rhythmically with theta (Vertes et al., 2001; Albo et al., 2003).

2.6 The prefrontal cortex (PFC)

Evidence from electrophysiological and lesion studies supports the critical role of HPC-PFC interactions in memory processing (Colgin, 2011). These interactions are of particular relevance to this thesis. The PFC is a large and heterogenous region. It occupies the anterior portion of the frontal lobe (Ongur & Price, 2000). It receives a plethora of highly processed sensory inputs, and plays a key role in cognitive and emotional processes. Although the PFC shows a high level of variability across species, particularly in terms of its granular to agranular ratio, its position and connectivity is remarkably conserved (Ongur & Price, 2000).

The medial prefrontal cortex (mPFC) has been consistently shown to be critical to memory function and thus is of particular significance. The medial prefrontal cortex includes both the prelimbic (PL) and infralimbic (IL) cortices which receive direct and indirect innervation from the HPC, as well as inputs from the mediodorsal nucleus, ATN, RSC and nucleus reuniens (Hoover & Vertes, 2007; Eichenbaum, 2017; Mathiasen et al., 2017). In the more recent 7th edition of "The Rat Brain in Stereotaxic Coordinates" (Paxinos & Watson,

2013) the medial PFC is now composed of area 32V of the anterior cingulate cortex (previously the prelimbic cortex - the terminology that will be used in the current thesis) and 32D of the anterior cingulate cortex (previously the anterior cingulate cortex). Both the PL and IL receive direct projections from the HPC, specifically area CA1 and the subiculum. There are an additional two key pathways which include an intermediate structure between the HPC and the mPFC. The thalamic pathway is bidirectional and passes from area CA1 to the thalamic nucleus reuniens (Re). Neurons in the Re then innervate all mPFC regions, including some cells that bifurcate between the PFC and HPC, supporting the idea that the nucleus reuniens may play a global role within the thalamocortical circuit in synchronising PFC-HPC interactions (Eichenbaum, 2017). The ATN also has dense reciprocal connections with the mPFC. In the case of the anteromedial thalamus, efferents to the mPFC are ipsilateral, whilst reciprocal projections to the AM are bilateral. By comparison, the AV cortical projections and reciprocal connections are both relatively ipsilateral (Mathiasen et al., 2017).

2.7 The retrosplenial cortex (RSC)

The location of the RSC differs across species. The RSC is proportionately larger in rodents than in humans and non-human primates, as the entirety of the posterior cingulate region is classified as the RSC (Vann et al., 2009). In humans and non-human primates the RSC is located directly behind the splenium of the corpus callosum, posterior to the cingulate cortex, identified as Brodman areas 29 and 30 (Mitchell et al., 2018). In the rat, the RSC is composed of three regions: a caudal granular a region (Rga; A29b), the more rostral and more extensive granular b RSC (Rgb; A29c) and an extensive region of dysgranular RSC (Rdg; A30). The Rga, Rgb and Rdg area are all interconnected, with up to 78% of RSC connections originating in or being received from other parts of the RSC. However, as previously mentioned, the RSC also exhibits subcortical connectivity as well as other cortical connections (Mitchell et al., 2018). The RSC receives direct unidirectional input from hippocampal area CA1 (Cenquizca & Swanson, 2007; Miyashita & Rockland, 2007) and the subiculum (Honda & Ishizuka, 2015), and forms reciprocal connections with the pre-, para- and post-subiculum. Similarly, the RSC is reciprocally connected with the PFC, cingulate cortex (only in humans and non-human primates), parietal and visual cortex. The RSC is also reciprocally connected to all three nuclei of the ATN (AV, AM and AD) and the laterodorsal

thalamic nucleus (Mitchell et al., 2018). The RSC also receives inputs from the primate medial pulvinars (Baleydier & Mauguiere, 1985). RSC inputs differ as a function of region, with the granular layers receiving inputs from the septal and temporal subiculum, whilst the dysgranular layer is densely connected to the visual cortex (Shibata et al., 2009).

The association of the RSC with memory function is largely driven by its interconnectedness with key memory structures, the HPC and ATN, as well as evidence from lesion studies and human cases of Alzheimer's disease (AD). The RSC has been suggested to act as a convergence point of information from the HPC and ATN, thus explaining the shared covert pathology observed in the RSC following lesions to either structure. This refers to instances where a structure appears functionally intact but there is evidence of an underlying loss of function (elaborated on in later chapters) and demonstrated in this instance by a profound reduction in neuronal markers, particularly immediate early gene markers (Aggleton, 2008; Dillingham et al., 2015; Powell et al., 2018). Furthermore, the RSC is one of the first brain regions to show pathological and metabolic changes in mild cognitive impairment and early AD (Nestor et al., 2003; Aggleton et al., 2016).

2.8 The fornix (Fx)

The Fx (meaning 'arch') acts as the major fibre output from the HPC forming connections with most structures implicated in learning and memory, the RSC being the sole exception (Aggleton, 2014). As previously mentioned, the body of the fornix splits at the level of the anterior commissure to form the pre- and post-commissural fornix. The fibres of the post-commissural fornix split in two and either turn caudally to innervate the ATN, or proceed towards the ventral surface as a compact bundle to terminate in the MB. Approximately half to one third of the post-commissural fibers terminate in the ATN, with the remainder innervating the MB (Powell et al., 1957; Guillery, 1956). Previously, rat lesion studies have suggested that selective damage of the descending portion of the post-commissural fornix (PCFx), i.e. innervating the MB, produces negligible behavioural impairments on standard memory tasks which are sensitive to targeted MB and MTT damage (Vann et al., 2009; Vann et al., 2010; Vann, 2013). This evidence has been used to support the importance of the brainstem influence on the MB and the extended hippocampal circuit via the MTT and ATN. However, it has also raised the question as to the role of the PCFx in memory, as the direct anatomical connection between the HPC and MB suggests a mnemonic capacity. Attempts

to explore the importance of the PCFx in human memory have been hindered by its being a component of a larger fibre pathway, however recent studies have suggested that the integrity of the PCFx may be critical for episodic memory function in mild cognitive impairment (MCI) and normal ageing (Christiansen et al., 2016; Coad et al., 2020).

2.9 The tegmental nuclei of Gudden

The tegmental nuclei of Gudden is a relatively new addition to the extended hippocampal system. Recent evidence suggests that this brainstem input may influence memory via its connection with the MB (Vann, 2013). The tegmental nuclei of Gudden are comprised of two nuclei, the VTNg, which has been strongly implicated in the 'theta circuit' involved in memory function and has dense reciprocal connections with the medial MB. The DTg is considered a part of the hierarchical head direction system and is densely interconnected with the lateral MB. Lesion studies have demonstrated that, unlike HPC inputs to the MB via the PCFx (Vann et al., 2009), the VTNg may provide the more crucial inputs for the role of the MB in memory (Vann, 2010; Vann, 2013). In line with the association of the VTNg with the 'theta circuit', electrophysiological evidence demonstrates that the cells of the VTNg discharge in rhythmic bursts at theta frequency. Thus the VTNg may either modulate or contribute to theta rhythm within the circuit (Kocsis et al., 2001; Bassant & Poindessous-Jazat, 2001).

2.10 Conclusions

The aforementioned structures comprise an extended hippocampal system critical for episodic memory function. Despite the often hippocampal-centric view of memory, following Scoville and Milner's paper in 1957 on the amnesic patient HM, recent years have demonstrated the importance of many different structures in hippocampal-related functions, and emphasised the interconnected nature of a distributed "episodic memory" system in the brain. Of particular note are the ATN, MTT and PCFx. The ATN and MTT have been consistently associated with cases of anterograde amnesia in humans and severe memory deficits in animal studies. Anterograde amnesia in humans and the underlying sites of pathology will be discussed in the following chapter, whilst the animal evidence implicating the MTT and ATN will be examined in chapter four. Surprisingly, the PCFx is associated with, thus far, negligible behavioural effects although its anatomical status suggests that it would have an important role in memory. Subsequent chapters will present

evidence for a comparison of the behavioural impact of MTT and PCFx lesions, explore the role of rhythmic oscillatory activity within the extended hippocampal system and examine the potential to improve memory function through selective optogenetic stimulation after MTT lesions in rats. The ATN is a critical node within the extended system facilitating cortical and subcortical communication as well as a convergence point of the 'theta circuit' and the propagation of head direction information, by virtue of its interconnected nature. Therefore, the ATN may present itself as a possible target structure for intervention following selective damage to component structures within the memory system.

Chapter 3:
Diencephalic Amnesia

This chapter summarises the literature on human neurodegenerative disease and brain injury associated with diencephalic amnesia. The focus of the current thesis is on components of the extended hippocampal system, particularly the MTT and PCFx. But, in human cases, pathology is often diffuse with other diencephalic structures also influencing clinical findings. As both the MTT and PCFx have direct connections with the MB, and MTT has direct connections to the ATN, clinical findings associated with damage to both the ATN and MB will be discussed. There are only a couple of studies that examines the role of the PCFx in memory. This lack is largely due to PCFx being a subcomponent of the fornix. Being a part, it is rarely analysed as a stand-alone structure; instead the status of the whole fornix is normally considered. The highly variable and diffuse damage in humans makes it difficult to elucidate the neural basis of diencephalic amnesia. Nonetheless, there is consistent evidence suggesting an important role of select diencephalic structures in amnesia. Human cases of diencephalic amnesia are typically observed in conditions such as Korsakoff's syndrome, as well as following damage to the diencephalon due to stroke, penetrating injuries or through the removal of colloid cysts. There is strong evidence from lacunar stroke supporting the importance of the MTT, but studies examining patients with Korsakoff's syndrome have also demonstrated a critical role for the ATN.

3.1 Lacunar stroke

The most consistent support for the role of the MTT (and, to a lesser extent, the ATN) is from cases of relatively selective thalamic stroke. Lacunar stroke resulting in diencephalic amnesia involves occlusions of the supply arteries to thalamic regions that include the ATN and MTT, the anterior choroidal or tuberothalamic arteries (Von Cramon et al., 1985; Carrera & Bogousslavsky, 2006). Unlike haemorrhagic stroke, ischemia-associated lacunar stroke is caused by occlusions of arteries supplying blood to the deep regions of the brain. This leads to comparatively focal infarcts in localised regions of the thalamus. These instances are informative as the pathology remains relatively localised due to the small penetrating arteries involved without the more diverse changes associated with conditions such as Korsakoff's syndrome (Van der Werf et al., 2003; Carlesimo, Lombardi, & Caltagirone, 2011) or Alzheimer's disease (Aggleton et al., 2016).

An early study examined the CT images of 6 patients who had ventral thalamic infarcts and presented with an amnesic syndrome (Von Cramon et al., 1985). Their findings suggested that the MTT and ventral portion of the lamina medullaris interna were associated with memory impairment. Furthermore, they suggested that localised damage to the MD was insufficient to cause amnesia, although this remains controversial (Von Cramon et al., 1985). In 2000, Van der Werf et al. reviewed 35 articles, encompassing 60 patients presenting with lacunar infarcts confined to the thalamus. They concluded that the only structure consistently associated with an amnesic syndrome was the MTT, with only one patient exhibiting an amnesic syndrome in the absence of damage to the MTT.

Later, Van der Werf et al. (2003) examined 22 further patients with thalamic infarction and used a lesion overlap analysis to establish a structure-function relationship. This entailed compiling the lesions of patients who shared a certain deficit, and then subtracting those structures that were lesioned in patients not presenting with the same deficit, leaving behind the structures of interest (Van der Werf et al., 2003). They found that damage to the MTT was again the most consistent predictor of an amnesic syndrome. However, the anterior and midline thalamic nuclei were also found to have predictive value (Van der Werf et al., 2003).

More recent cases also support these findings. A review of vascular thalamic amnesia focussed on potentially different roles played by thalamic regions, implicating the MTT and the ATN in recollection rather than familiarity (Carlesimo at al., 2011). This review of 41 papers provided evidence on 83 patients with lacunar infarcts in the anterior and mesial thalamus with the presence of an amnesic syndrome (with both retrograde and anterograde memory deficits) most strongly predicted by the presence of damage to the MTT. Carlesimo et al. (2011) provide support for an extended hippocampal system. The qualitative pattern of memory impairment observed following focal lesions to the medial and anterior thalamus is similar in nature to those impairments associated with damage to the medial temporal lobe. This pattern of memory impairment included a striking loss of declarative anterograde memory, a more variable deficit in retrograde long-term memory, but relatively intact short-term and implicit memory (Carlesimo et al., 2011). Lastly, Carlesimo et al. (2011) observed the differences in memory deficits between cases was attributable to differences in thalamic pathology. More specifically, the MTT/ATN axis

appears to be critically involved in recollective processes whilst the ventroamygdalofugal pathway/ MD axis was implicated in familiarity processes (Aggleton & Brown, 1999; Carlesimo et al., 2011).

Recently, Danet et al. (2015) examined the MRI images of 12 patients with left thalamic infarction compared with 25 healthy matched controls. They reported that damage to the MTT was associated with severe memory impairment. However the authors reported that MD lesions were also predictive of impaired memory function, although to a lesser extent, suggesting a role for the MD in mnemonic functioning (Danet et al., 2015). An advantage of this study over earlier imaging studies was the use of a thalamic atlas which allowed manual segmentation and automatic localisation of thalamic lesions. Thalamic atlas plates were superimposed onto the summed and overlapped lesions, thus producing a clear image of lesion distribution across thalamic nuclei. 11 out of 12 patients had damage to the MD and all had damage to the intra-lamina nuclei. Collectively, the patients showed impaired performance on verbal memory tasks, but those cases with MTT damage presented with a more severe memory impairment than cases where the MTT was spared.

Although the above evidence encourages a focus on particular neural structures, the report from Danet et al. (2015) highlights the difficulty inherent in human cases of diencephalic amnesia. The close anatomical proximity of thalamic nuclei and fibre tracts means that damage to the MTT typically also encompasses damage to local nuclei such as the ATN, MD and the MB. This is even apparent in the single case study of patient GP, who possessed possibly the most localised MTT lesion in the literature (Carlesimo et al., 2007). Patient GP suffered an acute episode of unconsciousness and upon awakening presented with a neuropsychological profile typical of an amnesic syndrome, in that he demonstrated impaired verbal and visuo-spatial recall, but relatively spared recognition memory, normal short-term and semantic memory function. MRI scans showed the presence of localised bilateral MTT damage (see Figure 3.1 for the MRI images and lesion reconstruction by Carlesimo et al. (2007). Although the prevailing amnesia was attributed to damage to the MTT, the authors note that the infarction most likely extends into adjacent structures such as the intralaminar nuclei, ventral anterior thalamus and mammillotegmental tract. These findings support the value of relatively precise animal lesion experiments to determine the mnemonic role of the MTT and other structures within the extended hippocampal system.

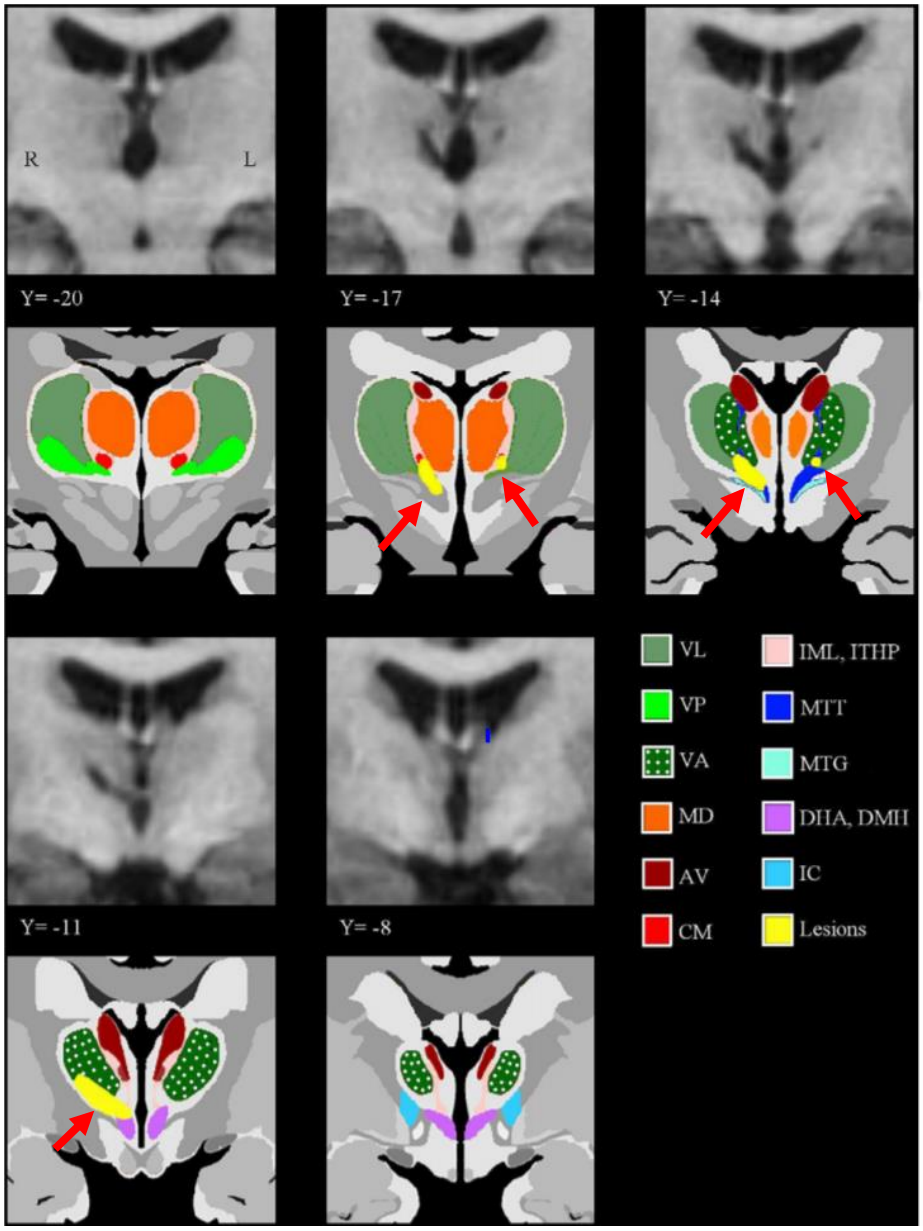

Figure 3.1. T1-weighted coronal slices (1 mm thick) through the thalamus (top row and third row down) with corresponding atlas plates upon which the lesion has been superimposed in yellow. Red arrows point to the lesion site of interest. Note the MTT has been shown here in blue. VL = ventrolateral thalamic nuclei; VP = ventroposterior thalamic nuclei; VA = ventroanterior thalamic nuclei; MD = mediodorsal thalamic nuclei; AV = anteroventral thalamic nuclei; CM = centromedian thalamic nuclei; IML = internal medullary lamina of thalamus; ITHP = inferior thalamic peduncle; MTT = mammillothalamic tract; MTG = mammillotegmental tract; DHA = dorsal hypothalamic area; DMH = dorsomedial hypothalamic nucleus; IC = internal capsule. Adapted from Carlesimo et al., (2007).

3.2 Traumatic brain injury

Instances of TBI, like localised infarction, are highly informative as they provide a clear

'before' and 'after' image of the patient, as opposed to cases of neurodegeneration which

can have an insidious onset involving a range of symptoms and associated neural damage. However, there are very few studies involving TBI to the diencephalon. The two most often cited cases (Squire et al., 1989; Dusior et al., 1990), whilst remarkable and informative, are both confounded by additional damage to other diencephalic nuclei.

The first case study concerns patient NA who sustained a penetrating injury to the base of the brain when a fencing foil was forced up his right nostril (Squire et al., 1989). MRI imaging carried out more than 20 years later revealed the key damaged locations. The authors found a large thalamic lesion in the left hemisphere, damaging the anterior and posterior intralaminar, mediodorsal and lateral nuclei. The lesion also likely transected the left MTT and PCFx, as well as damaging the hypothalamus and MB bilaterally. Lastly, there was substantial unilateral damage to the right temporal lobe and rostral amygdala (Squire et al., 1989). Patient NA presented with a predominantly verbal form of amnesia, suggesting that the effective lesion was located in the left hemisphere and implying that the resulting deficit could not be solely attributed to the bilateral damage to the MB. Squire et al. (1989) attributed NA's amnesia to damage of the intralaminar nuclei and MTT. However, patient NA sustained damage to a large number of memory-related structures, which all may have contributed to his memory dysfunction rather than an individual structure playing a causal role.

A second case of diencephalic TBI concerns patient BJ who developed severe memory dysfunction after sustaining a penetrating brain injury to the basal regions of the brain when a snooker cue entered his left nostril (Dusior et al., 1990). Although patient BJ initially presented with a dense amnesic syndrome (anterograde and retrograde amnesia), he later showed significant recovery of function. Twenty-one months after injury, formal memory testing demonstrated a significant deficit in verbal memory, comparable to patients with an amnesic syndrome. Conversely, BJ's memory for non-verbal material appeared to be only mildly affected, and his retrograde amnesia regressed to the six-month period prior to injury (Dusior et al., 1990). MRI imaging showed sparing of the thalamic nuclei, but relatively localised damage to the bilateral MB, and therefore implicating the MB as the primary cause of memory loss.

3.3 Removal of colloid cysts and cavernous angiomas

The role of the MB has been reinforced by evidence from the removal of colloid cysts in humans. A colloid cyst is a benign tumour which develops in the third ventricle, located adjacent to the fornix (see Figure 3.2). The surgical removal of colloid cysts is commonly associated with fornix atrophy. A study by Tsivilis et al. (2008) aimed to relate fornix volume to memory following the removal of colloid cysts, due to the assumption that the functional relationship between temporal lobe and diencephalic amnesia depended on the integrity of the fornix (Tsivilis et al., 2008). However, fornix volume was not consistently correlated with working memory performance, but was associated with impaired long-term memory. Instead, Tsivilis et al. (2008) found that MB volume was correlated with 13 out of 14 tests of episodic memory function, and moreover, patients with the smallest MB volume showed significantly greater impairments on tests of recall than those with comparatively larger MB volume (Tsivilis et al., 2008). Although discussed later in this chapter, it is also worth noting that damage to the fornix was still associated with long term memory impairment and that the post-commissural fornix constitutes the majority of fornical fibres. The authors used MRI-based volume estimates as a direct measure of fornix status and MB atrophy as an indirect measure as the MB commonly atrophy after fornix damage (Tsivilis et al., 2008).

Similar to colloid cyst removal, surgery for cavernous angioma can also cause damage to nearby structures, such as the pre- and post-commissural fornix. A cavernous angioma, or cavernoma, is a cluster of abnormal blood vessels which are usually found in the brain or spinal cord. Vann et al., (2008) examined the cognitive status of a patient who underwent cavernoma removal surgery for a large cavernoma extending ventrally from the anterior horn of the left lateral ventricle to the posterior gyrus rectus. MRI imaging and in depth neuropsychological assessment suggested that the memory deficits that arose were attributed to tissue loss in the pre- and post-commissural fornix and the surrounding septal area (Vann et al., 2008). It is likely that these structures were compromised prior to surgery by the size and position of the cavernoma, but that surgical procedures had created additional damage in the fornix and septal region. Additionally, it was found that there was no evidence of ventricular enlargement prior to and following surgery (a common occurrence in colloid cyst removal patients), which implies a lack of damage to other distal structures (Vann et al., 2008). Notably, the patient possessed unimpaired recognition

memory but a severe case of persistent anterograde amnesia. Human cases of damage limited only to the fornix are rare, and therefore instances of selective post-commissural damage are rarer still as it requires the partitioning of the pre- and post-commissural fornix (Christiansen et al., 2016; Coad et al., 2020). Hence, human evidence supporting the role of the fornix (and PCFx to a certain extent) in memory stems from neuroimaging studies in cases of neurodegenerative disease, mild cognitive impairment (MCI) and normal ageing. This will be addressed later in this chapter in the section devoted to neurodegenerative diseases (Christiansen et al., 2016; Coad et al., 2020).

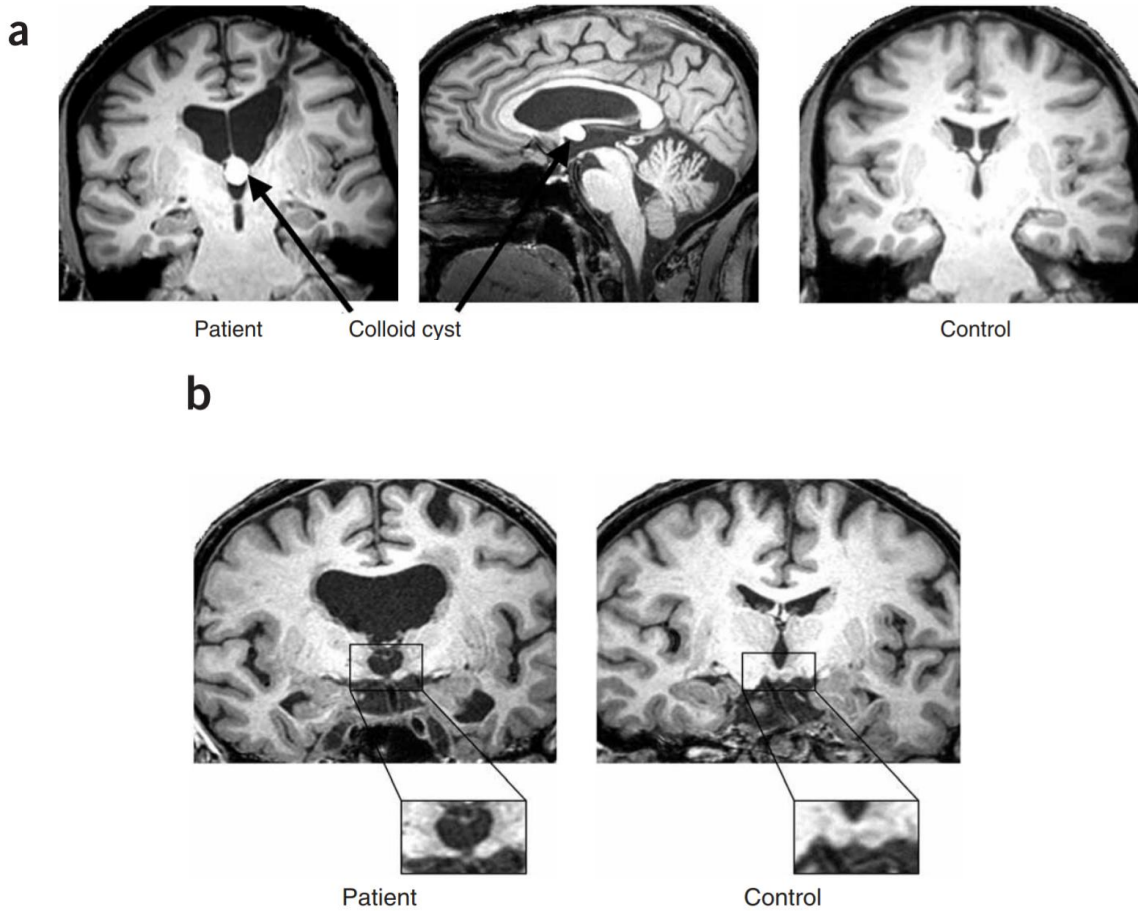

Figure 3.2. The fornix and mammillary bodies in colloid cyst surgery patients. (a) Structural MRIs showing the appearance and typical location of a colloid cyst before surgery, as seen in coronal and sagittal planes. Control brain shown on the right. (b) Structural MRIs showing an individual with the colloid cyst removed and subsequent fornix loss. From Tsivilis et al. (2008).

3.4 Korsakoff's amnesia

Korsakoff's syndrome (KS) is characterised by a striking and chronic loss of everyday memory (Sechi & Serra, 2007; Kopelman, 2015). More specifically, patients present with severe anterograde amnesia but retain implicit learning as they are able to learn new motor skills and develop conditioned reactions to stimuli (Korsakoff, 1887; 1889). In very severe cases, the amnesia can be more profound, with patients also demonstrating severe retrograde amnesia (Korsakoff, 1889). Thus, patients with Korsakoff's syndrome demonstrate symptoms closely related to temporal lobe damage (Squire & Wixted, 2011), but which are noticeably greater than instances of thalamic infarction (Harding et al., 2000; Van der Werf et al., 2003; Carlesimo et al., 2011; Kopelman, 2015). While both thalamic stroke and Korsakoff's amnesia are associated with impaired recollection, those with Korsakoff's amnesia further present with deficits in recognition memory and temporal context memory, as well as retrograde amnesia, a symptom that only presents in one third of thalamic infarct cases.

The associated neuropathology is most commonly linked to the diencephalon, with early studies consistently reporting the presence of MB atrophy in cases of probable KS. This has since been confirmed in more recent neuropathological studies (Harding et al., 2000; Kopelman, 2015). Other than pathology in the MB, both KS and Wernicke's encephalopathy (WE; see below) have been associated with other distributed changes such as neural loss, gliosis and micro-haemorrhages in the MD, paraventricular and periaqueductal grey matter (Harding et al., 2000; Sechi & Serra, 2007; Kopelman, 2015). The overlap between these two conditions has made it difficult to accurately assess the key site of pathology underlying the anterograde amnesia.

KS is often preceded by WE, which is the initial acute neuropsychiatric reaction to thiamine (also known as vitamin B1) deficiency. WE is characterised by confusion, poor balance and coordination, nystagmus (repetitive and uncontrolled eye movements) and opthalmoplegia (Kopelman et al., 2009). It is most commonly found in cases of alcohol abuse, as well as in illnesses where nutrient absorption has been compromised, such as anorexia nervosa (purging), peptic ulcers, and AIDS (Sechi & Serra, 2007). Thiamine pyruvate (its active form) is a critical coenzyme for several biochemical reactions in the brain, and thus a deficit causes brain lesions in regions with a normally high thiamine turnover in as

little as 2-3 weeks, which correlates with the length of time taken to deplete the body's thiamine stores (Sechi & Serra, 2007). It is also associated with carbohydrate and lipid metabolism, as well as the production of amino acids and glucose-derived neurotransmitters such as GABA. Those with a more insidious onset of WE are more likely to be brought to the attention of neuropsychologists or clinicians, however the lack or absence of a clear-cut WE period prior to KS makes it difficult to diagnose accurately and some cases may only be diagnosed post-mortem (Kopelman et al., 2009). The key observable difference between KS and WE is the memory impairment that accompanies the development of KS. More precisely, the extent of working memory dysfunction is disproportionate to other aspects of cognition, and normally occurs once the acute global confusion associated with WE has resolved (Sechi & Serra, 2007).

3.5 Pathological evidence from studies of Korsakoff's Syndrome

Nine years after Korsakoff's (1887) initial description, Gudden (1896) completed a study on the brains of patients with alcoholism, some of whom suffered from Korsakoff's syndrome. Post-mortem observations revealed patients that presented with memory deficits had mammillary body atrophy. Conversely, Victor et al. (1971) reported that pathology located within the mediodorsal thalamus was the critical point of difference between WE and KS as all 24 patients with lesions of the MD presented with chronic memory impairment. Most notably, the authors found that five patients with lesions of the MB but not the MD exhibited only transient WE symptoms with no evidence of amnesia. However, this study was later criticised for the lack of detailed neuropsychological testing validating their neuropathological observations.

Following this, Mair et al. (1979) and Mayes et al. (1988) completed similar neuropathological studies but using more rigorous and detailed neuropsychological testing, combined with extensive post-mortem examination of neural tissue. The subsequent results showed that unlike Victor et al's. (1971) study, the key sites of pathology underlying the observable memory deficits were in the MB, MTT and ATN (Mair et al., 1979; Mayes et al., 1988).

Harding et al. (2000) improved upon previous studies by including control groups and using unbiased stereology to estimate cell counts in the structures of interest. The authors compared five WE-only patients against eight WE/KS patients, as well as alcoholic

and non-alcoholic controls. They reported that WE and WE/KS patients demonstrate similar neuropathology in the MB and MD, but WE/KS patients exhibit more substantial neuronal loss in the ATN (Harding et al., 2000) (see Figures 3.3 and 3.4 and Table 3.1).

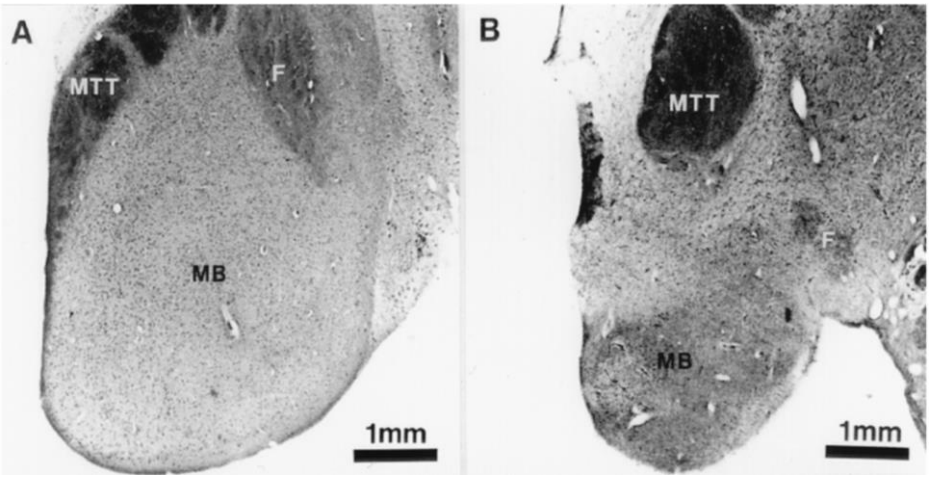

Figure 3.3.Photomicrographs of the MB and MTT from (a) a healthy control and (b) an alcoholic with chronic WE. The MB in (b) is shrunken and darker in appearance than in (a) due to severe gliosis and necrosis. Adapted from Harding et al. (2000).

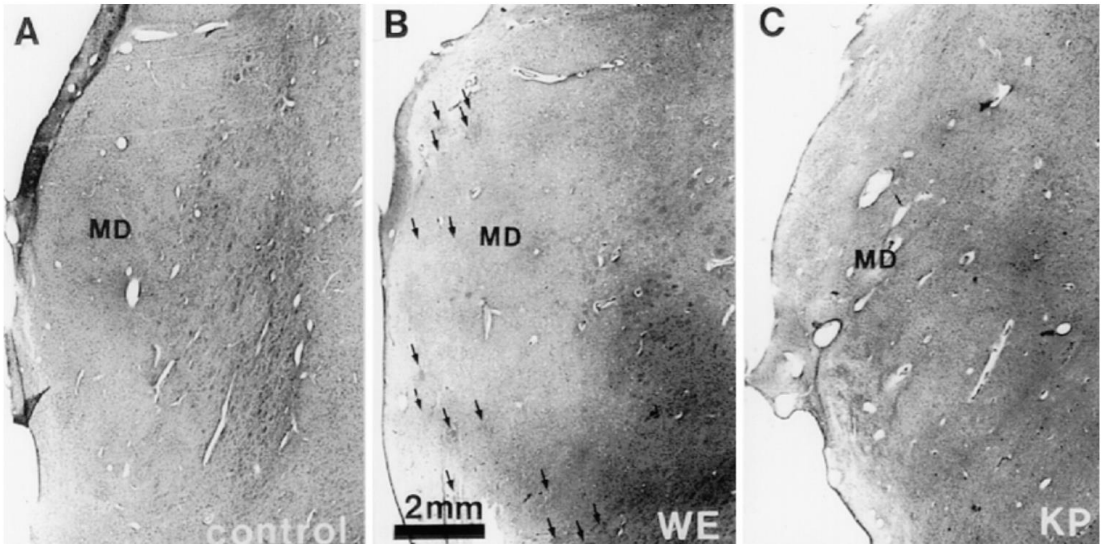

Figure 3.4. Photomicrographs of the MD. (a) the normal architecture of the MD in a healthy control, (b) an alcoholic patient with WE and (c) an alcoholic patient with KS. Note the vascular and parenchymal pathology particularly in the alcoholic with KS (c), as well as the petechial haemorrhages (arrows). Adapted from Harding et al. (2000).

*Table 3.1. The mean values and standard deviations of the volumes and estimated neuron numbers for the MM, AP and MD diencephalic nuclei in each of the diagnostic groups analysed. Volumes are given in mm³ and neuronal number is x10 000; the percent is that of the control mean. KP= Korsakoff's psychosis; WE= Wernicke's encephalopathy. *= p<.05 for comparison against controls. Adapted from Harding et al. (2000).*

Variable	Controls (n = 6)	Alcoholic controls (n = 5)	WE (n = 5)	WE and KP (n = 8)
MM volume	90 ± 30	80 ± 20 (89%)	70 ± 60 (78%)	30 ± 15 (33%)*
MM number	53 ± 18	52 ± 11 (98%)	28 ± 19 (53%)*	17 ± 14 (32%)*
AP volume	300 ± 50	280 ± 30 (93%)	260 ± 20 (87%)	190 ± 50 (63%)*
AP number	120 ± 22	121 ± 9 (100%)	103 ± 17 (86%)	56 ± 22 (47%)*
MD volume	1600 ± 200	1600 ± 150 (100%)	1400 ± 300 (88%)	900 ± 350 (56%)*
MD number	636 ± 44	643 ± 37 (100%)	330 ± 292 (52%)*	227 ± 157 (36%)*

3.6 Neural imaging evidence from studies of Korsakoff's Syndrome

Neural imaging studies have reinforced the neuropathological findings implicating the thalamus and MB in mnemonic deficits associated with KS. Pitel et al. (2012) compared grey and white matter volumes in alcoholics and alcoholics with KS and found that although there was much overlap across the two groups, the MB, medial thalamus and corpus callosum were more consistently damaged in cases of KS compared to the control group. Similarly, positron emission tomography (PET), which measures blood flow, oxygen levels and metabolism, has shown reduced glucose uptake in the thalamus, MB and basal forebrain/ orbito-frontal cortex (Reed et al., 2003; Pitel et al., 2012). Kim et al. (2009) examined the role of functional connectivity between structures in WE using fMRI scans. Seven alcoholics presenting with WE and recovering memory function, fourteen alcoholics not presenting with WE and 14 healthy controls underwent functional connectivity fMRI scans and verbal and non-verbal memory testing. Kim et al. (2009) found that the level of resting state functional connectivity between the MB and ATN in those patients recovering from WE correlated with their measured memory function.

3.7 Neurodegenerative diseases

Further support for the key role of the anterior thalamic nuclei in the control of memory stems for human cases of neurodegeneration such as multiple sclerosis (MS) (Houtchens et al., 2007), Lewy body dementia (LBD) (Janvin et al., 2006; Delli Pizzi et al., 2015), Alzheimer's disease (AD) and cases of mild cognitive impairment, which has been recognised as an early indication of eventual dementia (Aggleton et al., 2016). By contrast, there are only two

studies directly examining the role of the PCFx in MCI and/ or normal ageing in humans (Christiansen et al., 2016; Coad et al., 2020). Therefore studies exploring the association between the fornix and memory function have also been included here, as they in part reflect a loss of PCFx fibres.

MS is a disorder of the central nervous system, involving the demyelination of axons. MRI studies of MS have found that one of the most consistent predictors of cognitive status in MS is an observable reduction in the thalamus, with those exhibiting the most severe cognitive impairments presenting with the lowest thalamic volumes (Houtchens et al., 2007; Schoonheim et al., 2015). Moreover, Bisecco et al. (2015) reported that ATN atrophy and abnormalities in all cortico-thalamic tracts (using diffusion tensor MRI techniques) could enable differentiation between those MS patients with cognitive impairment and those without.

LBD is the second most common form of neurodegenerative dementia after AD and presents with symptoms such as severe attentional and visuo-perceptual impairments but sometimes less prominent deficits in memory function relative to AD (Delli Pizzi et al., 2015). A multimodal (MRI, diffusion tensor imaging and proton MR) study carried out by Delli Pizzi et al. (2015) examined the differences in pathology location in LBD and AD. The authors found that LBD patients had bilateral damage to thalamic regions, such as the mediodorsal thalamus, which largely project to the PFC. By contrast, AD patients showed bilateral disruption in the anterior thalamic and pulvinar regions. These regions show stronger connectivity with the medial temporal lobe and limbic cortex. Therefore, these findings suggest that the presence of severe memory dysfunction may be attributed to pathology in the ATN and pulvinar.

Findings such as Delli Pizzi et al.'s (2015) reflect a relatively recent push to extend the focus of AD research "beyond the temporal lobe" rather than continuing to assume that the HPC is the key site of damage (Aggelton et al., 2016). AD-related memory impairment has historically been linked to HPC dysfunction, and this idea is reinforced by the presence of severe neurofibrillary tangle pathology appearing in the medial temporal lobe in early AD. However, early AD changes are actually found in both the HPC and ATN (Braak & Braak, 1991a, 1991b; Delacourte et al., 1999). For example, de Jong et al. (2008) examined patients with probable AD and found that accompanying the reduction in global grey matter and

hippocampal volumes, there was also severe atrophy in thalamic regions and the putamen. In addition, all sites of atrophy were correlated with overall cognitive functioning, suggesting that hippocampal pathology alone could not account for the AD-related decline in cognition (de Jong et al., 2008).The findings reported thus far support the theory of an extended hippocampal system underlying memory function and also suggest that the anterior thalamic nuclei hold an important nodal position within this circuity.

The fornix as a whole has been shown to be critically involved in memory function, with alterations occurring in AD, mild cognitive impairment (MCI) and normal ageing. Reduced fornix fractional anisotropy (FA; a measure of diffusivity) and hippocampal atrophy are frequently associated with amnestic MCI (Liu et al., 2011; Zhuang et al., 2012, 2013; Zhang et al., 2013). MCI is considered as indicative of probable progression to AD (Kantarci, 2014). Furthermore, studies comparing elderly patients (over 70 years of age) with normal cognition to those with MCI have demonstrated that reduced fornix FA can be used to predict in advance the conversion from normal cognitive status to MCI and from amnestic MCI to AD (Oishi & Lyketsos, 2012), and can subsequently predict the cognitive decline observed in these patients with AD (Miekle et al., 2009; Oishi & Lyketsos, 2012). Moreover, lower fornix FA has been shown to accurately predict eventual hippocampal atrophy and cognitive decline (Miekle et al., 2012). Given the aforementioned evidence, it appears that fornix pathology is associated with impaired memory function. The mnemonic deficits that arise may in part reflect a loss of post-commissural fornix fibres given that the PCFx, which projects from the subiculum to the ATN and MB, comprises the majority of the fornical fibers (Kantarci, 2014) (see Figure 3.5). By contrast, the pre-commissural fornix constitutes the minority of the fornical projections, originating in area CA1 and CA3 and terminating in the septal complex.

Christiansen et al. (2016) attempted to separate out the differential contributions of the pre- and post-commissural fornix in an MRI tractography study comparing the status of the fornix in normal ageing and MCI. Diffusion weighted MRI, spherical convolution based tractography and Boolean logic (ie. “AND”, “OR” and “NOT” gates) were employed to reconstruct the separate divisions (see Figure 3.5 for gate location). In doing so, the authors were able to separate the majority of pre- and post-commissural fibres. Only those fibres located within the body of the fornix AND passing either anterior (pre-commissural fornix)

OR posterior (post-commissural fornix) to the anterior commissure were included (see Figure 6). Due to the location of the region of interest gates, those fibres of the post-commissural fornix that turn caudally (above the anterior commissure) to terminate in the ATN were excluded from PCFx analysis. Changes in both the pre- and post-commissural fornix were associated with ageing in both cohorts. Whilst there were no clear-cut dissociations between the two fibre tracts in MCI or normal ageing, the authors reported that alterations in PCFx diffusivity alone correlated with visual recall performance. The specific association between PCFx microstructure and visual recall performance is consistent with the view that PCFx fibres play a crucial role in mediating episodic memory function through facilitation of communication within the extended hippocampal network (Christiansen et al., 2016). The findings of Christiansen et al. (2016) are supported by more recent work that also examined the microstructure of the pre- and post-commissural fornix but in healthy ageing (Coad et al., 2020). Coad et al. (2020) reported that whilst ageing was associated with alterations in the microstructure of both tracts, only the status of the post-commissural was shown to predict paired-associate learning performance, again reinforcing its role in learning and memory (Coad et al., 2020).

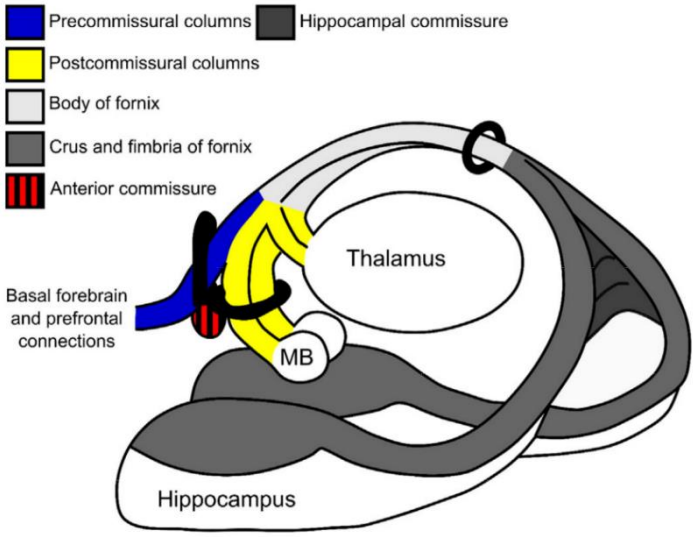

Figure 3.5. Schematic of the principal components of the fornix and main areas to which it connects. The black rings represent the placement of AND and NOT gates used for the tract reconstructions, as well as the seed ring around the body of the fornix. Abbreviations: MB mamillary bodies. Adapted from Christiansen et al. (2016).

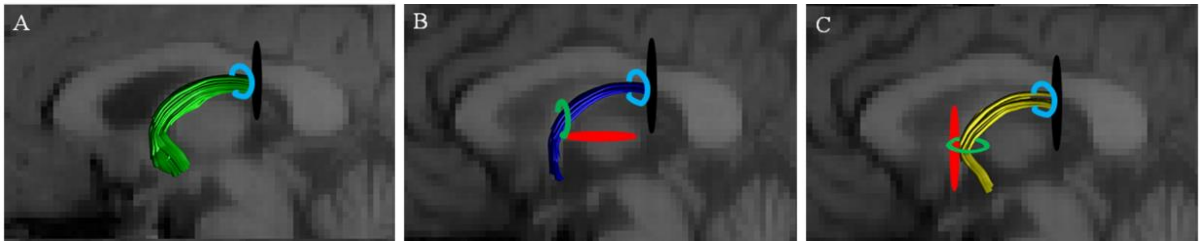

Figure 3.6. Depictions of the region of interest gates for the: (A) anterior body of the fornix, (B) the pre-commissural fornix and (C) the post-commissural fornix. NOT gates are in red, SEED gates are in light blue and AND gates are in light green. Adapted from Christiansen et al. (2016).

3.8 Developmental amnesia

Developmental amnesia (DA) provides strong supporting evidence for the role of the ATN and, most especially, the MB in mnemonic function. Developmental amnesia presents as a selective episodic memory disorder attributed to hypoxic-ischaemic events that occur in early life (Dzieciol et al. 2017). Previously, the resulting brain damage was largely thought to be restricted to the hippocampus due to its high oxygen requirements and susceptibility to glutamate-induced toxicity (Schmidt-Kastner & Freund, 1991). However, damage also occurs in both the thalamus and MB (Sie et al., 2000; Johkura & Naito, 2008; Kumar et al., 2008; Thayyil et al., 2010). Dzieciol et al. (2017) used MRI techniques to examine diencephalic damage in 18 patients with DA. All presented with episodic memory deficits but relatively spared semantic and recognition memory, compared to 18 controls. They found HPC atrophy as expected, but this was accompanied by severe damage to the MB and the anterior two-thirds of the thalamus. All patients with DA showed a decrease in MB size. Furthermore, in two thirds of those patients, the MB were atrophied to the extent that they were unidentifiable (see Figure 3.7). Additionally, the size of the anterior thalamus, which remained intact, was highly correlated with visual memory performance.

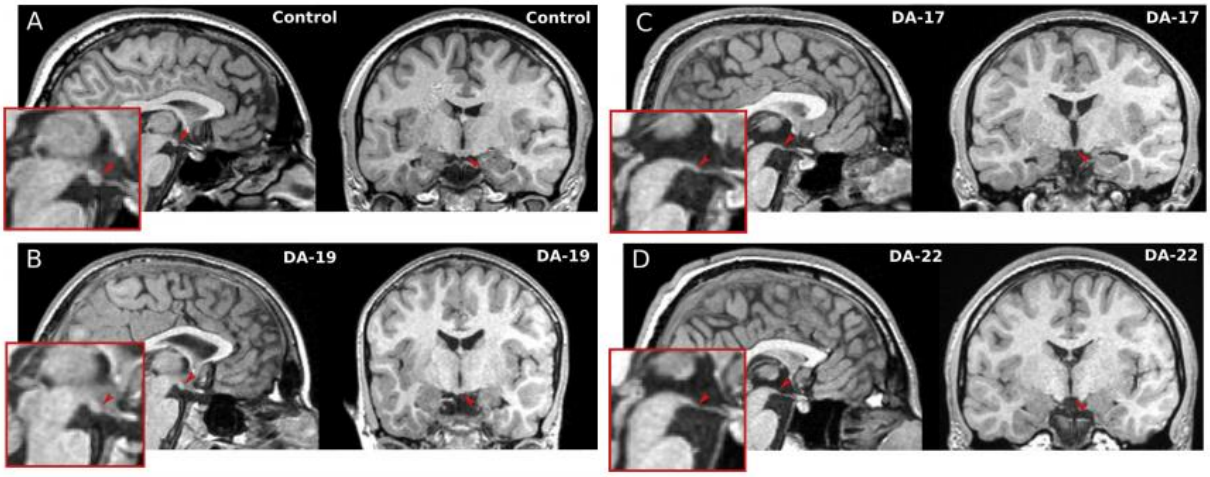

Figure 3.7. Mammillary bodies in a control participant (A) and in three DA patients (B-D).Red arrowheads show the location of the mammillary bodies. Note that in C and D the mammillary bodies are absent. Adapted from Dzieciol et al. (2017)

3.9 Evidence of aberrant oscillatory activity accompanying memory impairment in neurological disease

Neural oscillations are generated by the rhythmic activation and inactivation of neural assemblies, which cumulatively give rise to rhythmic activity in the brain (Fell & Axmacher, 2011; Buzsaki, 2011). The frequency of these oscillations can range from relatively slow oscillation periods of a couple of seconds, to faster activity wherein one oscillation may only take a few milliseconds (Colgin, 2011). Typically, oscillatory activity is divided into the bands specified in the introductory chapter as well as the following: beta (12-30Hz), and gamma (30-100Hz). Synchronisation (i.e. a high degree of phase correlation) of neural oscillatory activity across structures is referred to as coherence. Coherence is thought to be indicative of functional inter-structural interactions – it suggests that one structure is driving activity in another, although it cannot indicate which is in control. Interaction between structures is thought to be necessary for complex cognitive functions such as memory (Fell & Axmacher, 2011; Colgin, 2013). Moreover, slow-wave activity is capable of synchronising distally located neural ensembles and 'theta' rhythms have been consistently implicated in memory function (Colgin, 2013).

Aberrant neurological activity has been associated with various neurological conditions including AD, Parkinson's disease (PD) and schizophrenia, and may contribute to the impaired cognition associated with these conditions (Nimmrich et al., 2015; Senkowski & Gallinat, 2015; Basar et al., 2016; Palop & Mucke, 2016). Abnormal rhythmic activity has

been proposed to reflect a loss of neuromodulatory activity and interneuron depletion or dysfunction, both which contribute to the production of neural oscillations. The loss of these mechanisms impairs the recruitment of neuronal assemblies at frequencies necessary for complex cognitive functions such as memory (Nimmrich et al., 2015).

Abnormal increases in theta rhythmicity have been observed in patients with AD, PD and schizophrenia, as well as additional changes in other frequency bands (Herrmann & Demiralp, 2005; Nimmrich et al., 2015; Cozac et al., 2016; He et al., 2016; Chaturvedi et al. 2017). Pathology within the diencephalon has been implicated in all of the aforementioned conditions, suggesting a possible link between damage to the diencephalon and abnormalities in rhythmicity (Braak & Braak, 1991a, b; Delacourte et al., 1999; Young et al., 2000; Rub et al., 2002; Aggleton et al., 2016). For example, in patients with PD it was found that, at baseline, a global increase in theta activity in conjunction with reduced executive and working memory function could predict severe cognitive decline over three years (Cozac et al., 2016). Similarly, increased theta power in the temporal region has been shown to distinguish between patients with PD and healthy controls (Chaturvedi et al., 2017), whilst abnormalities in frontal theta have been associated with the presence of mild cognitive impairment (MCI) in PD patients (He et al., 2017). Similarly, patients with AD have changes in theta and delta power in the temporal and parietal lobes that have been associated with progression from MCI to AD over a 21 month period (Jelic et al., 2000). In schizophrenia, abnormal increases in the lower frequency bands, such as theta, have been reported within the default mode network (Burke et al., 2013). More recently, Barr et al. (2017) suggested that impaired theta-gamma coupling in the PFC of schizophrenic patients compared to controls may contribute to the working memory dysfunction observed in schizophrenia (see Figure 3.8 for a topoplot of theta-gamma coupling during the N-back working memory task).

Evidence of abnormal oscillatory activity occurring in neurological conditions in which pathology within the extended hippocampal system is also implicated suggests that pathology and electrophysiological aberrations may collectively contribute to the cognitive deficits that arise.

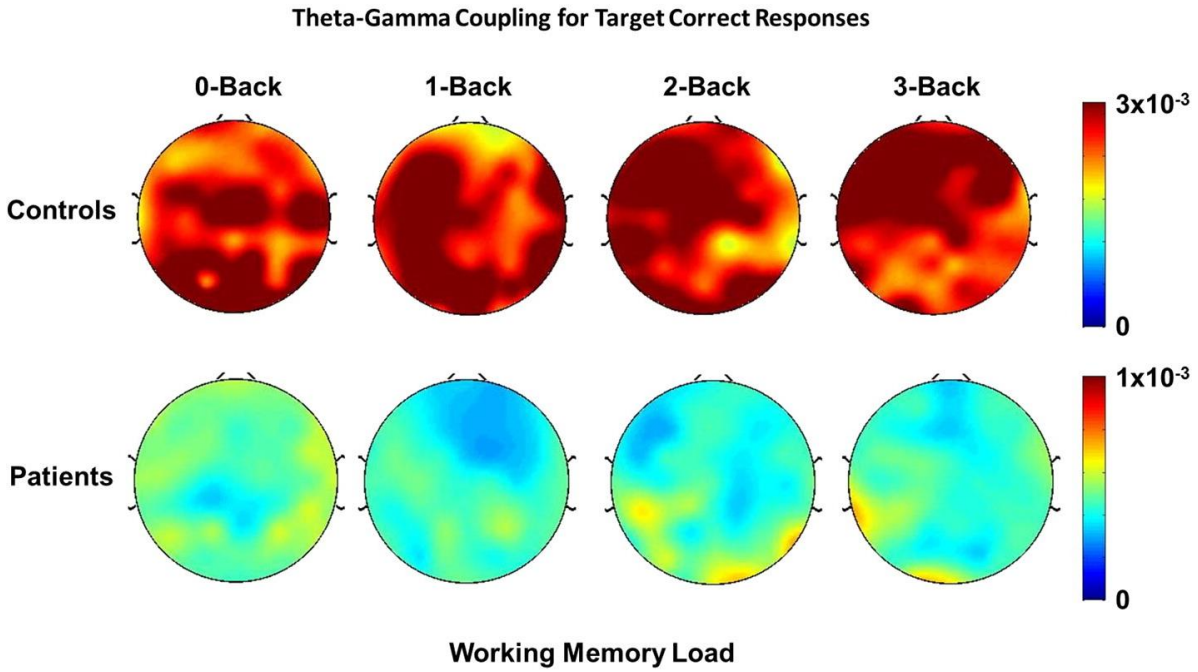

Figure 3.8. Topoplot of mean theta-gamma coupling for correct responses across the N-Back working memory task in patients with schizophrenia and healthy controls measured using the modulation index (MI). Hotter colours indicate a greater MI, cooler colours indicate lower MI. Adapted from Barr et al. (2017).

3.10 Conclusions

Damage to the MTT has been consistently associated with severe and persistent memory loss. The strongest evidence in support a critical role of the MTT in memory comes from studies of localised thalamic stroke. Evidence from cases of KS and neurodegeneration has also highlighted the importance of the ATN in the development of an amnestic syndrome. Conversely, clinical evidence for PCFx-related memory dysfunction is far less. However, this is largely attributed to its location and the difficulties in partitioning out its role from that of the fornix as a whole. Nonetheless, recent studies have suggested that the PCFx may play a crucial role in mediating episodic memory function.

Evidence from neurological conditions such as Alzheimer's and Parkinson's disease suggests that oscillatory dysfunction may contribute to the impaired cognitive function found in these conditions. Furthermore, pathology within the diencephalon is consistently found in such conditions and as such suggests a link between diencephalic damage and changes in rhythmicity.

Instances of diencephalic amnesia in humans have provided key evidence supporting the role of individual structures in memory function, as well as the concept of a wider

memory system. However, the additional brain injury to other sites that occurs in even the most localised cases precludes any definitive conclusions regarding each structure's precise contribution to memory. Animal lesion models are instrumental in addressing the issue of lesion specificity and allowing researchers to have precise control over outcome measures (ie. behavioural tasks). The lack of clinical cases involving localised PCFx damage highlights the need for animal lesion studies, as its location and connectivity suggest an important mnemonic capacity with a lack of clinical evidence. Therefore, the following chapter reviews the evidence from animal lesion studies, with a particular focus on the MTT and PCFx, highlighting the importance of assess the effect of both lesions on behaviour, as well as other key structures within the extended hippocampal network.

Chapter 4:
Animal Models of Diencephalic Amnesia

In this chapter, I review the experimental evidence from animal lesion studies that focused on subcortical neural structures in an "extended hippocampal memory system" (Aggleton & Brown, 1999). These lesions are intended to model brain injury that is associated with human diencephalic amnesia. The main focus in this chapter is the impact of lesions to the MTT and PCFx, as well as related work on ATN lesions.

As discussed in the previous chapter, the variability and diffuse nature of human cases of pathology can make it difficult to ascertain the key structure(s) underlying amnesia. Animal lesion models enable greater precision as they use targeted and relatively localised lesions. Animal models allow direct comparison between control and lesion animals and facilitate detailed post-mortem tissue examination. One major caveat associated with the use of animal models is that the paradigms used in animal behavioural testing may not reflect episodic memory function in humans. I will briefly discuss this issue in the next section. However, the primary aim of the chapter is to summarise the current rodent literature on lesions to the MTT or the descending limb of the PCFx in terms of their effects on memory. It is surprising that the literature on the effects of MTT lesions is limited. There is even less evidence on the impact of PCFx injury. The much larger literature on the effects of ATN lesions on memory tasks provides an important context for the effects of MTT and PCFx lesions. The review will then examine reports of "covert pathology" in structures distal to the site of thalamic damage, such as the retrosplenial cortex. This idea will be expanded upon in the following section, which will discuss the occurrence of electrophysiological rhythmicity within the extended hippocampal system and its role in memory. I will propose that memory deficits arising following damage to key components of the extended circuit may in part reflect aberrations in normal oscillatory interactions at between distal structures such as the prefrontal cortex, hippocampus and anterior thalamic nuclei. Abnormalities in rhythmic activity and covert pathology may reflect widespread diaschisis within the extended hippocampal network.

4.1 Examining episodic like memory in animals

An obstacle for researchers who examine memory in animals is how to capture something reflecting human episodic memory. In humans, episodic memory results in the conscious

recollection of a personal (first person) experience as well as its spatial and temporal context (Pause et al., 2013). This first-person subjectivity, which is a component of autonoetic consciousness, is regarded as a critical facet of episodic memory in humans (Tulving, 2002). It is impossible to model this aspect of human episodic memory. Nonetheless, the fundamental characteristics and neuroanatomy of overlapping aspects of memory function may be shared among all mammals. Over the past two decades, it has been shown that various animal species can demonstrate the behavioural manifestations of many aspects of episodic memory, such as remembering what occurred, where it occurred and when the items within the event occurred (Binder et al., 2015). The most widely cited example is the study by Clayton and Dickinson (1998). They showed that scrub jays were capable not only of searching for their favourite food (what), fresh wax worms, in a location they had previously cached them (where), but also that they could preferentially select the most recent locations in order to obtain the freshest worms (when). The most common animal used to model diencephalic amnesia in the literature is the rat, due to evidence supporting anatomical similarities as well as the ability to model a substantial amount of human behaviour (Cenci, Whishaw, & Schallert, 2002). In rats, analysis of neural systems relevant to episodic memory typically focusses on testing the 'where' component. Hence many tasks focus on spatial working memory in the T-maze, radial-arm maze and water-maze.

The T-maze relies on a rodent's natural tendency to alternate spatial responses. The T maze is an elevated or enclosed space in the form of a T, and testing is comprised of two parts, a 'sample' and a 'choice' phase. During the 'sample' run one arm of the T is blocked and thus directs the animal down the unblocked arm. During the 'choice' run, both arms are left open and the animal is rewarded if it chooses the arm not previously visited, reflecting memory of the first forced choice.

The water maze consists of a large circular pool filled with opaque water, with an escape platform hidden just beneath the surface. The water maze task relies on the rodent's motivation to get out of the water by locating the escape platform. Spatial memory in this task is shown by improved navigation to the platform location across successive trials. Furthermore, the water maze can be adapted to accommodate working memory testing.

The radial arm maze (RAM) has a central hub with eight or more arms extending off it in all directions. In the standard version of this task, all of the arms are baited only once. In this case, the optimal strategy is for the animal to visit each arm only once. If it does this, then it suggests that it has remembered which arms it has previously visited within that trial (i.e. spatial working memory). The RAM has been extensively used to assess both reference and working memory function in rodents. Moreover, the RAM task has been used to examine the effect of MTT and PCFx lesions, and was therefore selected as the primary task in this thesis. As electrophysiological activity during *correct* choices was of interest for the current thesis, a 12-arm RAM was selected. The increased number of arms provides the opportunity for impaired rats to make many correct choices, which can then be compared across lesion and control (Sham) groups.

4.2 MTT and PCFx lesion studies

Early MTT and PCFx lesion studies are difficult to interpret. They had poorly localised lesions with extensive damage to additional structures beyond the MTT and PCFx. For example, the electrolytic MTT lesions reported by Thomas and Gash (1985) were so extensive they likely included substantial damage to adjacent structures such as the nucleus reuniens and supramammillary area, both of which have been implicated in memory function (see Figure 4.1, panel A). Similarly, Tonkiss et al. (1990) severed the descending columns of the fornix, disconnecting the subicular inputs to the ATN and MB (see Figure X, panel B). However, the authors were unable to section the descending columns without also damaging the subicular outputs to the nucleus accumbens and stria terminalis. By contrast, more recent studies have made a concerted effort to create localised lesions to the MTT and PCFx using a radio frequency probe or small electrolytic lesion to generate more localised lesions (see Figure 4.1 for a comparison between earlier and more recent studies and respective damage to the MTT and PCFx; Winter et al., 2011; Vann, 2013). As a result, this section will focus on more recent studies from Vann, Aggleton & Honey (2003) onwards, summarised in Table 4.1.

A comparison between lesions of the MTT and PCFx would provide important insight into three different views on the key sites of pathology in diencephalic amnesia. One suggests that MB inputs from the HPC via the PCFx are important due to the role of the HPC in memory. This is supported by evidence implicating the PCFx in episodic memory function

in MCI and normal ageing (Christiansen et al., 2016). The second perspective emphasises the brainstem inputs from the tegmental nuclei of Gudden to the ATN via the MB and MTT and is supported by extensive evidence from thalamic stroke (Carlesimo et al., 2011). The third perspective is that the inputs from the hippocampus and the inputs from the VTNg may work in conjunction with one another, providing complementary inputs to the ATN and the wider circuit. Prior to Vann et al.'s 2011 study, the impact of localised PCFx lesions had received little attention. The lack of available PCFx literature reinforces the need for further investigation into the role of the PCFx in memory, as well as its relative contribution compared to the MTT.

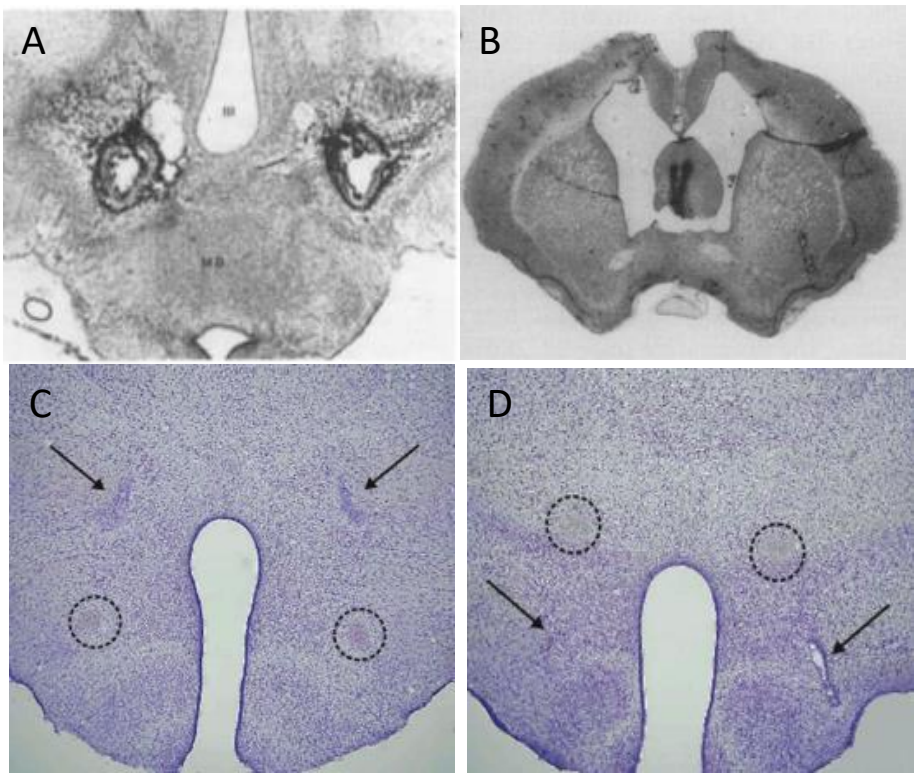

Figure 4.1. Photographs of an earlier MTT (A; adapted from Thomas & Gash, 1965) and descending PCFx (B; adapted from Tonkiss, Feldon & Rawlins, 1990) lesion showing extensive damage to adjacent structures, compared with a more recent study demonstrating more localised lesions to the MTT (C) and PCFx (D). Dotted circles show that the PCFx (C) and MTT (D) have been left intact. (C and D adapted from Vann, 2013).

MTT lesions typically result in spatial working memory deficits in the T-maze, although in some instances these impairments have been suggested to be only transient (Vann & Aggleton, 2003; Vann, 2013). For example, Vann (2013) found that rats with MTT lesions only showed sustained memory impairment in the T-maze when either: 1) intra-maze cues were removed by running the rats on different adjacent mazes between the

'sample' and 'choice' phase, or 2) when allocentric cues were additionally removed as well as intra-maze cues by further running rats in the dark on separate mazes. By contrast, more recent studies have found that rats with MTT lesions have persistent deficits in standard T-maze alternation (Frizzati et al., 2016; Dillingham et al., 2019), although this may reflect subtle differences in testing procedures. Similarly, PCFx lesions have been associated with mixed results in the T-maze. For example, the Tonkiss et al. (1990) study reported an initial transient impairment in PCFx rats during the standard T-maze task, but persistent deficits when a delay was implemented, or when proactive interference was increased. However, due to the extensive lesions, the results of this study are difficult to interpret. Nonetheless, a similar pattern of results was found by Vann et al. (2011), wherein PCFx lesions only transiently impaired performance on the standard T-maze task but showed sustained yet mild impairment when rats were forced to alternate continuously and when a rotation was also added. Conversely, Vann (2013) reported no observable deficits following PCFx lesions even when the task was run on adjacent mazes in the dark, thereby removing allocentric and intra-maze cues.

Unlike the T-maze, MTT lesions have been consistently associated with spatial working memory deficits in the 8-arm RAM (Vann & Aggleton, 2003; Vann, 2013; Nelson & Vann, 2014; Perry et al., 2018; Dillingham et al., 2019). Transection of the MTT has produced deficits in the 8-arm RAM comparable to neurotoxic MB lesions (Vann & Aggleton, 2003; Vann 2013). These MTT lesion-associated deficits are made worse by increasing task difficulty through introduction of a mid-trial delay and/ or rotation (Vann & Aggleton, 2003; Vann, 2013, Perry et al., 2018). A mid-trial rotation involves turning the RAM 45° mid-way through the task and moving the remaining rewards so that they remain in the same relative spatial location. Thus, intra- and extra-maze cues are placed in conflict to one another. Conversely, PCFx lesions produce negligible spatial working memory deficits in the standard 8-arm RAM task (Vann et al., 2011; Vann, 2013). Vann et al. (2011) found that rats with PCFx lesions demonstrated mildly impaired performance when the RAM was rotated mid-trial. By contrast, Vann (2013) failed to find any PCFx impairment even with mid-trial rotation.

MTT lesions also result in consistent working memory deficits in the water maze (see Table 4.1; Vann & Aggleton, 2003; Winter et al., 2011; Perry et al., 2018). In the standard, working memory version of the water maze, the location of the submerged platform

remains stable within a session of testing, but changes between sessions. Vann & Aggleton (2003) observed that rats with MTT lesions exhibited longer path length and escape latencies to the escape platform compared to sham rats. Conversely, Winter et al. (2011) found no significant working memory impairments following MTT lesions in the water maze. However, Winter et al. (2011) employed a simplified version of the water maze, in that rats only received two trials a day for four days and the location of the hidden platform relative to the edge of the pool was not changed. More recently, Perry et al. (2018) found that MTT lesions impaired spatial working memory in the standard task, as well as when extra-maze cues were minimised. Moreover, in the standard memory task i.e. with no delay or rotation, MTT lesions impaired performance to the same extent as lesions to the ATN (Perry et al., 2018). Unlike MTT lesions, PCFx lesions produce negligible memory deficits on the water maze task, although this has only been tested once: Vann et al. (2011) reported that whereas complete transection of the fornix impaired working memory on the delayed matching-to-place task in the water maze, lesions of the descending PCFx had negligible effects.

In addition to the tasks described above, MTT lesions have been tested on tasks not yet examined following PCFx lesions. For example, MTT lesions impair spontaneous object-in-place discriminations but not spontaneous object recognition (Nelson & Vann, 2014); and they impair contextual discrimination involving visual contexts, but not an equivalent discrimination where the context was thermal (Vann, Honey & Aggleton, 2003). MTT lesions impact recency judgements or temporal context (Nelson & Vann, 2017). Impaired recency memory is a common symptom of diencephalic amnesia, such as following Korsakoff's syndrome, and may be reflective of damage to the MB-ATN connection (Kopelman, 2014; Nelson & Vann, 2017). Nelson and Vann (2017) recently tested rats on multi-item recency memory. Rats were required to discriminate between pairs of objects that had previously been presented either in separate blocks of testing (between-block recency) or within the same continuous block (within-block recency), but at different time points. Rats with MTT lesions performed at chance level in both conditions. However, when MTT rats were required to differentiate between only two items that had been presented at different time points, recency memory was unaffected (Nelson & Vann, 2017). The authors suggested that the lesion effect only emerged when rats were required to make recency judgements

involving multiple objects, reflecting an impaired ability to cope with multiple items or events. Furthermore, the authors proposed that this may be indicative of a heightened sensitivity to proactive interference in lesion animals (Nelson & Vann, 2017).

4.3 Conclusions from MTT and PCFx lesion studies

Based on the MTT and PCFx lesion studies summarised in the previous section, a strong case can be made for the role of the MTT in memory, whereas the PCFx lesions appear to produce mild or no effects. Variable results have been found in both the T-maze and the RAM, with PCFx lesions suggested to only have a very mild effect and only when task difficulty is increased through the removal of intra- and extra-maze cues, or when proactive interference is increased (Vann et al., 2011; Vann, 2013). There appears to be little impact of lesions to the PCFx, although there are only two rat studies thus far. This limited evidence (Vann et al., 2011; Vann, 2013) warrants a further comparison of the behavioural effects of MTT and PCFx lesions given that these are two key fibre tracts in the extended hippocampal memory system (Aggleton & Brown, 1999; Aggleton et al., 2010; Aggleton, 2012). The next section provides a brief overview of the effect of ATN lesions on memory performance in order to reiterate the critical role of the ATN in memory function.

4.4 ATN lesion studies

A larger number of studies have examined the effects of ATN lesions in rats. A subset of these are summarised in Table 4.2. The value of rat ATN-lesion models is that in clinical studies implicating the ATN in cases of amnesia, the pathology is rarely localised to the ATN alone (Van der Werf et al., 2003). For example, while the effects of ATN neuronal loss is important in the alcoholic Korsakoff's syndrome, these patients also have neural injury to other brain regions (Harding et al., 2000; Kopelman, 1995). Animal lesion models allow researchers to circumvent the issue of diffuse damage.

Table 4.1. MTT and PCFx lesion behavioural studies

Task	MTT deficit	Authors	Comments	PCFx deficit	Authors	Comments
T-maze: delayed non-matching to sample	Yes	Dillingham et al. (2019); Frizzati et al. (2016); Vann (2013)*; Vann & Aggleton (2003); Thomas & Gash (1985)**; Field et al. (1978); Krieckhaus & Randall (1968)***	*MTT only impaired when intra- and extra-maze cues removed. **transient MTT deficit ***MTT not impaired	Mild deficit	Vann (2013)*; Vann et al. (2011)**; Tonkiss et al. (1990).	* No impairment ** Mild impairment
Water maze: Reference memory	No	Perry et al. (2018); Winter et al. (2011)*	* Mild transient impairment	-	-	-
Water maze: spatial working memory	Yes	Perry et al. (2018); Winter et al. (2011)*; Vann & Aggleton (2003)	*MTT not impaired	No	Vann et al. (2011)	
Radial arm maze: standard task	Yes	Dillingham et al. (2019); Perry et al. (2018); Vann (2013); Vann & Aggleton (2003)		No	Vann (2013); Vann et al. (2011)	
Radial arm maze: mid-trial delay and/ or rotation	Yes	Perry et al. (2018); Nelson & Vann (2014)*; Vann (2013); Vann & Aggleton (2003)	* MTT performance worse than standard task	Yes No	Vann et al. (2011)* Vann (2013)	* Mild impairment
Object recognition	No	Nelson & Vann (2017)*; Nelson & Vann (2014)	* Bow-tie maze	-	-	-
Object recency	Yes	Nelson & Vann (2017)*	*MTT deficit only found with multi-item recency	-	-	-
Context discrimination	Yes	Vann, Aggleton & Honey (2003)	*Context discrimination only impaired with spatial, but not thermal, cues	-	-	-

Abbreviations: MTT=mammillothalamic tract; PCFx= post-commissural fornix

The ATN has been strongly implicated in memory through the use of the memory tasks previously described. ATN lesions have been repeatedly shown to cause severe and pervasive impairments in the standard T-maze task (Aggleton et al., 1995; 1996; 2009; Dumont et al., 2014), at least in rats housed in standard conditions (Loukavenko et al., 2007). In these studies, rats typically demonstrate chance level performance at the beginning of testing and, although improvement may be observed, fail to reach Sham levels of accuracy, even when they have been trained on the task prior to surgery (Warburton et al. 1999). Moreover, ATN-associated working memory deficits are exacerbated when egocentric strategies are prevented through the use of a T-maze embedded within a cross maze as 'sample' and 'choice' runs can be started from opposing ends of the maze (Loukavenko et al., 2007, 2016; Aggleton & Nelson, 2015).

ATN lesions also produce severe spatial working memory deficits in the RAM (Mitchell & Dalrymple-Alford, 2006; Sziklas & Petrides, 2007; Perry et al., 2018). ATN lesions also produce deficits in alternative versions to the standard RAM, such as delayed non-matching to sample (Mair et al., 2003) or with extra-maze cues removed (Byatt & Dalrymple-Alford, 1996).

Unsurprisingly, ATN lesions impair spatial working memory performance in the water maze, in proportion to the extent of ATN damage (Van Groen et al., 2002); and impair reference memory in the water maze to a similar level to hippocampal lesions (Warburton & Aggleton, 1997; Warburton et al., 1999; Wolff et al., 2008a; 2008b; Perry et al., 2018).

The ATN lesion studies already mentioned in this section and those listed in Table 4.2 suggest a consistent and crucial role of the ATN in working memory function. Further, damage to the ATN may cause greater memory impairments than lesions to the MB or fornix (Aggleton et al., 1995; Aggleton et al., 2009).

The ATN has also been shown to work in conjunction with the HPC, reiterating the idea of a distributed neural network involving the diencephalon and temporal lobe. In a study by Warburton et al. (2001) rats were given unilateral lesions of the HPC and ATN either in the same side (HPC-ATN ipsi) or contralateral side (HPC-ATN contra). The authors found that spatial memory function in the T-maze, RAM and water maze was impaired to a greater extent in the HPC-ATN contra group compared to those animals where lesions were

located in the same hemisphere. A study by Henry et al. (2004) demonstrated that unilateral lesions of the HPC and ATN in opposite hemispheres also impaired working memory function. These findings suggest that the two structures may work in an inter-dependent fashion during spatial tasks and that spatial memory relies on both the ATN and HPC within an integrated neural network.

The next section examines the evidence of functional changes occurring in distal sites within the extended hippocampal system, following lesions to the ATN and MTT. Most of these studies have found hypoactivation of immediate early genes in structures within the circuit, especially in the retrosplenial cortex. These 'functional lesions' have been proposed to contribute to the lesion-associated deficits that arise and will be discussed in the following section. PCFx lesions do not appear to effect immediate early expression, however at present this has only been examined in one study (Vann, 2013).

Table 4.2. ATN lesion behavioural studies

Task	ATN deficit	Authors	Comments
T-maze: delayed non-matching to sample	Yes	Loukavenko et al. (2016); Ulrich et al. (2014); Harland et al. (2014); Dumont et al. (2013); Aggleton et al. (2009)	
T-maze spatial forced alternation	Yes	Warburton & Aggleton (1999); Warburton et al. (1999); Aggleton et al. (1996); Aggleton et al. (1995).	
Water maze: reference memory	Yes	Perry et al. (2018); Wolff et al. (2008a*; 2008b); Warburton & Aggleton, 1998; Warburton et al. (1999)	* ATN impaired for both fixed and variable release points
Water maze: spatial working memory	Yes	Perry et al. (2018)*; Van Groen et al. (2002)	* ATN more impaired severely impaired when extra-maze cues were reduced
Cross-maze: spatial working memory	Yes	Loukavenko et al. (2007)*	* ATN severely impaired 14, 75 and 120 days post-surgery
Radial arm maze: standard working memory task	Yes	Perry et al. (2018); Harland et al. (2014); Sziklas & Petrides (2007); Mitchell & Dalrymple-Alford (2006); Byatt & Dalrymple-Alford (1996)*; Aggleton et al. (1996)	* Lesioned subregions of the ATN (AV and AM), both impaired performance
Radial arm maze: mid trial delay and/ or rotation	Yes	Perry et al. (2018)	
Object recognition	No	Dumont & Aggleton (2013); Warburton & Aggleton (1999); Aggleton et al. (1995)	
Object recency	Yes	Dumont & Aggleton (2013)*	*ATN only impaired on within- but not between-block recency
Geometric learning	Yes	Aggleton et al. (2009)	

Abbreviations: AM= anteromedial nuclei; AV= anteroventral nuclei; ATN= anterior thalamic nuclei; ENR= environmental enrichment; RAM= radial arm maze

4.5 Distal 'covert pathology' following diencephalic damage

Lesions to the ATN produce 'covert pathology' in distally located structures within the extended hippocampal system. Covert pathology refers to when an area appears normal by standard histological criteria, but nonetheless shows evidence of a functional lesion (Aggleton, 2008). Immediate early genes are genes whose transcription is activated rapidly and transiently within minutes of cellular activation. They can therefore act as indicators of neuronal activation. There are other markers of covert pathology, such as CREB (a cAMP-associated transcription factor; Dumont et al., 2012) and cytochrome oxidase or COX (a cellular marker of metabolism and enzyme associated with the electron transport chain in respiration; Mendez-Lopez et al., 2013). The RSC has been shown to be particularly sensitive to lesions to the extended hippocampal circuit. Lesions to the ATN consistently produce a striking reduction in IEG expression in the RSC. The RSC is densely connected (both directly and indirectly) with the ATN and HPC (Aggleton, 2008).

As previously mentioned, IEGs are typically transcription factors that are rapidly encoded following cellular activation (Davis et al., 2003). Although activation of IEGs has not been directly linked to behavioural changes, increases in RNA levels of IEGs Zif268 (also known as EGR-1), c-Fos and Arc have been reported in the dorsal HPC following training in the water maze (Guzowski et al., 2001). Furthermore, the presence of c-Fos and CREB have been associated with improved spatial memory performance (Czajkowski et al., 2014). Some IEGs may play an important role in hippocampal plasticity and the consolidation of long-term memory. For example, Zif268 expression in mice enhances the capacity to form long-term memory of the spatial location of objects. Overexpression of Zif268 also enhanced long-term potentiation in the DG of the hippocampus (Penke et al., 2014). These findings from Penke et al. (2014) suggest that Zif268 may contribute to learning and memory processes.

Table 4.3 provides a summary of studies that have assessed the levels of IEG activation in rats following lesions to the MTT, PCFx and ATN, most of which examine the effects on IEGs c-Fos and Zif268. MTT lesions have been associated with reduced IEG expression in subregions of the RSC, hippocampal areas CA1, CA3 and DG, the prelimbic cortex and the para- and post-subiculum, suggesting widespread and systemic hypoactivity following MTT damage (Vann & Albasser, 2009; Vann, 2013; Perry et al., 2018). As the MTT

does not directly innervate these structures, it suggests that these functional changes are not a disconnection effect. ATN lesions also reduce marked reductions in IEG activation in structures such as the HPC, RSC and prefrontal cortex. Of note is that whilst MTT and ATN lesions consistently reduce IEG, PCFx lesions have been associated with negligible IEG effects (Vann & Albasser, 2009; Vann, 2013; Frizzati et al., 2016; Perry et al., 2018). However, the impact of PCFx lesions on IEG activation has only been explored in one study, which reported a negligible effect of PCFx lesions on c-Fos activity (Vann, 2013).

Expression of biomarkers such as CREB and phosphorylated CREB (pCREB) in the RSC and HPC have also been examined following lesions of the ATN (Dupire et al., 2013; Dumont et al., 2012). pCreb has been of particular interest due to its role in neural plasticity and IEG regulation. For example, Dumont et al. (2012) observed that ATN lesions reduced pCREB expression in the Rgb. By contrast, Dupire et al. (2013) found a striking reduction in pCREB in the amygdala, area CA1 and Rgb. However, these differences in IEG levels may reflect differences in the behavioural tasks used between studies to drive IEG activation: a context fear conditioning task was used in the study by Dupire et al. (2013); but a novel object task was used by Dumont et al. (2012).

Harland et al. (2014) reported that ATN lesions resulted in pronounced reductions in dendritic spine densities in hippocampal area CA1 and retrosplenial Rgb neurons (see Figure 4.2). Changes in dendritic spine density are indicative of alterations in neural plasticity. The reductions noted in area CA1 are of particular interest as CA1 is one of the primary sources of HPC outputs, but has no direct connections with the ATN. Therefore the ATN lesion-associated loss of CA1 spine densities reflects a systemic change in function rather than effects that might be expected following a loss of direct inputs.

Figure 4.2. Example photographs of Golgi-stained dendritic segments from a sham rat (left) and ATN-lesion rat (right) showing the relative loss of dendritic spine density following ATN lesions. Adapted from Harland et al. (2014).

Levels of neural activity markers are typically increased prior to perfusion by introducing animals to novel stimuli. This can be achieved in a number of ways including, but not limited to, using a new cage, testing or holding room, novel test cues, or a combination of these (Jenkins et al., 2002; Jenkins, 2004; Poirier et al., 2008; Poirier & Aggleton, 2009; Dumont et al., 2012). One task that is commonly used prior to perfusion involves forced runs in a RAM (Vann & Albasser, 2009; Dumont et al., 2012; Frizzati et al., 2016; Perry et al., 2018). This task enables the experimenter to control which and how many arms are accessible and therefore can match animals for motor responses and number of rewards received (Frizzati et al., 2016). A further consideration is the amount of time between the animal completing the task and perfusion. The majority of studies examining IEG activation typically place the animal in a dark quiet room for 90 minutes prior to perfusion as IEG protein accumulation peaks 90 minutes after exposure to a stimulus (Chadhuri et al., 2000). Additionally, although only examined following ATN lesions, shorter intervals between lesion surgery and perfusion have been shown to alter IEG expression (Poirier & Aggleton, 2009). For example, IEG changes were restricted to the superficial layers of the Rgb and Rga retrosplenial regions following a short interval. However, as the interval between surgery and perfusion increased, IEG activation extended into the deep laminae of the Rgb and Rga region, as well as involving the Rdg (Jenkins et al., 2004; Poirier & Aggleton, 2009).

Table 4.3. Summary of studies examining biomarkers of neural activation following MTT, PCFx and ATN lesions

Year	Authors	Lesion type	Behavioural deficits	Induction of neural marker	Neural marker and regions analysed	Outcome relative to neural marker
2018	Perry et al.	MTT ATN	ATN lesions impaired reference memory. ATN and MTT lesions both impaired spatial working memory, ATN to a greater extent.	RAM task with mid-trial delay and rotation, rats allowed a total of only 8 choices, with novel cues, followed by 90mins in a dark room prior to perfusion,	Zif268 in the RSC, CA1, DG, anterior cingulate cortex and posterior subiculum.	MTT lesions reduced Zif268 in sup. Rgb and CA1. ATN lesions reduced zif 268 in sup. and deep Rgb, ant sup Rdg, sup. Rga and CA1.
2016	Frizzati et al.,	MTT	MTT lesions severely impaired T-maze alternation.	Forced runs in an 8-arm RAM in a novel room with novel cues.	Cohort 1: Zif268 Cohort 2: cytochrome oxidase DG, CA1, CA3 and RSC	MTT lesions reduced zi268 in the sup. and deep Rgb and Rdg. MTT lesions reduced cytochrome oxidase in the sup Rdg, and the deep Rga and Rgb.
2013	Vann	MTT PCFx VTNg	MTT but not PCFx lesions impaired T-maze alternation when intra-maze cues were minimised and impaired spatial working memory in the RAM.	Forced runs in an 8-arm RAM in a novel room with novel cues, followed by 90mins in a dark room prior to perfusion.	c-Fos was examined in the RSC, HPC, IL, Prl, somatosensory cortex, SuM, lateral and medial septum.	MTT lesions reduced c-Fos counts in the posterior RSC, HPC and Prl. PCFx lesions did not reduce c-Fos counts.

2009	Vann & Albasser	MTT	No behavioural difference- forced runs	Forced runs in an 8-arm RAM in a novel room with novel cues, followed by 90mins in a dark room prior to perfusion.	c-Fos was examined in the RSC, DG, CA3, CA1, HPC, entorhinal cortices, perirhinal cortices, postrhinal cortex, Prl, IL, ACC, subiculum, para-, pre- and post-subiculum, as well as the somatosensory, auditory and visual cortices.	MTT lesions reduced c-Fos counts in the anterior and posterior sup. Rdg, Rgb and Rga, the deep Rdg and Rgb, Prl, DG, CA3, CA1, dHPC and the para- and post-subiculum.
2016	Loukavenko et al.	ATN	ATN lesions severely impaired T-maze alternation.	T-maze with 90mins in a dark room after the third trial	c-Fos examined in the Prl, IL, ACC, dHPC, RSC, somatosensory and motor cortex.	ATN lesions reduced c-Fos counts in the sup and deep Rgb.
2013	Mendez-Lopez et al.	ATN	ATN lesions severely impaired spatial discrimination in the RAM.	Delay of 90mins between final testing session in the RAM and perfusion.	Cytochrome oxidase examined in the RSC, DG, CA3, CA1, subiculum, Prl, IL, ACC, Pt, Entorhinal cortex and CPu.	ATN lesions reduced cytochrome oxidase activity in the sup Rgb and sup Cg1 region of the ACC.
2012	Dumont et al.	1) Unilateral (split into novel and familiar) and 2) bilateral ATN	1) only novel group showed improved recency discrimination 2) forced choices in the RAM so no group difference	1) Novel and familiar object exploration. 2) Forced runs in a RAM in a novel room with novel cues.	1) Zif268 was examined in the Prl, IL, PRC, HPC, RSC, dorsal subiculum and post-subiculum. 2) Zif268, CREB, pCREB and GAP-43 were examined in the same regions.	1) Lesions reduced Zif268 counts in the Rgb and post-subiculum. 2) Lesions reduced Zif268 counts in the Rgb and post-subiculum and pCREB in the Rgb.
2008	Poirier et al.	Unilateral ATN	N/A	Novel room and cage with visual stimuli	c-Fos and multiple other transcription factors examined in the Rgb region.	Rdeuction in c-Fos and transcription factors in the Rgb in the lesioned hemisphere relative to the intact hemisphere.

2004	Jenkins et al.	ATN	ATN lesions impaired spatial alternation in the T-maze and spatial working reference memory in the RAM	Spatial working memory task in the RAM in a novel room, followed by 90mins in a dark room.	c-Fos examined in 24 regions from within the HPC, subicular and limbic cortices.	ATN lesions reduced c-Fos in the Prl, ACC, RSC, dorsal and ventral HPC.

Abbreviations: ACC=anterior cingulate cortex; ATN= anterior thalamic nuclei; CA1=area CA1 of the hippocampus; CA3= area CA3 of the hippocampus; CREB= c-AMP response element binding protein; deep= deep layer; DG= dentate gyrus; dHPC= dorsal hippocampus; GAP-43= growth associated protein 43; HPC= hippocampus; IL= infralimbic cortex; pCREB= phosphorylated c-AMP response element binding protein; Prl= prelimbic cortex; RAM= radial arm maze; Rdg= dysgranular retrosplenial cortex; Rga= granular a retrosplenial cortex; Rgb= granular b retrosplenial cortex; sup= superficial layer.

4.6 Oscillatory activity changes are associated with behavioural performance

Whilst IEG expression is a useful tool for examining the systemic effects of localised diencephalic lesions, and may be indicative of functional lesions in certain structures, such findings may be complemented by exploring the 'online' impact of localised MTT and PCFx lesions. For example, recording local field potentials (LFPs) in key structures within the circuit during behavioural performance may reinforce the evidence provided by IEG activity. LFP activity within (measured by local power) and between (measured by coherence) structures may shed light on functional changes occurring following localised lesions, as well as following intervention.

Due to the well-documented role of theta activity in memory, electrophysiology in the current thesis will focus on the 'theta' frequency, although the exact definition of theta frequency varies between humans and rodents and across studies (see general introduction chapter). Slow-wave theta activity is capable of synchronising distally located neural ensembles (Colgin, 2013). Coherence, or phase correlation, is used as a measure of synchrony across structures and an absence of theta rhythmicity can be indicative of dysfunction (Fell & Axmacher, 2011; Colgin, 2013).

Human evidence typically uses word recall/ recognition paradigms paired with recording electrodes placed on the scalp when investigating the electrophysiological correlates of memory. Such studies have consistently reported that in healthy controls increased cortical theta phase synchronisation was predictive of successful memory function (Fell et al., 2003). Depth recording in epileptic patients showed that increased cortico-hippocampal theta coupling was associated with improved memory performance (Weiss et al., 2000; Weiss & Rappelsberger, 2000; Mölle et al., 2002; Fell et al., 2003; Mormann et al., 2005; Colgin, 2013). However, different definitions of theta were used across studies, i.e. theta was defined as 5-7Hz by Weiss et al. (2000) and Weiss and Rappelsberger (2002), whilst Mölle et al. (2002) and Mormann et al. (2015) defined theta as 4-8Hz. Sweeney-Reed et al. (2014) demonstrated that neocortical-ATN theta/alpha phase synchrony was able to predict memory recall of complex photographic scenes. Similarly, Sweeney-Reed et al. (2015) showed that ATN theta phase alignment with stimulus onset increased during successful compared with unsuccessful encoding. These findings demonstrate the importance of theta activity in structures such as the ATN, HPC and PFC in memory function.

Animal studies have reinforced the critical role of theta in learning and memory. The animal literature has typically focussed upon cortical and hippocampal theta oscillatory activity and its relation to memory performance. For example, McNaughton et al. (2006) showed that abolishing hippocampal theta (with a septal block) resulted in severe spatial memory impairments in the water maze. Upon reinstatement of hippocampal theta, memory performance improved towards baseline levels. Reinstatement of theta activity was achieved via a bypass circuit triggered by recording from the supramammillary nucleus (McNaughton et al., 2006). There is also considerable evidence suggesting that coupling between the HPC and PFC is critical for spatial memory in rodents, as increased synchrony of hippocampal theta rhythm and phasic firing of mPFC neurons have been consistently reported during key decision points during working memory tasks (Jones & Wilson, 2005; Hyman et al., 2010; O'Neill et al., 2013). For example, in a delayed non-matching to place task, Hyman et al. (2010) reported that 46% of theta-modulated neurons in the mPFC become phase-locked to hippocampal theta rhythmicity during correct, but not incorrect, trials. Phase-locking of mPFC neural spiking with CA1 theta rhythm has been demonstrated during correct object-place association (Kim et al., 2011). Furthermore, the authors reported high CA1-PFC theta coherence during the decision point within this task, suggesting that mPFC-CA1 theta coherence may play a crucial role during specific epochs involving high cognitive demand (Kim et al., 2011). In line with this, the current thesis will focus on the electrophysiological activity occurring during 'choice points', examining changes in power spectral density (PSD) and coherence.

4.7 Anatomy and phenomenology of theta activity

The medial septum/vertical limb of the diagonal band of Broca (MS/vDBB) possess rhythmically discharging cells that fire synchronously with theta and thus have been strongly implicated as a likely source of hippocampal theta (Vertes et al., 2004). Additionally, MS/vDBB stimulation with pulses at theta frequency has been shown to drive hippocampal theta (Vertes et al., 2004). By contrast, disruption or lesions (both permanent and temporary) of the MS/vDBB eliminate theta activity in the HPC and parahippocampal regions (Vertes et al., 2004). Medial septum inactivation not only diminishes theta activity in the HPC and MB but also impairs memory performance (Kirk et al., 1996; McNaughton et al., 2006). However, there is also evidence suggesting that the supramammillary nucleus

(SuM) may modulate HPC theta activity (Kirk & McNaughton, 1991) and this was further supported by MS/vDBB retrograde tracing studies which showed a direct projection from the SuM and terminating in the MS/vDBB (Vertes & McKenna, 2000). Previous investigation of the SuM had shown that SuM cells fire rhythmically at theta rhythm and that inactivation of SuM activity disrupts medial septum rhythmicity and suppresses HPC theta in anesthetised rats (Kirk & McNaughton, 1993; Thinschimdt et al., 1995). In awake rats however, suppression of SuM theta activity via chemical inhibition or lesion only reduces theta frequency rather than eliminating oscillatory activity (McNaughton et al., 1995; Sharp & Koester, 2008). These findings have led to the proposal that SuM activity codes the frequency of theta rhythm, whilst the medial septum determines the amplitude of the theta wave form (Kirk & McNaughton, 1993; Vertes et al., 2004).

The historical focus of theta propagation has been largely focused on the control of HPC theta. However, theta oscillatory activity is ubiquitous throughout the extended hippocampal system (see Chapter 2). This reinforces the concept of theta as a coordinating rhythm underlying memory function (Kirk & Mackay, 2003; Ketz et al., 2015). For example, as discussed in Chapter 2, cells in the ATN and medial MB exhibit theta bursting activity in synchrony with HPC theta, suggesting a common rhythmic input (Kocsis & Vertes, 1994). However, theta activity in the ATN and MB must be driven by afferent inputs as the ATN and MB, unlike the HPC and entorhinal cortex, do not contain interneurons and thus are incapable of independent generation of theta, at least in the rat (Wang et al., 1999; Dillingham et al., 2015). The most likely source of ATN theta activity is either the direct HPC input via the post-commissural fornix or the MB input via the MTT. MB theta activity is also likely driven by either the HPC input via the descending limb of the post-commissural fornix, or from the brainstem VTg. Firing of VTg cells at theta precedes HPC theta, and the presence of VTg interneurons suggests that theta may be independently generated by the VTg (Bassant & Poindessous-Jazat, 2001). Currently, control of hippocampal theta appears to rely on multiple modulatory structures, with the overarching coordinating input yet to be determined (Buzsaki, 2002).

4.8 Evidence of aberrant rhythmic activity in animal models

As was discussed in chapter three, human evidence suggests that aberrant oscillatory activity may contribute to the cognitive deficits observed in neurological conditions. Similar

rhythmic abnormalities have been observed in animal models of neurodegenerative diseases. AD rodent models, which typically focus on amyloid beta (Aβ) and tau protein pathology, have been instrumental in expanding our understanding of AD progression and symptomology. Severe memory impairments and aberrant oscillatory activity have been reported in studies using mouse models of AD. In line with clinical findings, Scott et al. (2012) reported decreased theta power in transgenic mice (APP/PS1) over-producing Aβ. Moreover, the observed decreases in hippocampal theta activity correlated with amyloid plaque formation. Jyoti et al. (2010) reported an abnormal increase in delta and theta power at pre-plaque stages in a different mouse model that also overexpresses Aβ. Another study reported substantial decreases in theta-gamma cross-frequency coupling in the subiculum prior to any amyloid beta pathology in mice with Aβ pathology (Goutagny et al., 2013). Evidence from animal models of conditions such as AD suggests that oscillatory dysfunction, particularly within the theta band, may be of critical importance in the cognitive deficits associated with neurological disease.

A recent study using MTT lesions as a model for diencephalic amnesia in rats reported lesion-induced alterations in oscillatory activity in the HPC and RSC (Dillingham et al., 2019). MTT-lesions were shown to reduce peak 'theta' frequency (6-12Hz) in the HPC and RSC relative to control rats during locomotion in a bow-tie maze. Peak 'theta' frequency was also reduced by MTT lesions in the HPC, but increased in the RSC, during paradoxical rapid eye movement sleep (Dillingham et al., 2019). Rats with MTT lesions also exhibited excessive HPC-RSC coherence during both locomotion and paradoxical rapid eye movement sleep compared to control animals. These findings suggest that localised damage to the MTT may induce oscillatory dysfunction within the wider memory circuit (Dillingham et al., 2019).

4.9 Conclusions

Animal lesion studies have demonstrated a critical role for both the MTT and ATN in episodic memory function (Sziklas & Pertrides, 2007; Vann, 2013; Perry et al., 2018; Dillingham et al., 2019), whilst localised lesions of the PCFx have been associated with negligible behavioural effects (Vann et al., 2011; Vann, 2013). Damage to the ATN and MTT have been associated with covert pathology in regions distal to the site of pathology (Dumont et al., 2012; Loukavenko et al., 2015; Vann, 2013; Perry et al., 2018). Another means of assessing the systemic impact of lesions is through examining rhythmic activity

within and between key structures within the extended hippocampal system. For example, Dillingham et al. (2019) recently demonstrated that localised MTT lesions alters theta power and coherence within and between the HPC and RSC.

The current thesis will compare the impact of PCFx and MTT lesions on spatial working memory function, examine the systemic effect of damage, and explore whether recovery of function is possible. In order to assess the impact of lesions and subsequent intervention on the extended memory system, IEG activation and LFP activity in key structures will be explored as a measure of functional change. The background and impetus for our novel intervention is provided in the following chapter on optogenetics.

Chapter 5:
Optogenetics

Although diencephalic damage, either following human cases of pathology or localised lesions in rodent models, may be permanent, the associated memory impairments may not be. Human studies have revealed that approximately 75% of those with alcoholic Korsakoff's syndrome may show recovery of memory function following abstinence despite the permanent pathology in the ATN and MB (Kopelman et al., 2009). In rodents, exposure to enriched environments following permanent damage to the ATN can also improve memory (Loukavenko et al., 2007, 2016; Wolff et al., 2008; Harland et al., 2014). These instances of recovery suggest that there may be a degree of compensation occurring elsewhere in the circuit, and therefore the extended hippocampal circuit may be amenable to intervention. As has already been discussed in previous chapters, aberrations in rhythmic activity may contribute to the memory impairments observed in neurological conditions (Nimmrich et al., 2015; Cozac et al., 2016; Chaturvedi et al., 2017). It may be that improved oscillatory activity within the extended memory circuit is able to compensate for the loss of function attributed to permanent structural damage. Indeed, it has already been shown that reinstatement of hippocampal theta rhythmicity, following septal blockade, can significantly improve memory function (McNaughton et al., 2006). Therefore, a possible intervention worth investigating is the selective stimulation of a nodal structure within the circuit in an attempt to improve circuit-wide rhythmicity. The ATN is indeed a key nodal structure due to its anatomical connections with the HPC, PFC, RSC and MB (Aggleton et al., 2010; Dalrymple-Alford et al., 2015). Evidence from Korsakoff's syndrome and ATN lesions in animal models has shown that the ATN is critically involved in memory (Harding et al., 2000; Aggleton & Nelson, 2015). Electrical stimulation of the ATN can improve cognitive performance in both humans and rats (Hamani et al., 2010; Oh et al., 2012). However there are particular limitations associated with the use of electrical stimulation, such as lack of cellular specificity and unnatural stimulation parameters, suggesting that optogenetic techniques may be a superior means of intervention (Wells et al., 2005). Therefore the following chapter makes a case for the use of optogenetic stimulation of the ATN with the potential to gain recovery of function following permanent damage to a component of the extended hippocampal system. This chapter has been adapted from Barnett et al. (2018): *Optogenetic stimulation: Understanding memory and treating deficits.*

Optogenetic stimulation has revolutionized biomedical research on brain function. The term describes light activated modulation (increases or decreases) in cell activity. This chapter begins by briefly explaining optogenetics, the advantages it offers over other stimulation methods, the advantages and disadvantages of methods used to transduce neurons, as well as covering the range of opsins available. Optogenetic techniques have been used to dissect the components of particular circuits, such as the role of specific structures within the extended hippocampal system in memory function (Shipton et al., 2014; Spellman et al., 2015) and exploring how optogenetic stimulation may be used to treat memory deficits in animal models (Roy et al., 2016; Yang et al., 2016). As previously stated, this chapter will lastly present a case for targeting the ATN to improve spatial working memory function in rats following localised damage. Optogenetics is a powerful tool for exploring how defined neural ensembles or networks contribute to complex behavioural processes.

5.1 Development of optogenetics

Optogenetics encompasses knowledge from the fields of optics, microbial biology, virology, biochemistry, and neuroscience (see Kim, Adhikari, & Deisseroth, 2017 for the history of optogenetics). Transmembrane proteins, called rhodopsins, become permeable to ions when exposed to specific wavelengths of light. They were first reported in 1971 (Oesterhelt & Stoeckenius, 1971). Rhodopsin-type proteins are found in algae and archaebacterial, and they have now been isolated, adapted, and refined so that they can be expressed in mammalian tissue (Kim et al., 2017). Researchers selectively transduce a subpopulation of neurons to express these light-sensitive transmembrane proteins. The activity of these transduced neurons is then modulated through light-induced cellular hyperpolarisation or depolarization (Fenno, Yizhar, & Deisseroth, 2011).

5.2 Optogenetics: Genetic manipulation of cells and study design considerations

Optogenetics is governed by three core features: (1) microbial opsins. A gene family consisting of different genes that code for a unique proteins to permit a change in the electrical status of a neuron in response to exposure to a particular wavelength of light; (2) the ability to deliver the appropriate opsin genes to specific cells within a neural population

of interest; and (3) delivery of a sufficiently strong and precisely timed light to the correct neural location.

The specificity afforded by optogenetics allows researchers to target a particular subset of neurons in a brain region and selectively influence neural pathways. Neurons are genetically transduced via local infusion of a recombinant replication-defective viral vector and/or through manipulation of the genome to produce transgenic animals (Fenno et al., 2011; Yizhar, Fenno, Davidson, Mogri, & Deisseroth, 2011). A less common method of transduction is through electroporation, which is typically used in embryonic and perinatal rodents to selectively transduce neurons in a particular brain location based on the developmental trajectory (Gu et al., 2012; Taniguchi, Young-Pearse, Sawa, & Kamiya, 2012). Electroporation involves permeating membranes by using electric pulses to induce an electrophoretic influx of selected DNA into the target cell (Dezawa et al., 2002); it permits large (and multiple) genes to be inserted. For the purpose of this thesis, this chapter will focus on transducing neurons using viral vectors because these methods are most commonly used in memory based experiments in adult and aged animals and is the technique employed in the current thesis.

The viral vector typically involves either a lentivirus (LV) or adeno-associated virus (AAV). These have different properties with associated advantages and disadvantages. LV has a relatively large particle size (100 nm), which restricts its diffusion through neural tissue (Parr-Brownlie et al., 2015). This property of LVs is useful when the aim is to transduce neurons in a small nucleus. Larger brain regions can still be targeted by administering multiple injections within the target. Another advantage is that LV vectors have greater genome capacity; recombinant genetic information containing 8–10 kilobases (kb) can be inserted (Parr-Brownlie et al., 2015; Rein & Deussing, 2012). The use of longer gene sequences and multiple genes is discussed below. Conversely, AAV particles are much smaller (20 nm), permitting them to diffuse further and enabling larger nuclei and brain regions, such as cortical areas, to be transduced for a given volume (Sizemore, Seeger-Armbruster, Hughes, & Parr-Brownlie, 2016). For AAV9 and AAVrh10, an additional advantage is that they can cross the blood brain barrier, so that brain neurons can be transduced when the viral vector is administered peripherally (Sizemore et al., 2016). However, the genomic capacity for AAVs is only 4 kb (Rein & Deussing, 2012), which restricts

the use of large gene complexes. AAV is the vector most often used for gene therapy in humans (Feigin et al., 2007; Kaplitt et al., 2007; Marks et al., 2008; LeWitt et al., 2011; Coune, Schneider, & Aebischer, 2012; Palfi et al., 2014; Rafii et al., 2014; Olanow et al., 2015; Tuszynski et al., 2015) and optogenetic stimulation in nonhuman primates (Diester et al., 2011; Lerchner, Corgiat, Der Minassian, Saunders, & Richmond, 2014; Galvan, Hu, Smith, & Wichmann, 2016).

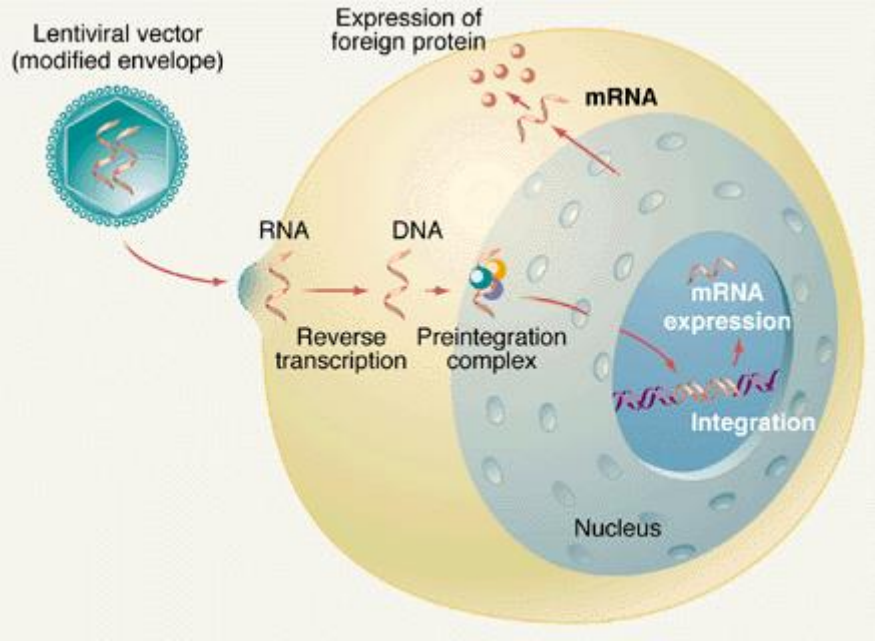

Figure 5.1. Gene transfer by a lentivirus, showing integration into the host genome. Adapted from Amado & Chen (1999).

A key consideration is the type of viral vector that is required. More specifically, this pertains to the selection of different capsids (AAV) or glycoproteins (LV), which determine which cells (e.g., neurons versus cardiac myocytes etc.) will endocytose the vector. AAV single-stranded DNA is incorporated as an episome (non-chromosomal double-stranded DNA), whilst the LV will be reverse transcribed into DNA and integrated into the host genome, and is therefore more likely to maintain opsin expression long-term (see Figure 5.1; Amado & Chen, 1999). LV viral vectors are commonly used in studies where effective and sustained transduction is required, such as in the current thesis in which extended behavioural testing is necessary. Each specific vector contains a particular native genome, and then a set of proteins are expressed on the capsid for AAVs and virus membrane for LVs. However, with engineering it is also possible to improve vector functionality or targeting, a process called pseudotyping. For AAVs, the genome of one serotype (e.g.,

serotype 2) can be packaged in the capsid from another serotype (e.g., serotype 5). For LVs, glycoproteins from other viruses (e.g., rabies (Rb) or vesicular stomatitis virus (VSV)) can be packaged with the LV (e.g., human immunodeficiency virus (HIV)) genomic background. Pseudotyping can alter the viral vectors tropism and trafficking properties, thereby limiting or expanding the range of cells susceptible to transduction. For example, VSV G-pseudotyped lentivirus is able to infect an almost universal set of cells, a tropism characteristic of the VSV G-protein with which the vector is coated.

AAV serotypes and LV glycoproteins also influence whether the vector will be transported anterogradely or retrogradely. For example, AAV2 and AAV5 serotypes usually exhibit an anterograde pattern of transport, although some retrograde transport has been observed using AAV5 in the entorhinal cortex (Aschauer, Kreuz, & Rumpel, 2013). AAV6 usually undergoes retrograde transport, although this functionality varies across brain regions and neuronal phenotypes (Salegio et al., 2013; Hadaczek et al., 2016). For LVs, packaging with the VSVg glyoprotein causes transduction of the soma of neurons and astrocytes at the injection site, permitting anterograde labeling of axonal projections. By contrast, pseudotyping LV with the Rb glycoprotein means that the vector is taken up at axonal terminals in the injected region and transported retrogradely so that cell bodies at local and distant sites are transduced (Parr-Brownlie et al., 2015). In addition, intraventricular infusion of some vectors (such as AAV1) will transduce neurons and glia in several brain regions simultaneously (eg. hippocampus, striatum and adjacent cortex) (Li et al., 2006). However, the efficacy of injectable viral vectors using cell specific promotors is limited by the size of the virus. Targeting a wider range of cell types is impeded by the size of the sequences that would need to be packaged into viruses.

Selective expression in a particular neuronal phenotype is achieved by adding a specific promoter to the genetic construct within the vector. Promoters determine the type of cell that will encode the transgene. Once transcribed it can also determine the subcellular component (e.g., cell membrane or a kinase in the cytoplasm) that will express the opsin protein (Nathanson, Yanagawa, Obata, & Callaway, 2009; Olson & Tabor, 2014; Sizemore et al., 2016). The length of promoter sequences differs between genes being controlled (Dimidschstein et al., 2017). The complete promoter sequence is not needed to restrict transduction to the target neuronal phenotype, but using a more complete (longer)

promoter sequence will generally ensure expression is restricted to the target phenotype. The minimum promoter sequence needed for targeted expression varies for each cell phenotype (Li & Zhang, 2014). This can occasionally affect which vector is used for experiments. For example, the smallest promoter used to target inhibitory neurons is 3 KB long, which fits in an AAV vector but may not permit other genes to be included. Across brain regions and nuclei, the synapsin promoter allows expression in all neuronal types (Zhang et al., 2007). Further cell type specificity can be gained through the use of specific promotors to drive gene expression in select cells. Glial fibrillary acidic protein (GFAP) is astrocyte-specific (Gradinaru, Mogri, Thompson, Henderson, & Deisseroth, 2009). Glutamic acid decarboxylase 67 (GAD67) provides specific expression in GABAergic neurons (Denyer & Douglas 2012; Sizemore et al., 2016). Calmodulin-dependent protein kinase II (CamKII) targets glutamatergic neurons (Yizhar et al., 2011; Gradinaru et al., 2009). There is a long list of potential promoters providing different levels of selectivity (for comprehensive lists see Carter & de Lecea, 2011; Yizhar et al., 2011; Parr-Brownlie et al., 2015; Sizemore et al., 2016). The current thesis aimed to selectively target the excitatory glutamatergic neurons of the ATN, and thus used the CamKII promotor sequence.

For optogenetic stimulation, selection of the vector and promoter provide the first level of specificity. Local injection of the vector(s) into the brain permits a second level of control. A third level of specificity can occur depending on where the optical fiber is implanted. For example, if LV_{VSVg} injections are made into the ATN, the fiber can be implanted there too. With this arrangement, stimulation would then influence all of the nuclei that ATN neurons innervate, and experiments will clarify what the ATN does. Alternatively, the function of a specific pathway from the ATN can be tested by stimulating axon terminals at one of its targets, e.g., subiculum (Bubb et al., 2017). Typically, around six weeks is required to ensure that there is sufficient opsin expression in the terminals of long-range axonal projections. Recent developments, however, suggest that the provision of a fused neuritin 3' untranslated region accelerates the expression of specific proteins over long-range projections (Ye et al., 2016).

Transgenic rodents have the genome of germ cells altered so that opsins are expressed at functionally relevant levels in specific cell types in progeny. Therefore, one of the benefits of using transgenic rodent lines is the ability to overcome the limitations

associated with AAV and LV vector gene capacities, facilitating the use of larger promoter sequences, and thus highly restricted control of transgene expression (Fenno et al., 2011). In addition, the use of Cre recombinase cell lines in combination with viral vector infusion within these animals enables cell-type and site specificity afforded by the use of viral vectors (reviewed in Zhang et al., 2010). Cre is a bacterial enzyme that is used for site specific recombination of DNA between two loxP sites, i.e., the floxed transgene is reversed so the gene can be transcribed. For example, injecting an AAV virus with a relatively small but powerful promotor into a recombinase-driver transgenic mouse results in targeted opsin expression in only those recombinase-expressing cells in the injected brain region of interest (Kim et al., 2017). Nonetheless, transgenic mouse lines also have inherent caveats. These largely pertain to the costs required, in terms of time and effort to produce, maintain and validate these knock-in animals (Fenno et al., 2011). Transgenic rodent lines are also associated with biological and developmental complications, including epigenetic effects, random integration of transgenes into the DNA (Matthaei, 2007), and the presence of undesirable genes in some transgenic lines such as the bacterial artificial chromosome (BAC) (Ting & Feng, 2014).

5.3 Optogenetics: Opsin variants and cellular impact

A diverse range of opsins are currently available, either naturally occurring genetic forms or variants engineered to achieve new functionality (Kim et al., 2017). Opsin-encoding genes determine the precise type of channel or carrier protein that will be expressed by target cells. These proteins control whether excitatory (increased neuron activity) or inhibitory (decreased activity) effects will occur when the opsin is activated with the appropriate wavelength of light (Yizhar et al., 2011). Here, I provide a general overview of the major subclasses of microbial genes encoding opsins, the colour of light required for activation, and their physiological effect on the target cell. I also briefly mention engineered alterations that have been made to enhance optogenetic capabilities.

Presently, the most widely used construct for cellular activation is channelrhodopsin-2 (ChR2), which is activated by blue light. When activated, ChR2 allows the net passage of cations into the cell, resulting in depolarization and spiking (Kim et al., 2017). As ChR2 is a nonspecific cation channel, one photon of light is accompanied by the movement of multiple cations (Yizhar et al., 2011). For inhibition, the most common constructs are

halorhodopsin-type chloride (Cl-) pumps, which induce hyperpolarisation by pumping one chloride ion into the cell for every photon of yellow light (Fenno et al., 2011; Yizhar et al., 2011). By contrast, archeorhodopsins (Arch/ArchT) are inhibitory bacteriorhodopsin-type proton (H+) pumps that induce hyperpolarisation by pumping one proton out of the cell for every photon of green light. However, extrusion of protons means that cell pH and pH sensitive functions may also be altered (Fenno et al., 2011; Yizhar et al., 2011).

The field of optogenetics has expanded through the engineering of ion-selective variants of these major classes of opsin. For example, ChR2 has been molecularly altered to permit higher stimulation rates by reducing deactivation kinetics (ChETA), and others have been modified so they can inhibit activity (e.g., ChloC, iC1C2) (Berndt, Lee, Ramakrishnan, & Deisseroth, 2014; Gunaydin et al., 2010; Wietek et al., 2015). Unlike the aforementioned Cl- and H+ pumps that move one ion per photon of light, molecularly altered opsins are much more efficient as they allow the passage of thousands of Cl- ions into the cell for one photon of light (Berndt et al., 2014; Wietek et al., 2015). Furthermore, ChloC exhibits comparatively slower off-kinetics, resulting in sustained decreases in cell activity lasting several seconds (Wietek et al., 2015). Similarly, step-function opsins deactivate even more slowly, by inducing prolonged changes with a comparatively short light delivery epoch, in some instances inducing a deactivation period of up to ten minutes. Examples of this include the excitatory stabilized step-function opsin (SSFO, a bi-stable variant of excitatory ChR2) and the step-waveform inhibitory ChR2 or SwiChR which is a step-function form of the inhibitory ChRs which conduct Cl- ions (Kim et al., 2017).

Other adaptations include altering the wavelength activation peak for ChR2, shifting it from blue to red (Zhang et al., 2008; Kim et al., 2017). The wavelength of activation light is important because it also determines light penetrance through tissues. Red-shifting the activation wavelength confers several benefits; it reduces spectral overlap should multiple opsins be present in the neural tissue and allows a larger neural region to be stimulated because red light is less divergent in tissue than other wavelengths, which means it travels further through the tissue (Zhang et al., 2008). To improve penetrance, sometimes more light (mW/mm^2) is applied to the brain. However, depending on the wavelength, light density and duty cycle, this can cause heat to accumulate (Stujenske et al., 2015), particularly when a laser light source is used rather than LEDs, which may alter neuronal

activity or cause tissue damage (Thomsen et al., 1991; Deng et al., 2014). Viral vector modifications have also been made to achieve greater cellular control. For example, both ChR2 and halorhodopsin have been incorporated into the same vector, which enables both excitation and inhibition of the same population of transduced cells using blue and yellow light, respectively (Yizhar et al., 2011). This latter approach enables the effects of increases and decreases in activity in the same neuronal population to be directly compared within a dynamic network and behaving animal.

5.4 Optogenetics: Advances on traditional techniques

The spatial and temporal resolution afforded by optogenetics distinguishes it from traditional methods of neuromodulation, such as local application of electrical currents or pharmacological agents. For example, while electrical stimulation is temporally specific, we do not know the volume of tissue that is stimulated. Furthermore, locally applied electrical currents produce activation (or inactivation) of all cell types, as well as fibres of passage, in the immediate vicinity of the electrode tip (Merrill, Bikson, & Jefferys, 2005). Although pharmacological approaches spare fiber tracts and some selectivity is possible, cell specificity is lacking and altered cellular activity may persist for hours after administration (van Duuren et al., 2007). In an effort to address some of the inadequacies of electrical and chemical modulation, chemogenetic lock and key approaches have been employed. This technique uses cell specific expression of mutated muscarinic receptors that might be exclusively activated by an otherwise biologically inert substance, clozapine-N-oxide (CNO; Urban & Roth, 2015). The technology was given the acronym DREADDs because mutated designer receptors are exclusively activated by designer drugs (Armbruster, Li, Pausch, Herlitze, & Roth, 2007). This approach relies on metabotropic receptors and requires intraperitoneal or intracranial administration of CNO. As a result, its effects have a delayed onset, which can then last for many hours, making it more suited to extended manipulations, but unable to mimic the spatial and temporal characteristics of local circuit activity (Urban & Roth, 2015). Furthermore, Gomez et al. (2017) demonstrated that activation of DREADDs is not solely caused by CNO binding but also by the CNO metabolite, clozapine. While DREADDs are relatively specific, clozapine has multiple endogenous targets such as serotonin and dopamine neurons, which requires the addition of CNO-only controls (Gomez et al., 2017).

Optogenetics has the distinct advantage of being able to modulate specific cellular activity at time scales relevant to neural networks (Fenno et al., 2011; Yizhar et al., 2011). In some cases, light stimulation effects may be instantly terminated when a short stimulation period (less than a minute) and/or low stimulation rates have been used. Optogenetic stimulation effects may outlast the stimulation when high frequencies or complex patterns are used (Seeger-Armbruster et al., 2015). In addition, the intensity and duration of stimulation effects are dependent on the type of receptors (ionotropic versus metabotropic) the underlie pre and/or postsynaptic effects. Furthermore, this precise and potentially reversible control of cellular activity theoretically allows multiple conditions to be examined within a single subject over one experimental session, providing a more efficient means of investigating neural network dynamics (Tye & Deisseroth, 2012). An additional benefit of optogenetics is that it can be used to selectively stimulate different terminal regions of selectively transduced cells. As previously mentioned, this is achieved by infusing neurons within a structure and waiting for expression in their terminals at a downstream region of interest and then optically stimulating by implanting the optical fiber at this precise location, thereby selectively targeting a specific directional connection (Stuber et al., 2011). Moreover, as optogenetics evokes cellular responses with light pulses, rather than electrical currents, it is highly compatible with neural and electrochemistry recordings (Kim et al., 2017). Hence, sophisticated experiments are feasible, in which optogenetic interventions are made highly biologically relevant by constantly adapting stimulation parameters based on real time activity within neural circuits (Siegle & Wilson, 2014).

5.5 Pairing optogenetics and electrophysiological techniques

Patch-clamp electrophysiology (measuring the currents in individual cells) is perhaps the most recognised means of monitoring high-speed single-cell synaptic activity, but it is difficult to link this with in vivo recordings made during behavioural performance. However, the combination of optogenetics and patch-clamp techniques has enabled researchers to study these long-range functional connections with cellular specificity. For example, monosynaptic responses to optogenetic stimulation have been studied using acute brain slices in tetrodotoxin and 4-aminopyridine to abolish polysynaptic responses. Adhikari et al. (2015) obtained whole-cell recordings from neurons in the amygdala during optogenetic stimulation of ChR2 expressing cells in the mPFC. The results of this study demonstrated

that excitatory projections from the dorsomedial PFC synapse onto the fear-suppressing GABAergic cells in the amygdala.

Similarly, the combination of optogenetic stimulation and in vivo electrophysiological recording has greatly improved our understanding of the impact of stimulation on both the cellular and circuit-wide level. For example, where previously in vivo electrophysiological recordings could provide insight into the changes in local field potentials as they pertained to behaviour, the addition of optogenetics has meant that stimulation of a particular input or cell type can be directly linked to an observed behavioural change, and this can then also be related to circuit-wide alterations (Kim et al., 2017). For example, Jennings et al. (2013) demonstrated that although the lateral hypothalamus is crucially involved in feeding behaviours, input from the extended amygdala helps to regulate these feeding behaviours. This was shown by optogenetic activation of GABAergic inputs from extended amygdala to the lateral hypothalamus which resulted in rapidly increased food consumption. Optogenetic stimulation may be more effective or produce differential effects if delivered during particular aspects of behaviour (eg. Encoding vs. retrieval) or during different rhythmic epochs (e.g. Trough vs peak of an electrophysiological rhythm such as theta; Siegle & Wilson, 2014; Seeger-Ambruster et al., 2015).

The real-time fast readouts gained from using in vivo electrophysiological techniques has presented the possibility of using closed-loop techniques. Closed-loop techniques use real-time electrophysiological activity to drive optogenetic stimulation. Combining electrophysiology and optogenetic techniques enables the design of simultaneously precise and diverse studies which can elegantly partition out the roles of particular cells, pathways and structural subregions.

5.6 Optogenetic dissection of neural circuits

The main focus of this section is the role of optogenetics in both the deconstruction of memory circuits and subsequently its applicability to treat amnesic disorders, such as diencephalic amnesia and Alzheimer's disease. However, it is important to highlight how optogenetics has been widely used to link behaviour and neural circuitry, and has enabled the design of highly selective preclinical treatments across a range of disorders (Tye & Deisseroth, 2012; Parr-Brownlie et al., 2015). The specificity of transduced brain cells and placement of the optic fibre are instrumental in elucidating the exact nature of the

connection of interest; careful selection of behavioural tasks enables precise improvements or deficits in behaviour to be characterized (Fenno et al., 2011; Parr-Brownlie et al., 2015).

Optogenetics has confirmed the circuitry involved in a plethora of behaviours including anxiety, reward, aggression, and predation (Stuber et al., 2011; Tye et al., 2011; Adhikari et al., 2015; Falkner, Grosenick, Davidson, Deisseroth, & Lin, 2016; Han et al., 2017). In a previously mentioned example, Adhikari and colleagues (2015) showed that glutamatergic neurons in the ventral part of medial prefrontal cortex (mPFC) that project to the amygdala play an important modulatory role in anxiety in rodents. Glutamatergic cells in the rodent mPFC innervate the basomedial amygdala, intercalated cells in the amygdala and other cortical and subcortical targets (Sesack, Deutch, Roth, & Bunney, 1989; Hurley, Herbert, Moga, & Saper, 1991; Öngür & Price, 2000). Interestingly, no anxiolytic effect was found when ChR2 was injected and the optical fibre implanted in the ventral mPFC, thus potentially activating glutamatergic neurons projecting to all targets (Adhikari et al., 2015). By contrast, selective optogenetic stimulation of only ChR2 expressing ventral mPFC neuron terminals in the basomedial amygdala, by placement of the fiber there, resulted in a profound anxiolytic effect, highlighting the influential role of the direct connection from ventral mPFC to the basomedial amygdala. This experiment clearly illustrates the importance of selectively stimulating specific connections, in this case only the ventral mPFC-basomedial amygdala pathway, to induce cortically controlled fear and anxiety behaviors (Adhikari et al., 2015). In another example, Gradinaru and colleagues (2009) showed that high frequency (130 Hz) stimulation in the rodent subthalamic nucleus produced different behavioral outcomes depending on whether subthalamic nucleus neurons, or glia, or afferents to the subthalamic nucleus were stimulated. Here, selective optogenetic stimulation of subthalamic neurons, or glia, did not alter pathological rotational movements, whereas selective stimulation of motor cortex inputs to the subthalamic nucleus therapeutically reduced these movements (Gradinaru et al., 2009). This study confirmed in behaving animals that selective activation of collaterals from corticospinal neurons contribute to the therapeutic effect of deep brain stimulation (DBS) in the subthalamic nucleus in the parkinsonian state (Li, Arbuthnott, Jutras, Goldberg, & Jaeger, 2007; Li et al., 2012). Alongside the ability to precisely define the neural circuitry underlying behavior is the potential to selectively treat abnormal neurological states. The

following provides an initial overview of preclinical research dedicated to treating neurological conditions and demonstrating how optogenetic targeting of select structures or cell types has made this possible.

5.7 Optogenetics to treat non-memory aspects of neurological conditions

The ability to locate critical components of neural circuits and selectively influence relevant pathways is an important step when considering the design of therapeutic interventions for neurological conditions. Optogenetics, therefore, may provide a powerful therapeutic tool for conditions such as Parkinson's disease (PD), drug abuse, epilepsy (Chen et al., 2013; Krook-Magnuson, Armstrong, Oijala, & Soltesz, 2013; Paz et al., 2013; Suthana & Fried, 2014; Seeger-Armbruster et al., 2015) and Alzheimer's disease (AD; which will be addressed later). DBS targeted in the subthalamic nucleus or globus pallidus internus is a common treatment for some of the motor symptoms of PD, such as bradykinesia and postural rigidity (Suthana & Fried, 2014). The motor thalamus is of particular interest for DBS as it integrates basal ganglia and cerebellar motor information that is sent to the motor cortex. Electrical high frequency DBS in the motor thalamus is associated with improvements in tremor, but is ineffective in treating other symptoms (Benabid et al., 1991; van Someren et al., 1993; Boecker et al., 1997; Atkinson et al., 2002; Beuter & Titcombe, 2003; Okun & Vitek, 2004; Duval, Panisset, Strafella, & Sadikot, 2006; Klein et al., 2012). Using optogenetics, Seeger-Armbruster and colleagues (2015) demonstrated that pattern-dependent optogenetic activation of glutamatergic neurons in the motor thalamus effectively treated akinesia in a haloperidol-induced parkinsonian rat model. In this study, the drug-induced impairment in forepaw reaching was ameliorated by optogenetically stimulating the motor thalamus using a pre-recorded physiological pattern of neuronal activity from a control rat or theta burst stimulation (Seeger-Armbruster et al., 2015). Therefore, optogenetic stimulation of the motor thalamus with complex patterns may be a future treatment for akinesia in PD patients.

Optogenetics has also been applied to the treatment of compulsive drug seeking behaviour (Chen et al., 2013). Prolonged cocaine self-administration has been shown to decrease excitability in deep layer pyramidal neurons of the mPFC in a rat model of compulsive drug seeking. To compensate for this prefrontal hypoactivity, the authors used optogenetics to stimulate ChR2 expressing pyramidal neurons in the prelimbic area of the

mPFC at a low frequency (1 Hz). Here an animal model of addiction was employed, in which the authors selected a subpopulation of rats that demonstrate foot-shock resistance. Stimulation successfully attenuated cocaine self-administration in these rodents, as shown by a decrease in earned cocaine infusions and an increase in lever-press latency (Chen et al., 2013). The authors further demonstrated that this effect did not result from reduced motor control or increased motivational behavioral responding. Conversely, the authors demonstrated that inhibiting the prelimbic area of the mPFC, via halorhodopsin activation, in foot-shock sensitive rats increased cocaine seeking confirming that bidirectional (increases versus decreases) manipulation of neural activity can produce opposite behavioral effects.

Promising optogenetic treatment has also been explored in the context of epilepsy. A particularly effective form of treatment for temporal lobe epilepsy in mice is the use of closed-loop optogenetic control (Krook-Magnuson et al., 2013; Paz et al., 2013). As previously mentioned, closed-loop studies typically involve using the activity of a key nodal structure in the circuit of interest to drive the onset or type of modulatory intervention. In the aforementioned studies, seizure onset was detected in real time and in response either closed-loop optogenetic inhibition of granule cells in the dentate gyrus or thalamocortical neurons was used to abolish seizure activity (Krook-Magnuson et al., 2013; Paz et al., 2013). The use of real time feedback for intervention combined with optogenetics, electrophysiological, electrochemical or microdialysis techniques enables greater understanding of how altered activity in a selective part of a circuit controls behavior. Furthermore, using optogenetic stimulation to modulate specific neurons in a precise nucleus to treat epilepsy reduces the probability of triggering another seizure, a side effect associated with electrical stimulation (Coley et al., 2009).

5.8 Optogenetics to improve memory in neurological conditions

5.8.1 The neuroanatomical basis for memory: The hippocampus

Optogenetic techniques are being increasingly used to improve our understanding of the role of the hippocampus in memory function. One study by Spellman and colleagues (2015) used the light activated H+ extrusion protein, Arch, to disrupt interactions between the ventral hippocampus and PFC. They found that selective inhibition of this pathway during encoding impaired spatial memory performance. However, this effect was not observed if

inhibition occurred during recall of spatial information, reinforcing a specific spatial memory role for hippocampal-PFC interactions. Shipton and colleagues (2014) optogenetically silenced CA3 pyramidal neurons (using halorhodopsin) and reported a left-right dissociation in hippocampal memory processing. Silencing of CA3 pyramidal neurons in either the left or right dorsal hippocampus was sufficient to impair short term spatial memory, but only inhibition of neurons in the left CA3 impaired long-term memory (Shipton et al., 2014).

5.8.2 The hippocampal formation and Alzheimer's disease

The hippocampus proper (CA1-CA3 and the dentate gyrus) is the core structure within a larger hippocampal formation. However, the entorhinal cortex is among the first of the medial temporal lobe regions to exhibit dysfunction in early AD (Khan et al., 2014). Yang and colleagues (2016) demonstrated that entorhinal cortex layer II pyramidal neurons directly innervate parvalbumin positive GABAergic neurons in area CA1 of the hippocampus. The authors then used a mouse model of AD (EC-APP/ Tau line), which expresses an isoform of the human amyloid precursor protein and exhibits similar plaque pathology to human AD patients. These mice showed degeneration of the entorhinal cortex layer II-area CA1 pathway and impaired spatial learning and memory. However, selective optogenetic activation of these entorhinal cortex layer II pyramidal neurons at theta burst frequency prior to symptom onset rescued degeneration of entorhinal cortex-hippocampal synapses and improved learning and memory function (Yang et al., 2016). Theta burst stimulation is commonly used to induce long-term potentiation in target structures, especially the hippocampus (Bowden, Abraham, & Harris, 2012) and may provide a mechanism for synchronising activity of neural network activity during mnemonic processes (Colgin, 2013).

Hippocampal cells, thought to represent “memory engrams,” have also been optogenetically targeted in an effort to better understand the circuitry involved in AD-related memory impairments (Roy et al., 2016). A mouse AD model that incorporates the human-mouse β-amyloid precursor protein transgene is associated with severe deficits in memory retrieval, but selective optogenetic activation of memory engram cells in the dentate gyrus attenuated the expected deficits in contextual fear learning. The authors also noted that prior to amyloid plaque deposition and in the absence of optogenetic stimulation, spine density progressively reduced in dentate gyrus neurons. Furthermore, this reduction was correlated with age-related memory loss. Memory performance was

improved with 100 Hz stimulation of dentate gyrus neurons, and was associated with restored spine density and innervation by the perforant pathway, which might provide an opportunity for an early treatment intervention.

5.8.3 The extended hippocampal system: a recap

As mentioned in previous chapters, memory is supported in the brain by an extended network of cortical, limbic and brainstem structures (see figure 2). Extensive rodent experimental lesion work supports a functional role of the ATN on the structure and function of cortical regions in the system (Aggleton, 2008; Dalrymple-Alford et al., 2015; Perry et al., 2018; Savage et al., 2011; Vann & Nelson, 2015; Zhang et al., 2015). Clinical studies have also demonstrated the role of these diencephalic and cortical structures, including the ATN, in patients with anterograde amnesia, Alzheimer's disease and other neurodegenerative dementias (Harding et al., 2000; Tsivilis et al., 2008; Carlesimo et al., 2015; Kopelman, 2015; Aggleton et al., 2016; Dzieciol et al., 2017).

Designing therapeutic optogenetic stimulation interventions to treat memory deficits by targeting the whole extended hippocampal circuit will not be possible. Instead, key thalamic structures, particularly the ATN within the extended hippocampal system, provide a strategic opportunity to selectively modify a relatively small brain structure, yet have widespread impact on the extended hippocampal circuit as a whole via extensive connections (see Figure 2.1 for a schematic representation of the extended hippocampal system).

5.8.4 Potential targets for optogenetic intervention in memory

Optogenetic investigation into the contribution of extra-hippocampal regions to mnemonic function is largely unexplored. To date, the importance of each extra-hippocampal constituent has largely been demonstrated by lesion and electrophysiology research. However, the interconnected nature of the circuit and the need to circumvent sites of permanent damage suggest that activity in the whole system should be considered when designing interventions to treat memory deficits. This would create significant technical challenges given the distributed nature of the circuit and the size of some constituents.

As discussed in previous chapters, it has been suggested that modulation of selective structures can improve memory function. These improvements could occur via changes in rhythmic activity or improvements in neural plasticity. Such interventions may provide

therapeutic avenues for neurological conditions, and in particular diencephalic amnesia and AD. To date, electrical brain stimulation has achieved some success in treating memory impairment in patients with AD (Suthana & Fried, 2014). A phase one clinical trial of DBS to the fornix/hypothalamus in 6 patients with AD found that high frequency stimulation increased activity within the circuit, as measured by fMRI (Laxton et al., 2010). This coincided with upregulated glucose metabolism in temporal and parietal lobes, an effect that remained after 12 months of stimulation. However, despite these promising functional markers, only moderate improvements in mnemonic function were observed in some patients (Laxton et al., 2010). The precise locus for these functional improvements is difficult to determine because the electrode had four stimulation contacts located along the entire vertical segment of the fornix (immediately anterior to the thalamus), thereby activating a large region, and potentially many structures. The fornix innervates many structures, such as the MB, ATN and basal forebrain, at different points along its axis, and any one of these might have been critical for functional improvements (Vann & Nelson, 2015).

Initially, the most obvious structure to target for optogenetic stimulation to enhance memory appears to be the hippocampal formation (Drapeau et al., 2003; Neves, Cooke, & Bliss, 2008; Deng, Aimone, & Gage, 2010). Targeting major input or output regions such as the entorhinal cortex and/or area CA1 may be effective (Ramirez et al., 2013; Lux, Bindrich, Markowitsch, & Fink, 2015; Ryan, Roy, Pignatelli, Arons, & Tonegawa, 2015; Yang et al., 2016). Early stimulation of the hippocampus may be useful during the mild cognitive impairment stage in AD (Braak & Braak, 1991; Price & Morris, 1999). For example, optogenetically-induced recovery of spine density in cells in the hippocampus could be exploited during the early stages of medial temporal lobe neurodegeneration in AD (Roy et al., 2016). Currently, translating optogenetic stimulation of the hippocampal formation to clinical trials would require enhanced pre-diagnostic criteria before excessive degeneration occurs.

Frontal and retrosplenial cortices work in conjunction with the hippocampus during memory consolidation, and could be targeted to recover memory (Vann, Aggleton, & Maguire, 2009; Preston & Eichenbaum, 2013; Buckley & Mitchell, 2016; Eichenbaum, 2017). Metabolic decline in the retrosplenial cortex is evident during early AD and animal work

shows that secondary dysfunction in this region occurs after injury to the ATN, MB and hippocampus (Aggleton, 2008; Dumont, Amin, Poirier, Albasser, & Aggleton, 2012; Mendez-Lopez, Arias, Bontempi, & Wolff, 2013; Vann, 2013; Perry et al., 2018). However, like the hippocampus, cortical regions are highly diverse and present an excessive expanse for transduction, which precludes interventions in patients. Specifically, it is not practical to infuse large volumes of virus across multiple sites and introduce multiple implanted light sources for optogenetic stimulation. Nonetheless, de Sousa et al. (2019) recently used a c-Fos/ ChR2 variant transgenic mouse to explore the effect of optogenetic stimulation in the retrosplenial cortex. This circumvented the need for large volume infusions and multiple optic fiber implants as they instead adopted a cranial window approach, allowing the researchers to selectively stimulate a $1mm^2$ cortical area of the RSC. de Sousa et al. (2019) demonstrated that high frequency stimulation of neural ensembles representing a contextual fear memory one day after learning produced a recent memory. However, this recent memory presented with features normally associated with a remote memory. That is, decreased hippocampal dependence, context generalisation and the recruitment of neocortical areas during retrieval. Similarly, Benn et al. (2016) found that selective ChR2 optogenetic stimulation of medial PFC glutamatergic neurons enhanced recognition memory in rodents. Moreover this was attributed not only to activation of the prelimbic and infralimbic cortices but also to activation of the mediodorsal thalamus (Benn et al., 2016). Whilst these studies suggest that cortical structures may present potential target structures for memory improvement, they are impractical targets in human subjects at this time.

A feasible approach with translatable potential is to treat memory dysfunction by optogenetically modulating small structures that innervate and regulate both hippocampal and cortical regions. Therefore, small thalamic nuclei are ideal because small volumes of viral vector will transduce the majority of neurons that innervate many memory-relevant brain structures (Dalrymple-Alford et al., 2015; Tsanov, 2015; Vertes, 2015; Bubb et al., 2017).

For example, the MD provides a potential site for optogenetic stimulation to improve memory. In a recent study, Bolkan et al. (2017) found directionally-specific functional interactions between the MD thalamus and mPFC during a spatial working memory task. Selective inhibition of MD terminals in the mPFC in a T-maze during the 60 sec

delay phase, but not the sample or choice phases, impaired task performance by preventing maintenance of working memory. Conversely, optogenetic activation of the MD may sustain cortical representations in the PFC (Schmitt et al., 2017). The MD plays a critical role in sustaining prefrontal activity during working memory maintenance (Bolkan et al., 2017). Hence, the MD thalamus may provide another relatively tractable site to facilitate memory enhancement via modulation of the large expanse of PFC in the human brain.

The Re is a second thalamic region of interest due to its dense reciprocal connections with both the hippocampus and PFC. The Re directly innervates hippocampal CA1, a main output region of the hippocampal formation (Vertes, 2015). Its connections suggest a vital role in mediating hippocampal formation-PFC interactions critical for mnemonic function (Cassel et al., 2013; Loureiro et al., 2012). As yet, there is limited exploration regarding Re stimulation effects on memory processing. Duan et al. (2015) confirmed that delta frequency optogenetic stimulation of transduced Re terminals in the hippocampus impairs working memory. Similarly, Maisson et al. (2018) showed that Re inhibition during the sample phase, but not the delay or choice phase, of a spatial working memory task impaired memory function. However, the authors noted that viral expression spread laterally, as well as along the anterior-posterior, and dorsal-ventral axes. As the Re is located beneath the main body of the thalamus and is closely surrounded by other structures implicated in memory function (such as the AM and MTT) it is difficult to attribute the behavioural effects to inhibition of only the Re.

Another small structure in the extended hippocampal system, the MB, may be another option as the majority of cells within the medial MB fire at theta frequency and all MB neurons are thought to project to the ATN (Dillingham et al., 2015). Unfortunately, the location of the MB on the ventral surface of the brain makes this a difficult target for transduction and optic fiber implantation (Figure 1). Furthermore, the dichotomy between the lateral and medial MB would need to be considered when designing an intervention as stimulation of the lateral head direction cells compared to the medial theta pathway may produce distinct responses (see Butler et al., 2017 for the effects of optogenetic stimulation of head direction cells).

The most suitable nodal structure for optogenetic intervention within the extended hippocampal system is the ATN. As described earlier, it occupies a strategic position within

the extended hippocampal system with extensive reciprocal connections with the prefrontal and retrosplenial cortices and subicular regions of the hippocampal formation (Jankowski et al., 2013; Bubb et al., 2017; Mathiasen et al., 2017). Both clinical and animal experimental lesion studies implicate the ATN in episodic memory and related tasks (Harding et al., 2000; Aggleton & Nelson, 2015; Dalrymple-Alford et al., 2015; Kopelman, 2015; Aggleton et al., 2016). The ATN has been a major target for DBS treatment in refractory epilepsy and proven promising in reducing seizure activity via its ability to modulate activity in both the hippocampus and PFC. DBS of the ATN has also resulted in cognitive improvements in some patients (Oh et al., 2012). The anteroventral nucleus (AV) of the ATN, in particular, contains a large population of cells that fire at theta frequency. Therefore the ATN likely plays a key role in the medial theta pathway previously described (see Chapter 2; Tsanov and O'Mara, 2015). Real-time communication between the neocortex and the ATN has implicated in successful memory encoding (Sweeney-Reed et al., 2014). Simultaneous intrathalamic and scalp EEG recordings were taken from patients receiving intrathalamic electrode implantation for the treatment of epilepsy. Both neocortical-ATN theta oscillatory phase synchrony of LFPs and neocortical theta-ATN gamma cross-frequency coupling have been shown to predict later memory recall of complex scenes, demonstrating the importance of ATN-neocortex interactions in human memory encoding (Sweeney-Reed et al., 2014). Furthermore, ATN theta phase alignment has since been shown to correlate with theta-gamma cross-frequency coupling, and is enhanced during successful encoding (Sweeney-Reed et al., 2015). Phase alignment, the re-setting of phase in a particular frequency range with each new stimulus, is regarded as a pre-requisite for the synaptic plasticity underlying memory encoding (Sweeney-Reed et al., 2015).

Electrical stimulation of the ATN in rats has also been shown to increase hippocampal neurogenesis and improve memory performance (Hamani, Stone, Garten, Lozano, & Winocur, 2011). Using the increased selectivity and specificity afforded by optogenetics, it may be possible to build upon these early findings. The glutamatergic cells of the anterior thalamus (largely those of the anteroventral but also present in the majority of all other subnuclei) are predominantly thalamo-cortical projection neurons (Zakowski, 2017). These neurons project to many cortical regions, such as the entorhinal cortex, subiculum, anterior cingulate and the granular dysgranular retrosplenial cortices. For

example, 70% of the neurons projecting from the AV to the Rgb and Rga contain glutamate (Zakowski, 2017).

5.9 Conclusions

Optogenetic stimulation affords much greater cellular and temporal specificity for neural control than electrical or pharmacological techniques. The ability to target specific cells and then use light to stimulate them with spatial and temporal precision means researchers can elucidate the contributions made by individual structures to behaviour, and also permits selective stimulation for therapeutic recovery or maintenance of memory function. This prospect is encouraged by evidence that optogenetics is improving our understanding of the neural mechanisms underlying neurological disorders, such as epilepsy and PD, and the design of therapeutic interventions that target specific symptoms.

As mentioned in chapter 2, memory is supported by a distributed neural network that includes cortical, diencephalic and brainstem structures. Due to their compact size and dense connections with the hippocampal formation and cortical regions, thalamic nuclei appear to be ideal structures amenable to therapeutic intervention. Of these, the anterior thalamus presents itself as the most translatable target due to its nodal position within the system. Evidence supports its role in theta propagation and the cellular specificity of the glutamatergic projections to cortical regions, including the hippocampal formation and retrosplenial cortex, highlight the interconnected nature of the ATN.

A clear first step would be to explore whether optogenetic stimulation of the anterior thalamus can ameliorate memory function following focal damage to a key structure within the extended hippocampal system. In this instance, the MTT would be an obvious target due to its assumed role in propagating theta rhythmicity from the medial MB to the ATN and the wider system, as well as its location downstream of the ATN. Stimulation of a densely interconnected structure such as the ATN and beyond the site of damage may serve to reinstate inter-structural rhythmicity in the wider circuit and improve mnemonic functioning. Due to the emphasis on theta rhythmicity within the system, its crucial role in memory function, and the suggestion that theta burst stimulation can improve memory function, employing theta burst parameters with optogenetics may be an effective intervention.

In the subsequent chapters (6-7) the effects of lesions to key fibre tracts, as well as the potential to achieve recovery of memory function, will be examined. In Chapter 6, a direct comparison between MTT and PCFx lesions is made to provide greater understanding into the relative contribution of these two key fibre tracts to memory and the functionality of the extended hippocampal system. In Chapter 7, I will investigate whether selective optogenetic stimulation of the ATN can ameliorate the memory deficits caused by MTT lesions. A general discussion of the overall findings will then be provided in Chapter 8.

Chapter 6:
MTT and PCFx comparison

6.1 Introduction

As discussed in Chapters 2 and 3, the MTT and post-commissural fornix are key fibre pathways in an extended hippocampal memory circuit. The post-commissural fornix provides direct hippocampal innervation of the MB and ATN, whilst the MTT provides the unidirectional afferent path from the MB to the ATN. The fibres of the post-commissural fornix split in two and either turn caudally to innervate the ATN or proceed towards the ventral surface as a compact bundle, known as the descending post-commissural fornix (PCFx), to terminate in the MB. Injury to the MTT is the most consistent predictor of an amnesic syndrome following thalamic infarction (Van der Werf et al., 2000, 2003; Carlesimo et al., 2011, 2014). Similarly, moderate to severe working memory impairments are observed in the T-maze, water maze and RAM following MTT lesions in rodents (Vann & Aggleton, 2003; Vann, 2013; Nelson & Vann, 2014; Perry et al., 2018; Dillingham et al., 2019). By contrast, there is relatively little human or animal model evidence supporting the role of the PCFx in memory. To reiterate, only two human studies have examined the role of post-commissural fornix microstructure in MCI and normal ageing. Christiansen et al. (2016) examined the PCFx, thus only innervation of the MB, whilst Coad et al. (2020) included the post-commissural fornix innervation of both the MB and ATN. Christiansen et al. (2016) found that the integrity of the PCFx was associated visual recall performance, whilst Coad et al. (2020) reported that post-commissural fornix microstructure was associated with object-location paired-associate learning (Christiansen et al., 2016; Coad et al., 2020). These findings suggest that the PCFx plays an important mnemonic role. Surprisingly, however, two animal lesion studies have thus far suggested that transection of the descending limb of the post-commissural fornix has a negligible impact on spatial working memory in the T-maze and 8-arm radial arm maze (Vann et al., 2011; Vann, 2013). The contrast between human and animal lesion model findings suggests that further investigation is needed into the relative contributions of the PCFx in memory.

In addition, MTT lesions produce ‘covert pathology’ in distal sites within the extended hippocampal system (see Chapter 4). Covert pathology refers to when an area appears normal by standard histological criteria, but nonetheless shows evidence of a

functional lesion (Aggleton, 2008; Aggleton & Nelson, 2015). Typically, this is reflected by a loss of immediate early gene (IEG) neural activity markers such as c-Fos and Zif268. MTT lesions reduce IEG immunoreactivity in subregions of the RSC, hippocampal areas CA1, CA3 and DG, the prelimbic cortex and the para- and post-subiculum, suggesting widespread and systemic hypoactivity following MTT damage (Vann & Albasser, 2009; Vann, 2013; Perry et al., 2018). By contrast, there is no evidence suggesting that PCFx lesions cause functional lesions elsewhere in the extended memory system (Vann, 2013). Whilst MTT lesions reduced c-Fos activation in the HPC, posterior RSC, and prelimbic cortex, PCFx lesions had negligible effects on c-Fos expression (Vann, 2013).

Examining alterations in oscillatory activity is another means of quantifying the 'online' systemic effects of localised damage to structures within the neural network. For example, recording local field potentials (LFPs) in key structures within the circuit during behavioural performance may reinforce the evidence provided by IEG activity. LFP activity within (measured by local power) and between (measured by coherence) structures may shed light on functional changes occurring following localised lesions. Theta rhythmicity has been consistently implicated in memory function in both humans and animal models (Fell et al., 2003; McNaughton et al., 2006; Kim et al., 2011; Sweeney-Reed et al., 2014; 2015) and it is ubiquitous throughout the extended hippocampal system (Kirk & Mackay, 2003; Ketz et al., 2015). In humans, the distinction is made between theta (4-7 Hz) and alpha (8-12 Hz), but in freely-moving rats 'theta' frequency typically ranges from 5-14 Hz (Mitchell et al., 2008). The slow-wave nature of theta means that it is capable of synchronising distally located ensembles (Colgin, 2013) and may act as a coordinating rhythm within the neural network (Kirk & Mackay, 2003; Ketz et al., 2015). It may be that damage to structures within the extended hippocampal system disrupts normal oscillatory activity, and this aberrant rhythmicity may contribute to the memory deficits observed. Indeed, a recent study has demonstrated that transection of the MTT attenuates peak theta frequency (theta defined as 6-12 Hz in this instance) in the HPC and RSC during locomotion and causes aberrant coherence between the HPC and RSC (Dillingham et al., 2019). The effect of MTT lesions on HPC theta is unsurprising, as it has previously been demonstrated that the MB-ATN axis is critical for HPC theta functionality (Zakowski et al., 2017).

The current Chapter directly compared the behavioural and neural systemic effects of removal of key inputs to the MB-ATN axis. That is, the HPC input to the MB via the PCFx and the MB input to the ATN, via the MTT. System-wide neural changes were measured by Zif268 IEG activation and oscillatory activity. We determined the relative impact of MTT and PCFx lesions on spatial working memory in the 12-arm radial arm maze. As discussed in Chapter 4, the standard RAM task has been reported to be sensitive to MTT lesions but not PCFx lesions (Vann et al., 2011; Vann, 2013; Perry et al., 2018). In order to assess the effect of lesions on oscillatory activity during critical decision points within the maze, oscillatory activity in lesion and control groups was analysed during correct 'choice' epochs. Correct choice epochs refer to the epoch just before the rat proceeded down an arm that was not counted as an error. PSD and coherence for correct choice epochs across the ATN-HPC-PFC axis were analysed across a frequency band encompassing rat 'theta' (5-14 Hz), akin to human theta (3-7 Hz) and alpha (8-12 Hz) frequencies (Mitchell et al., 2008). The ATN-HPC-PFC axis was of particular interest as all three structures have been consistently implicated in memory function (Aggleton & Brown, 1999). Aberrant oscillatory activity across this axis may reflect dysfunctional theta propagation to the ATN and into the wider network from either the hippocampus or from brainstem inputs. Prior to perfusion, rats were tested in a novel room using a novel maze, as this manipulation has been shown to increase IEG activation in regions within the extended hippocampal system (Jenkins et al., 2002; Vann, 2013). Rats were run on a forced-choice version of the RAM task so that sensorimotor behaviour could be controlled for and reward contingencies could be matched. We then compared Zif268 expression in the RSC, dorsal HPC and mPFC across lesion and control groups. Zif268 was selected as this marker is associated with spatial memory formation and long-term plasticity (Jones et al., 2001; Penke et al., 2014; Farina & Commins, 2016, Gallo et al., 2018). The aim of this chapter was to directly compare the impact of MTT and PCFx lesions on spatial working memory and their effects on function across the wider memory system.

6.2 Methods

6.2.1 Animals

Thirty-six male Piebald Virol Glaxo cArc (PVGc) hooded rats were used. These were bred in the University of Canterbury facility and maintained in standard housing of three or four rats per opaque plastic cage (50 cm long by 30 cm wide by 23 cm high). They were maintained in reversed lighting conditions and behavioural testing conducted during the lights off period (8 am-8 pm). Rats were 16 months old at the time of lesion surgery and weighed between 300 g and 400 g. Triplets of rats were randomly allocated to MTT lesion, PCFx lesion or Sham surgery groups. Rats were housed individually for about seven days after lesion surgery, and then group-housed for six to eight weeks before electrode implantation surgery. Rats were randomly allocated to group housing. Food and water were available *ad libitum* prior to surgery and during recovery. For behavioural testing food was restricted to maintain 85% of the rats' free feeding body weight; water was available *ad libitum* at all times. All procedures complied with the University of Canterbury animal ethics committee guidelines and approval (2016/24R).

6.2.2 Spatial memory in the 12-arm Radial Arm Maze

Spatial working memory was tested using a 12-arm Radial Arm Maze (RAM) located in the centre of a large, windowless room (4m by 4.7m; Figure 6.1). Rats were attached to the headstage cable throughout the session. Pulleys beneath the maze enabled the clear Perspex guillotine doors (10 cm by 28 cm) to be manually raised at the entrance to each arm around the perimeter of the 35 cm wide central hub. The RAM was raised 70 cm above the floor and had 12 equally-spaced aluminium arms (65 cm long by 10 cm wide, with 3 cm high walls). A clear Perspex barrier (19 cm high by 25 cm long) extended from the central hub along one side of each arm to prevent rats from jumping across arms. A wooden block (5 cm by 9 cm by 3 cm) was located at the end of each arm, with a recessed food well (3 cm by 1 cm) for 0.1 g chocolate food rewards; inaccessible chocolate was also placed underneath the food wells to provide constant odour cues. Extra-maze cues were located on the four walls surrounding the RAM, positioned roughly 1-2m from the maze. These cues consisted of a computer, tables, posters, curtains, orange cones and boxes.

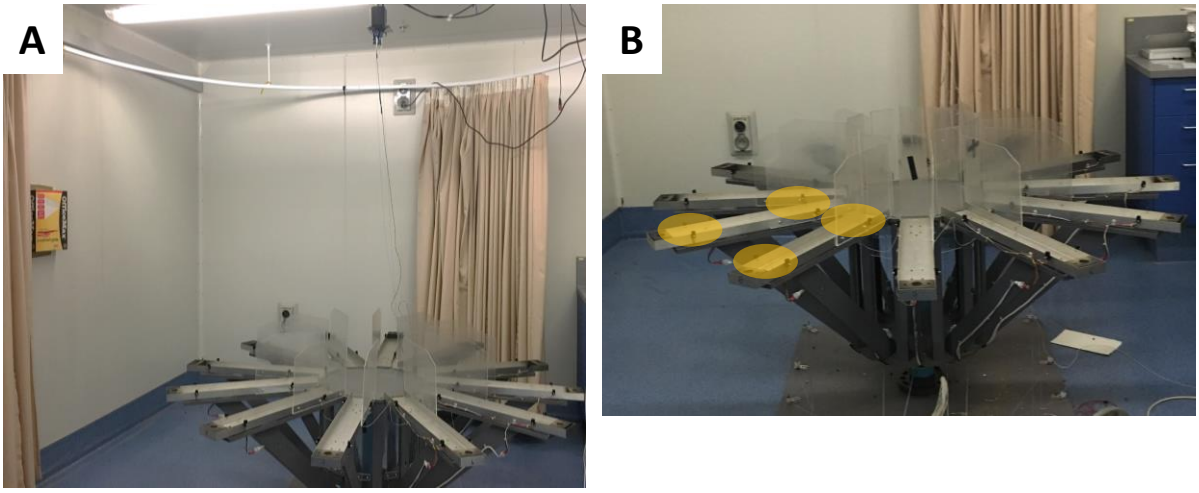

Figure 6.1. Photograph of the 12-arm radial arm maze used for this experiment. Figure A shows the relative position of the maze within the testing room. Infrared beam locations have been highlighted in yellow on two of the arms (B).

6.2.3 Habituation

Prior to lesion surgery rats were placed on food restriction, handled over three weeks, familiarised with chocolate drop food rewards (0.1 g) and habituated in the 12-arm RAM. For the first three days of habituation rats were placed in the maze in cage groups for ten minutes with chocolate drops scattered throughout the maze (lightly in the central hub and more densely towards the end and food well of each arm). Rats were then habituated individually for three minutes per day for 4 days, during which time the chocolate drops were gradually moved until they were present only in the food wells on the final day. The rats were familiarised to opening and closing of the guillotine doors during individual habituation.

6.2.4 Lesion surgery

Rats were anesthetised with an intraperitoneal injection of ketamine (80 mg/kg; Provet, NZ) and Domitor (medetomidine, 0.35 mg/kg; Provet, NZ) and placed in a stereotaxic device with atraumatic ear bars (Kopf, Tujunga, CA). The head was positioned so the skull was horizontal for MTT and PCFx lesions, which were made using a Radionics TCZ radio frequency electrode (0.25 mm diameter, 0.3 mm long exposed tip; RFG4-A, Radionics, Burlington, VT; see Figure 6.2 for relative positioning of target structures). Radiofrequency rather than excitotoxic, methods were used in the current experiment as the target structures were fibre pathways. Excitotoxic lesions specifically damage neurons whilst

sparing axons, where as radiofrequency lesions damage everything within the vicinity of the electrode tip. Methopt Forte (Aspen Pharm, NZ) eye drops were applied, and a moist gauze was then placed above and clear of the eyes. The site of incision was cleaned with sterilised gauze soaked in 4% chlorhexidine gluconate. The rat was given subcutaneous local analgesia to the scalp (0.2 ml of 2 mg/mL of Mepivacaine). The rat's core temperature was maintained by insulating the rat's body in bubble wrap. One of four anterior–posterior (AP) coordinates from bregma was used to accommodate different bregma to lambda (B–L) distances. For MTT lesion surgery: -0.245 mm for B-L distance of ≤ 0.64 mm; -0.25 mm for B-L 0.65-0.68 mm; -0.255 mm for B-L 0.69-0.72 mm; and -0.260 mm for B-L ≥ 0.73 mm. The lateral target was ±0.09 from midline and ventral target was -0.71 mm from dura. For PCFx lesion surgery: -0.145 mm for B-L distance of ≤ 0.64 mm; -0.15 mm for B-L 0.65-0.68 mm; -0.155 mm for B-L 0.69-0.72 mm; and -0.160 mm for B-L ≥ 0.73 mm. The laterality was ±0.12 mm from midline and ventrality was -0.77 mm from dura. The electrode was lowered vertically to the lesion coordinate and the temperature of the tissue surrounding the electrode tip was raised slowly to 65 °C for MTT lesions or 66 °C for PCFx lesions and then maintained at this temperature for 60 s. Sham rats received the same procedure as either MTT or PCFx lesion surgery except the electrode was lowered to 1.0 mm above the lesion site to prevent any damage to the structure and the temperature was not raised.

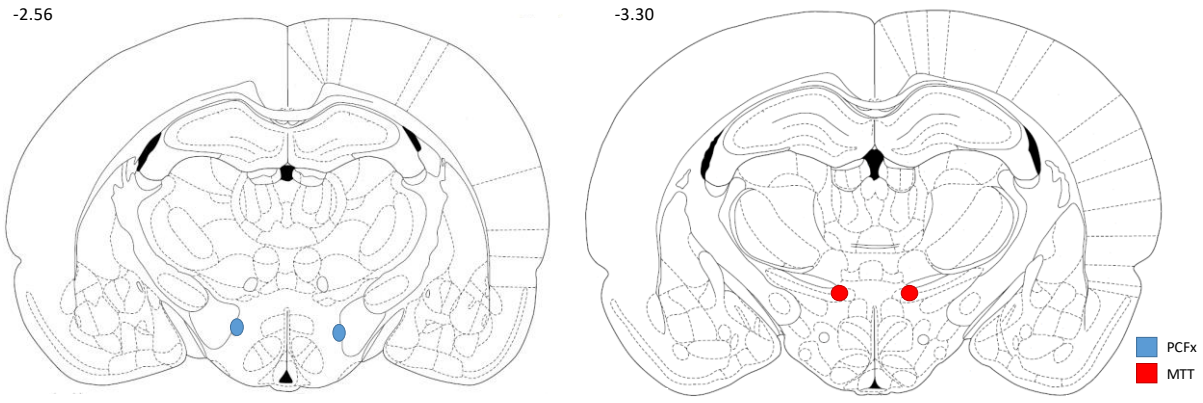

Figure 6.2. Rat atlas plate depicting the relative positioning of the two target lesion structures. Adapted from Paxinos and Watson (1982). Abbreviations: MTT= mammillothalamic tract; PCFx= post-commissural fornix. -2.56 and -3.30 denote values in mm from bregma.

6.2.5 Electrode fabrication

Electrodes were prepared for implantation in the hippocampus, anterior thalamus, and prefrontal cortex. Electrodes were constructed by twisting together four 50 µm platinum-

iridium wires which had a heavy polyamide coating (90% platinum, 10% iridium; California Fine Wire, CA, USA). Four wires per electrode provided additional strength to the implant and allowed selection of the most conductivechannel for electrophysiological analysis from each structure. The insulation of the wires were then fused by applying heat from three different directions with a heat gun and then sealed with a thin layer of cyanoacrylate (Selleys, NZ). The four twisted wires were then threaded through a 3 mm long section of 26 gauge stainless steel cannula (PlasticsOne; see C and D in Figure 6.3) so that roughly 10 mm of the electrode protruded from the base of the cannula, and secured to the cannula with cyanoacrylate to provide further structural strength for when the electrodes were implanted into the brain. The electrode was then attached to a Mill-Max gold pin (Mill-Max, USA) with cyanoacrylate to facilitate implantation (see B in Figure 6.3). Once dry, the length of the electrode beneath the base of the cannula was cut using a scalpel to the approximate length based on the target structure: 4 mm for the prefrontal cortex and hippocampus and 6 mm for the anterior thalamus. The two ~ 6 cm loops of wires at the distal (untwisted; see A in Figure 6.3) end were then cut to yield four wires, separated out, the coating removed with a naked flame and each wire soldered separately using flux and Duratech solder (Jaycar, NZ) to one male silver-coated pin on a four-pin block of Mill-Max connectors (male/female pins; see E in Figure 6.3). The soldered connections were strengthened by applying a coat of epoxy resin and left to set for 24 h. Each electrode was tested for conductivity and to ensure there were no shorts between channels using a bubble test and a digital multi-meter. Shorts were indicated by the multi-meter by an audible beep. Ground electrodes were constructed from 12 cm lengths of 200 µm diameter silver wire (California Fine Wire, CA, USA). One end of the ground wire was soldered with flux and Duratech solder to a block of four male/female Mill-Max pins, bridging the male pins to create a ground electrode. The other end of the wire was looped just beneath the head of the ground screw, hydrochloric flux was applied and the wire was soldered in place.

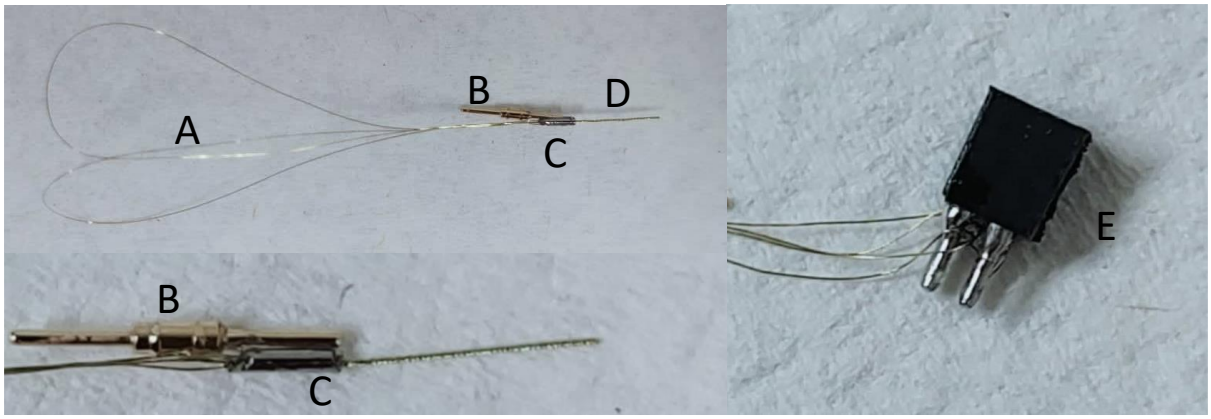

Figure 6.3. Example of electrode construction steps. The two loops of platinum iridium wire (A) were cut to yield four untwisted wires, which were then soldered to a Mill-Max connector containing four male to females pins (E). The twisted wires (D) were passed through and secured to a 3mm length of cannula (C), which was then attached to a gold pin (B) to facilitate implantation.

6.2.6 Electrode implantation surgery

Rats were implanted with the recording electrodes ~6 weeks after lesion surgery. General anaesthesia was achieved by placing the rat in an induction chamber with 4% isoflurane (Provet, NZ) mixed with oxygen at a flow rate of 1500 ml/min. Once an anaesthetic plane was reached the rat was given a subcutaneous injection of Carprofen (5mg/kg; Provet, NZ) for pain relief, as well as 1 mL of Hartmann's solution (sodium lactate, Intraperitoneal; Baxter, NZ) for hydration. The top of the head was then shaved and cleaned. Before the rat was transferred to the stereotaxic, the rat was placed in the induction chamber briefly. Depth of anaesthesia was tested by checking for tail pinch and plantar reflex. Tail pinch, plantar, and visual checks of colour and respiration were performed every ten minutes during surgery. Following this, the rat was transferred to the nose cone and mounted in the stereotaxic frame. Anaesthesia was maintained throughout surgery at 2% isoflurane with an oxygen flow rate of 1000 mL/min during surgery. Waste gases were actively scavenged into the outside atmosphere via an exhaust system. All anaesthesia equipment was cleaned and disinfected with medi-wipes before and after use. If the animal appeared responsive to tail pinch or plantar reflex the isoflurane rate was increased back to 4% until the reflex disappeared. Surgery was then carried out in the same way as lesion surgery, with the following changes.

Following incision, six angled holes were drilled around the perimeter of the incision and five anchoring screws inserted (see Figure 6.4 for a representation of screw

placements). The sixth screw was placed in the orbital bone to act as the ground/reference channel. The uninsulated silver ground wire was wrapped first around the ground screw and then around all remaining screws. Small craniotomies were then made above the site of the PFC, HPC and AV for implanting the electrodes (see Table 6.1 for coordinates). Electrodes were sterilised in 70% ethanol; and implanted using a mounting arm with a specialised socket that held a female connector pin. The male gold pin of each electrode slotted into the matching connector pin. After each electrode was implanted, it was secured in place using a small amount of dental acrylic, and allowed to dry before the mounting arm was removed. Once all electrodes were secured in place, a thin layer of dental acrylic was applied over the entire area of skull confined within the grounding wire. The top half of each gold pin was removed. A dummy Mill-Max connector in a rectangular configuration (see Figure 6.5) was used to line up the connectors attached to the electrodes and then the ground/reference electrode was also connected to the dummy.

Dental acrylic was used to cover all exposed electrode wires, and the anchoring and reference screws. The incision surrounding the head cap was then cleaned with sterile saline and closed with sutures (if needed). Emla analgesic (Aspen Pharma, NZ) cream was applied to the scalp area following suturing and the rat was given additional Hartmann's solution. At the completion of the surgical procedure, the isoflurane was switched off and the animal was administered 2 min of pure oxygen through either the nose cone or induction chamber before being transferred back to a clean cage for recovery. I then remained with the rat until it became ambulatory again. Post-operatively, especially during the first week, both the laboratory technicians and I monitored recovery twice daily to check that the rat was not in pain, returned quickly to being bright, alert and responsive, was drinking (water bottle weighed daily), and eating (food reduced, faeces present). The wound was checked for healing (no discharge, inflammation or pulled stitches). The rat was weighed every second day.

Table 6.1. Electrode coordinates (mm). Abbreviations: B= bregma; L=lambda; AP= anterior-posterior; DV= dorsal-ventral.

PFC			
Distance B to L	AP coordinate	Lateral coordinate	DV (from dura
≥0.64	+0.300	± 0.06	-0.35
0.65-0.68	+0.305		
0.69-0.72	+0.310		
< 0.72	+0.315		
AV			
Distance B to L	AP coordinate	Lateral coordinate	DV (from dura
≥0.64	-0.131	± 0.145	-0.488
0.65-0.68	-0.136		
0.69-0.72	-0.141		
< 0.72	-0.146		
HPC			
Distance B to L	AP coordinate	Lateral coordinate	DV (from dura
≥0.64	-0.285	± 0.21	-0.28
0.65-0.68	-0.290		
0.69-0.72	-0.295		
< 0.72	-0.300		

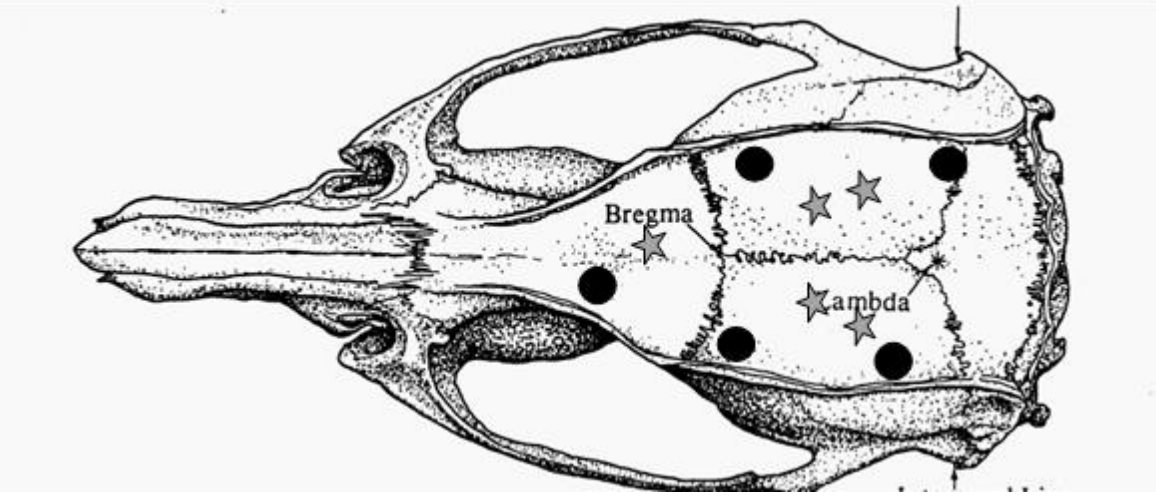

Figure 6.4. Diagrammatic representation of electrode (stars) and screw locations (black circles). Image adapted from Paxinos, Watson & Topple (1985).

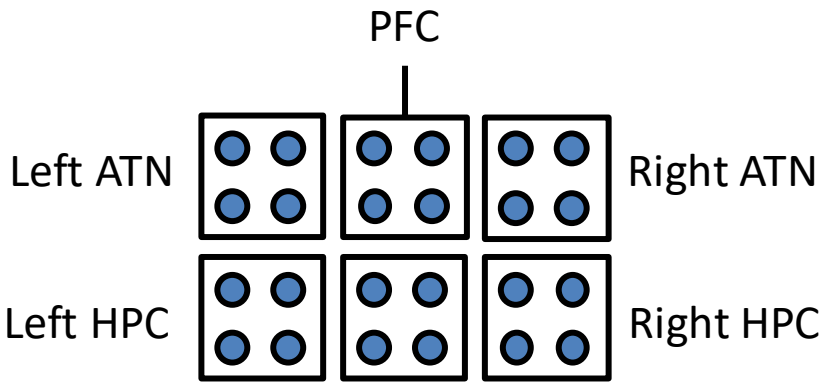

Figure 6.5. Diagram indicating the topographical layout of the Mill-Max plug on the rats head. Abbreviations: G=ground.

6.2.7 RAM testing

Around 14 days after electrode surgery, rats were re-habituated to the 12-arm RAM, and then given 20 days of testing in the working memory task. The 12 arms were each baited with one chocolate drop and optimal behaviour was to avoid revisiting any arm. At the beginning of the trial, the rat was placed in the central hub with all doors raised to block access to the arms. After a 5-10 s delay, all 12 guillotine doors were dropped and the rat was allowed to make an arm choice. An arm choice was defined as both hind legs entering the arm. Once the rat had entered an arm, all the doors were raised, confining the rat to the arm for ~10 s while it consumed the food reward and then the rat was allowed back into the central hub. If the rat had selected an arm that it had previously visited, it would not receive a reward and was still confined to the arm for ~10 s and this was considered an error. Once the rat returned to the central hub, it was kept there for ~5-10 s before all of the doors were dropped again and the rat was allowed to make another arm choice. The trial concluded when the rat had either visited all 12 arms, made 20 arm choices or 10 min had elapsed.

6.2.8 Electrophysiological recording

Before each trial began, the rat was plugged into the Open Ephys headstage, which connected to the Open Ephys data acquisition board via a carousel commutator (Plexon, Tx) attached to the roof above the central hub. The headstage cable connected to the commutator via a Harwin adaptor. The Open Ephys programme was activated, and the trial began. Electrophysiological data during RAM testing was recorded using the open-source Open Ephys graphical user interface and data acquisition system. Implanted electrodes were

connected to this system via a custom-made Mill-Max/Omnetics adapter consisting of a bank of Mill-Max pins with an identical configuration to the rat's headcap, then soldered onto a 32-channel electrode interface board (Open Ephys). Electrode signals were referenced to the ground. The Open Ephys software recorded the wideband local field potential (LFP) signals, which were notch (50 Hz) and bandpass filtered (1 -100 Hz) and sampled at 1 KHz. All recorded channels were saved to the computer running the Open Ephys software to allow for later offline analysis of LFP activity in Neuroexplorer version 5, Matlab, Plexon Offline Sorter, Windows Excel, SPSS and Statistica.

To synchronise behaviour with recorded electrophysiology, a pair of 3 mm diameter infrared beams (each with sender and receiver) were fixed above the walls of each arm. One beam was located 15 cm along the arm, to record when the rat had entered the arm; the second was located 12 cm from the end of the arm, just before the rat reached the food well, producing a distance between beams of 38 cm in each arm. The beams were powered via the 3.3 V lines of an Arduino Mega 2560 that was in turn powered by an Open Ephys Input/Output (I/O) 5 V line extension. Each beam signal was held logic high (3.3 V) by a dedicated 1 KΩ pull-up resistor wired between the signal and power lines of each infrared detector unit. When the beams were broken the signals became logic low (0 V or 'ground') and the Arduino read, processed, then sent an output signal(s) to the Open Ephys I/O. Due to the high number of infrared detector units (24) and the low number of Open Ephys I/O lines (8) a basic program was run on the Arduino to firstly invert the logic signals (0 V becomes 3.3 V; or 0 V becomes 1 V; or on becomes off), then convert the 24 outputs into a combination of 3.3 V I/O signals based on which beam was broken. Open Ephys interpreted these logic high signals as "events" on the timeline to timestamp behavioural events with the electrophysiology recording.

Open Ephys only has 8 possible digital inputs. We wanted to have beam breaks at the beginning and end of each arm and to match electrophysiology with behaviour using timestamps. To work around the missing 24 digital inputs, an Arduino was programmed to produce a combination of signals for each arm. For example, arms 1-6 produced a timestamp, each labelled with the number of the arm (5 for example). Arms 7-12 were labelled as a zero and another number. For example, arm eight was denoted by a zero and a

2. The beam breaks at the end of the arms were all connected as a single signal, indicated by the number 8.

6.2.9 Electrophysiology data processing

Local field potentials from anterior thalamic, hippocampal and prefrontal electrodes were processed using Neuroexplorer version 5.128, Microsoft Excel and SPSS. One patent LFP channel per structure per rat was selected for analysis. For coherence analyses, only patent electrodes located in the same hemisphere were used. The filtered LFP channels were then visually inspected, and any movement artefacts appearing across channels were removed before spectral and coherence estimates were calculated. Neuroexplorer used a fast Fourier transform for power and coherence calculations. As justified in the general introduction chapter to this thesis, we focus here on 2-14 Hz. Group differences in power spectral density (PSD) and coherence across the frequency spectrum were calculated during the 500ms choice epochs (see data analysis). Spectral analyses were performed separately for the ATN, HPC and PFC in each rat in Neuroexplorer using a single taper spectral estimation (Hanning window) with 25% overlap. Data were normalised using a log transform (i.e. converted to log μV^2 for analysis), extracted across a range of 2-14 Hz and sent to Microsoft excel for further processing before analysis in SPSS. Coherence coefficients were calculated between the ATN-HPC, ATN-PFC and HPC-PFC with only ipsilateral electrode pairs used in each analysis.

6.2.10 Immediate Early Gene activation

Following the final day of testing, the rats were habituated to a novel, dark holding room for three days. They were placed in individual holding cages in the dark room for 90 min each day, for three days. Four days after the previous RAM testing, the rats were returned to the RAM but using a new procedure. All arms were baited to promote immediate early gene activation (Zif268) expression in the extended hippocampal circuit (Vann & Aggleton 2002; Vann, 2013). They were run in a novel room that had a different spatial configuration and novel extra-maze cues, and completed three massed trials in a single session per day for three days. One configuration was used on the first two days, each with three trials to adjust the rat to the new environment; then a different novel configuration was used on the final day of testing to further increase activation of the extended hippocampal system. During each trial, the rat was allowed to make eight arm choices. The rat was first allowed to make

four arm choices as per standard RAM testing (all rats were making correct choices in the first four arms following the 20 days of testing in the RAM). After the rat had been held in the central hub after the fourth arm choice, a single door was lowered allowing access to an arm the rat had not previously visited. Once the rat entered the arm to consume the food reward, the door was raised and the rat was confined there for ~15 s, before the door to the arm was again lowered for the rat to re-enter the central hub. The next three arm choices proceeded in the same fashion; this ensured that all rats entered the same number of arms and performance differences were not a confound across rats. Once all eight arm choices had been made, the rat was removed from the maze and placed in a separate opaque box (50 cm long by 30 cm wide by 23 cm high) for 2 min while the maze was reset. The rat was then returned to the maze and completed the same procedure for trial two and trial three. Once the rat returned to the central hub after the eighth choice on the third trial , it was removed from the maze, and placed in the quiet and dark room that it had been familiarised to for 90 min to facilitate immediate early gene activation (Chadhuri et al., 2000).

6.2.11 Perfusion

After 90 min in the dark room rats were anaesthetised with sodium pentobarbital (125 mg/kg; Provet, NZ). Once deeply anesthetised (cessation of plantar and tail pinch reflexes), the tip of each electrode was marked by passing 20 µA through the electrode for 20 s. Rats were then perfused transcardially with ~200 mL of chilled saline followed by ~200 mL of 4% paraformaldehyde in a 0.1 M phosphate buffer (PB) solution (pH 7.4). Once the rat was perfused, the head-cap and electrodes were removed carefully to minimize damage to the brain; and the brain was post-fixed in 4% paraformaldehyde solution overnight at 4°C. Brains were then transferred into a solution for long term storage (20% glycerol, 0.1M PB), for a minimum of 48 h.

6.2.12 Histology

Continuous 40 µm coronal sections were taken from approximately +3.70 to -9.16 from bregma (anterior prefrontal cortex to start of cerebellum) using a sliding microtome with a freezing stage (Thermofisher, NZ). To capture both electrode placements and lesion sites, sections were collected in sequential series of four sections (1 per vial) so that lesion verification and immunohistochemistry could be performed on the same regions. Sections

were collected into 3 mL vials containing cryoprotectant solution (40% 0.1 M PB, 30% glycerol and 30% ethylene glycol) for long-term storage at -20 °C.

6.2.13 Lesion verification

Luxol blue, a myelin specific stain, was used to assess the completeness of the fibre pathways, with sections counterstained with cresyl violet (Nissl stain) to confirm lesion extent and placement relative to surrounding structures. Two out of four vials per rat used for lesion verification (and corresponding electrode verification in the dorsal hippocampus) were collected between -1.80 to -4.30 from bregma. Mounted sections were delipidised in graduated concentrations of alcohol (3 minutes in 100% ethanol, 3 min in 95% ethanol and 1 hour in 70% ethanol). The slides were then placed in Copland jars containing ~250 mL of Luxol blue solution (0.1% solvent blue 38 from Sigma Aldrich, in 95% ethanol with acetic acid added (0.1% of the total solution)). Half-submerged Copland jars were preheated in a water bath (55 ºC) for one hour before the slides were incubated in Luxol blue solution overnight (~15 h). Slides were then differentiated, counterstained with cresyl violet, dehydrated and cover slipped as follows. Slides were removed from the Luxol blue solution in batches and submerged in 95% ethanol for 15 sec before being rehydrated in deionised water for 3 min. Next, the slides were differentiated in 0.1% lithium carbonate (Sigma Aldrich) for three minutes to remove non-specific staining, before being transferred to 70% ethanol for three minutes. In order to thoroughly remove excess background staining, the rehydration and differentiation steps were repeated three times each: that is submerged in deionised water, lithium carbonate and then 70% ethanol then back to deionised water and so forth. After the third differentiation, the slides were rinsed in deionised water for one minute and then submerged in 0.5% cresyl violet solution for eight minutes before being rinsed twice in deionised water for two min each. The slides were subsequently dehydrated in 70% ethanol for two min, 95% ethanol for two minutes, and then differentiated in 95% acid alcohol solution for 30 seconds. The slides were then submerged in 100% ethanol twice for two minutes each to complete the dehydration steps, before being cleared twice in xylene for five minutes each and finally cover slipped with DPX mounting medium (see results section 7.1 for example photographs of staining).

Sections were viewed on a Leica DM6 B upright microscope and images captured using the DFC7000T proclass microscope camera (Leica Microsystems) using the 10x

objective. Outlines of the MTT and PCFx were initially made on copies of the Paxinos and Watson (1998) atlas plates by Professor John Dalrymple-Alford, blinded to condition, and the approximate area of fibre pathways estimated using in-house software. Average areas of the MTT and PCFx tracts in Sham rats were calculated using the open-source Fiji software (ImageJ software, https://imagej.net/Fiji/Downloads). The approximate area of the MTT or PCFx fibres was traced in the lesion rats and calculated using the Fiji automated area calculation tool. For MTT lesions, only cases with 80% or more damage bilaterally were included in analyses. For PCFx lesions, only those with 100% bilateral damage were included.

6.2.14 Electrode verification

Sections from one of the four vials from each rat were mounted onto gelatin-coated slides and allowed to dry overnight before being stained with cresyl violet only. Slides were delipidated, hydrated, stained, rinsed, dehydrated and differentiated as follows. Slides were delipidated by receiving 10 dips in 70%, 95% and 100% ethanol, followed by 5 min in 100% ethanol, a further 10 dips in 95% ethanol and an additional 5 min in 70% ethanol. Slides were then rinsed in distilled water for one minute before being stained with 0.5% cresyl violet solution for approximately 8 min, and then rinsed again in distilled water for 4 min. Dehydration and differentiation of slides required 2 min in both 70 and 95% ethanol, before being submerged in 95% acid/alcohol for approximately 6-8 min. Following this, slides were submerged twice in 100% ethanol for 5 mins each, before being cleared twice in xylene for 5 mins each and finally cover slipped with DPX mounting medium. The approximate location of each electrode tip was independently determined by Professor John Dalrymple-Alford and indicated on corresponding atlas plates.

6.2.15 Zif268 immunohistochemistry and regions of interest

Tissue sections from one of the four vials from each rat were initially washed in 0.1 M phosphate buffered saline (PBS) containing 0.2% Triton X-100 (PBS-Tx) for 3x 10 min. Endogenous peroxidase activity was blocked by washing tissue sections for 30 mins with peroxidase blocking buffer (30% hydrogen peroxidase), 100% methanol, PBS-Tx at 2% in distilled water. Excess blocking solution was removed by washing tissue sections for 3x 10 min in PBS-Tx before being incubated for 72 h at 4°C with rabbit polyclonal zif268 antibody (also known as Egr-1; 1:1500; Santa Cruz Bio) in PBS-Tx with 1% normal goat serum (NGS).

Tissue was then rinsed in PBS-Tx for 3x 10 min and then incubated in a biotinylated goat anti-rabbit secondary antibody (1:1000; Vector) with 1% NGS in PBS-Tx for 24 h. Tissue sections were then washed in PBS-Tx for 3 x 10 min, before incubation in Extravadin (Peroxidasae Conjugated; 1:1000; Sigma) in PBS-Tx with 1% NGS. Sections were then rinsed in PBS for 3 x 10min and PB for 3 x 10min, washed in 0.05 M Tris buffer (pH 7.4) for 2 x 5min and then developed for 20 min in 0.05% diaminobenzidine (Sigma, Castle Hill, Aus) in 0.05 M Tris buffer with 30% hydrogen peroxidase added just prior to incubation. Sections underwent 3x 10 min washes in Tris buffer to stop the reaction, rinsed in PB for 3 x 10 min and then mounted on gelatinised slides, allowed to dry and then run through graded alcohols (70%, 95% and 100%) before being cleared in xylene and cover-slipped with DPX mounting medium.

Zif268 sections were viewed on a Leica DM6 B upright microscope and images captured using the DFC7000T proclass microscope camera (Leica Microsystems) using the 10x objective. Automated cell counts were obtained using the open-source Fiji software. Images were gray-scaled, the background subtracted using rolling 20 light, the autothreshold set using Max Entropy (built in thresholding algorithm) and the image converted to a binary mask. The same threshold was used across all rats. Labelled cell bodies in each region of interest were determined by counting the number of cells above threshold with a circularity between 0.7 - 1 (for a circle, Circularity = 1). Cell counts were made blind to group condition but were not stereological, providing a relative number of cells rather than absolute levels. Between four and six sections per hemisphere were analysed for each brain region. The cell count of zif268-positive neurons in each sub-regional area was expressed as the number of cells per mm^2, by dividing the total cell count by the corresponding area measured per um^2, multiplied by 1,000,000.

6.2.16 Regions of interest for zif268

Zif268 expression was examined in the retrosplenial cortex, dorsal hippocampus, dorsal subiculum and prelimbic cortex (see Figure 6.6), as well as in the auditory cortex (control region; see Figure 6.6). Zif268 positive cell counts were made separately for the superficial and deep granular b and dysgranular regions of the retrosplenial cortex, layers 2, 3, 5, and 6 of the prelimbic cortex and hippocampal areas CA1, CA3, hilus of the DG and the dentate gyrus.

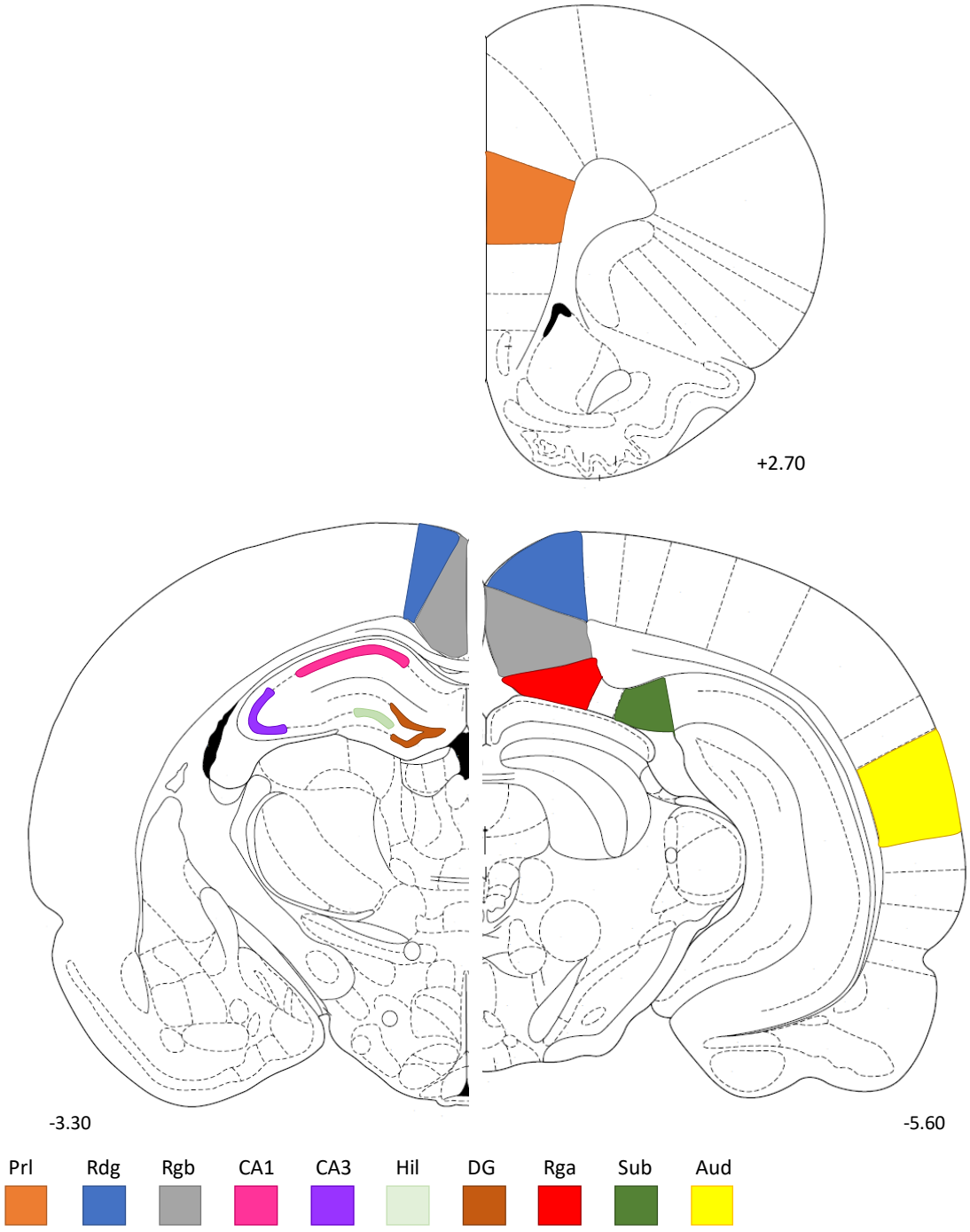

Figure 6.6. Regions of interest for zif268 immunostaining. Atlas plates from Paxinos & Watson (1998) indicating the relative location (from bregma) of the cortical and hippocampal regions of interest. Abbreviations: Prl= prelimbic cortex; Rdg= dysgranular retrosplenial cortex; Rgb= granular b retrosplenial cortex; CA1= CA1 of the hippocampus; CA3= CA3 of the hippocampus; Hil= hilus of the DG; DG= dentate gyrus; Rga= granular a retrosplenial cortex; Sub= subiculum; Aud= auditory cortex. +2.70, -3.30 and -5.60 denote distance in mm from bregma.

6.2.17 Data Analysis

Repeated measures ANOVA were used for behavioural data (between subjects factor= Group; repeated measures factor= Block) and comparisons of immediate early gene zif268 expression in the hippocampus, subiculum, retrosplenial, medial prefrontal and auditory cortex. Lesion effects were analysed in each brain region separately with additional repeated measures factors as required. Significant interaction terms were examined with separate ANOVAs of conditions x and y. Given the significance of original interaction terms we did not Bonferroni correct the resultant p values. These separate ANOVAs are referred to as post-hoc ANOVAs as they are justified by the original ANOVA.

Similarly, repeated measures ANOVA was used for analysis of each individual electrode (PSD) and each pair of structures (coherence), with the between subjects factor of Group (MTT, PCFx or SHAM) and the repeated measures factor of Block. Post-hoc analyses were carried out using split repeated measures ANOVAs. The critical alpha value was set at 0.05 for all statistical tests.

Electrophysiological data were analysed in Neuroexplorer using the power spectra and coherence analyses. Neuroexplorer calculated a standard power spectrum using the Welsh periodogram method. Our focus on theta band was driven by the involvement of theta in memory. The frequency band analysed was from 2-14 Hz, thus encompassing the conventional theta band in rats (see Chapter 1). This bandwidth includes some lower frequency bands (frontal delta rhythmicity not linked to HPC theta) and higher frequency bands (frontal rhythmicity similar to human alpha frequency, linked to HPC).

The focus for electrophysiological data was the ‘choice’ epoch, the epoch during which the rat is choosing whether to go down an arm or not and defined here as a 500 ms epoch beginning 700 ms prior to the rat crossing the first beam break, before it begins running down any given arm (see Figure 6.7). Due to the possibility that electrophysiological activity may differ between correct and incorrect choices, but as Sham rats made relatively fewer errors, LFP and coherence data were only analysed from epochs when rats made a correct arm choice. The last eight correct choice epochs were analysed across rats to ensure the same number of correct choices were analysed per rat. Repeated measures ANOVA (with 30 frequencies) was used for analysis of each individual electrode (PSD) and each pair of structures (coherence).

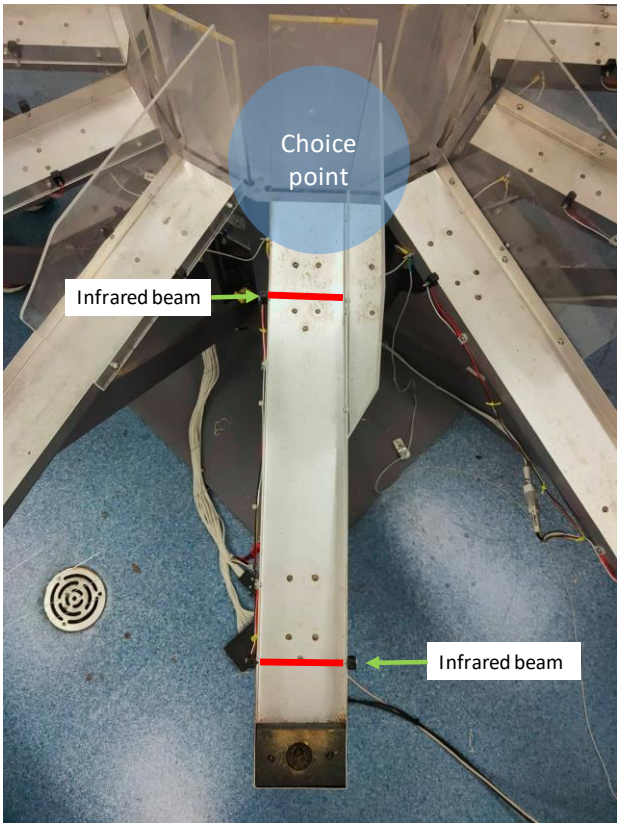

Figure 6.7. Location of infra-red beams and choice point used during RAM testing.

6.3 Results

6.3.1 Lesion verification

Six of the ten rats given descending PCFx lesions met the criterion of 100% bilateral transection of the tract based on Luxol blue and cresyl violet histology. The successful lesions were all complete lesions (100% bilateral damage to the tract; see Figure 6.8). The excluded PCFx lesion rats included two with complete unilateral lesions but only 10% (left PCFx) and 55% contralateral damage (right PCFx), respectively; and two rats with partial damage bilaterally (61% left and 62% right-sided damage; and 53% left and 59% right-sided damage, respectively). Nine of the twelve rats in the MTT lesion group met the inclusion criterion of at least 80% transection bilaterally of the tract (see Figure 6.8). Eight of the included MTT lesion rats had 100% bilateral lesions; the ninth exhibited 85% damage on the left and 100% damage on the right. The three excluded MTT lesion rats had complete unilateral MTT damage but only 30%, 28% and 21% (respectively) damage on the contralateral side.

None of the included MTT or PCFx lesions had observable damage to supramammillary nuclei, mammillary bodies or mammillotegmental tract. There was also no

evidence of damage to the mammillary bodies as the furthest extent of lesion damage in the MTT (-3.80 from Bregma), and especially the PCFx (-3.60 from Bregma) groups did not extend posterior enough to impact the MB (observable from -4.20 from Bregma). All ten Sham rats were included. In addition, due to surgical complications one MTT lesion rat and two PCFx lesion rats died surgery.

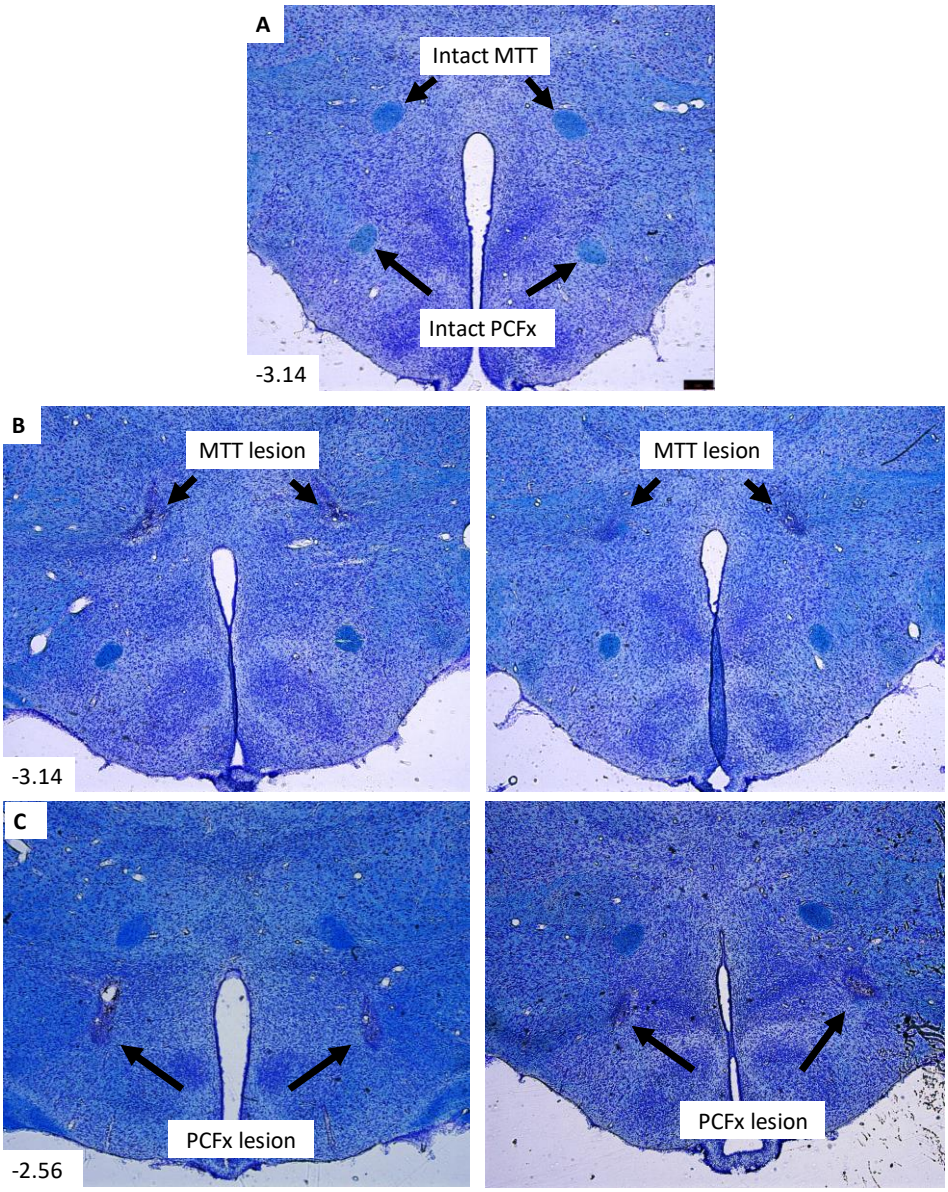

Figure 6.8. Photomicrographs of luxol blue (myelin specific) and cresyl violet (Nissl stain) counter-stained sections. Coordinates are from bregma. (A) Example of a Sham lesion, showing intact MTT and PCFx; (B) An example of the largest (100% bilateral damage; left) and smallest (85% damage left and 100% damage right; right) bilateral MTT lesion; (C) An example of the largest (left) and smallest (right) total PCFx lesion. Abbreviations: MTT= mammillothalamic tract; PCFx= descending post-commissural fornix.

6.3.2 Electrode verification

ATN electrode

The anteroventral and dorsal anteromedial regions were the primary targets for electrode placement due to their involvement in the diencephalic-hippocampal theta circuit (Vertes, Albo & Di Prisco, 2001). Electrodes located in the stria medullaris and anterodorsal nucleus were removed from data analysis, particularly as the anterodorsal nucleus is implicated in the lateral head direction circuit (see Chapter 2, section 2.5 for further information on the distinction between the head direction and theta circuits).

In total, 14 of the 18 bilateral ATN electrodes in the included MTT rats were located within the target anteroventral and dorsal anteromedial regions. Of the four excluded electrodes, three were located in the AD or along the AD-SM border, and one was located in the DG of the dorsal HPC (see Figure 6.9). All the included Sham and PCFx rats had ATN electrodes located in the target region.

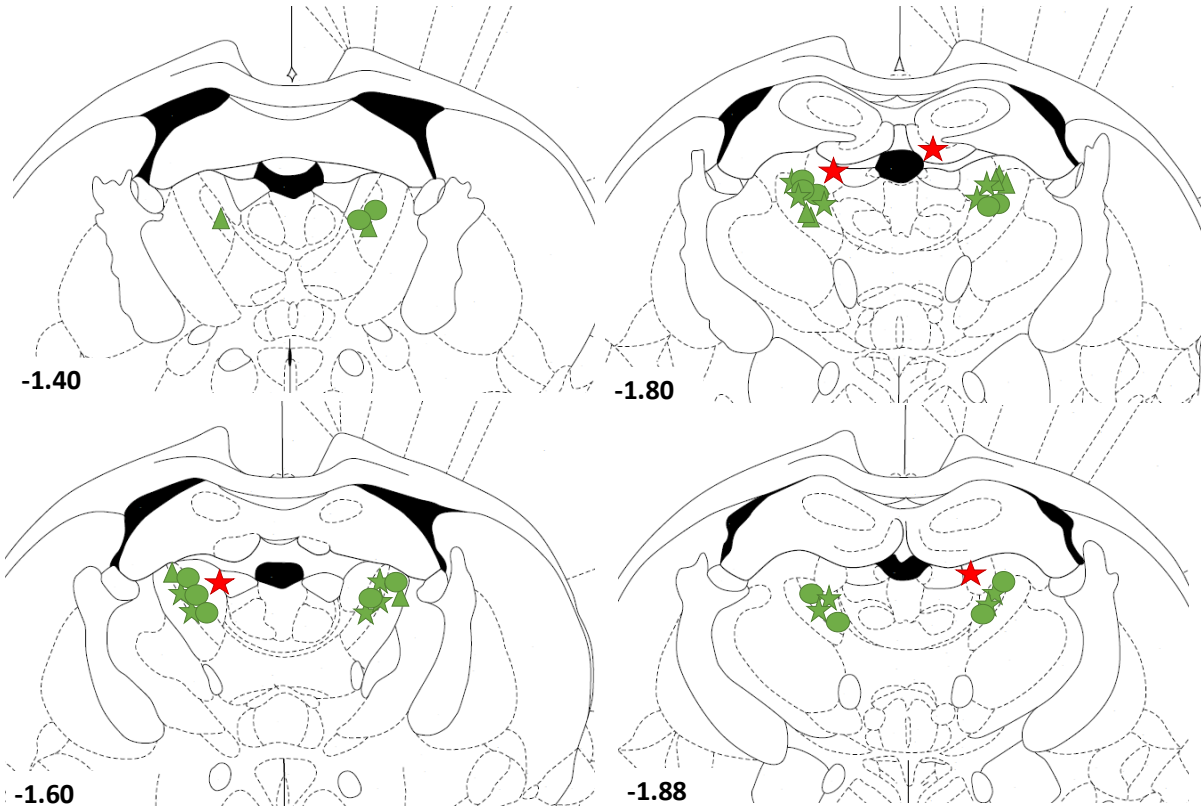

Figure 6.9. Coronal atlas plates through the AV indicating the approximate placement of electrodes for the MTT (star), PCFx (triangle) and Sham (circle) groups. Included electrodes are shown in green, excluded electrodes are shown in red; some placements overlap.

HPC electrode

The dorsal hippocampal target was the striatum lacunosum moleculare of CA1, due to its documented oscillatory output in the theta band (Buzsaki, 2002). As a result of the inversion of phase that occurs along the dorso-ventral aspect of the HPC, only those electrodes located in area CA1 but above the dorsal blade of the DG were included. Figure 6.10 shows that ten out of 20 bilateral electrodes were excluded in the Sham group, 9 out of 18 bilateral electrodes were excluded in the MTT group and 3 out of 12 were excluded in the PCFx group. This left a total of one HPC electrode per rat in the Sham and MTT groups. Three rats in the PCFx group had correct bilateral HPC placement and three had only correct unilateral placement. All excluded electrodes were removed from analyses due to their placement being too ventral in HPC, either at or below the dorsal blade of the DG (see Figure 6.10).

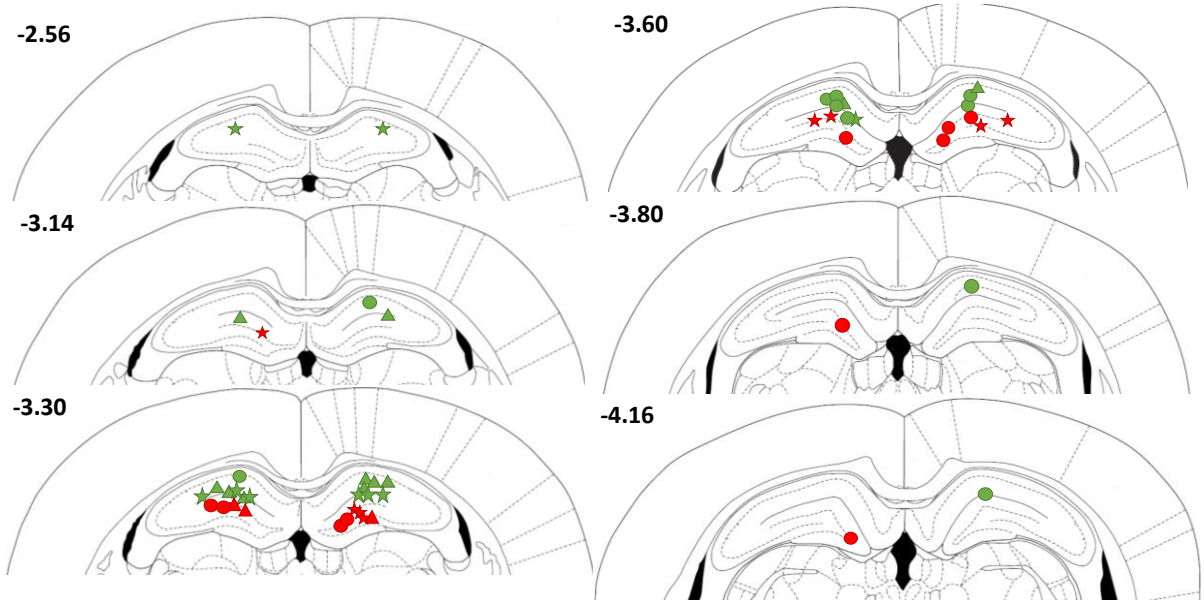

Figure 6.10. Coronal atlas plates showing the approximate location of electrodes in the dorsal hippocampus in the MTT (star), PCFx (triangle) and Sham (circle) groups. Included electrodes are shown in green, excluded electrodes are shown in red.

Medial prefrontal electrode (mPFC)

The primary target for the mPFC electrode was the infralimbic and prelimbic cortices (see Figure 6.11). In all cases, the mPFC electrodes were located within one of these two target regions (see Figure 6.12). In the MTT, PCFx and Sham groups all mPFC electrodes were located in the prlimbic cortex.

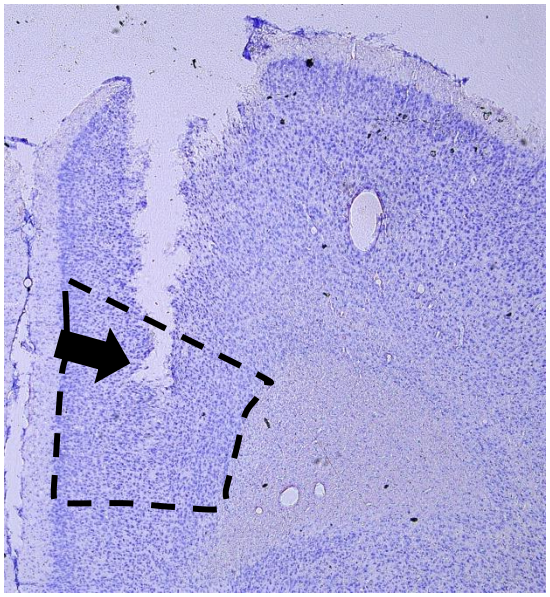

Figure 6.11. Photograph of a PFC section stained with cresyl violet showing an electrode placement in the prelimbic cortex (black arrow). The outline of the prelimbic cortex is shown by a dashed black line.

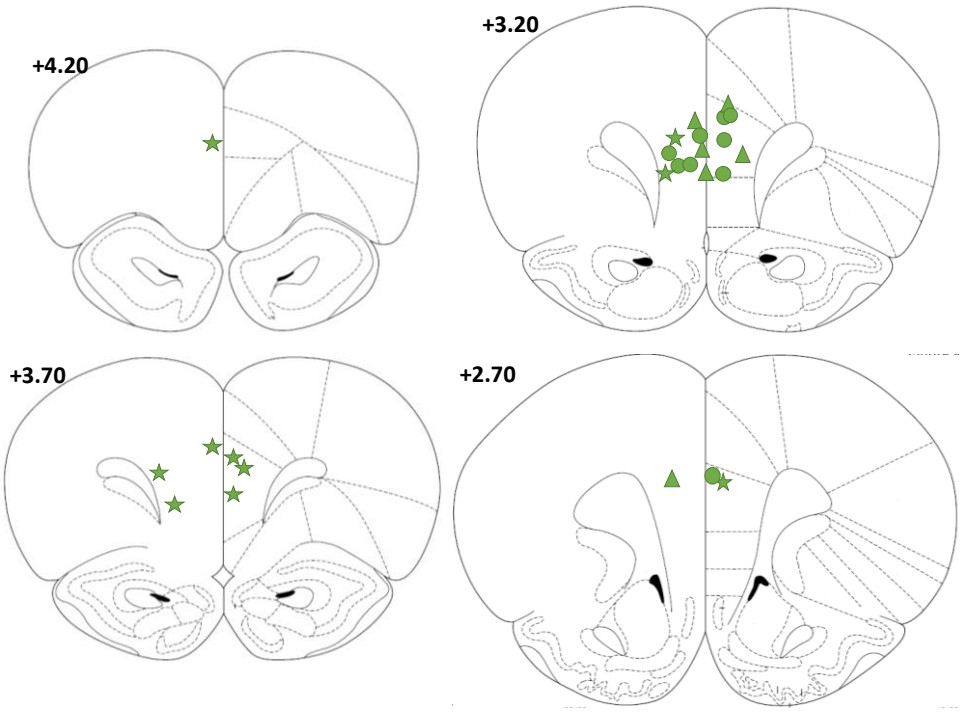

Figure 6.12. Coronal atlas plates indicating the approximate location of electrodes in the medial prefrontal cortex in the MTT (star), PCFx (triangle) and Sham (circle) groups. All electrodes were included electrodes and are shown in green.

6.3.3 Spatial working memory in the 12-arm radial arm maze (RAM)

As shown in Figure 6.13 (panel A), both lesion groups showed minimal, if any, improvement in spatial working memory in the 12-arm maze across training blocks, and equally poor

performance; whereas the Sham group showed steadily improving performance (Group x Block [lin], F(2, 22)=14.05, p<0.001). Overall, the Sham group made fewer errors (Group, F(2,22)=22.77, p < 0.001) than both the PCFx and MTT lesion groups (Newman-Keuls post-hoc: PCFx vs Sham, p<.001; MTT vs Sham, p<0.001). Neither Lesion group improved significantly over Blocks (post-hoc PCFx data only, Block[lin], F(1,5)=2.88, p=0.15; post-hoc MTT data only, Block[lin], F(1,8)=4.48, p=0.07), whereas the Sham group showed significant improvement over time (post-hoc Sham data only, Block[lin], F(1,9)= 27.47, p=0.001).

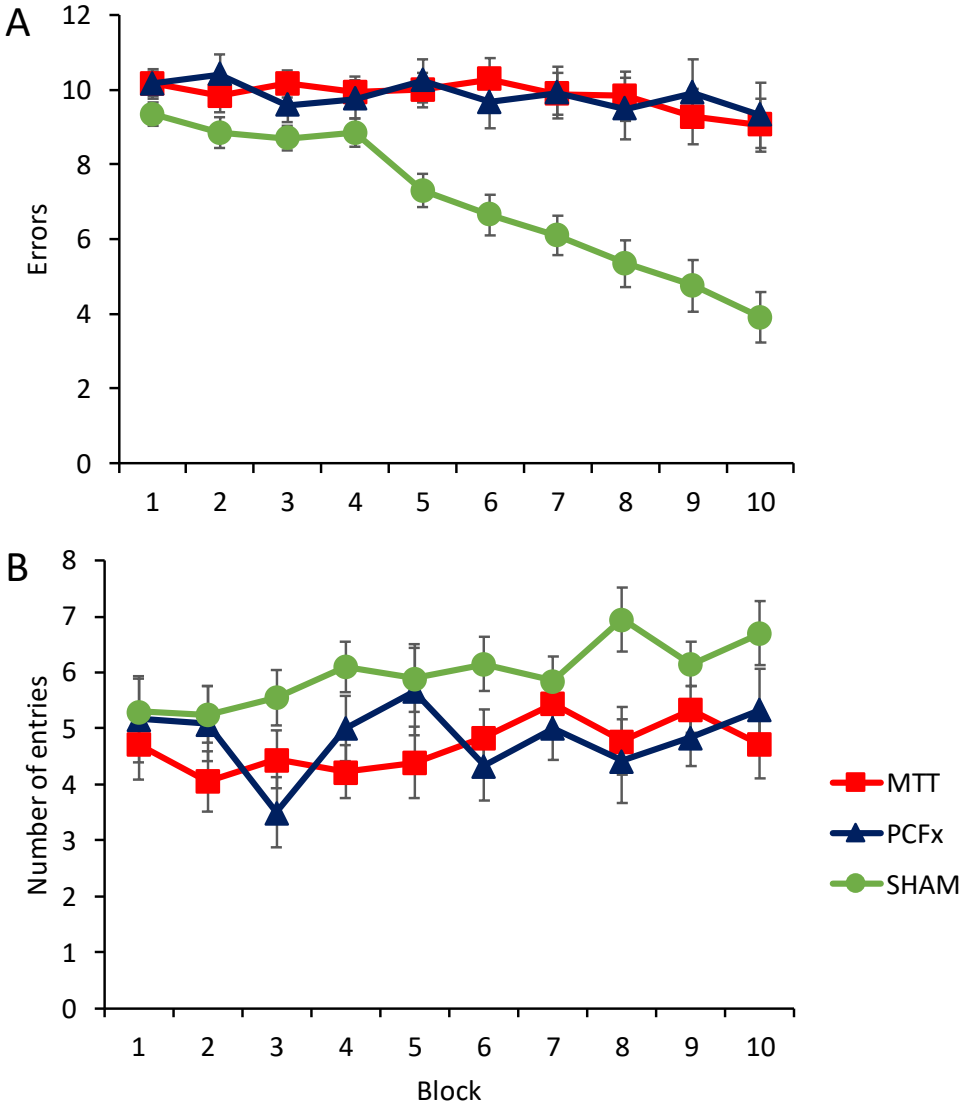

Figure 6.13. Behavioural performance across 10 two-day blocks during acquisition training after electrode surgery. A) Mean ± SE of errors across blocks. B) Average number of correct entries made before the first error across blocks. Abbreviations: MTT=mammillothalamic tract lesion group; PCFx= post-commissural fornix lesion group; SHAM= Sham lesion group.

The Sham group also made consistently more entries before making the first error (Group, F(2,22)=9.39, p = 0.001) compared to both MTT groups (Newman-Keuls post-hoc: PCFx vs Sham, p=.004; MTT vs Sham, p=.004) (see Figure 6.13, panel B). Overall, no group showed significant improvement across test (Block[lin], (F(1,22) = 3.24, p = 0.09), and there was no Group by Block interaction (Group x Block[lin], F(2, 22) = 0.63, p = 0.54).

Running speed was measured between beam breaks on the arms and did not differ between Sham, PCFx and MTT groups (Group, F(2,21) = 2.78, p = 0.09; Group x Block[lin], F(18,198) = 0.92, p = 0.41; mean and SD per group across the 10 blocks: SHAM, Mean = 0.65, SD = 0.06; MTT, Mean =0.69, SD = 0.06; PCFx, Mean = 0.66, SD = 0.06) (see Figure 6.14).

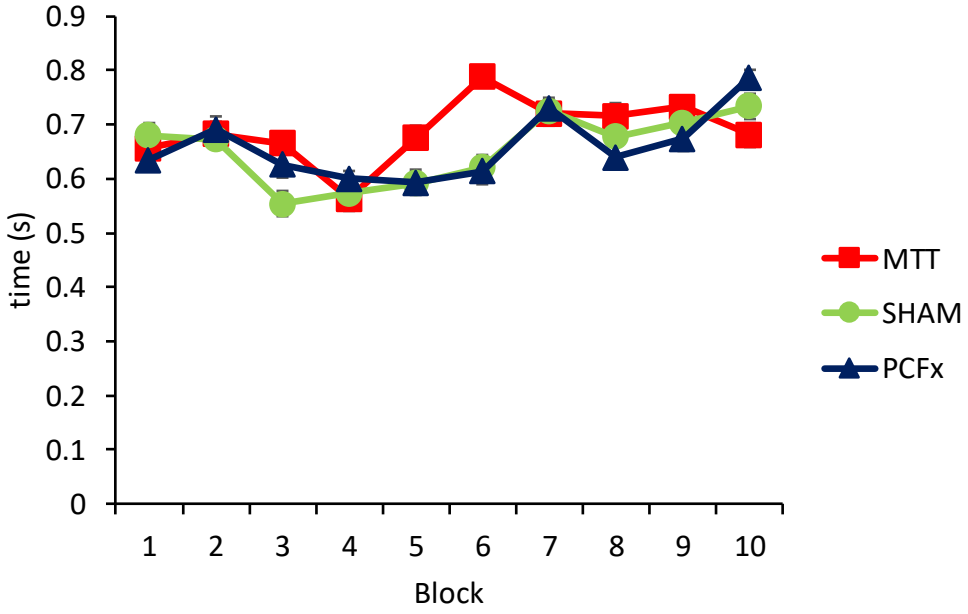

Figure 6.14. Time taken to run from the first to the second beam across 10 two-day blocks. Abbreviations: MTT=mammillothalamic tract lesion group; PCFx= post-commissural fornix lesion group; SHAM= Sham lesion group.

By the final 2 blocks of testing (Block 9 and 10), MTT rats were making on average between 9.0 and 9.5 errors, PCFx rats were making between 9.5 and 10.0 errors, and Sham rats were making between 3.9 and 4.8 errors. The average number of errors made in Blocks 9 and 10 by lesion rats that had been excluded from analyses due to incomplete lesions of the PCFx or MTT is shown in Table 6.2 and suggests an intermediate level of impairment in those rats with partial damage.

Table 6.2. Average number of errors made by excluded MTT and PCFx lesion rats in blocks 9 and 10.

Group	Damage	Block 9	Block 10
MTT	100% Unilateral damage + partial damage to the contralateral side	7.5	8.0
MTT	100% Unilateral damage + partial damage to the contralateral side	7.5	8.0
MTT	100% Unilateral damage + partial damage to the contralateral side	9.0	9.5
PCFx	100% Unilateral damage + partial damage to the contralateral side	6.0	7.5
PCFx	Partial bilateral sparing	5.5	8.0
PCFx	Partial bilateral sparing	8.0	7.5
PCFx	100% Unilateral damage + partial damage to the contralateral side	10.0	9.0

6.3.4 Electrophysiological activity during correct arm choices across the last 5 days of working memory testing: *Power spectral density (PSD)*

An omnibus repeated measures ANOVA was run including all electrodes, with electrode as a repeated measure. PSD for each electrode is graphed separately, to allow easy relation to post-hoc testing, in Figure 6.15.

There was variation in PSD across electrodes with regards to the peak (in the region of 8.5 Hz) and a largely linear trend in PSD across frequency. For all electrodes there was a decrease in PSD with frequency. This downward linear trend in PSD was noticeably less in the Sham than the other two groups, and the difference between groups decreases steadily across electrodes (ordered as ATN then HPC then PFC) (Electrode x Group x Freq[lin], $F(2, 19) = 4.88$, $p = 0.02$). Due to the significant differences in PSD between electrodes, post-hoc split ANOVAs were run in order to clarify the effects at each electrode separately.

To test for any reliable changes across the 5 days, an ANOVA was run on each electrode. No changes across days were found in the ATN electrode (Day, $F(1,19) = 0.53$, $p = 0.47$; Day x Group, $F(2,19)=0.35$, $p=0.71$), the HPC electrode (Day, $F(1,19)=0.52$, $p=0.48$; Day x Group, $F(2,19)=2.87$, $p=0.08$) and PFC electrode (Day, $F(1,19)=1.12$, $p=0.30$; Day x Group, $F(2,19)=1.11$, $p=0.35$). For further analyses, therefore, PSD for the last five days was collapsed across days to give an average PSD value.

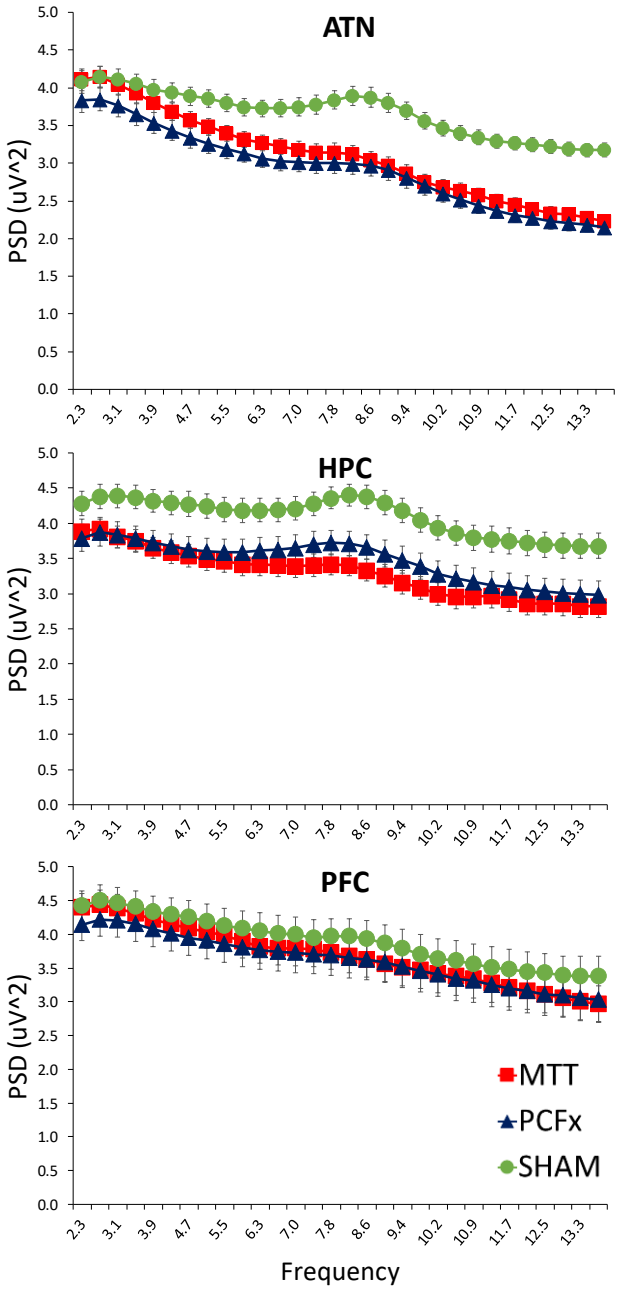

Figure 6.15. PSD ± SE in the ATN (top), HPC (middle) and PFC (bottom) across the final 5 days of testing. Abbreviations: MTT= mammillothalamic tract lesion group; PCFx= post-commissural fornix lesion group; SHAM= Sham lesion group.

ATN post-hoc test (Figure 6.15, top panel): Both MTT and PCFx lesions reduced global (i.e. averaged across frequency) PSD compared to Sham rats (Group, $F(2,19)=11.94$, $p=0.001$). Whilst PSD in Sham rats clearly differs from both lesion groups (post-hoc Sham and PCFx data only, Group, $F(1,11)=13.46$, $p=0.004$; post-hoc Sham and MTT data only, $F(1,13)=11.21$, $p=0.005$), the MTT group also exhibited higher PSD than the PCFx rats (post-hoc PCFx vs MTT data only, $F(1,12)=5.56$, $p=0.036$).

The slope is steeper in both lesion groups compared to Shams, reflecting that both MTT and PCFx lesions cause a greater linear decrease in PSD across the frequency band than Sham rats (Group x Freq[lin], $F(2,19)=33.25$, $p<0.001$). Furthermore, in Figure 6.15 it can also be seen that both lesions reduce peak PSD, observable in Sham rats ~8.5 Hz (Group x Freq[quad], $F(2,19)=12.80$, $p<0.001$), although the reduced peak PSD is greatest in the MTT group (post-hoc MTT and Sham data only, Group x Freq[quad], $F(1, 13)=21.24$, $p<0.001$; post-hoc PCFx and Sham data only, Group X Freq[quad], $F(1,11)=8.90$, $p=0.012$). There was no difference in peak PSD between the two lesion groups (post-hoc PCFx and MTT data only, Group x Freq[quad], $F(1,12)=3.09$, $p=0.10$).

HPC post-hoc test (Figure 6.15, middle panel): Both MTT and PCFx lesions reduced global PSD compared to Sham rats (Group, $F(2,19)=6.80$, $p=0.006$). However, the greatest reduction in PSD was observed in the MTT group (post-hoc MTT and Sham data only, Group, $F(1,13)=16.42$, $p=0.001$; post-hoc PCFx and Sham data only, Group, $F(1,11)=4.985$, $p<0.05$). Furthermore, the MTT and PCFx rats did not differ (post-hoc MTT and PCFx data only, Group, $F(1,12)=0.61$, $p=0.45$).

Peak PSD is observable in the Sham group at ~8.5 Hz (Group x Freq[quad], $F(2,19)=3.96$, $p=0.04$). The peak in PSD is reduced by MTT lesions (post-hoc MTT and Sham data only, Group x Freq [quad], $F(1,13)=23.70$, $p<0.001$), but not by PCFx lesions (post-hoc PCFx and Sham data only, Group x Freq[quad], $F(1,11)=0.07$, $p=0.80$), relative to Shams. Although not significant, a trend for a reduced peak PSD is also observable in the MTT group relative to PCFx rats (post-hoc PCFx and MTT data only, Group x Freq[quad]=3.45, $p=0.088$).

PFC post-hoc test (Figure 6.15, bottom panel): Any lesion-associated reduction in PFC PSD was much less than for the ATN and HPC and was not statistically significant (Group, $F(2,19)=0.30$, $p=.75$; Group x Freq[lin], $F(2,19)=0.80$, $p=0.47$).

6.3.5 Electrophysiological activity during correct arm choices across the last 5 days of working memory testing: *Coherence*

The individual electrode pairs were each submitted to an ANOVA to test for any reliable changes across days. No changes across days were found between the HPC and ATN (Day, $F(1,19)= 3.65$, $p=0.7$; Day x Group, $F(2,19)=0.36$,$p=0.70$), ATN and PFC (Day, $F(1,19)=0.04$, $p=.85$; Day x Group, $F(2,29)=1.00$, $p=0.39$) or the HPC and PFC (Day, $F(1,19)=0.04$, $p=0.84$;

Day x Group, F(2,19)=0.28, p=0.76). For further analyses, therefore, coherence for the last five days was collapsed across days to give an average coherence value.

An omnibus repeated measures ANOVA was run including all electrode pairs. These are graphed separately, to allow easy relation to post hoc testing, in Figures 6.15, 6.16 and 6.17.

There is a complex variation of coherence across frequencies that decreases steadily across electrode pairs (ordered as ATN-HPC then HPC-PFC then PFC-ATN). The strongest variation in coherence across the frequency band (with a clear peak in the region of 8.5 Hz) is seen with ATN-HPC, this becomes moderate with HPC-PFC and minimal with PFC-ATN (Pair[lin] x Freq[quad], $F(1,19)=5.93$, $p<0.03$; Pair[lin] x Freq[order 4], $F(1,19)=21.10$, $p<0.001$; Pair[lin] x Freq[order 6], $F(1,19)=28.04$, $p<0.001$; Pair[lin] x Freq[order 8], $F(1,19)=25.95$, $p<0.001$; Pair[lin] x Freq[order 10], $F(1,19)=18.62$, $p<0.001$). However, the shape of the curves was not affected by treatment group (all interactions with group $F(2,19)< 1.9$, $p>0.18$).

For all pairs there was a steady decline in coherence with frequency that was greater for the Sham than the other two groups (Group x Freq[lin] $F(2,19) = 8.55$, $p<0.002$). Due to the complex difference in trend in coherence across frequency for the different electrode pairs noted in the previous paragraph, post-hoc split ANOVAs were run in order to analyse each pair separately and, particularly, confirm the presence of the linear group trend in each case separately.

ATN-HPC post hoc test (Figure 6.16): Both MTT and PCFx lesions reduced global (i.e. averaged across frequency) ATN-HPC coherence compared to Sham rats (Group, $F(2,19)=21.50$, $p<0.001$). However there is no observable difference between the two lesions group (post-hoc PCFx and MTT data only, Group, $F(1,12)=0.14$, $p=0.72$).The greatest reduction in ATN-HPC coherence was observed in the low frequencies, where Sham coherence was highest (Group x Freq[lin], $F(2,19)=8.32$, $p=0.003$). In all groups, a peak in coherence ~8.5 Hz was observed (post-hoc 7-9 Hz data only, Freq[quad], $F(1,19)=25.59$, $p<0.001$).

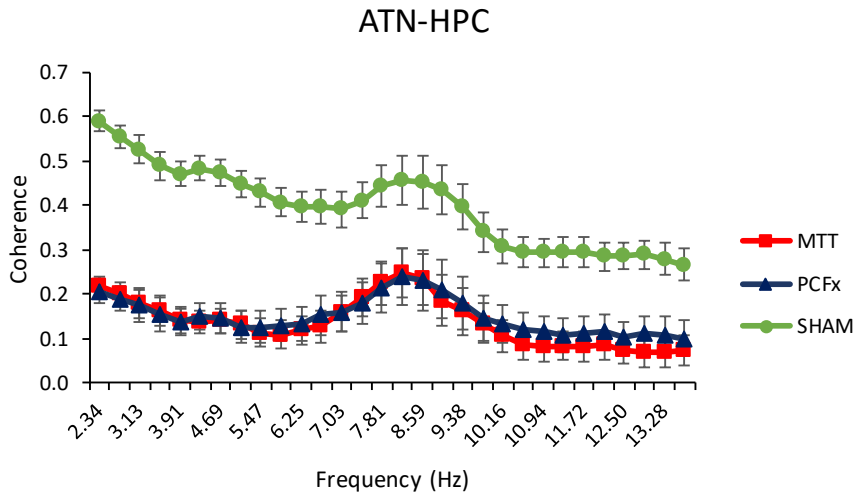

Figure 6.16. Coherence ± SE between the HPC and ATN across the final 5 days of testing. Abbreviations: MTT= mammillothalamic tract lesion group; PCFx= post-commissural fornix lesion group; SHAM= Sham lesion group.

HPC-PFC post hoc (Figure 6.17): Both MTT and PCFx lesions reduced global PFC-HPC coherence (Group, $F(2,19)=21.26$, $p<0.001$) compared to Sham rats. MTT and PCFx rats did not differ (post-hoc PCFx and MTT data only, Group, $F(1,12)=1.71$, $p=0.22$). As with ATN-HPC, the greatest lesion-associated reduction in coherence compared to Sham rats was observed in the lower frequencies, where Sham coherence was highest (Group x Freq[lin], $F(2,19)=4.36$, $p=0.03$). Similarly to in ATN-HPC coherence, a peak in coherence ~8.5 Hz is observed in all groups (post-hoc 7-9 Hz data only, Freq[quad], $F(1,19)=17.51$, $p=0.001$).

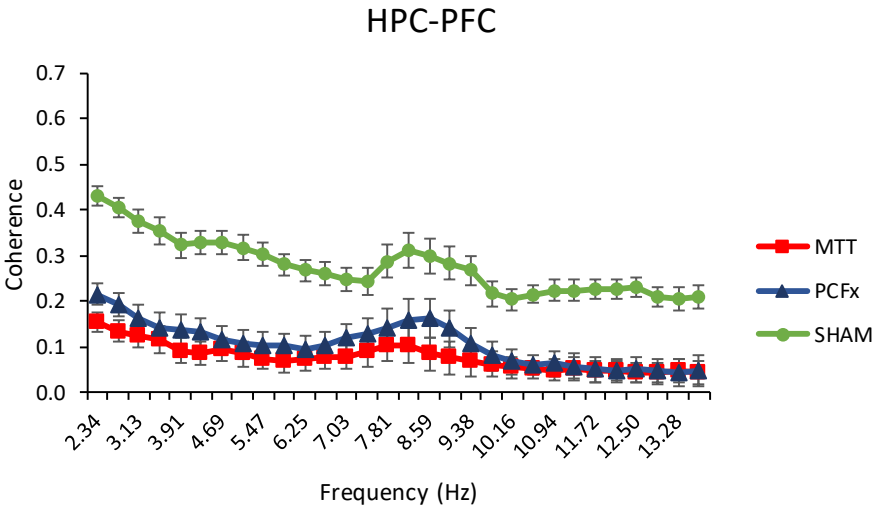

Figure 6.17. Coherence ± SE between the HPC and PFC across the final 5 days of testing. Abbreviations: MTT= mammillothalamic tract lesion group; PCFx= post-commissural fornix lesion group; SHAM= Sham lesion group.

PFC-ATN post hoc (Figure 6.18): PFC-ATN coherence was significantly reduced by both MTT and PCFx lesions compared to Sham rats (Group, $F(2,19)=43.44$, $p<0.001$). In contrast to the previous two electrode pairs, MTT lesions appeared to show lower coherence than PCFx lesions (post-hoc PCFx and MTT data only, Group, $F(1,12)=5.07$, $p=0.04$) but this difference is small as well as on the borderline of significance and does not survive Bonferroni correction ($p=0.12$). Although the absolute reduction in PFC-ATN coherence associated with both MTT and PCFx lesions is greatest at low frequencies where Sham coherence is highest (Group x Freq[lin], $F(2,19)=3.91$, $p=0.04$), the relative change within group in coherence across the frequency band is greatest at higher frequencies. Notably, the peak in coherence previously observed ~8.5 Hz between the ATN-HPC and HPC-PFC, is absent between the PFC-ATN across all groups (post-hoc 7-9 Hz data only, Freq[quad], $F(1,19)=0.53$, $p=0.51$).

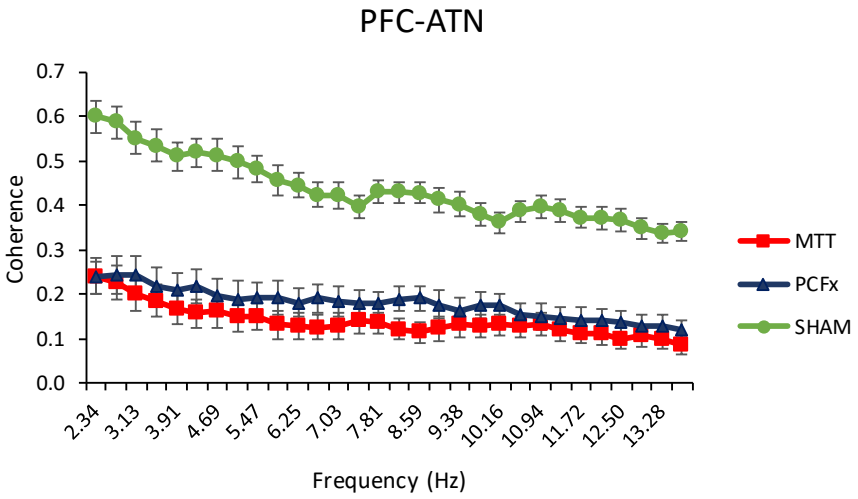

Figure 6.18. Coherence ± SE between the PFC and ATN across the final 5 days of testing. Abbreviations: MTT= mammillothalamic tract lesion group; PCFx= post-commissural fornix lesion group; SHAM= Sham lesion group.

Linear trend differences: Table 6.3 shows that, across all electrode pairs Sham rats exhibit a higher mean and steeper slope than both lesion groups reflecting the higher overall coherence observed in the Sham group in Figures 6.15, 6.16 and 6.17, as well as the greater downwards slope across the frequency band.

Table 6.3. Slope (lin) and average coherence values (mean) across the HPC-ATN, ATN-PFC and PFC-HPC in the SHAM, PCFx and MTT groups. Abbreviations: HPC=hippocampus, ATN= anterior thalamus, PFC= prefrontal cortex, Sham= Sham surgery group, PCFx= post-commissural fornix lesion group, MTT= mammillothalamic tract lesion group.

		ATN-HPC	HPC-PFC	PFC-ATN
lin	**SHAM**	**-0.0096**	**-0.0062**	**-0.0079**
	PCFx	-0.0021	-0.0044	-0.0038
	MTT	-0.0036	-0.0029	-0.0034
mean	**SHAM**	**0.5459**	**0.3742**	**0.5591**
	PCFx	0.1833	0.1743	0.2375
	MTT	0.1932	0.1221	0.1927

6.3.6 Zif268 expression

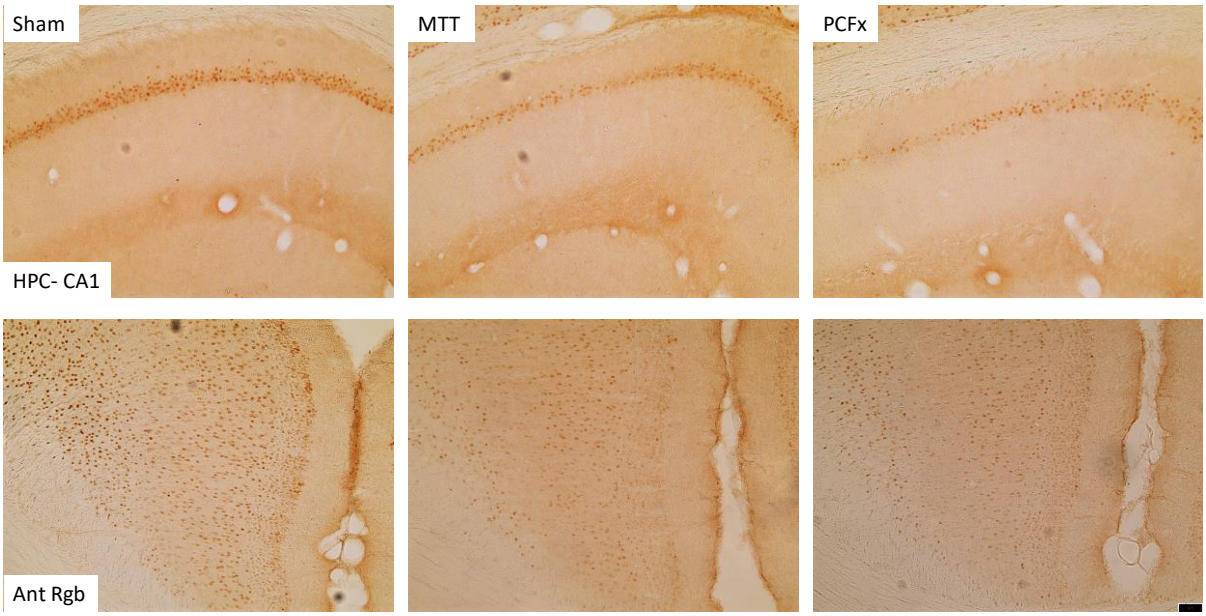

Figure 6.19. Example photographs (10x objective) of Zif268 immunostaining in the HPC and RSC. Zif268 expression shown for area CA1 of the dorsal hippocampus (top panel) and the anterior granular b retrosplenial cortex (Rgb; bottom panel) from a Sham (left), MTT (middle) and PCFx (right) rat.

Zif268 expression (Figure 6.19) after rats were tested in a forced choice RAM procedure (see Methods 6.2) was analysed separately for each region (cell counts per mm²) with post-hoc

ANOVA to determine lesion and region/layer effects when required. Raw cell counts were transformed with a square root transform in order to normalise error variance and make them suitable for analysis with ANOVA.

Retrosplenial cortex - Rgb

Both MTT and PCFx lesions reduced Zif268 expression in the Rgb (Group, $F(2,21)=22.37$, $p<0.001$), but more so in the MTT group than the PCFx group (Sham vs PCFx, $F(1,21)=5.04$, $p<0.05$; Sham vs MTT, $F(1,21)=40.59$, $p<0.001$; MTT vs PCFx, $F(1,21)=9.26$, $p<0.01$; Figure 6.20A). In terms of anterior vs posterior Rgb, higher expression was observed in the posterior (AP, $F(1,21)=44.95$, $p<0.001$), but there was also a Group x AP interaction ($F(2,21)=3.91$, $p<0.04$). Increased expression in the posterior Rgb was evident in both Sham and PCFx groups (Sham, $F(1,21)=22.05$, $p<0.001$; PCFx, $F(1,21)=21.11$, $p<0.001$), but not in the MTT group (MTT, $F(1,21)=2.07$, $p=0.16$). Compared to the Sham group, both MTT and PCFx lesions reduced Zif268 expression in the anterior Rgb (MTT, $F(1,21)=34.35$, $p<0.001$; PCFx, $F(1,21)=12.11$, $p<0.01$), but reduced expression in the posterior Rgb was only present in the MTT group (MTT, $F(1,21)=28.28$, $p<0.001$; PCFx, $F(1,21)=1.12$, $p=0.29$). Higher Zif268 cell counts in the superficial layers relative to deep layers of the Rgb (Layer, $F(1,21)=4.47$, $p<0.05$) was only evident in the Sham group (Layer x Group, $F(2,21)=3.58$, $p<0.05$; Sham only, $F(1,21)=12.82$, $p<0.01$). Compared to the Sham group, MTT lesions reduced Zif268 expression in both superficial and deep layers (Superficial, $F(1,21)=39.54$, $p<0.001$; Deep, $F(1,21)=28.61$, $p=<0.001$), whereas PCFx lesions only reduced expression in the superficial layers (Superficial, $F(1,21)=5.92$, $p<0.03$; Deep, $F(1,21)=2.61$, $p=0.12$). Although the Group x Layer x AP interaction was not significant ($F(1,21)=0.77$, $p=0.47$), higher Zif268 expression in the superficial layer in the Sham group was only evident in the posterior region (Sham only, Layer effect in the anterior Rgb, $F(1,21)=0.11$, $p=0.73$; Layer effect in the posterior Rgb, $F(1,21)=14.72$, $p<0.001$).

Retrosplenial cortex - Rdg

Only MTT lesions significantly reduced overall Zif268 expression in the Rdg relative to the Sham group (Group, $F(2,21)=7.42$, $p<0.005$; Sham vs MTT, $F(1,21)=14.08$, $p=0.001$; Sham vs PCFx, $F(1,21)=2.91$, $p=0.10$), but the two lesion groups did not significantly differ (MTT vs PCFx, $F(1,21)=1.99$, $p=0.17$). In terms of anterior vs posterior Rdg, higher cell counts were observed in the posterior Rdg irrespective of group (AP, $F(1,21)=13.79$, $p=0.001$; AP x Group,

F(2,21)=0.34, p=0.71; Figure 6.20A). Although higher Zif268 counts were evident in the superficial layers relative to deep layers (Layer, F(1,21)=52.13, p<0.001), this was only evident in the anterior Rdg (AP x Layer, F(1,21)=8.28, p<0.01; Anterior, F(1,21)=102.42, p<0.001; Posterior, F(1,21)=1.88, p=0.18). Compared to the Sham group, both MTT and PCFx lesions reduced Zif268 expression in the superficial and deep layers of the anterior but not posterior Rdg (AP x Layer x Group, F(1,21)=4.79, p<0.02; Anterior superficial Rdg, MTT, F(1,21)=56.72, p<0.001; Anterior superficial Rdg, PCFx, F(1,21)=14.45, p<0.001; Anterior deep Rdg, MTT, F(1,21)=4.60, p<0.05; Anterior deep Rdg, PCFx, F(1,21)=5.09, p<0.05; Posterior superficial Rdg, MTT, F(1,21)=1.31, p=0.26; Posterior superficial Rdg, PCFx, F(1,21)= 0.07, p=0.78; Posterior deep Rdg, MTT, F(1,21)=3.00, p=0.10; Posterior deep Rdg, PCFx, F(1,21)= 0.28, p=0.59).

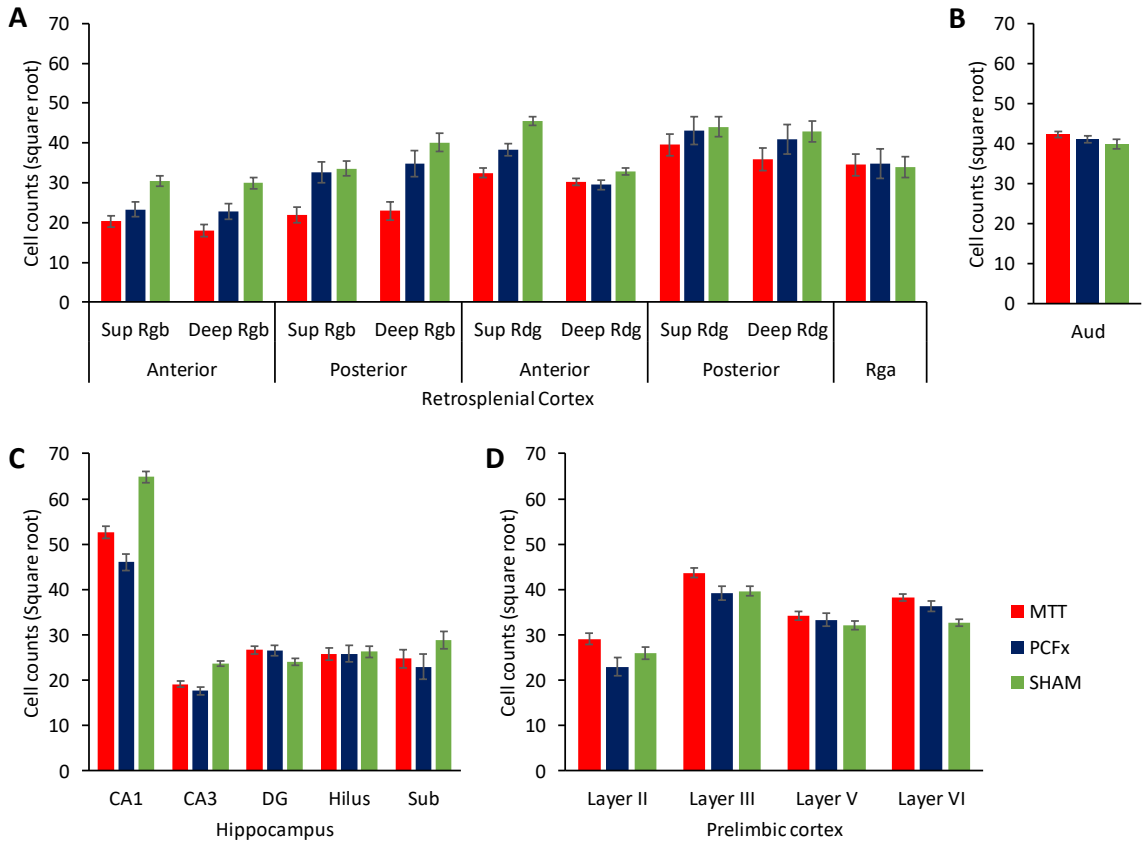

Figure 6.20. Mean ± SE of square root of Zif268 cell counts for MTT, PCFx and Sham groups across the subregions of the anterior and posterior retrosplenial cortex (A), auditory cortex (B), hippocampal subregions (C) and prelimbic cortex (D). Abbreviations: Aud= auditory cortex; CA1= area CA1 of the hippocampus; CA3= area CA3 of the hippocampus; DG= dentate gyrus; Hilus= hilus of the DG; Rga= granular a retrosplenial cortex; Rgb= granular b retrosplenial cortex; Rdg= dysgranular retrosplenial cortex; Sub= dorsal posterior subiculum; sup= superficial.

Retrosplenial cortex - Rga

No group main effect was observed in the Rga (Group, $F(2,21)=0.03$, $p=0.97$; Figure 6.20A).

Hippocampus and Subiculum

Overall, both MTT and PCFx lesions reduced Zif268 expression in the hippocampus relative to the Sham group (Group, $F(2,22)=35.54$, $p<0.001$), but more so in the PCFx group than the MTT group (MTT, $F(1,22)=64.68$, $p<0.001$; PCFx, $F(1,22)=101.82$, $p<0.001$; PCFx vs MTT, $F(1,22)=10.74$, $p<0.005$). As shown in Figure 6.20C, the highest Zif268 immunoreactivity was observed in area CA1 of the hippocampus (Region, $F(1,22)=455.53$, $p<0.001$). Both MTT and PCFx lesions reduced expression in hippocampal areas CA1 and CA3 relative to Sham rats (Region x Group, $F(2,22)=15.72$, $p<0.001$), but only MTT lesions reduced Zif268 expression in the DG (CA1, MTT vs Sham, $F(1,22)=50.89$, $p<0.001$; CA1, PCFx vs Sham, $F(1,22)=77.68$, $p<0.001$; CA3, MTT, $F(1,22)=26.72$, $p<0.001$; CA3, PCFx, $F(1,22)=30.84$, $p<0.001$; DG, MTT, $F(1,22)=4.68$, $p<0.05$; DG, PCFx, $F(1,22)=2.61$, $p=0.12$). Neither MTT nor PCFx lesions altered Zif268 expression in the hilus of the DG (MTT, $F(1,22)=0.03$, $p=0.86$; PCFx, $F(1,22)=0.02$, $p=0.87$). Although both PCFx and MTT lesions appear to reduce activity in the subiculum, the main effect of group did not reach significance (Group, $F(2,21)=1.91$, $p=0.17$; Figure 6.20C).

Prelimbic Cortex

Unlike the pattern of lesion effects observed in the retrosplenial cortex and hippocampus, MTT lesions increased Zif268 activation across the prelimbic cortex relative to the Sham and PCFx group (Group, $F(2,19)=8.79$, $p=0.002$; MTT vs Sham, $F(1,19)=16.19$, $p<0.001$; MTT vs PCFx, $F(1,19)=7.06$, $p<0.02$; Sham vs PCFx, $F(1,19)=0.25$, $p=0.62$; Figure 6.20D). The highest Zif268 cell counts were observed in prelimbic layer III (Layer, $F(1,19)=42.33$, $p<0.001$; Layer III vs Layers II, V and VI, $F(1,19)=144.61$, $p<0.001$). Although the Region x Group interaction was non-significant, both MTT and PCFx lesions appeared to increase Zif268 expression in Layer VI of the prelimbic cortex relative to the Sham group (Region x Group, $F(6,57)=2.14$, $p=0.06$; MTT, $F(1,19)=29.48$, $p<0.001$; PCFx, $F(1,19)=7.21$, $p<0.02$).

Auditory cortex

No group differences were found in this “control” region (Group, $F(2,22)=1.69$, $p=0.21$) (see Figure 6.20B).

6.4 Discussion

This Chapter is the first to demonstrate that lesions of the PCFx impair memory to a similar extent as MTT lesions in the 12-arm RAM. Moreover, this Chapter showed that both MTT and PCFx lesions disrupt rhythmic interactions between three key memory structures. Specifically, both lesions reduced spectral power in the ATN and HPC, and reduced coherence between the ATN, HPC and PFC during correct choice epochs. These findings suggest that aberrant oscillatory activity may contribute to the memory deficits observed in cases of diencephalic amnesia.

The anatomical connectivity of the MTT and PCFx suggests that both fibre tracts are critically involved in memory (Poletti & Creswell, 1977; Aggleton, 2012), and this is reinforced by clinical evidence (Van der Werf et al., 2000, 2003; Carlesimo et al., 2011, 2014; Christiansen et al., 2016; Coad et al., 2020). However, animal lesion studies have shown that whilst MTT lesions are consistently associated with memory deficits (Vann & Aggelton, 2003; Vann, 2013; Perry et al., 2018; Dillingham et al., 2019), transection of the PCFx results in negligible behavioural impairments (Vann et al., 2011; Vann, 2013). In the current Chapter, both MTT and PCFx lesions showed sustained impairment across the 20 days of testing in the RAM, whilst the Sham lesion group showed improved performance from day 8.

In addition to the severe memory deficits observed, both MTT and PCFx lesions resulted in a consistent reduction in PSD in the ATN and HPC, but not the PFC, during correct choice epochs. In the ATN, both lesions reduced the peak in PSD at ~8.5 Hz, although this was to a greater extent in the MTT group than the PCFx group. In the HPC, only MTT lesions reduced the 8.5 Hz peak in PSD. These findings are consistent with previous work, showing that MTT lesions reduced hippocampal peak theta frequency across 6-12 Hz during locomotion (Dillingham et al., 2019). A steady linear decrease in variation in coherence was observed across electrode pairs. The steady decrease in signal (i.e. peak coherence) is consistent with the ATN sending input to the HPC and then from the HPC to the PFC, with signal attenuation at each step and with minimal return signal from the PFC to the ATN. MTT and PCFx lesions also resulted in a profound reduction in coherence between the ATN-HPC, HPC-PFC and PFC-ATN, with the greatest reduction occurring at the lower frequencies where Sham coherence was highest. A peak in coherence was observed at ~8.5 Hz in all

groups between the ATN-HPC and HPC-PFC, but not the PFC-ATN. These novel findings suggest that damage to the MTT and PCFx results in oscillatory dysfunction across key memory structures within an extended neural network.

The present Chapter also examined the effects of MTT and PCFx lesions on immediate early gene activity. As the effects of PCFx lesions have only been previously examined in one study which used c-Fos as a marker of neuronal activation (Vann, 2013), the current Chapter provided novel insight into the effect of PCFx lesions on Zif268 expression. MTT lesions reduced IEG activation in subregions of the RSC, HPC and prelimbic cortex (Vann & Albasser, 2009; Vann, 2013; Frizzati et al., 2016; Perry et al, 2018), with the most prominent reductions observed in the RSC (Vann & Albasser, 2009; Dupire et al., 2013; Mendez-Lopez et al., 2013; Vann, 2013; Harland et al., 2014; Frizzati et al., 2016; Perry et al., 2018). More specifically, MTT lesions reduced Zif268 expression in the anterior and posterior superficial and deep layers of the Rgb, as well as the superficial layers of the anterior and posterior Rdg, replicating previous findings (Vann, 2013; Frizzati et al., 2016; Perry et al., 2018). Additionally, MTT lesions reduced Zif268 expression in hippocampal areas CA1, CA3 and DG, paralleling the findings of Vann & Albasser (2009) and Vann (2013), both of which examined the effect of MTT lesions on c-Fos activity. By contrast, the current Chapter found that both MTT and PCFx lesions increased Zif268 activation in layer VI of the prelimbic cortex, which may be indicative of a compensatory shift from diencephalic to cortical activation. Furthermore, PCFx lesions reduced Zif268 expression in the anterior Rgb and Rdg, as well as hippocampal areas CA1 and CA3.

The similar mnemonic effects of both lesion types suggest that both the MTT and PCFx are critical for memory function. This is further supported by evidence that both lesions disrupt normal rhythmic activity within and between structures heavily involved in memory, the HPC, ATN and PFC. The shared systemic effects imply that the subicular input to the MB may be equivalent in importance to the MB efferents to the ATN. However, differences in the effect of MTT compared to PCFx lesions suggests that damage to the MTT may impact the extended hippocampal system more severely than PCFx lesions. For example, MTT lesions resulted in an attenuation of the theta peak in both the ATN and HPC whereas PCFx lesions only led to a slight reduction in peak theta in the ATN and had no impact in the HPC. Similarly, both PCFx and MTT lesions reduced Zif268 expression in

subregions of the anterior RSC, but only MTT lesions reduced expression in the posterior RSC. These findings suggest that rather than the hippocampal input via the PCFx being redundant in the presence of the brainstem input from the VTNg, it may also contribute to memory function. The electrophysiological and IEG effects following transection of the PCFx and MTT are not equivalent, this suggests that inputs from the VTNg and HPC may work in conjunction to support working memory function.

One limitation of examining IEG expression as an indicator of systemic effects is that it relies on the examination of isolated structures post-mortem, constraining the ability to draw conclusions concerning altered or dysfunctional interactions. In the current Chapter, electrophysiological recording enabled the direct pairing of behaviour with neural activity within multiple distinct brain regions simultaneously, in addition to IEG analyses.

Theta rhythmicity is critically involved in memory function and is present throughout structures of the extended memory circuit (Kirk & Mackay, 2003; McNaughton et al., 2006; Ketz et al., 2015). The presence of theta bursting cellular activity in synchrony with HPC theta within the MB and ATN suggests a shared rhythmic input (Kocsis & Vertes, 1994). Of the two possible inputs, the findings of the present Chapter emphasise the importance of the HPC input into the diencephalon. More specifically, this highlights the rhythmic propagation from the medial septum to the MB, via the HPC and PCFx, and onto the ATN and wider circuit via the MTT. By contrast, if rhythmic input from the VTNg into the MB rendered HPC innervation redundant, only MTT lesions would be expected to impact rhythmicity across the ATN-HPC-PFC axis. The current Chapter found striking reductions in ATN-HPC, ATN-PFC and HPC-PFC coherence, as well as reduced spectral power in the ATN and HPC, following both lesions. These findings suggest that disconnection of either fibre tract causes rhythmic dysfunction within the extended hippocampal system. This is in line with previous findings showing that septal blockade eliminates theta rhythm within the HPC and MB (Kirk et al., 1996) and that MB lesions modulate HPC rhythmicity (Kirk & Mackay, 2003). The reductions in peak PSD, as well as aberrant coherence within the extended hippocampal system demonstrated in the current Chapter are also similar to recent findings by Dillingham et al. (2019). Dillingham et al. (2019) reported an attenuation of peak theta in the HPC and RSC, as well as dysfunctional coherence between the RSC-HPC following MTT lesions. Perhaps most importantly, the reductions in theta PSD and coherence in the current

Chapter were observed during 'choice point' epochs, reinforcing the role of theta in successful memory function. These findings are consistent with previous studies in rodents which have demonstrated the importance of HPC-PFC theta synchrony during spatial memory performance in rodents (Jones et al., 2005; Hyman et al., 2010; Kim et al., 2011; O'Neill et al., 2013). For example, Kim et al. (2011) showed that HPC-PFC theta coherence was enhanced just prior to decision making during a spatial memory task. Additionally, in humans, cortical- ATN theta/ alpha synchrony has also been implicated in successful encoding and later recall, highlighting the importance of ATN-PFC interactions (Sweeney-Reed et al., 2014, 2015).

One possible explanation for the changes observed in rhythmic oscillatory activity following MTT and PCFx lesions is disrupted cholinergic activity within the extended hippocampal system. MB lesions have been shown to alter cholinergic activity in the hippocampus and cortex, as well as reducing acetylcholine binding to muscarinic receptors in the ATN (Sikes & Vogt, 1996; Béracochéa et al., 1995). Acetylcholine activity in the HPC is thought to be primarily driven by cholinergic neurons located in the medial septum/ diagonal band. In line with this, chemogenetic inhibition of cholinergic neurons in the medial septum has been shown to disrupt theta rhythmicity in the HPC (Carpenter et al., 2017). Neurons in the medial septum are reciprocally innervated by the RSC (Gonzalo-Ruiz & Morte, 2000), and thus Savage et al. (2012) have postulated that the reduced cholinergic activity in the hippocampus following ATN lesions may be a result of modulation of descending RSC projections to the medial septum. As the current Chapter demonstrated, both MTT and PCFx lesions result in profound functional changes in the RSC, indicated by a loss of IEG activity, and thus may similarly impact HPC theta via disruption of the cholinergic system.

Whilst the current PCFx findings do not replicate the findings by Vann et al. (2011) or Vann (2013) in which PCFx lesions were associated with negligible behavioural and IEG effects, procedural differences may account for the discrepancy in results. Here, complete loss of PCFx fibres was assessed using luxol blue (myelin) and cresyl violet (Nissl) counterstain. Previously the loss of PCFx fibres had been assessed using cresyl violet only (Vann et al., 2011; Vann, 2013) and thus some myelinated fibres may have been left intact. Nonetheless, Vann et al. (2011) used Fluoro-Gold retrograde tracing to demonstrate that

the PCFx lesions removed the majority of subicular inputs to the MB. Whilst there was evidence of some fibre sparing it is unlikely that this accounts for the complete lack of mnemonic deficits observed in these studies. Where previously the effect of PCFx lesions had been tested using an 8-arm RAM and T-maze task (Vann et al., 2011; Vann, 2013), the present Chapter used a 12-arm RAM, thus increasing task difficulty through increased proactive interference. The difficulty of the 12-arm RAM is reflected by the Sham group only beginning to show task acquisition by day 8 of testing in the RAM, where previously Sham rats have shown task acquisition around days 4-6 (Vann et al., 2011; Vann, 2013; Perry et al., 2018). Additionally, in the current Chapter rats were aged between 28-30 months at the time of behavioural testing. As memory performance decreases with age in rodents (Barnes, 1979; Geinisman et al., 1986), this may also have contributed to the extent of the memory impairments observed. In terms of IEG activation, changes in neuronal activation were measured in the present Chapter using Zif268 as opposed to c-Fos (Vann, 2013). As mentioned in the introduction of this chapter, there are subtle differences between these two markers of neuronal activation. Zif268 is a zinc finger protein closely linked to spatial learning and memory, as well as long-term plasticity (Farina & Commins, 2016; Gallo et al., 2018). By contrast, c-Fos has been used to investigate a wide range of systems and provides a more general measure of neuronal activation (Jones et al., 2001; Penke et al., 2014; Gallo et al., 2018). Based on the mnemonic deficits observed in the current Chapter following PCFx lesions, the use of Zif268 may have been more sensitive to PCFx damage than c-Fos.

One limitation of the current Chapter was that it did not provide a direct comparison with previous PCFx lesion studies or provide a clear justification for the discrepancy in results found when compared to these studies. Future work could address this issue by testing rats with PCFx lesions in both an 8-arm and 12-arm RAM using a counterbalanced design to address the question of whether task difficulty contributes to the PCFx lesion deficit observed here. To ascertain whether the advanced age of the rats in the current Chapter was also a contributing factor, a cohort of young and a cohort of old rats could be run on both tasks. An additional experiment could examine the relationship between memory impairment and the degree of mammillary body disconnection through the use of retrograde tracing. It may be that only a few spared PCFx fibres are required for apparently normal memory function. Therefore rats could be given variable degrees of PCFx damage (as

indicated by luxol blue and cresyl violet staining), tested on a variety of working memory tasks such as the 8- and 12-arm RAM, the water maze and T-maze, and infused with a retrograde tracer in the MB three days prior to perfusion (Vann et al., 2011). Such a study would allow a direct comparison between the severity of the memory deficit observed relative to the degree of PCFx damage as quantified by Nissl and Myelin staining as well as retrograde tracing of fibres from the MB to the subiculum.

The findings of the present Chapter provide a significant contribution to our current understanding of the propagation of rhythmic oscillatory activity within the extended hippocampal system. Here we provide evidence suggesting that damage to two key fibre tracts, the MTT and PCFx, impairs spatial working memory, causes functional lesions in distal regions and leads to aberrant rhythmic interactions between other structures critical for memory, namely the HPC, ATN and PFC. Importantly, oscillatory dysfunction was shown to occur during epochs of successful memory recall. These findings suggest that rhythmic input from the medial septum to the MB and onwards to the ATN is of critical importance for oscillatory interactions between the ATN, HPC and PFC. Moreover, it seems likely that these aberrant interactions contribute to the memory deficits observed. In the following chapter, I will examine whether the memory deficits described here following MTT lesions are amenable to intervention via optogenetic stimulation of the ATN, and what effect such an intervention may have on oscillatory activity within the extended hippocampal system.

Chapter 7:
Optogenetic stimulation of the ATN following MTT lesions

7.1 Introduction

As outlined in Chapter 3, damage to the MTT is the most consistent predictor of an amnesic syndrome following thalamic stroke (Van der Werf et al., 2000, 2003; Carlesimo et al., 2011). Experimental evidence also shows that selective transection of the MTT results in severe spatial working memory impairments in rats (Vann & Aggleton, 2003; Vann, 2013; Frizzati et al., 2016; Perry et al., 2018). This was confirmed in Chapter 6, which showed that an enduring deficit was evident in a 12-arm maze. Chapter 6 also confirmed that MTT lesions cause a striking reduction in Zif268 expression in subregions of the RSC and HPC. New evidence in Chapter 6 showed that MTT lesions reduced PSD in the ATN, HPC and PFC, and reduced ATN-HPC, HPC-PFC and PFC-ATN coherence across the 2-14 Hz frequency range.

The primary question addressed in this chapter was whether optogenetic stimulation of the ATN could ameliorate the memory deficits observed following MTT lesions. Recovery of memory function after experimental MTT lesions has not been assessed previously, although amelioration of memory deficits after ATN lesions is found when rats have been housed in environmental enrichment (Loukavenko et al., 2007; Wolff et al., 2008; Harding et al., 2014; Dalrymple-Alford et al., 2015). This ATN lesion evidence suggests that improved functionality in the wider system is possible after diencephalic injury. The MTT provides a unidirectional connection between the MB and the ATN, so the memory deficits caused by MTT injury are most likely mediated by its impact on ATN function. This is consistent with the distal IEG and electrophysiological effects of MTT lesions, described in Chapter 6. Given the ATN itself remains intact after MTT lesions, we hypothesised that stimulation of the ATN would reduce the severity of memory deficits after MTT lesions. ATN stimulation may be particularly effective because they occupy a strategic position within the extended system, with dense reciprocal connections with the PFC, RSC and subicular regions of the hippocampal formation (Jankowski et al., 2013; Bubb et al., 2017; Mathiasen et al., 2017). As discussed in Chapter 5, other support comes from evidence that deep brain electrical stimulation of the ATN for the treatment of refractory epilepsy can improve cognitive performance (Oh et al., 2012). In rats, ATN electrical stimulation was associated with increased HPC neurogenesis and improved memory performance (Hamani et al., 2012).

As described in Chapter 5, optogenetic stimulation of the ATN, rather than electrical stimulation, provides an ideal experimental approach to test the hypothesis. Optogenetic techniques target molecularly defined neurons that can be activated by relatively specific wavelengths of light at physiologically-relevant time-scales. It avoids the non-specific activation of cells and, in particular, any non-specific fibres of passage that would be caused by electrical stimulation (Barnett et al., 2018). We selectively stimulated the glutamatergic neurons, which represent 40% of ATN neurons and provide the majority of ATN efferents to hippocampal formation frontal cortex and RSC (Gonzalo-Ruiz et al., 1997; Zakowski et al., 2017). If the hypothesis is correct, it would indicate potential treatment strategies in the clinical field for people with amnesia after MTT injury.

Negative effects on functional connectivity after MTT lesions were evident in Chapter 6. Similarly, Dillingham et al. (2019) also reported that MTT lesions disrupt normal theta rhythmicity within and between the HPC and RSC. Improving memory after diencephalic lesions may therefore require enhanced inter-structural communication in the extended hippocampal system, particularly at theta frequency (Dalrymple-Alford et al., 2015). In support of this, enrichment after ATN lesions increases functional connectivity between the PFC and HPC (Ulrich et al., 2019). Other work also suggests that increased PFC-HPC theta coupling is associated with stronger memory traces (Jones & Wilson, 2005; Hyman et al., 2010; Colgin, 2011; Fell & Axmacher, 2011).

Optogenetic stimulation also enables electrophysiological recordings to be made in different neural structures during stimulation, including the ATN itself. The pattern of optogenetic stimulation can also be experimentally controlled, which can influence whether specific behavioural benefits are found, at least in non-memory models (Seeger-Armbruster et al., 2015). We delivered optogenetic activation of the ATN using theta burst stimulation (TBS). Theta burst stimulation (TBS) has been shown to improve memory function in humans and rats (Sweet et al., 2014; Hoy et al., 2016). In humans, non-invasive transcranial magnetic TBS of the PFC can improve working memory performance (Hoy et al., 2016). Moreover, in rats, the deficits in learning and memory observed following traumatic brain injury can be significantly improved through TBS of the HPC (via a fornix electrode). Electrical HPC theta stimulation at 7.7 Hz has been shown to restore rhythmicity and improve memory performance in rats (McNaughton et al., 2006) but frequencies below 6.5

Hz been associated with behavioural impairments (Pan & McNaughton, 1997), suggesting that stimulation frequencies above ~7 Hz may be more relevant for memory function. For the current Chapter, TBS was delivered at 8.5 Hz, as a clear peak in spectral theta power was observed in Sham rats ~8.5 Hz when running in the RAM in Chapter 6. We therefore examined whether a regular pattern of optogenetic TBS of the ATN, in rats with MTT lesions, would improve (1) memory performance in the 12-arm maze, as well as (2) theta rhythmicity in and coherence between memory structures and (3) IEG expression in the extended hippocampal system. For (1) and (2), we also examined the effects of closed-loop optogenetic TBS of the ATN that was triggered by the rat's own HPC theta rhythm.

7.2 Methods and Materials

7.2.1 Subjects

Subjects were 30 male PVGc hooded rats bred in-house. Rats were between 8 and 9 months of age and weighed between 290-320 g at the time of lesion and infusion surgery. They were randomly allocated to MTT opsin, MTT non-opsin or Sham opsin groups. Three or four rats per cage were housed in standard opaque plastic cages (50 cm length, 30 cm wide and 23 cm high) in a vivarium under reversed lighting (lights turned off from 8 am to 8 pm, when behavioural testing was conducted). Following both surgical procedures (lesion plus viral vector infusion; optrode and electrode implantation), rats were housed individually for seven to eight days. Food and water were available ad libitum during surgery and recovery. During periods of RAM testing, rats received restricted access to food and were maintained at 85% of their free-feed body weight with water available ad libitum. All procedures were approved by the University of Canterbury Animal Ethics Committee, New Zealand (2016/07R).

7.2.2 Radial Arm Maze

Spatial memory (2 separate tasks) was tested using a 12-arm radial arm maze, located in the centre of a large windowless room (4 m by 4.7 m). When needed, rats were connected to the Open Ephys electrophysiological recording system (see Chapter 6 methods) and optogenetics stimulator (Plexon, Tx) via a headstage cable and fibre optic cables (Plexon, Tx), respectively. The same radial arm maze, placement and room configuration, as detailed previously (see Chapter 6), were used for this experiment.

7.2.3 Preoperative Habituation to the RAM

Rats were handled and habituated to the 12-arm RAM in the same manner detailed in Chapter 6.

7.2.4 Preoperative spatial working memory training in the RAM

Following habituation, rats were trained for ~25 daily trials (±4 days) to reach the criterion of a maximum of three errors within a trial for three consecutive days. Standard RAM testing was carried out in the same manner detailed in Chapter 6.

7.2.5 MTT lesion and ATN infusion surgery

MTT lesions were made in the same manner as detailed in Chapter 6. About 40 min later, bilateral viral vector infusions of the lentivirus (LV-CaMKII.hChR2(H134R).mCherry.WPRE; Otago Viral Vector Facility; pseudotyped with vesicular stomatitis virus glycoprotein, genomic viral titre 5.34E+09 genomes/mL; Best et al., 2018) were made that targeted the anteroventral region in the ATN. Each infusion was 0.24 µL, with two infusion sites per hemisphere and thus giving a total of 0.48 µL per hemisphere. ATN infusions were made with vertically-held 10 µL nanofil syringe (blunt tip, 30-gauge needle; World Precision Instruments, USA) at a rate of 0.07 µL/ min and with incisor bar at -7.5mm below the inter-aural line, which minimised damage to the fimbria-fornix. One of four anterior-posterior (AP) coordinates behind bregma was used to accommodate different bregma to lambda (B-L) distances (see Table 7.1 for infusion coordinates). The syringe needle was lowered slowly to each coordinate (dorsal then ventral on each side) and left in situ for five minutes post-infusion at each site to allow diffusion. Sham and MTT lesion opsin rats received infusions of viral vectors carrying the channelrhodopsin gene construct (ChR2) whereas the MTT lesion non-opsin rats (opsin control group) received the same viral vector but without the ChR2 gene. Following surgery, rats were given a recovery period of 7 - 10 days.

Table 7.1. Coordinates for AV infusion. Abbreviations: B= bregma; L= lambda; AP= anterior-posterior, DV= dorsal-ventral.

Distance B to L	AP coordinate	Lateral coordinate	DV (from dura)
≤0.64	-0.245	±0.144	-0.525 (top infusion site)
0.65-0.68	-0.250		-0.555 (lower infusion site)
0.69-0.72	-0.255		
>0.72	-0.260		

7.2.6 Post-lesion and infusion surgery RAM Testing

The spatial working memory task was run for 12 days beginning about 14 days after lesion / viral vector surgery. This testing checked the patency of the lesion and re-familiarized the rats to the task before the next surgery. Rats were first re-habituated to the RAM for three days following the same habituation procedure detailed in Chapter 6. Following re-habituation, rats received 12 consecutive days of testing in the standard working memory RAM (procedure described in Chapter 6), but without being plugged into the Open Ephys headstage.

7.2.7 Electrode and optrode fabrication

Electrodes were implanted bilaterally in the hippocampus and unilaterally in the prefrontal cortex. Optrodes were implanted bilaterally in the anteroventral portion of the ATN. Once electrodes were completed they were tested for patency and to check for shorts between wires as per Chapter 6.

PFC and HPC electrodes

Electrodes were constructed in the same manner as described in section 6.2.5 aside from the following changes. Stepped stereotrodes were implanted unilaterally in the prelimbic cortex, with the bottom electrode recording local field potentials in the prelimbic cortex and the upper electrode acting as a local reference. Two wires were twisted together to form each electrode to provide additional strength. One electrode was pulled up alongside the other until it extended approximately 5 mm out of the cannula and the second electrode was several millimetres below the first electrode. Due to the strong dipole in the dorsal HPC a local reference was not required, so two pieces of wire were looped and the four ends

twisted together to form a non-stepped stereotrode which were referenced to ground during analyses. Instead of the 2 wires being cut to give four separate wires, a small section at the tip of each loop was briefly exposed to a naked flame to remove the wire coating and each loop was soldered (Duratech solder; Jaycar, NZ) to two Mill-Max pins on a block of Mill-Max connectors containing four male/female pins (i.e. pin and socket). For the PFC, the lower electrode was cut to about 200-300 um longer than the length of the upper electrode. For the HPC, the tip of the four wires was then cut flat to a length of 4 mm, producing a non-stepped stereotrode.

ATN Optrode

Optrodes were constructed from a stepped stereotrode and one optic fibre (Doric Lenses Inc; Canada). Optic fibres had a fibre core with a diameter of 200 µm, 0.66 NA and were 8 mm in length. The ferrule was made of silica and had two sets of grooves at its base to aid in securing it to the skull. A stepped stereotrode was constructed in the same fashion as the PFC electrode except that rather than threading the two wires through a cannula they were pulled alongside each other and held in place with cyanoacrylate, being careful to leave each tip exposed. The upper pair of twisted wire had a tip of ~5 mm in length, and the lower pair was pulled ~2 mm further to be cut later. Once the wires were secured together, the stereotrode was secured to the optic fibre with cyanoacrylate. The upper electrode was positioned so that it extended ~100-200 µm below the tip of the optic fibre and the lower electrode was cut to length, an additional ~200 µm from this. Once secured, the two loops were separated out and wound around and soldered to two pins on a block of Mill-Max connector, the same as for PFC and HPC. The optic fibre was plugged into an optic fibre cable attached to the Plexon Radiant Software and tested to ensure patency and functionality by testing the output at the tip using a Power Meter Kit (Thorlabs).

Ground electrode

Ground electrodes were constructed in the same manner as described in Chapter 6.

7.2.8 Electrode Implantation Surgery

Rats were implanted with the recording electrodes 12-14 weeks after lesion and infusion surgery in the same manner as described in Chapter 6. However, due to the need to implant bilateral optrodes in ATN, the nose was set at -7.5mm relative to the interaural line in order

to minimise damage to the fornix (see Table 7.2 for the adjusted electrode and optrode coordinates and Figure 6.5 for the topographical layout of the head-cap on the rat's head).

Table 7.2. Electrode coordinates. Abbreviations: B= bregma; L=lambda; AP= anterior-posterior; DV= dorsal-ventral.

Distance B to L	AP coordinate	Lateral coordinate	DV (from dura)
PFC	+0.131	±0.05	-0.39
≤0.64	+0.136		
0.65-0.68	+0.141		
0.69-0.72	+0.146		
>0.72			
AV			
≤0.64	-0.240	±0.142	-0.54
0.65-0.68	-0.245		
0.69-0.72	-0.250		
>0.72	-0.255		
HPC			
≤0.64	-0.420	±0.21	-0.31
0.65-0.68	-0.425		
0.69-0.72	-0.430		
>0.72	-0.435		

7.2.9 Re-habituation in the RAM and habituation to cables

Following the recovery period, rats were re-habituated to the RAM for three days. On the first day, rats were placed in the maze in cage groups with chocolate drops sprinkled down the arms and piled up in the food wells, which also housed inaccessible chocolate drops to control for odour cues. On the second and third days, rats were habituated individually for 3 minutes each. Approximately 6 chocolate drops were placed in each well and the doors

were lowered and raised repeatedly at random intervals. Rats were also connected to the Open Ephys headstage and two high durability fibre-optic patch cables with LC ferrule tips (Plexon, Tx) so that they would be habituated to running the maze whilst connected to the tethers allowing electrophysiological recording and optogenetic stimulation.

7.2.10 RAM testing with simultaneous electrophysiological recording

Following the last day of re-habituation, rats returned to testing in the RAM with simultaneous electrophysiological recording for 12 days. Testing in the 12-arm RAM followed the same procedure as detailed in Chapter 6 except that, in this instance, rats were plugged into all three cables (one Open Ephys cable and two optic fibre patch cables). Rats were plugged into the fibre optic patch cables to keep the number of cables consistent across RAM testing with only electrophysiological recording and RAM testing with electrophysiological recording and optogenetic stimulation. Optogenetic stimulation was not given during the 12-days of RAM testing.

7.2.11 Electrophysiological recording

Electrophysiological data were recorded in the same manner described in Chapter 6, aside from the following changes. In order to allow the electrophysiological recording tether and both fibre-optic cables to be plugged in simultaneously, the interface board was cut to allow room for the patch cables to plug in directly in front of the interface board (see Figure 7.1, panels A, B and C). This left sixteen remaining channels. A thirty-two pin Omnetics connector was then soldered to the interface board, and all the soldered connections reinforced with a thin layer of epoxy. The Omnetics connector directly connected to the Open Ephys digital headstage (see Figure 7.1, panel D). The connections of the headstage cable to the carousel commutator and the Open Ephys data acquisition board are illustrated in Figure 7.2.

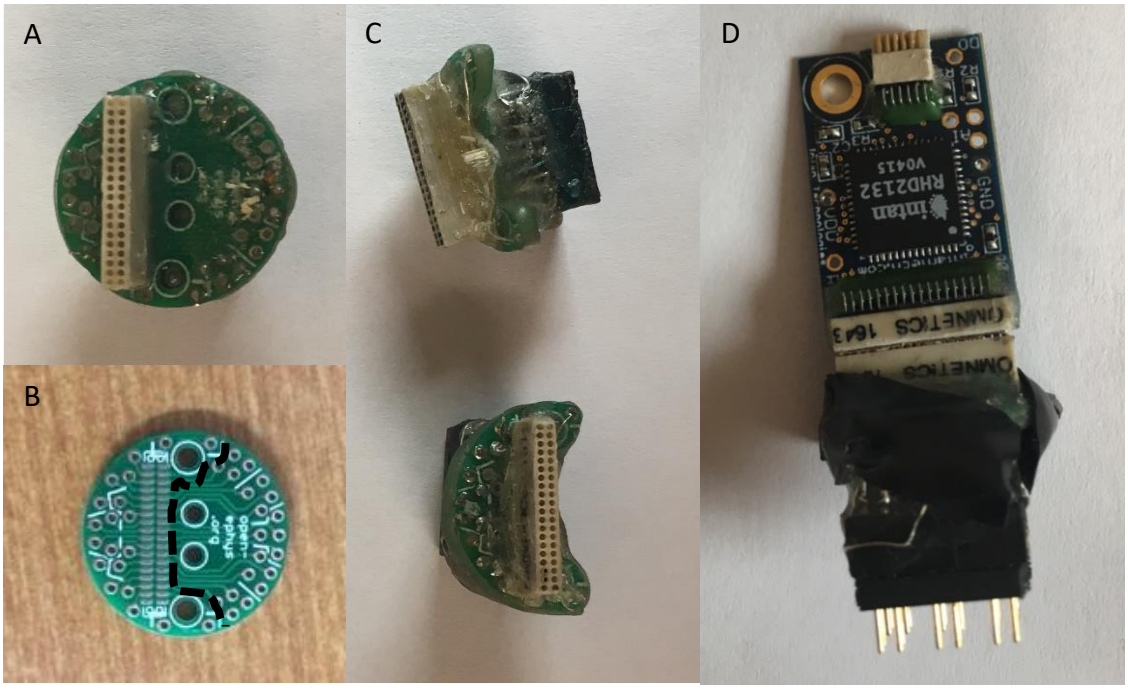

Figure 7.1 Open Ephys interface board and headstage construction. (A) normally constructed Open Ephys interface board as used in experiment 1, (B) example of cut made in Open Ephys interface board to facilitate plugging in of fibre optic patch cables, (C) various views of the adapted interface board once constructed, (D) Open Ephys digital headstage connected via the two banks of Omnetics connectors to the interface board.

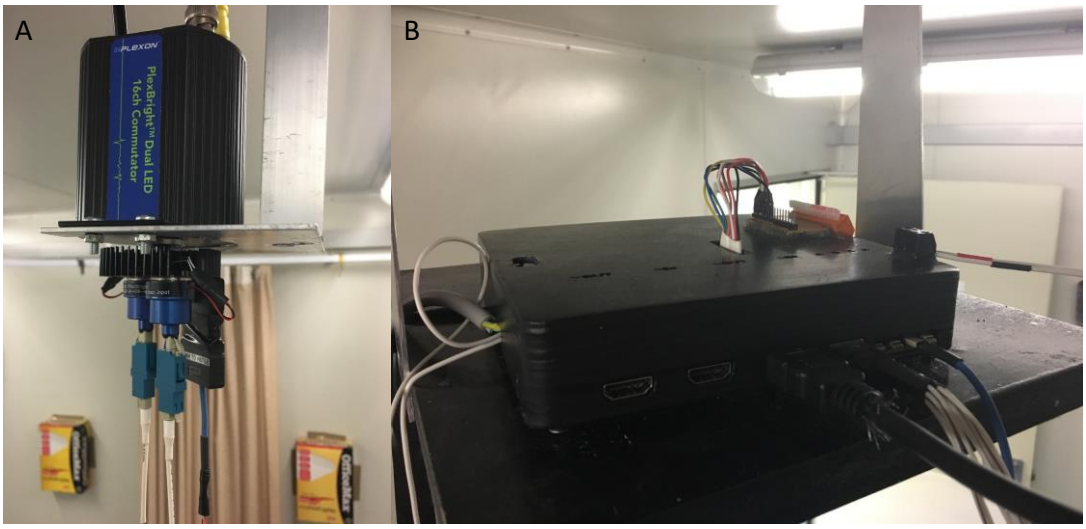

Figure 7.2 Open Ephys recording set-up. (A) Plexon dual-LED commutator connected to both patch cables and the Open Ephys headstage cable (via the Harwin adapter), (B) Open Ephys data acquisition board.

7.2.12 Electrophysiology data processing

Electrophysiological data were processed as described in chapter 6, section 6.2.9.

7.2.13 RAM testing with electrophysiological recording and optogenetic stimulation

Following standard testing, the RAM rats were run for a total of 24 days in the RAM to test the effects of optogenetic stimulation. First (Part 1), we tested the effect of blue light stimulation using regular theta burst stimulation (TBS; 480 nm blue light activates channelrhodopsin) by comparison with two control conditions. One control condition was orange light stimulation (620 nm), delivered using the same stimulation parameters; orange light (620 nm) would not activate the ChR2 protein channels. The second control condition was “no stimulation”, wherein rats were attached to all three cables but no optogenetic stimulation was delivered.

Regular TBS optogenetic stimulation was delivered via the PlexBright 4 Channel Optogenetic controller (Plexon, Tx) which was triggered using pre-set parameters (described later in this section) programmed into the Radiant software. The PlexBright Optogenetic controller connected to compact LED modules via the commutator (Plexon, Tx). Rats were connected to the Plexbright compact LED modules via the two fibre-optic patch cables.

Output was recorded from the tip of the attached patch cables (Power meter kit; Thorlabs) at the beginning and end of every testing day to verify the power output at the end of the optic cable. Normal power output using the blue (465 nm) LED was between 17.5-18.5 mW and 9-10 mW using the orange (620 nm) LED. For regular TBS, bursts of 3 x 5ms pulses at 40 Hz were delivered at a frequency of 8.5 Hz using Radiant software v2.

Rats were run on the RAM task for a total of 16 days: 4 days of regular TBS with blue light; 4 days of regular TBS with orange light; and 8 days of no stimulation. The order of presentation was counterbalanced: [NOON][NBBN][NBBN][NOON] where N= no stimulation, B= regular TBS with blue light and O= regular TBS with orange light.

At the start of each trial, rats were connected to all three tethers and then placed in the central hub. The electrophysiological programme was then activated, and, once the recording appeared stable, optogenetic stimulation and electrophysiological recording were turned on and the trial began. Optogenetic stimulation was delivered continuously for the duration of the task and only switched off once the task was completed. As in experiment 1, IR beams and IR detector units were used to synchronise behaviour with electrophysiological activity.

Five days after the final day of Part 1, rats began Part 2. Part 2 replicated the effects of blue regular TBS. Rats were run on the task for 4 days (2 using blue light and 2 using orange light) whilst receiving regular TBS. The four day blocked was counterbalanced using an OBBO design, where O= orange and B= blue.

One day after the end of Part 2, rats began Part 3. Part 3 assessed the effects of closed-loop TBS. For closed-loop stimulation, the online hippocampal electrophysiological recording was filtered between 8-9 Hz (to yield an average of 8.5 Hz) in Open Ephys. The Open Ephys Phase Detector module triggered stimulation when the filtered HPC signal arrived at the upward zero-crossing, or "rising phase". Upon triggering of the Plexbright Optogenetic controller, via a pulse pal, a burst of 3x5ms pulses at 40 Hz was delivered. In the absence of theta in the original recording, or if theta was beyond the narrow Bandpass Filter, stimulation would not be triggered. In Part 3, rats were run on the task for 4 days of closed-loop TBS (2 using blue light and 2 using orange light) counterbalanced using the same OBBO design used in Part 2.

7.2.14 Simultaneous Spatial Discrimination in the RAM

Three days after the last day of working memory RAM testing, rats were returned to the RAM for a simultaneous discrimination task to test the rapid acquisition of spatial reference memory. Rats were placed in the central hub for ~10 s before two doors were lowered simultaneously and the rat was permitted to make a choice. The two available arms were separated by a single closed arm and black electrical tape was used to mark the two choice doors. Only one arm of the pair was consistently baited with one chocolate pellet across the 20 trials on any given day, requiring that rats learn that only one of the presented arms would be rewarded. Once a rat had made its choice, both doors were raised simultaneously, the rat consumed the food reward, and was then allowed to return to the central hub for ~10 s before the next trial began. The pair of arms remained the same for all trials on a given day, but changed across days with no pair of arms repeated across the 3 days of testing. A different, fourth discrimination was used on both of the 2 days prior to days using optogenetic stimulation. The latter familiarized the rats to the new spatial memory task after the previous spatial working memory RAM testing. During the two initial days of this fourth discrimination task, rats were plugged into all three tethers (one recording cable and two optic fibre cables), but did not receive optogenetic stimulation. On the next three test

days, rats received optogenetic TBS using an OBO sequence of optogenetic stimulation across the three days. That is, on day one of testing rats received orange light regular TBS, on day two they received blue light regular TBS and on day three rats were returned to orange light regular TBS.

7.2.15 Immediate Early Gene activation

Following the final day of testing, rats were habituated to a dark holding room for three days. Rats were placed in individual holding cages in this room for 90 min each day. The following day, rats were placed in a 50 cm high x 1 m wide x 1 m long black open field with approximately 20 chocolate drops scattered across its base. A non-spatial task was used to avoid any confound with spatial memory testing in rats with MTT lesions. Rats were plugged in to all three tethers and allowed to explore for 60 s before receiving unilateral orange and blue regular TBS (counterbalanced across rats) for a five-minute period. Once five min had elapsed, rats were placed in an individual holding cage in the dark quiet room for 90 min prior to perfusion to facilitate immediate early gene activation (Chadhuri et al., 2000).

7.2.16 Perfusion

Rats were perfused in the same manner as described in Chapter 6.

7.2.17 Histology

Sections (40 µm) were taken in the coronal plane from approximately +3.70 mm to -9.16 mm from bregma using a sliding microtome with a freezing stage (Thermofisher). To document infusion, lesion sites, and electrode and optrode locations, sections were collected in four series – with each series consisting of a series of 4-6 sections so that infusion visualisation, lesion verification, and immunohistochemistry could be performed on the same regions. The first series of sections spanned from +3.70 mm to +1.20 mm from bregma, the second from -1.30 mm to -2.12 mm from bregma, the third from -2.12 mm to -3.80 mm from bregma and the fourth from -3.80 mm to -6.72 mm from bregma. This tissue, taken from the anterior portion of the prefrontal cortex to the beginning of the cerebellum, was put into vials containing -20°C cryoprotectant long-term solution (40% 0.1 M PB, 30% glycerol and 30% ethylene glycol) for long-term storage.

7.2.18 Lesion Verification

For MTT lesion verification, one of six vials from the third series of each brain was mounted onto gelatin-coated slides and allowed to dry overnight. Lesion verification was carried out as detailed in Chapter 6.

7.2.19 Electrode and optrode verification

One vial from each of the first, second and third series of sections were used per rat to verify the location of the PFC, ATN and HPC electrodes. Electrode verification was carried out as detailed in Chapter 6.

7.2.20 Visualisation of LV.CaMKII.hChR2(H134R) mCherry.WPRE in the ATN

One vial from the second series was removed from -20°C storage and used for infusion location verification. Sections were washed in PBS for 3 x 10 min to remove the cryoprotectant solution, before being washed in 0.1 M PBS-Tx 0.2% (biological detergent) to increase the permeability of the tissue. The tissue sections were then incubated for 1 h in 0.1 M PBS-Tx 0.2% containing 10% normal goat serum (1:100 Thermofisher) to block non-specific binding and then transferred to separate culture well-plates containing the primary antibody solution. Sections were double-stained with two primary antibodies (RFP antibody 5F8 rat for mCherry, Chromotek, 1:1000 and mouse-monoclonal anti-CamKIIα, Merck Millipore, 1:300) which were added to 0.1 M PBS-Tx 0.2% containing 5% normal goat serum. The tissue sections were incubated in primary antibody solution for 24 h at 4°C with gentle agitation. After the incubation period, tissue sections were removed from the primary antibody solution and washed twice in PBS-Tx for 20 min each. The tissue sections were then subsequently incubated for four hours at room temperature in the secondary antibody solution, whilst wrapped in foil as the fluorescent secondary antibodies are light sensitive. The secondary antibody solution consisted of goat anti-rat Alexafluor-594 (Thermofisher, 1:1500) and goat anti-mouse Alexafluor-488 (Thermofisher, 1:1500) added to 0.1 M PBS-Tx 0.2% containing 5% normal goat serum. The tissue was then washed twice in PBS for 10 min each, and then once in PB for 10 min. The tissue sections were then mounted onto gelatin-coated slides in the dark, and allowed to dry for approximately 30 min, before being coverslipped with Vectashield hardset mounting medium with DAPI (Vectorlabs). Once dry, the slides were sealed with nail polish and stored in the freezer in containers wrapped in aluminium foil.

Infusion location was visualised in the dark using a Leica DM6 B upright fluorescence microscope (Leica Microsystems) and captured using LAS X 1 imaging and analysis software (Leica Microsystems). Additional images were taken using a confocal microscope (40x and 60x, Leica TCS SP5).

7.2.21 Zif268 immunohistochemistry

Zif268 immunohistochemistry, image capturing, processing, and calculations were carried out in the same manner as described in Chapter 6.

7.2.22 Regions of interest for zif268

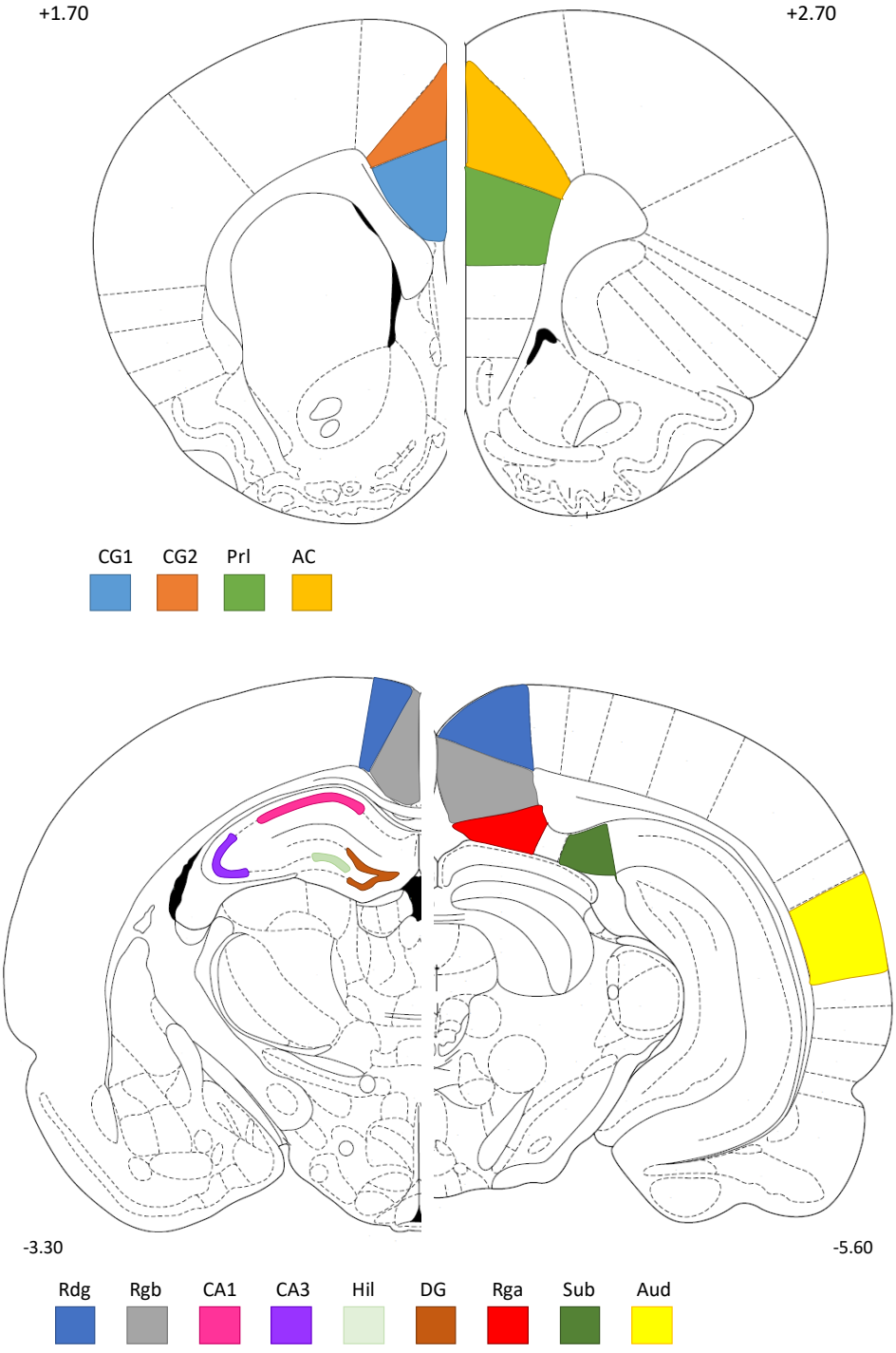

Figure 7.3. Regions of interest for zif268 immunostaining. Atlas plates from Paxinos & Watson (1998) indicating the relative location (from Bregma) of the cortical and hippocampal regions of interest. Abbreviations: Prl= prelimbic cortex; AC= anterior cingulate cortex; CG1= cingulate cortical area 1; CG2= cingulate cortical area 2; Rdg= dysgranular retrosplenial cortex; Rgb= granular b retrosplenial cortex; CA1= CA1 of the hippocampus; CA3= CA3 of the hippocampus; Hil= hilus of the dentate gyrus; DG= dentate gyrus; Rga= granular a retrosplenial cortex; Sub= subiculum; Aud= auditory cortex.

Zif268 expression was examined in the retrosplenial cortex, hippocampus, subiculum and prefrontal cortices (prelimbic, anterior cingulate, and cingulate (CG1 and CG2); see Figure 7.3). Zif268 positive cell counts were made separately for the superficial and deep granular b and dysgranular regions of the retrosplenial cortex, as well as layers 2, 3 and 5 in CG1 and CG2, layers 2, 3, 5 and 6 in the prelimbic and anterior cingulate, hippocampal areas CA1, CA3, CA3 hilar and the dentate gyrus.

7.2.23 Data Analysis

The critical alpha value was set at 0.05 for all statistical tests.

Behavioural data

Repeated measures ANOVAs were used for all behavioural analyses. Spatial memory performance after lesions, both prior to and after implant surgery, was analysed to show the linear and quadratic trends across the six two-day blocks and the effects of lesion group (Sham versus MTT lesion).

A five factor ANOVA with four repeated measures (2 x 2 x 2 x 2 x 2) was used to assess the effects of regular optogenetic TBS (Part 1). Part 1 used the sequence, NOON NBBN NBBN NOON, which was rearranged for analysis as NONO NBNB NONO NBNB. The four repeated measures were: first eight days versus second eight days (Half) to assess whether effects changed over time; orange phase (NONO) versus blue phase (NBNB; Colour phase); the order of stimulation versus no stimulation delivery (Order: no stim→stim versus stim→ no stim); non-stimulation versus stimulation (Stim). An effect of blue light stimulation relative to other conditions was therefore indicated by the Colour phase x Stim interaction. The effect of lesion status as a function of type of stimulation was indicated by the Group x Colour phase x Stim interaction. If this three-way interaction was significant, then two post-hoc analyses were used. (1) The post-hoc Group x Stim interaction for orange phase data only was assessed. It was anticipated that there would be a simple main effect of group (i.e. lesion effect), but no simple main effect of Stim or Group x Stim interaction. This pattern of results would confirm that orange stimulation had no effect. (2) The post-hoc Group x Stim interaction for blue phase data only was assessed. Here, we anticipated a significant interaction. Our expectation was that blue stimulation compared to non-stimulation would improve performance. If only the Colour phase x Stim interaction was significant, then the same two post-hoc were used but in this instance to demonstrate that

(1) orange light stimulation had no effect and that, (2) blue light stimulation improved performance irrespective of group.

A three factor ANOVA was used to assess Part 2 (the replication of the effects of blue regular TBS). The two repeated factors were: the counterbalance of OB versus BO (Order); orange versus blue (Colour). The same analysis was used to assess the effects of closed-loop TBS in Part 3. In Part 4 a two factor ANOVA compared the three stimulation days (OBO).

Electrophysiological data

Data analysis for electrophysiological data was carried out in the same manner as described in chapter 6, aside from the following changes. LFP data were sampled at 30 KHz in order to enable multi- and single-unit analyses at a later date. Therefore, raw local field potential data were first downsampled to 128 Hz. Similar analyses were run as for the behavioural tasks but with the additional factor of electrode location (PSD) or electrode pair (coherence). In addition, 24 power values were used to assess linear and quadratic trends across the 2-14 Hz frequency band based on a 1s window. For all omnibus ANOVAs, only rats with electrodes in all three locations (PFC, ATN and HPC) were included to allow for repeated-measures trend analysis of electrode effects. Post-hoc ANOVAs of individual electrodes/electrode pairs are reported for all the data from rats with appropriate placements in those areas to increase N and so increase power. These supplemented post hoc ANOVAs were compared with post hoc splits from the original omnibus analysis to confirm that the basic patterns were the same.

Immediate Early Gene data

Raw cell counts were normalised using a square root transform. Lesion and stimulation effects were analysed in each brain region separately with additional repeated measures factors as required.

7.3 Results

7.3.1 Lesion verification

Based on luxol blue and cresyl violet histology, thirteen of the fifteen rats in the MTT opsin group met the inclusion criterion of at least 80% bilateral damage to the MTT (see Figure 7.4). Eleven MTT opsin rats had 100% bilateral MTT damage, while one had 100% and 83% MTT damage in the left and right hemispheres respectively and one had 82% bilateral damage. One excluded MTT lesion rat had 96% left-sided MTT damage but only 63%

contralateral damage; the second exclusion had 67% and 80% MTT damage on the left and right respectively. In the MTT non-opsin group, two rats met the MTT lesion criterion (90% bilateral damage; and 88% bilateral damage), but two were excluded (one with 86% and 63% MTT damage on the left and right; one with 74% and 79% MTT damage on the left and right). The maximum extent of damage in rats with MTT lesions was at -3.80 from Bregma, with no impact on the supramammillary nuclei, mammillary bodies or mammillotegmental tract, which begin at -4.16 to -4.30 from bregma. One Sham lesion rat died before post-operative behavioural testing from an unknown cause. One rat met the MTT lesion inclusion criteria but was removed from analyses due to incorrect optic fibre placement (see section 7.3.2). The final groups were 12 MTT lesion opsin rats, 9 Sham opsin rats, and 2 MTT lesion non-opsin (viral vector control) rats.

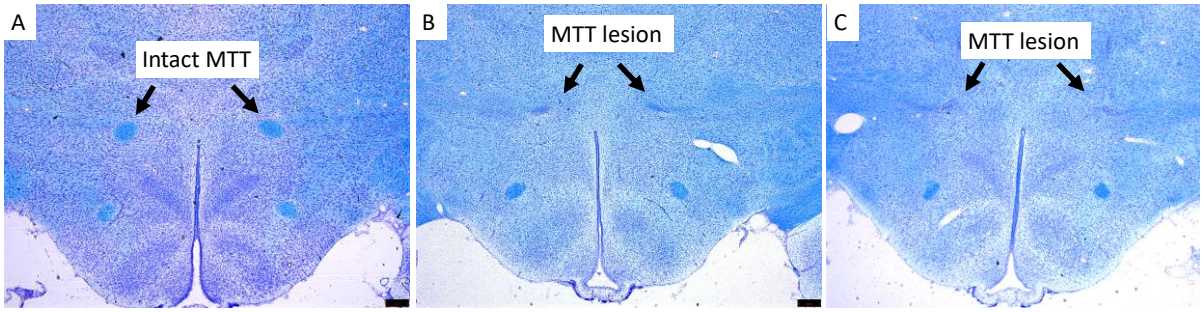

Figure 7.4. Photographs of luxol blue (myelin stain) plus cresyl violet (Nissl stain) counter-stained sections. Sections show an intact MTT (A; Sham surgery), the smallest included MTT lesion (B; 82% bilateral damage) and a 100% bilateral MTT lesion (C). Photographs taken at ~ -3.30- -3.60 mm from bregma.

7.3.2 Optic fibre verification

All optrodes implanted in the included opsin and non-opsin rats were located in the dorso-medial AV (Figure 7.5). The average AP placement was -1.80 mm from Bregma. In one rat (mentioned in section 7.3.1), one optrode was correctly placed but the other was located in the anterior MD; this rat was removed from analyses.

Triple-stained sections (mCherry, CamKIIα and DAPI) and cresyl violet stained sections in the ATN verified that that transduced cells were located beneath all optic fibres (Figure 7.6). The light irradiance required to activate ChR2 at a “blue” wavelength of 473 nm is between 1-5 mW. The output at the end of the optic fibre cable was between 18.5-19.5 mW, so optogenetic stimulation would cause ChR2 activation up to a depth of ~0.80 mm below the fibre tip, affecting both dorso medial AV and ventrolateral AV (calculated using

the Deisseroth lab “Brain tissue light transmission calculator”; https://web.stanford.edu/group/dlab/cgi-bin/graph/chart.php). The two included MTT lesion non-opsin rats also had optic fibre placements in the AV.

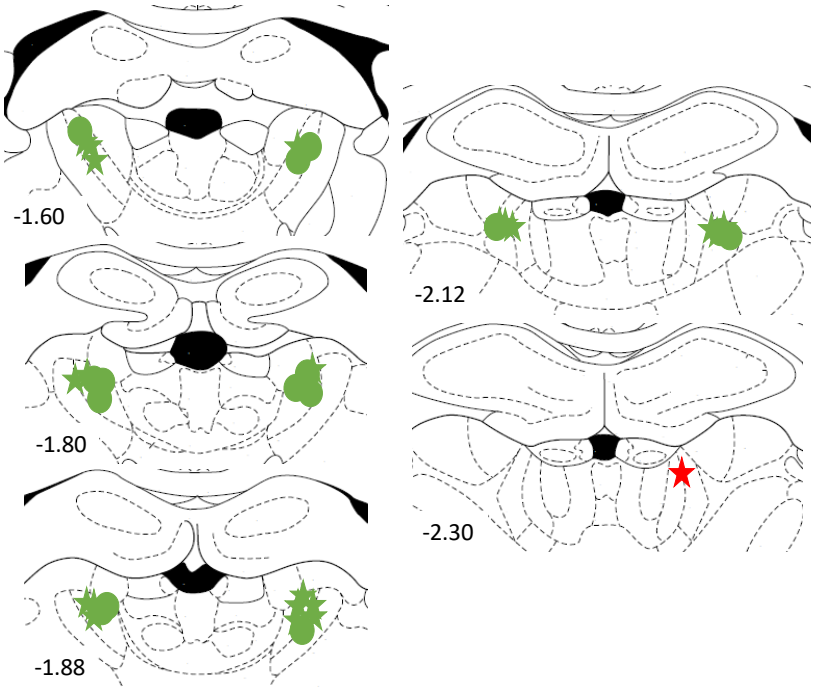

Figure 7.5. Coronal atlas plates through the AV -1.60 to -2.30 mm from Bregma. Symbols indicate the placement of optrode tips in the MTT opsin group (star) and Sham group (circle). The rat with the red fibre tip placement was excluded. Adapted from Paxinos & Watson (1998).

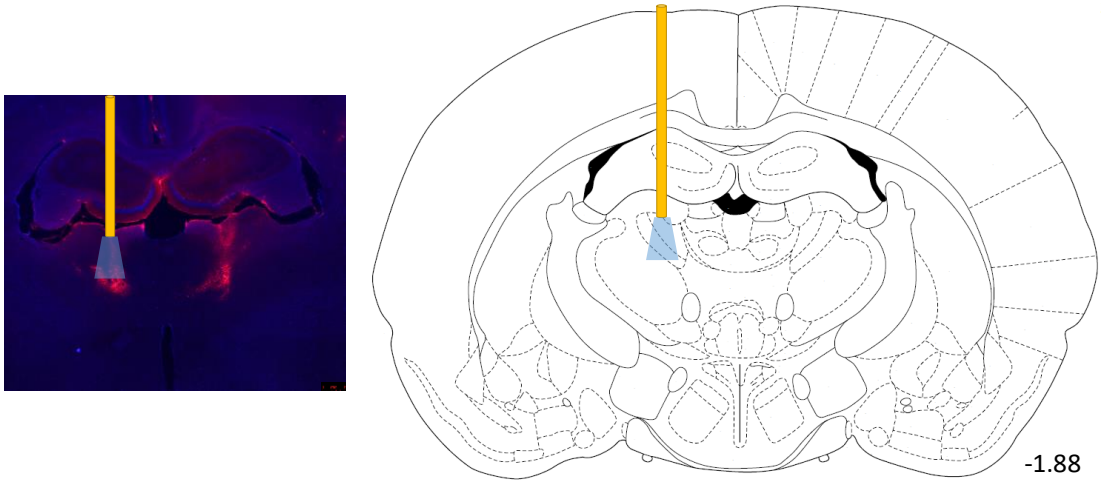

Figure 7.6. Example photograph of viral spread in the AV and surrounding structures and optic fibre location (left) and the estimated location in the brain (right). The anticipated spread of light from the fibre tip is shown: blue cone, about 0.8 mm vertical distance based on the “Brain tissue light transmission calculator”; https://web.stanford.edu/group/dlab/cgi-bin/graph/chart.php). Right panel adapted from Paxinos & Watson (1998).

7.3.3 Verification of viral vector

Sections approximately -0.92 mm to -2.80 mm from bregma were mounted using DAPI medium (cell nuclear stain) to confirm that the transduced thalamic neurons in all rats co-expressed mCherry (viral vector expression in opsin and non-opsin rats) and the CamKIIα (glutamatergic neuron) markers (Figures 7.7 and 7.8). Although there were transduced cells outside the ATN, light activation would only affect cells below the optrode fibre tip, which was in the dorsal AV in all accepted cases. The MTT lesion rat that was excluded because one optic fibre was in the MD nonetheless had unilateral transduction of the posterior AV.

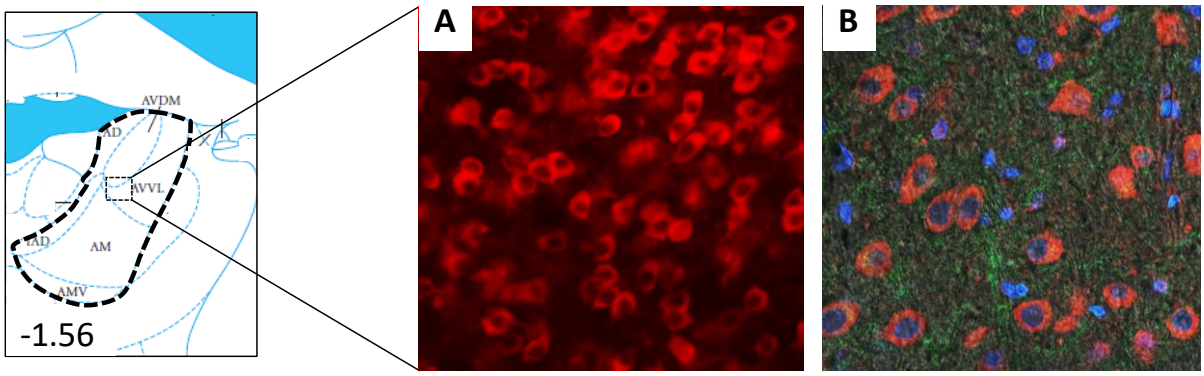

Figure 7.7. Left panel (adapted from Paxinos & Watson, 2014) shows approximate location in the brain of example photomicrographs of viral vector expression in the AV. A) mCherry only (red) stained section showing transduced AV neurons (left; 40x objective). B) The presence of DAPI cell nuclei (blue) in the absence of mCherry shows that not all cells of the ATN were transduced; the co-localisation, shown by orange to yellow emission in the cytoplasm, due to the combination of green (CamKIIa) and red (mCherry), confirms transduction of glutamatergic AV cells. Abbreviations: AD= anterodorsal thalamic nuclei; AM= anteromedial thalamic nuclei; AVDM= anteroventral thalamic nuclei dorsomedial; AVV= anteroventral thalamic nuclei ventrolateral; AMV= anteromedial thalamic nuclei ventral; IAD= interanterodorsal thalamic nuclei.

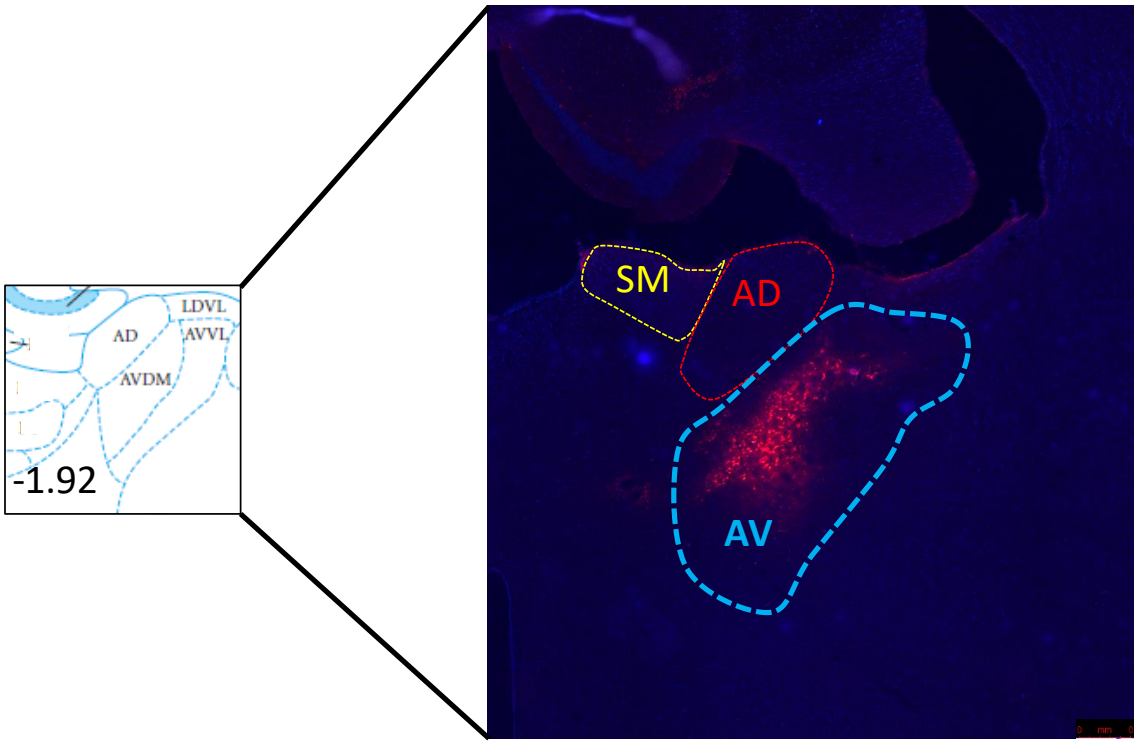

Figure 7.8. Location of viral vector infusion in the AV (right panel; AV outlined by dashed blue line). For clarity, the photomicrograph is posterior to the site of infusion and optic fibre to show the relative location of transduced cells within the AV. Abbreviations: AD= anterodorsal thalamic nuclei; AVDM= anteroventral thalamic nuclei, dorsomedial; AV= anteroventral thalamic nuclei; AVVL= anteroventral thalamic nuclei, ventrolateral; LDVL= laterodorsal thalamic nuclei, ventrolateral; SM= stria medullaris. Left panel, ATN structures adapted from Paxinos & Watson, 2014.

7.3.4 Viral vector expression in terminals

A preliminary investigation into the expression of mCherry in terminals located in distal regions was examined in several rats. mCherry / glutamatergic fibre expression (ATN efferents) was observed bilaterally in the posterior dorsal subiculum (Figure 7.9A, B and C), as well as the anterior (Figure 7.10) and posterior RSC (Figure 7.11).

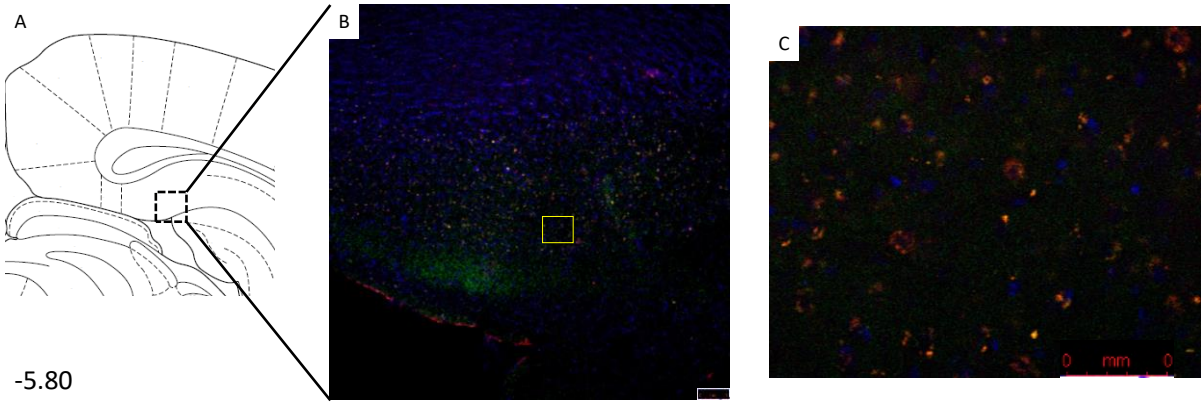

Figure 7.9. Terminal expression in the subiculum. Approximate location (shown in Figure A adapted from Paxinos and Watson, 1998) of the example confocal photographs of triple-stained (mCherry, CamKIIa and DAPI) sections showing expression of mCherry in ATN efferents to the posterior dorsal subiculum at 10x (B) and 40x (C) objective. The yellow box in B shows the relative location of B. Co-localisation of mCherry and CamKIIa is revealed by orange/yellow emission.

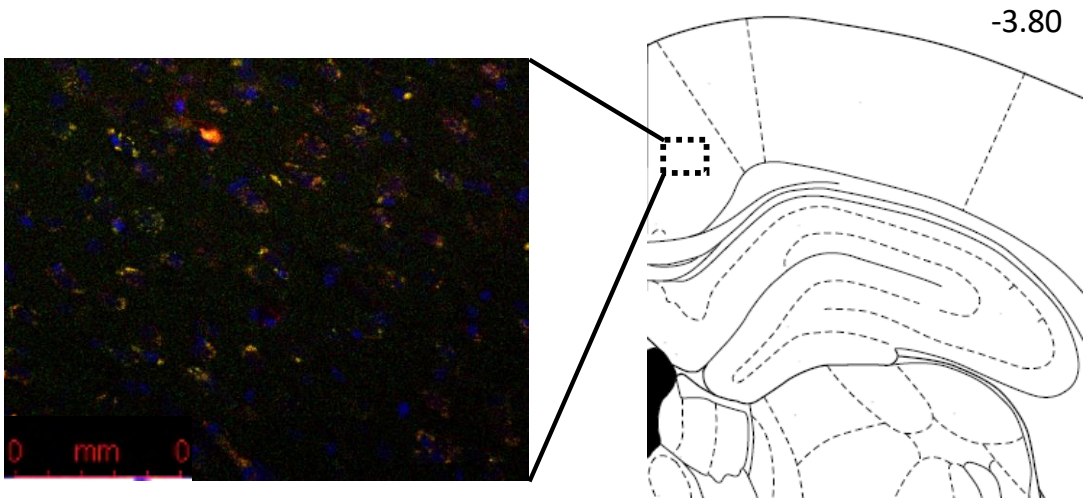

Figure 7.10. Terminal expression in the anterior retrosplenial cortex. Example confocal photograph of a triple-stained (mCherry, CamKIIa and DAPI) section showing the anterior deep granular B retrosplenial cortex. Co-localisation of mCherry and CamKIIa shown by orange/ yellow emission. The relative location in the brain at -3.80 mm from bregma is shown in the right-hand diagram adapted from Paxinos & Watson (1998). Co-localisation of mCherry and CamKIIa can be seen in the deep layers of the Rgb.

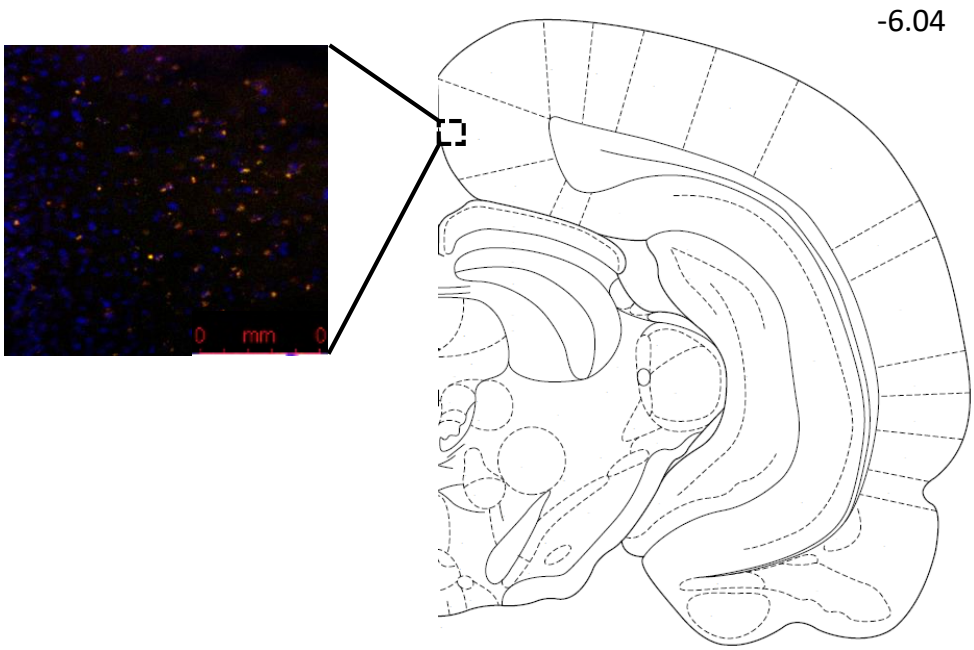

Figure 7.11. Terminal expression in the posterior retrosplenial cortex. Example confocal photograph of a triple-stained (mCherry, CamKIIa and DAPI) section showing the posterior superficial and deep granular B retrosplenial cortex. Co-localisation of mCherry and CamKIIa shown by orange/ yellow emission. The relative location in the brain at -6.04 mm from bregma is shown in the right-hand atlas plate adapted from Paxinos & Watson (1998). Co-localisation of mCherry and CamKIIa can be seen in the superficial and deep layers of the Rgb.

7.3.5 Electrode verification

One patent and correctly located electrode per rat, with minimal noise or artefacts, was selected for the ATN, HPC and mPFC. Patent electrodes in the same hemisphere were used for coherence analyses.

ATN electrodes

ATN recording electrodes extended 200 µm from the tip of the optic fibres. Correct placement of the optic fibres resulted in 12 electrodes in the MTT-lesion opsin group and 9 in the Sham group.

HPC electrodes

Only those electrodes located in CA1 cell layers above the dorsal blade of the DG were included (Figure 7.12). Six HPC electrodes from the MTT-opsin group were excluded, but only two MTT-opsin rats were removed due to bilateral exclusion of their electrodes. All other MTT opsin rats had a minimum of correct unilateral HPC placement. Similarly, three electrodes were excluded in the Sham group, but only one rat removed from analyses with

bilateral exclusion of HPC electrodes. Excluded electrodes were too ventral in the HPC, located either at or below the dorsal blade of the DG. Figure 7.13 shows the electrode placements for accepted and rejected hippocampal electrodes.

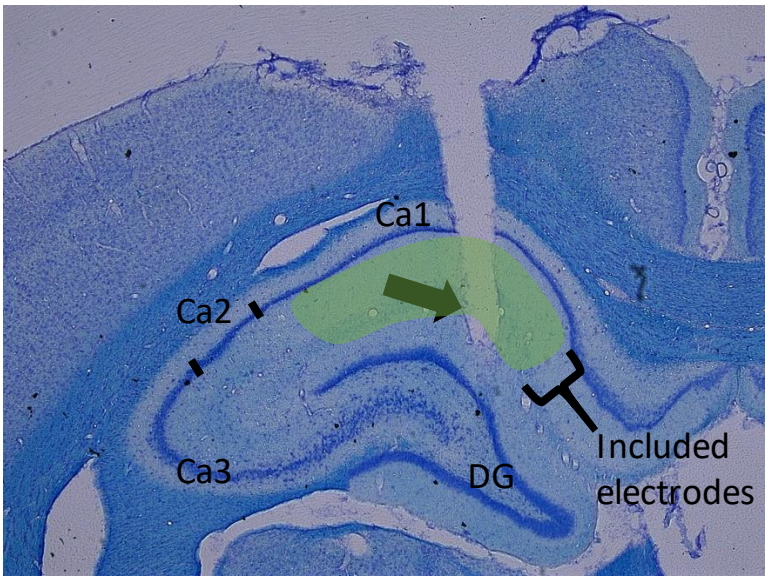

Figure 7.12. Example photograph showing an example of an acceptable electrode placement (black arrow) in a section stained with luxol blue and cresyl violet. Hippocampal sub-regions are indicated. The green area shows the area within the dorsal HPC where electrodes were located.

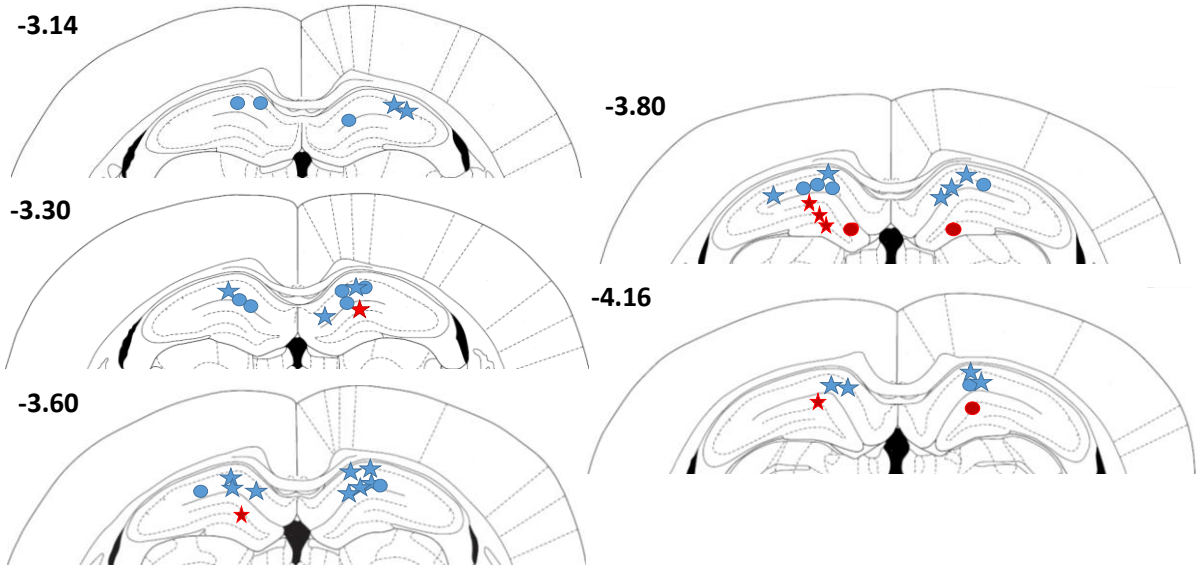

Figure 7.13. Coronal atlas plates showing the approximate location of electrodes in the dorsal hippocampus in the MTT opsin (star) and Sham (circle) groups. Excluded electrodes are shown in red.

mPFC electrodes

The primary target for the mPFC electrode was the infralimbic and prelimbic cortices. Four out of the 12 unilateral mPFC electrodes were excluded in the MTT opsin group and four out of 9 mPFC electrodes were excluded in the Sham group. The excluded electrodes were too posterior, in the cingulate cortex (see Figure 7.14 for electrode location in the mPFC).

Final Ns for all electrodes were as follows: 21 ATN electrodes (12 MTT, 9 Sham), 18 HPC electrodes (10 MTT, 8 Sham) and 13 PFC electrodes (7 MTT and 5 Sham). For the requirement of patent electrodes in the same hemisphere for coherence analysis, this left 7 MTT and 5 Sham rats for ATN-PFC and HPC-PFC coherence analyses and 10 MTT and 8 Sham for HPC-ATN coherence.

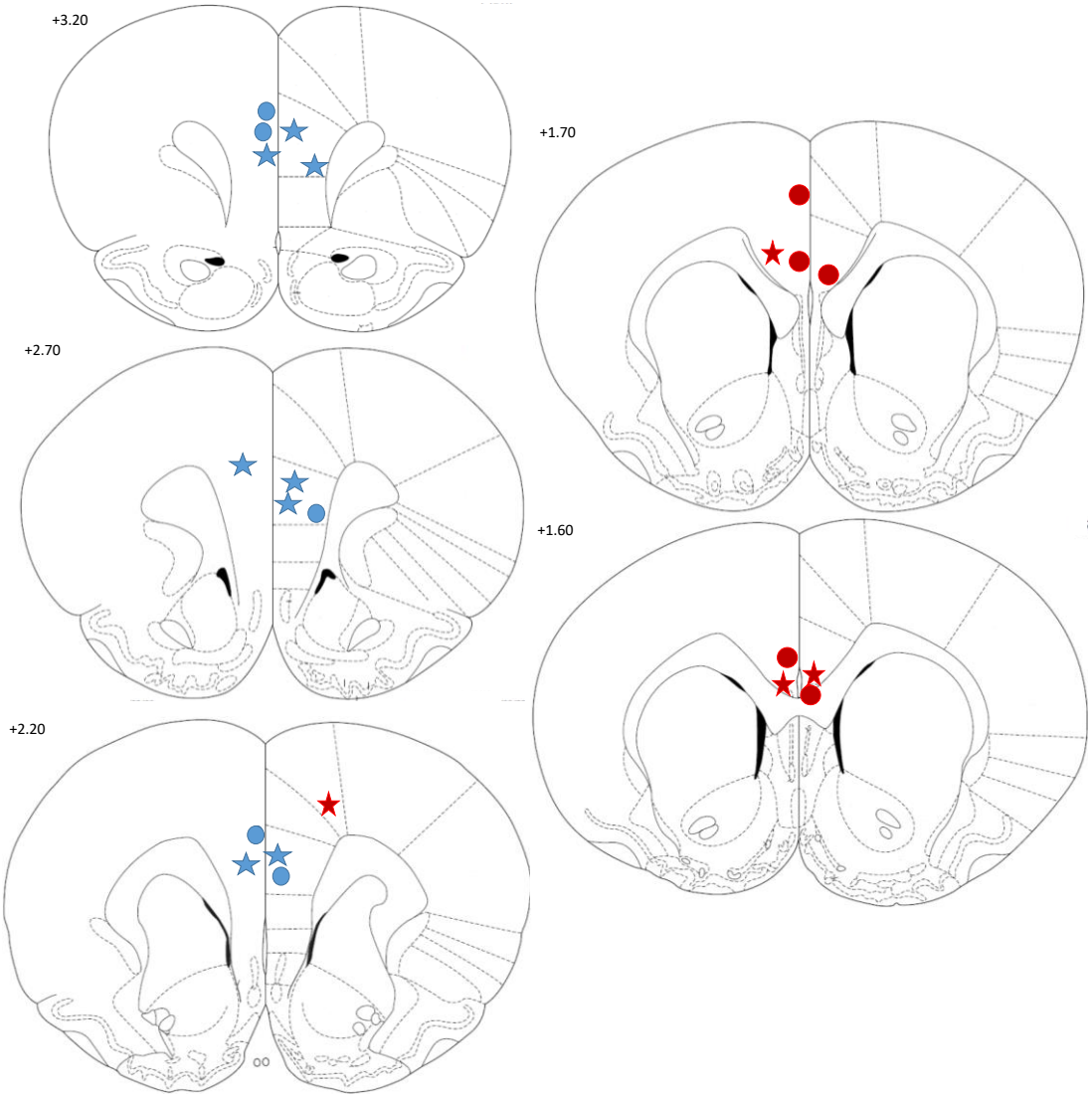

Figure 7.14. Location of electrodes in the medial prefrontal cortex in the MTT opsin (star) and Sham (circle) groups. Excluded electrodes are shown in red.

7.3.6 Spatial memory: effects of MTT lesions and optogenetic stimulation

7.3.6.1 Post-lesion RAM testing

During acquisition of the spatial working memory task in the 12-arm RAM, conducted after lesion surgery, the Sham group made progressively fewer errors across the second half of post-surgery training, whereas performance of the MTT group did not change (Group, $F(1,20)=7.92$, $p=0.01$; Group x Block[lin], $F(1,20)=6.92$, $p=0.02$; Figure 7.15A and B). The MTT group also made fewer correct entries before the first error than the Sham group, but this difference did not change significantly across training (Group, $F(1,20)=7.92$, $p=0.01$; Block[lin], $F(1,20)=1.90$, $p=0.19$; Group x Block[lin], $F(1,20)=1.72$, $p=0.21$; Figure 7.15C and D). The MTT group visited 6 or 7 arms before making an error, which suggests that their poor performance was at least partly due to the memory load associated with the task.

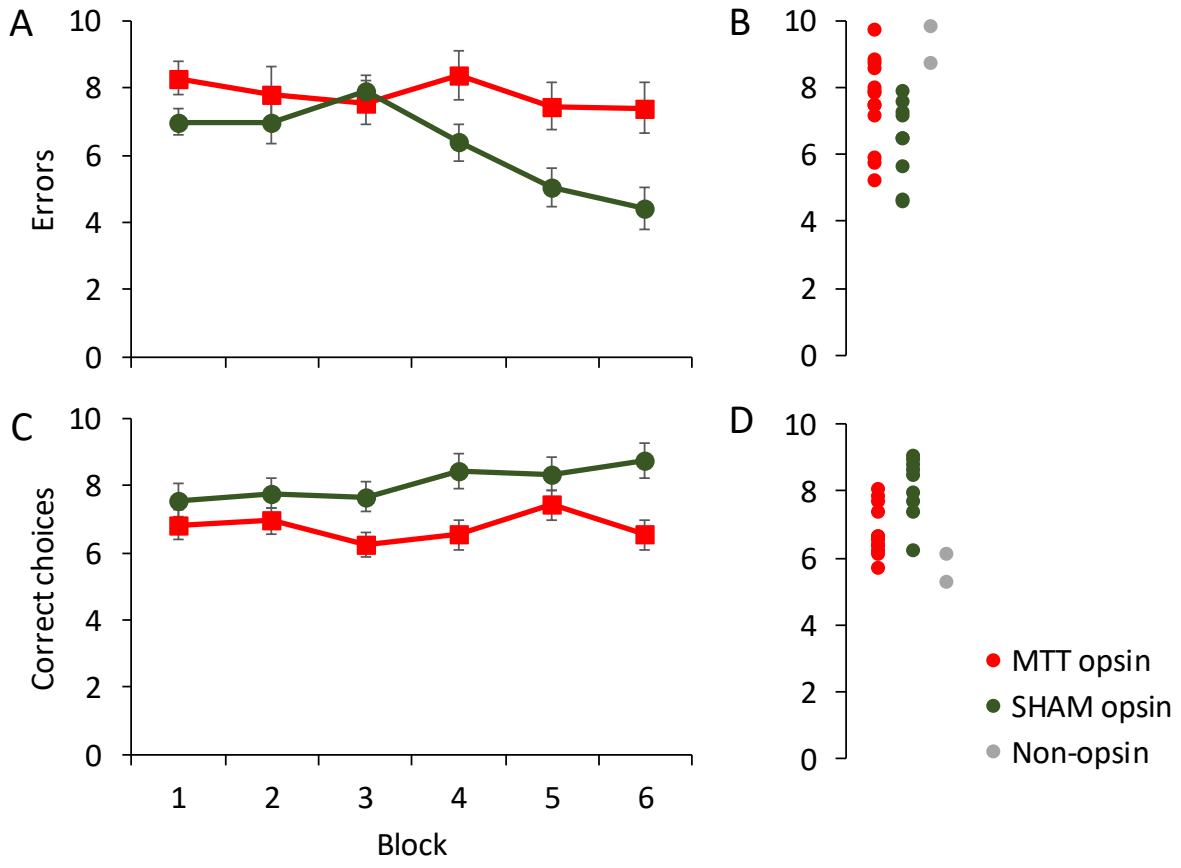

Figure 7.15. Acquisition of spatial working memory in the 12-arm radial arm maze after lesion surgery. A) Mean ± SE spatial working memory errors. C) Correct choices made before an error. B) and D) are dot plots of the performance of individual rats in the MTT opsin, Sham and MTT non-opsin rats averaged across the six blocks of testing.

7.3.6.2 Post-implant RAM testing

Rats were retrained on the working memory task after the electrode / optrode implantation surgery prior to optogenetic stimulation. The Sham group rapidly reacquired the task, making few errors by the end of the 12 sessions (7.16 A and B). By contrast the MTT group showed no improvement (Group, $F(1,20)=53.91, p<0.001$; Group x Block[lin], $F(1,20)=45.72$, $p<0.001$). As before, the MTT group made fewer entries before their first error, but did not show a difference across training (Group, $F(1,20)=8.85$, $p<0.01$; Block[lin], $F(1,20)=1.73$, $p=0.20$; Group x Block[lin]$=3.28$, $p=0.09$; Figure 7.16 C and D). By the final 2 blocks of testing (Blocks 5 and 6), MTT rats were making about 8 errors on average and Sham rats were making about 2 errors on average. Rats with MTT lesions that did not meet the criterion for lesion size made more errors than Sham rats but fewer than rats meeting the MTT lesion criteria (Table 7.3).

Table 7.3. Average number of errors made by the two excluded MTT opsin rats and the two non-opsin rats in blocks 5 and 6.

Group	Damage	Block 5	Block 6
Opsin	96% left; 63% right	5.5	6
Opsin	67% left; 80% right	5	3.5
Non-opsin	86% left; 63% right	8.5	4.5
Non-opsin	74% left; 79% right	6.5	6

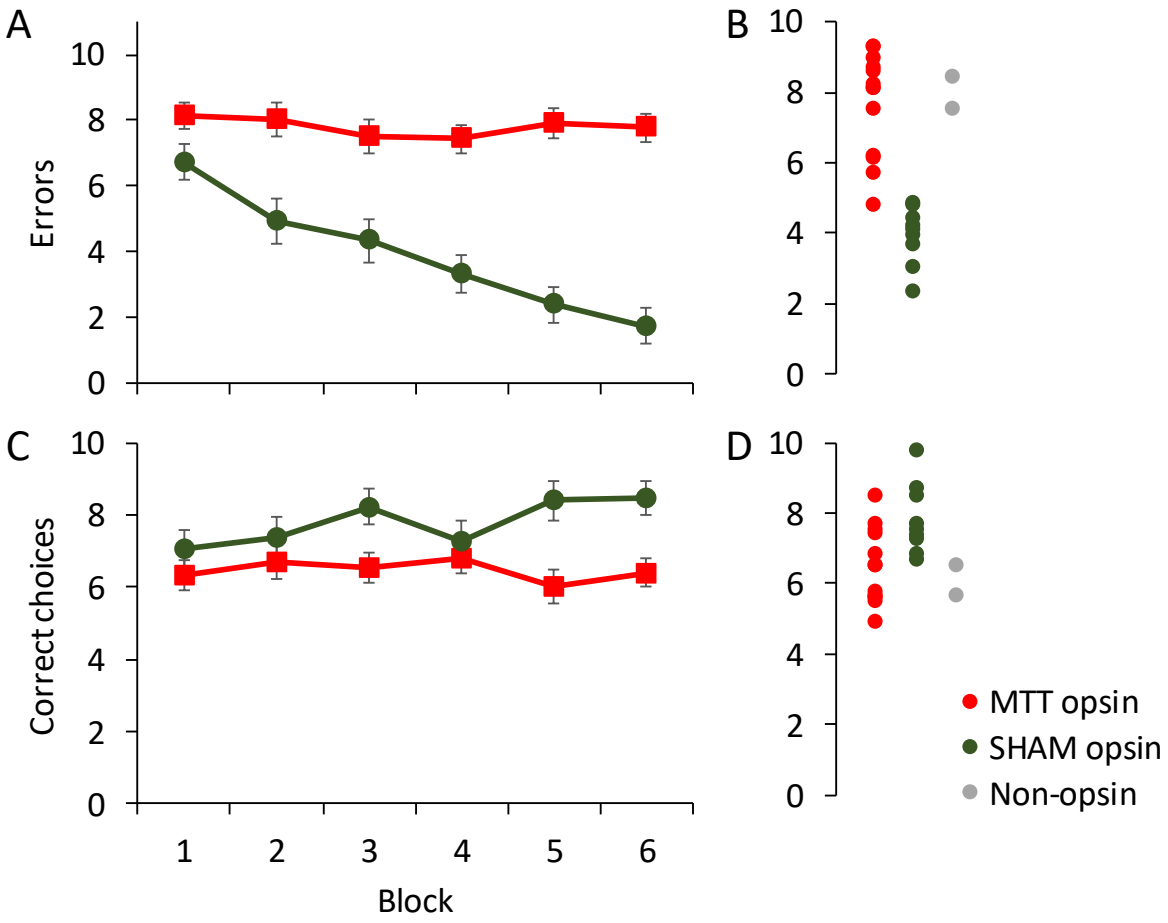

Figure 7.16 Performance in the radial arm maze task post implantation surgery. A) Mean ± SE spatial working memory errors. C) Correct choices made before an error. B) and D) are dot plots of the performance of individual rats in the MTT opsin, Sham and MTT non-opsin rats averaged across the six blocks of testing.

7.3.6.3 Optogenetic stimulation and spatial memory: Part 1

In Part 1 rats received optogenetic stimulation using regular TBS parameters. Overall, performance for the first half versus the second half of testing was similar across groups (Half, $F(1,20)=0.20$, $p=0.66$; Half x Group, $F(1,20)=0.58$, $p=0.45$). The order of stim versus no stim within each four day block also showed no effect (Order, $F(1,20)=0.01$, $p=.91$; Order x Group, $F(1,20)=0.09$, $p=0.77$). Blue light stimulation in the MTT-lesion group markedly and selectively improved performance on the RAM task (Colour phase x Stim x Group, $F(1,20)=28.69$, $p<0.001$; Figure 7.17A). Some, but not all, MTT opsin rats improved to the performance level of the Sham group (Figure 7.17B). Further analysis of this triple interaction showed that, during the orange colour phases (orange stimulation versus corresponding No Stim days), MTT opsin rats made more errors compared to Shams (post-hoc orange phase data only, Group, $F(1,20)=87.92$, $p<0.001$) but no difference in

performance was observed under orange light stimulation in either group (post-hoc orange data only, Stim, F(1,20)=0.30, p=0.59; Stim x Group, F(1,20)=2.01, p=0.17). By contrast, blue light stimulation dramatically improved performance in the MTT group (post-hoc blue phase data only, Stim x Group, F(1,20)=39.23, p<0.001). MTT non-opsin rats showed an improvement with neither blue nor orange light stimulation (Figure 7.17B).

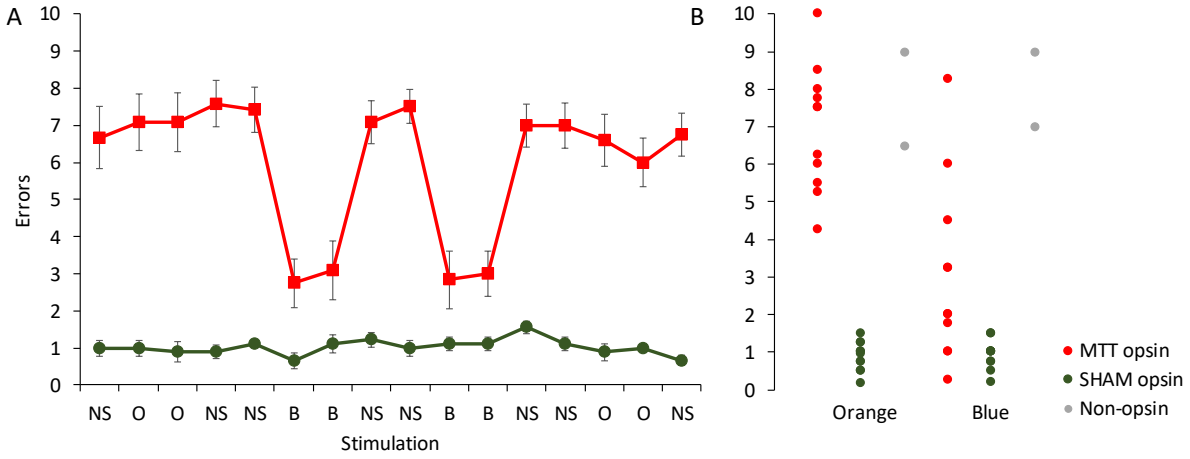

Figure 7.17. Performance in the radial arm maze task with optgenetic stimulation. A) Mean ± SE spatial working memory errors on the standard radial arm maze task with optogenetic stimulation. B) Average errors across blue light and orange light stimulation days for individual rats in the MTT opsin positive (MTT), Sham and MTT non-opsin group. Abbreviations: NS= no stimulation day; O= orange light optogenetic stimulation; B= blue light optogenetic stimulation.

7.3.6.4 Optogenetic stimulation and spatial memory: Part 2

Part 2 replicated the stimulation conditions used in Part 1, here with an OBBO design without non-stimulation days. The order of orange and blue stimulation had no effect (Order, F(1,19)=0.05, p=0.82; Order x Group, F(1,19)=0.15, p=0.70). Overall, MTT opsin rats continued to make a greater number of errors compared to Sham rats (Group, F(1,19)=96.43, p<0.001). As in Part 1, however, regular blue light TBS improved spatial working memory performance in the MTT opsin rats (Colour, F(1,19)=38.64; Colour x Group, F(1,19)=36.57, p<0.001; Figure 7.18A). No change in performance was observed in the two MTT non-opsin rats in Part 2 (Figure 7.18B).

7.3.6.5 Optogenetic stimulation and spatial memory: Part 3

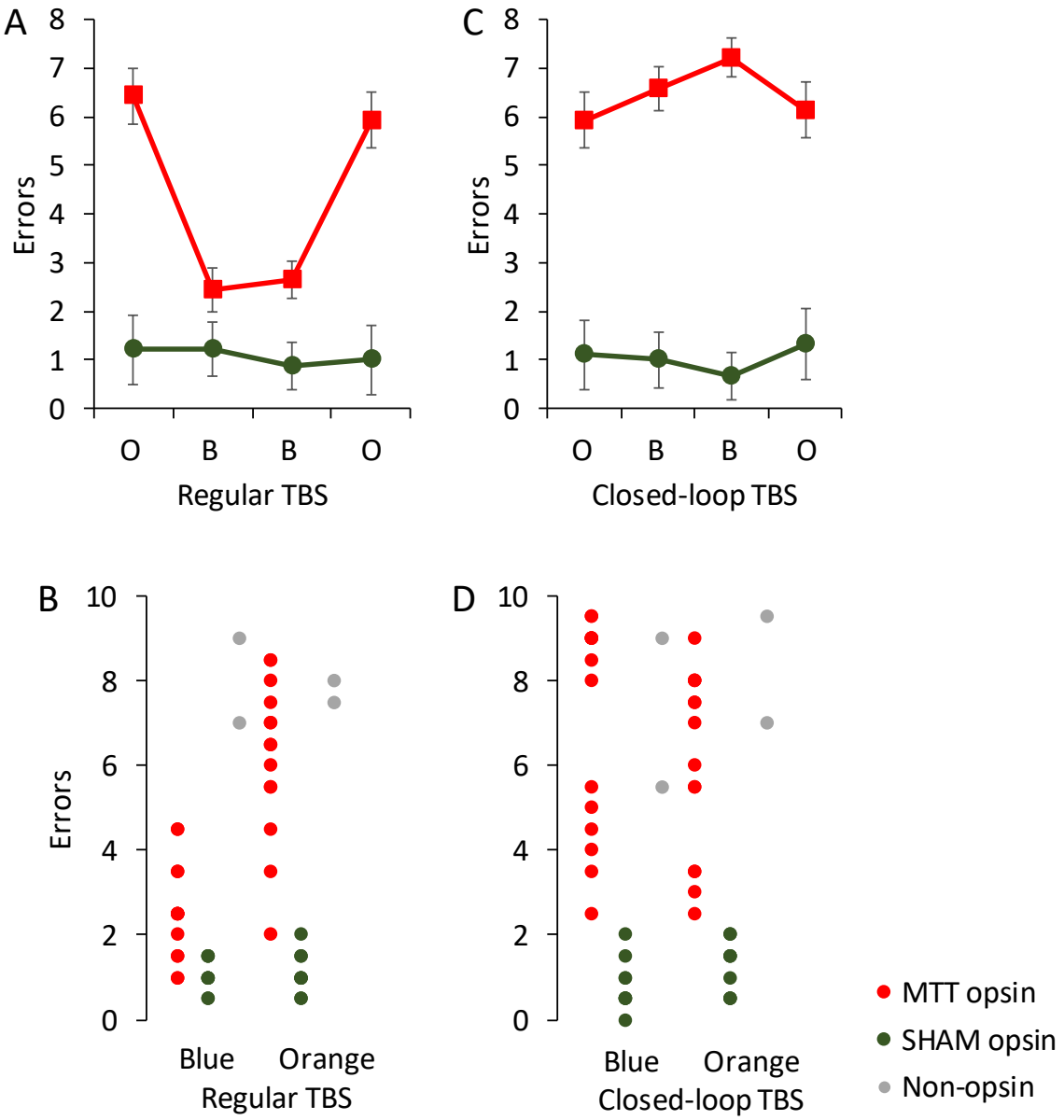

Figure 7.18. Mean ± SE spatial working memory errors on the standard radial arm maze task comparing optogenetic stimulation using regular (A) and closed-loop TBS (B). (C) Average number of errors made under blue and orange regular TBS and (D) closed-loop TBS for individual rats in the MTT opsin positive (MTT), Sham and MTT non-opsin group. Abbreviations: O= optogenetic stimulation using orange light; B=optogenetic stimulation using blue light.

Part 3 tested the effects of TBS with blue light, again using an OBBO design, but now used closed-loop stimulation, with TBS triggered by the rising phase of hippocampal theta. The order of orange and blue stimulation had no effect (Order, $F(1,19)=0.05$, $p=0.82$; Order x Group, $F(1,19)=0.15$, $p=0.70$). Unlike regular TBS, closed-loop TBS with blue light did not

improve performance in the MTT opsin rats (see Figure 7.18C), but may have mildly worsened performance in the Sham rats, although the latter did not reach significance (Colour, F(1,19)=0.62, p=0.44; Colour x Group, F(1,19)=4.17, p=0.06). Post-hoc split ANOVA of Sham rat data only revealed a small effect of blue light stimulation (post-hoc Sham data only, Colour, F(1,8)=5.77, p=0.04), and no effect of blue light was found in the MTT opsin group (post-hoc MTT data only, Colour, F(1,11)=2.84, p=0.12). As before, MTT opsin rats made a greater number of errors compared to Sham rats (Group, F(1,19)=80.98, p<0.001). No change in performance was observed in the two MTT non-opsin rats in Part 3 (see Figure 7.18D).

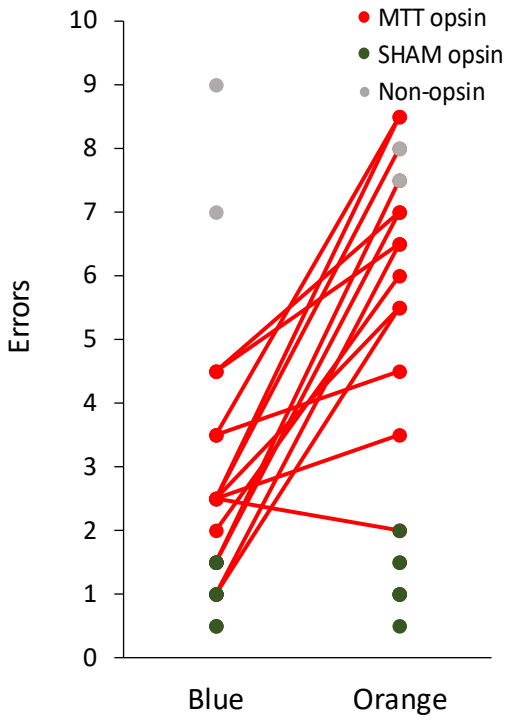

Figure 7.19. Average number of errors made in Part 2 for individual rats in the MTT opsin positive, Sham and MTT non-opsin group in orange and blue light conditions. Red lines show change in performance of each individual MTT opsin rat between blue and orange days. Overlap between Sham and MTT opsin rats has occurred in cases where a red line connects to a green dot.

The degree of improvement with regular TBS was variable across MTT opsin rats in both part 1 and part 2, with the reduction in number of errors made ranging from 3 to 7. However, in Part 2, all bar one MTT opsin rats with bilateral AV expression and optrode placement showed an improvement (see Figure 7.19).

7.3.6.6 Performance of excluded rats

The individual rat with only unilateral AV optrode and infusion placement did not initially show an improvement when regular TBS stim was delivered with blue light in Part 1. However, in Part 2, this rat did show a mild improvement. On days when the rat received regular TBS using blue light fewer errors were observed, i.e. under orange light an average of 7 errors were made compared to 6 and 3 errors on respective blue light days.

By contrast, the two excluded MTT opsin rats (with less than 80% bilateral damage to the MTT) demonstrated variable behaviour across all conditions. Both rats showed relatively intact spatial memory function, though not to the same level as Shams, making between 2.8 and 4.1 errors under control conditions. In Part 1, there was no indication that blue light regular TBS improved performance and in Part 2, it appeared that regular TBS may have improved performance in one rat but only by 1.5 errors (Table 7.4).

Table 7.4. Average number of errors across part 1 and part 2 for the excluded MTT opsin positive rats on no stimulation days (NS), blue light stimulation days (B) and orange light stimulation days (O) across the regular (Reg) and closed-loop (CL) TBS conditions.

	Part 1			Part 2		
Group	NS	O	B Reg	O	B Reg	B CL
MTT Opsin	3.1	4.0	3.8	4.0	2.5	5.0
MTT Opsin	4.1	4.3	5.3	2.8	2.5	2.5

7.3.6.7 Optogenetic stimulation and spatial memory: Part 4

The simultaneous discrimination task examined the rapid acquisition of a spatial reference memory. Rats first received two days with no stimulation on a single discrimination to ensure familiarity with the new task procedures. They then received a sequence of regular TBS stimulation, first orange light, then blue light and finally orange light on three consecutive days, each of which tested a new simultaneous discrimination (new pair of arms, one rewarded). As shown in Figure 7.20A, Sham rats made more correct choices than MTT opsin rats on control condition days (i.e. only NS and O days; Group, $F(1,19)=6.72$, $p=0.02$). Furthermore, mean performance increased steadily across time in both groups (Day, $F(3,57)=3.22$, $p=0.03$; Group x Day, $F(3,57)=1.40$, $p=0.25$), demonstrating task acquisition.

Across stimulation conditions (i.e. only O and B days) both groups showed an increase in the number of correct choices made on blue light stimulation days compared to

orange (O1 versus B versus O2, Day, F(2,38)=5.70, p=0.007; Day x Group, F(2,38)=0.90, p=0.41; planned comparison B versus average of O1 and O2, F(1,19)=14.43, p=0.001). Post-hoc comparisons show that accuracy increased under blue light stimulation compared to the first (F(1,19)=10.09, p=0.005) and second (F(1,19)=6.34, p=0.02) orange light stimulation day. There was no significant difference in correct performance for O1 versus O2 (F(1,19)=1.93, p=0.18) (Figure 7.20A). Performance did not differ between the MTT and Sham group in the simultaneous discrimination task (Group, F(1,19)=0.35, p=0.56). Blue light stimulation did not appear to affect the two MTT non-opsin rats (see Figure 7.20B).

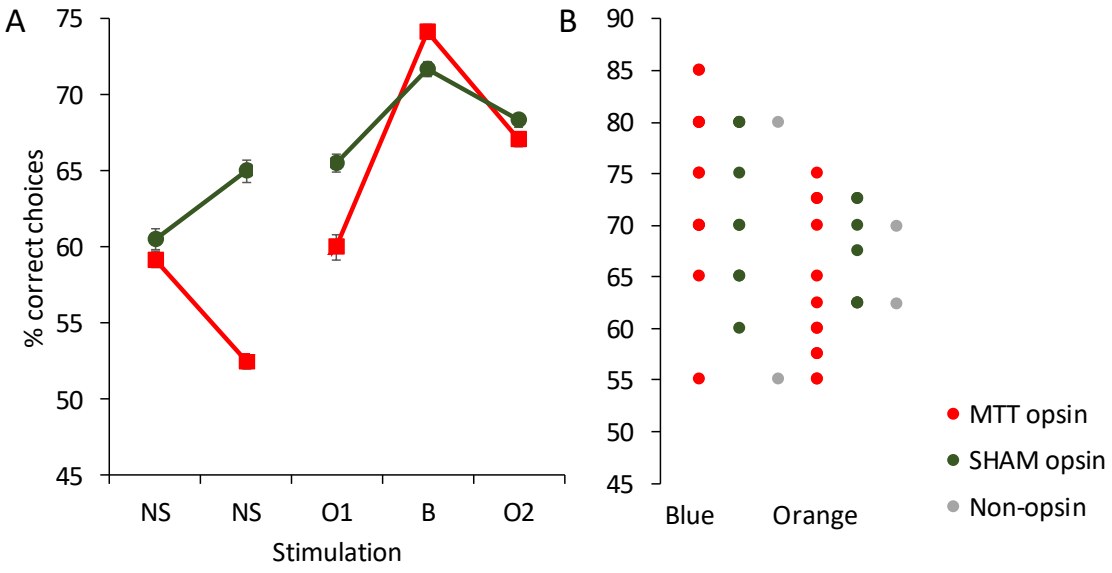

Figure 7.20. Performance on the simultaneous discrimination task in the RAM. A) Percentage ± SE correct choices on the simultaneous discrimination task in the RAM comparing no stimulation and blue and orange regular TBS. B) Average percent correct choices on blue and orange light stimulation days. Abbreviations: NS= no stimulation day; O1= first day of orange light regular TBS; B= blue light regular TBS; O2=second day of orange light regular TBS.

7.3.6.8 Part 1: Electrophysiology- Power Spectral Density

An initial repeated measures ANOVA was run including electrode placement as a repeated measure (ATN versus HPC versus PFC). There were significant PSD differences between electrodes (Electrode, F(1,11)=14.64, p=0.001), so post-hoc ANOVAs were run to examine the effects of each electrode separately. PSD for each electrode is graphed separately. No changes across first and second half of testing in Part 1 was found for any electrode (ATN electrode, Half, F(1,20)=1.28, p=.27, Half x Group, F(1,20)=0.35, p=0.71; HPC electrode, Half,

F(1,18)=0.74, p=0.40, Half x Group, F(1,18)=0.52, p=0.48, PFC electrode: Half, F(1,11)=2.12, p=0.17, Half x Group, F(1,11)=0.39, p=0.69).

No significant difference was found between the right and left ATN electrodes, or between the right and left HPC, so the data were pooled across right and left for the ATN and HPC.

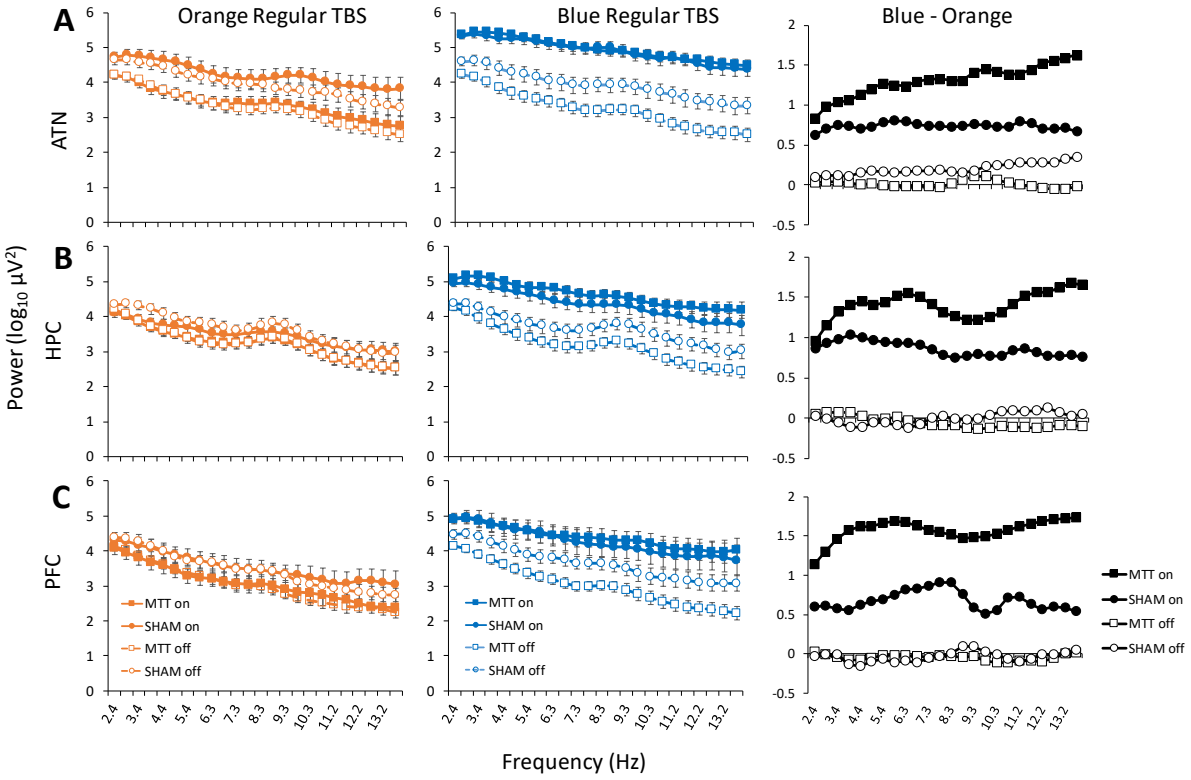

Figure 7.21. PSD comparisons of stimulation and no-stimulation days for phases when orange stimulation was used (left column) and blue stimulation was used (middle column) in Part 1. The absolute differences blue and orange "stimulation" and their corresponding "no stimulation" days, are shown on the right column. Optrodes were placed in the ATN (A), and electrodes in HPC (B) and mPFC (C). Abbreviations: on= stimulation on; off=stimulation off; MTT= mammillothalamic tract lesion opsin group; SHAM= Sham lesion opsin group.

ATN post-hoc test (Figure 7.21A): Blue light stimulation globally increased ATN PSD in the MTT group, and to a lesser extent in the Sham group (Colour phase x Stim x Group, F(1,19)=11.8, p<0.01; Colour phase x Stim, F(1,19)=72.92, p<0.001). Importantly, the increase in PSD associated with TBS did not occur under orange light stimulation (post-hoc orange phase only, Stim, F(1,9)=1.90, p=.18) and was only found on blue light stimulation days rather than associated no stimulation days (post-hoc blue phase data only, Stim, F(1,19)= 255.01, p<0.001).

As shown by figure 7.21A, MTT lesions reduced PSD in the ATN compared to Sham animals under control conditions (Post-hoc orange phase only, Group, $F(1,19)=21.94$, $p<0.001$; Group x Stim, $F(1,19)=0.38$, $p=0.54$).

HPC post-hoc test (Figure 7.21B): Blue light TBS increased global HPC PSD in both groups relative to orange light stimulation, however this effect was noticeably greater in the MTT-lesion rats compared to Sham rats (Colour phase x Stim x Group, $F(1, 18)=5.62$, $p=0.01$; Colour phase x Stim, $F(1,18)=64.54$, $p<0.001$).

The effect of TBS was only observed under blue light conditions, with no change in PSD observed under orange light conditions (post-hoc orange phase only, Stim, $F(1,18)=1.04$, $p=0.32$). As at the ATN electrode, the increase in PSD was observed on blue light stimulation days rather than associated no stimulation days (post-hoc blue phase only, Stim, $F(1,18)= 75.05$, $p<0.001$). The difference between blue and orange stimulation remained consistent in the Sham group across frequency, whilst the effect of blue light compared to orange in the MTT group appeared to increase linearly across the frequency band (Colour phase x Stim x Group x Freq[lin]=6.71, $p=0.02$).

MTT lesions reduced global overall PSD in the hippocampus under control conditions (post-hoc orange phase only, Group, $F(1,18)=4.31$, $p=0.04$; Group x Stim, $F(1,18)=0.66$, $p=0.43$; Figure 7.21B).

PFC post-hoc test (Figure 7.18C): Blue light TBS produced an increase in global PSD in both Sham and MTT rats compared to orange light stimulation (Figure 7.21C) (Colour x Onoff, $F(1,11)=6.3451$, $p=0.03$). Although the increase in PSD associated with blue light stimulation appears greater in the MTT group than the Sham group, this failed to reach significance (Colour x Onoff x Group, $F(1,11)=3.05$, $p=0.11$). The increase in PSD was unique to blue light as negligible changes in PSD were observed under orange TBS conditions (post-hoc orange phase only, Onoff, $F(1,11)=0.34$, $p=0.57$). The effect of blue light stimulation was consistent across frequency in the Sham group, but in the MTT group the difference in PSD increased linearly across frequency in the MTT group, although this also did not reach significance (Colour x Onoff x Group x Freq[lin], $F(1,11)=4.25$, $p=0.06$).

At the PFC electrode MTT-lesions reduced global PSD compared to Sham rats, under control conditions, that is, when orange light stimulation was delivered (post-hoc orange phase only, Group, F(1,11)=4.76, p=0.04).

7.3.6.9 Part 1: Electrophysiology- Coherence

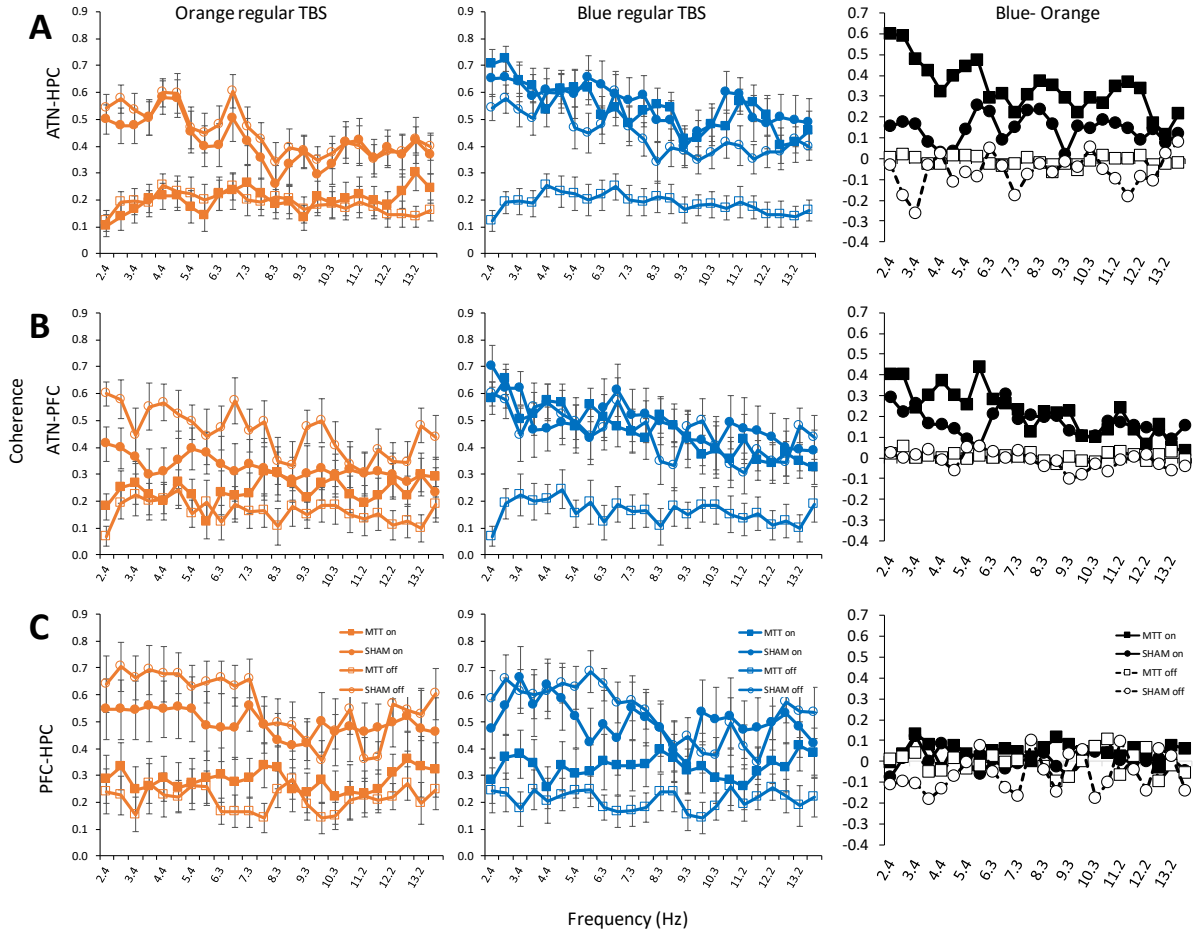

Figure 7.22. Coherence between the ATN, HPC and PFC in the orange and blue light conditions on stimulation and no-stimulation days (left and middle panels; collapsed across part 1 and part 2) and the difference in coherence between blue and orange light conditions on stimulation and no-stimulation days (blue minus orange; right panels). A) ATN-HPC coherence, B) ATN-PFC coherence, and C) HPC-PFC coherence. Abbreviations: on= stimulation on; off=stimulation off; MTT=mammillothalamic tract lesion group; SHAM= Sham lesion group.

An initial repeated measures ANOVA was run including all electrode pairs as a repeated measure. There is complex variation in coherence across frequencies that decreases steadily across electrode pairs, ordered HPC-ATN, then ATN-PFC, then PFC-HPC (Pair[lin] x Freq[lin], F(1,11)=8.05, p=0.02). For all pairs there was a steady decline in coherence with frequency that was greater for the Sham group than the MTT group (Group x Freq[lin], F(1,11)=7.84, p=0.02). Due to the complex difference in trend in coherence across frequency for the

different electrode pairs, post-hoc split ANOVAs were run in order to analyse each pair separately. Each of these focuses on a specific row in Figure 7.22.

Each pair of electrodes was submitted to an ANOVA to test for any reliable changes between the first and second half of testing. No changes across halves were found between the ATN and HPC (Half, $F(1,18)= 0.004$, $p=0.95$; Half x Group, $F(1,18)=0.38$, $p=.55$), ATN and PFC (Half, $F(1,11)=.30$, $p=.60$; Half x Group, $F(1,11)=0.12$, $p=.73$) or the HPC and PFC (Half, $F(1,11)=.54$, $p=.48$; Half x Group, $F(1,11)=0.33$, $p=.58$). The two halves were therefore combined for further analyses.

ATN-HPC post-hoc test: The difference panel in Figure 7.22A shows that TBS stimulation using blue light increased global ATN-HPC coherence in the MTT lesion group, with minor changes observed in the Sham rats (Colour phase x Stim x Group, $F(1,18)=8.15$, $p=.01$). Conversely, orange light TBS does not affect ATN-HPC coherence in either group (post-hoc orange phase only, Stim, $F(1,18)=0.22$, $p=.64$).This increase in coherence in MTT lesion rats was only observed on blue light stimulation days (post-hoc blue phase only, Stim x Group, $F(1,18)=22.34$, $p<.001$).

Under control conditions, MTT lesions reduced global ATN-HPC coherence relative to Sham rats (post-hoc orange phase only, Group, $F(1,18)=37.79$, $p<0.001$; Figure 7.22A). The greatest reduction in ATN-HPC coherence was observed at the lower frequencies where Sham coherence was greatest and decreased steadily as frequency increased (post-hoc orange phase only, Group x Freq[lin], $F(1,18)=14.74$, $p=0.001$).

ATN-PFC post-hoc test: The difference panel in Figure 7.22B shows that TBS stimulation with blue light increased ATN-PFC coherence in both the MTT and Sham group (Colour phase x Stim, $F(1,11)=81.14$, $p<0.001$). The increase in ATN-PFC coherence in MTT rats was greatest at lower frequencies and decreased steadily across the frequency band (Colour phase x Stim x Group x Freq[lin], $F(1,11)=11.35$, $p=0.003$). The increase in ATN-PFC coherence associated with TBS stimulation was only observed under blue light conditions, with negligible effects observed in either group when TBS was delivered using orange light (post-hoc orange phase only, Stim x Group, $F(1,11)=2.61$, $p=.14$).

Under control conditions MTT lesions reduced global ATN-PFC coherence compared to Sham rats (post-hoc orange phase only, $F(1,11)=22.62$, $p=0.001$; Figure 7.22B). As with

ATN-HPC coherence, the greatest reduction in ATN-PFC coherence was observed at the lower frequencies where Sham coherence was greatest, however this interaction failed to reach significance (Group x Freq[lin], F(1,11)=3.40, p=0.09).

HPC-PFC post-hoc test: The bottom difference panel in Figure 7.22C shows that in contrast to the effects on ATN-HPC and ATN-PFC coherence, neither blue nor orange TBS significantly altered coherence in either Sham or MTT-lesion rats (Colour phase x Stim, F(1,11)=0.30, p=0.59; Colour phase x Stim x Group, F(1,11)=1.50, p=0.25). No effects were found under control conditions (post-hoc orange phase only, Stim, F(1,11)=.11, p.75; Stim x Group, F(1,11)=2.89, p=.12).

MTT lesions reduce global PFC-HPC coherence compared to Sham rats under control conditions (post-hoc orange phase only, Group, F(1,11)=18.11, p=0.001; Figure 7.22C). The greatest reduction in HPC-PFC coherence was observed at the lower frequencies where Sham coherence was greatest (post-hoc orange phase only, Group x Freq[lin], F(1,11)=5.61, p=0.04).

7.3.6.10 Part 2: Electrophysiology- Power Spectral Density

An initial repeated measures ANOVA was run including all electrodes as a repeated measure. Due to significant differences in PSD between electrodes (Electrode, F(1,11)=5.42, p=0.01), post-hoc split ANOVAs were run in order to clarify the effects of each electrode separately. PSD for each electrode is graphed separately in Figure 7.23.

Each electrode was submitted to an ANOVA to test for any reliable changes across the order of orange and blue days. No effects of order were found at the PFC electrode (Order, F(1,11)=1.97, p=0.19; Order x Group, F(1,11)=1.64, p=0.23), the HPC electrode (Order, F(1,18)=2.63, p=0.12; Order x Group, F(1,18)=0.60, p=0.45) or the ATN electrode (Order, F(1,19)=0.26, p=0.87; Order x Group, F(1,19)=0.24, p=0.87).

As can be seen in Figure 7.23, there was no observable overall difference in PSD between Sham and MTT-lesion rats in the ATN (Group, F(1,19)=0.41, p=0.53),HPC (Group, F(1,18)=2.71, p=0.12) or PFC (Group, F(1,11)=0.24, p=0.63). Under control conditions (i.e. orange light stimulation) PSD decreases linearly across frequency across all electrodes, and to a greater extent in the MTT group (post-hoc orange light only: PFC, Group x

Freq[lin]=11.51, p=0.006; HPC, Group x Freq[lin], F(1,19)=19.25, p<0.001; ATN, Group x Freq[lin]=7.37, p=0.01).

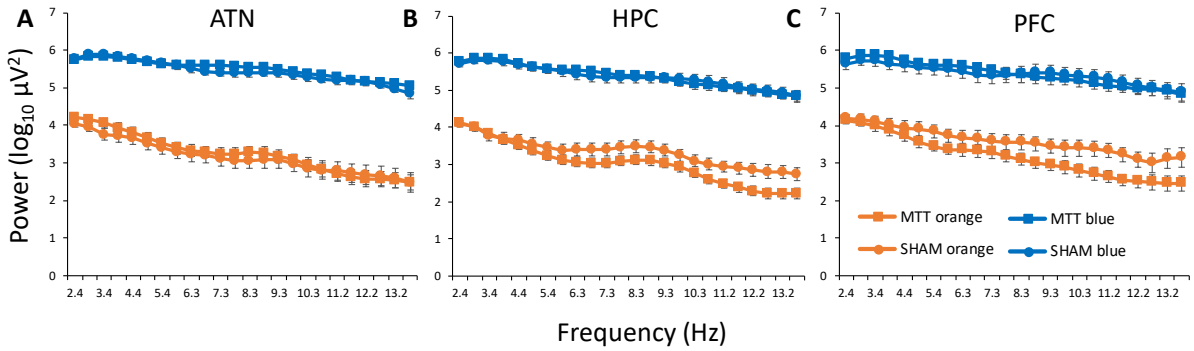

Figure 7.23. PSD in the regular theta burst stimulation (TBS) condition (collapsed across daypair 1 and 2) in the ATN (A), HPC (B) and PFC (C). Abbreviations: MTT=mammillothalamic tract lesion group; SHAM= Sham lesion group.

ATN post-hoc test (Figure 7.23A): Regular TBS delivered using blue light increased PSD in the ATN in both groups compared to orange (Colour, F(1,19)=748.98, p<0.001). This increase in PSD was equivalent in both groups (Colour x Group, F(1,19)=0.03, p=0.87).

HPC post-hoc test (Figure 7.23B): Regular TBS blue light stimulation was associated with an increase in global PSD in the HPC in both groups compared to orange light stimulation (Colour, F(1,18)=814.55, p<0.001), although this was to a greater extent in MTT rats (Colour x Group, F(1,18)=4.71, p=0.04).

PFC post-hoc test (Figure 7.23C): Regular TBS using blue light was associated with a global increase in prefrontal PSD in both groups compared to orange light stimulation (Colour, F(1,11)=380.56, p<0.001). It appears that (as in the HPC) the increase in PSD was greatest in the MTT lesion group, although this interaction failed to reach significance (Colour x Group, F(1,11)=4.62, p=0.055).

7.3.6.11 Part 2: Electrophysiology- Coherence

An initial repeated measures ANOVA was run including all electrode pairs as a repeated measure. There is complex variation in coherence across frequencies, with coherence decreasing steadily across electrode pairs ordered HPC-ATN, the ATN-PFC, and then PFC-HPC (Pair x Freq[lin], F(1,10)=9.49, p=0.01). Coherence also varies as a function of colour across electrode pairs, with a differential effect occurring across the ATN-PFC under blue light conditions compared to the ATN-HPC and HPC-PFC (Colour x Pair[quad], F(1,10)= 12.48,

p=0.005). Due to the complex difference in coherence across frequency and between colour conditions for the different electrode pairs, post-hoc split ANOVAs were run in order to analyse each pair separately. Each pair is also graphed separately in Figure 7.24.

Each pair of electrodes was submitted to an ANOVA to test for any effect of order of orange and blue days within the four-day block of stimulation. No changes OB and BO were found between the ATN and HPC (Order, F(1,18)=0.00, p=0.99; Order x Group, F(1,18)=0.02, p=0.90), ATN and PFC (Order, F(1,10)=0.15, p=0.71; Order x Group, F(1,10)=2.97, p=0.12) or the HPC and PFC (Order, F(1,10)=0.07, p=0.80; Order x Group, F(1,10)=2.03, p=0.19).

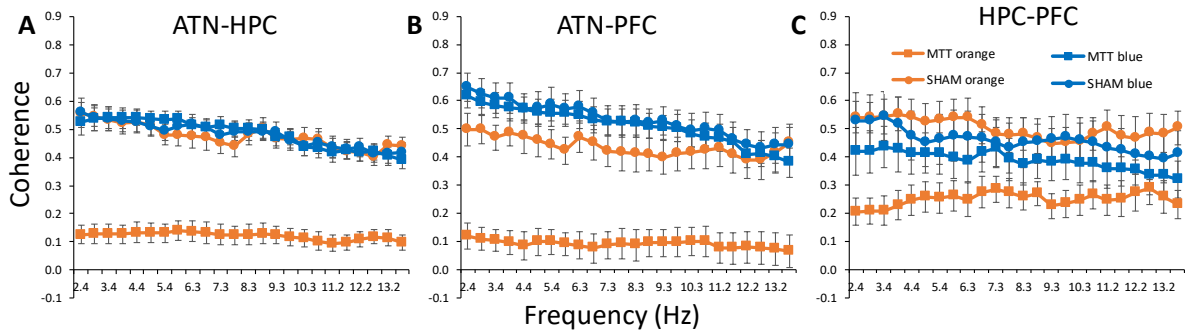

Figure 7.24 Coherence between the ATN (A), HPC (B) and PFC (C) in the regular TBS conditions (collapsed across daypair 1 and 2). Abbreviations: orange= orange light stimulation; blue=blue light stimulation; MTT=mammillothalamic tract lesion group; SHAM= Sham lesion group.

ATN-HPC post-hoc test (Figure 7.24A): Overall blue light stimulation increased coherence in MTT rats relative to Shams (Colour x Group, F(1,18)=53.31, p<0.001). Moreover, the increase in ATN-HPC coherence in MTT rats was greatest at lower frequencies (Colour x Group x Freq[lin], F(1,18)=5.39, p=0.03).

MTT lesions reduce global ATN-HPC coherence relative to Sham rats under control conditions (post-hoc orange data only, Group, F(1,18)=126.25, p<0.001). The greatest reduction in ATN-HPC coherence was observed at lower frequencies where Sham coherence was greatest, with a modest decrease as frequency increased (post-hoc orange data only, Group x Freq[lin], F(1,17)=5.18, p=0.04).

ATN-PFC post-hoc test (Figure 7.24B): Under blue light conditions regular TBS increases coherence between the ATN and PFC in both groups, but this effect is greater in MTT-lesion rats compared to Sham rats (Colour, F(1,10)=97.53, p<0.001; Colour x Group,

F(1,10)=38.30, p<0.001). The increase in coherence observed under blue light stimulation was greatest at lower frequencies in both groups (Colour x Freq[lin], F(1,10)=9.25, p=0.01).

MTT lesions reduced ATN-PFC coherence relative to Sham rats under control conditions (post-hoc orange data only, Group, F(1,10)=14.15, p=0.001), but that this did not differ across frequency (post-hoc orange data only, Group x Freq[lin], F(1,10)=0.31, p=0.59).

HPC-PFC post-hoc test (Figure 7.24C): Regular TBS under blue light conditions mildly increased HPC-PFC coherence in the MTT-lesion group only (Colour x Group, F(1,10)=4.94, p<0.05; Colour, F(1,10)=1.42, p=0.26).

MTT lesions reduced HPC-PFC coherence compared to Sham rats to a greater extent under control orange light conditions (post-hoc orange data only, Group, F(1,10)=87.03, p<0.001).

7.3.6.12 Part 3: Electrophysiology- Power Spectral Density

An initial repeated measures ANOVA was run including all electrodes as a repeated measure. Due to significant differences in PSD between electrodes (Electrode, F(1,11)=5.97, p=0.03), post-hoc split ANOVAs were run in order to clarify the effects of each electrode separately. PSD for each electrode is graphed separately in figure 7.25.

Each electrode was submitted to an ANOVA to test for any reliable changes across order of OB and BO. No effects of order were found in the PFC electrode (Order, F(1,11)=1.86, p=0.20; Order x Group, F(1,11)=0.01, p=0.66), the HPC electrode (Order, F(1,18)=0.47, p=0.50; Order x Group, F(1,18)=0.02, p=0.88) or the ATN electrode (Order, F(1,19)=1.44, p=0.25; Order x Group, F(1,19)=1.57, p=0.23).

There was no observable overall difference in PSD between Sham and MTT-lesion rats in the PFC (Group, F(1,11)=0.20, p=0.66),HPC (Group, F(1,18)=0.15, p=0.70) or ATN (Group, F(1,19)=0.05, p=0.82). PSD decreases linearly across frequency across all electrodes, and to a greater extent in the MTT group (post-hoc orange light only: PFC, Group x Freq[lin], F(1,11)=7.60, p=0.02; HPC, Group x Freq[lin], F(1,19)=8.87, p=0.01; ATN, Group x Freq[lin]=6.20, p=0.02).

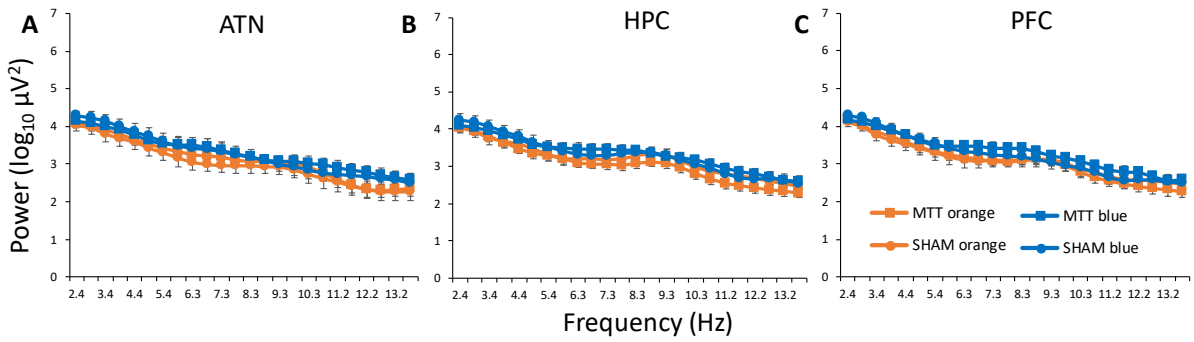

Figure 7.25. PSD in the closed-loop theta burst (TBS) condition (collapsed across daypair 1 and 2) in the ATN (A), HPC (B) and PFC(C). Abbreviations: MTT=mammillothalamic tract lesion group; SHAM= Sham lesion group.

ATN post-hoc test (Figure 7.25A): Closed-loop TBS delivered using blue light did not affect overall ATN PSD in either group (Colour, F(1,19)=3.21, p=0.09). However, at higher frequencies, closed-loop blue light stimulation did mildly increase PSD in the MTT group compared to orange light stimulation (Colour x Group x Freq[lin], F(1,19)=5.93, p=0.03).

HPC post-hoc test (Figure 7.25B): Closed-loop TBS blue light stimulation was associated with a small increase in global PSD in the HPC in both groups compared to orange light stimulation (Colour, F(1,18)=8.02, p=0.01). As was observed in the ATN, although relatively small in size, PSD in the MTT group increased more at higher frequencies, relative to orange light stimulation (Colour x Group x Freq[lin], F(1,8)=9.40, p=0.006).

PFC post-hoc test (Figure 7.25C): Closed-loop TBS using blue light did not increase prefrontal PSD in either group relative to orange light stimulation (Colour, F(1,11)=3.33, p=0.09). Unlike PSD in the HPC and ATN, no increase in PSD was observed at higher frequencies in the MTT group (Colour x Group X Freq[lin], F(1,11)=1.73, p=0.22).

7.3.6.13 Part 3: Electrophysiology- Coherence

An initial repeated measures ANOVA was run including all electrode pairs as a repeated measure. There is complex variation in coherence across electrode pairs, with coherence varying following a quadratic trend across electrode pairs ordered HPC-ATN, ATN-PFC, PFC-HPC (Pair[quad], F(1,10)=19.38, p=0.001). Coherence also varies across electrode pairs as a function of colour with a differential effect occurring across the ATN-PFC under blue light conditions compared to the ATN-HPC and HPC-PFC (Colour x Pair[quad], F(1,10)= 16.56, p=0.002). Due to the complex differences in coherence for the different electrode pairs,

post-hoc split ANOVAs were run in order to analyse each pair separately. Coherence for each electrode pair is graphed separately in Figure 7.26.

Each pair of electrodes was submitted to an ANOVA to test for any effect of order of orange and blue days within the four-day block of stimulation. No changes between OB and BO were found between the ATN and HPC (Order, $F(1,18)=1.30$, $p=0.27$; Order x Group, $F(1,18)=0.01$, $p=0.93$), ATN and PFC (Order, $F(1,10)=1.16$, $p=0.31$; Order x Group, $F(1,10)=4.61$, $p=0.10$) or the HPC and PFC (Order, $F(1,10)=0.20$, $p=0.67$; Order x Group, $F(1,10)=0.47$, $p=0.51$).

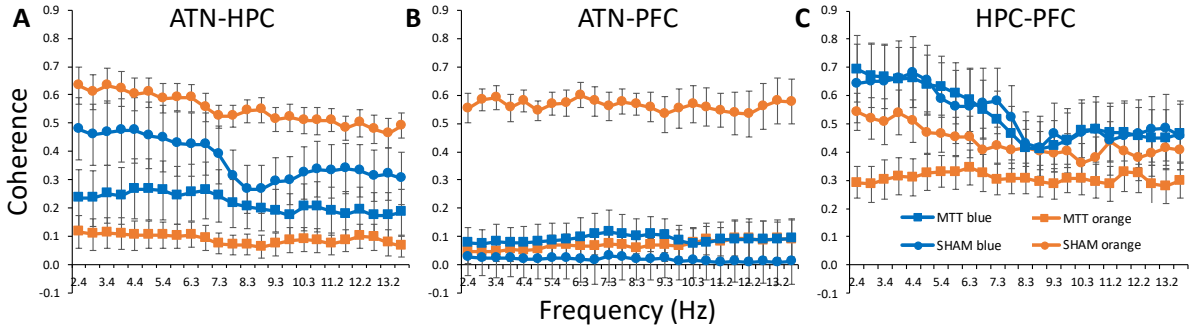

Figure 7.26. Coherence between the ATN (A), HPC (B) and PFC (C) in the regular TBS conditions (collapsed across daypair 1 and 2). Abbreviations: orange= orange light stimulation; blue=blue light stimulation; MTT=mammillothalamic tract lesion group; SHAM= Sham lesion group.

ATN-HPC post-hoc test (Figure 7.26A): Blue light stimulation mildly increased coherence in MTT rats relative to Shams (Colour x Group, $F(1,18)=4.80$, $p=0.04$). The increase in ATN-HPC coherence in MTT rats appears to remain relatively uniform across the frequency band (Colour x Group x Freq[lin], $F(1,18)=0.07$, $p=0.80$).

MTT lesions reduce global ATN-HPC coherence relative to Sham rats under orange light conditions (post-hoc orange data only, Group, $F(1,18)=100.56$, $p<0.001$). The greatest reduction in ATN-HPC coherence was observed at lower frequencies where Sham coherence was greatest (post-hoc orange data only, Group x Freq[lin], $F(1,17)=5.33$, $p=0.03$).

ATN-PFC post-hoc test (Figure 7.26B): Under blue light conditions closed-loop TBS decreases coherence between the ATN and PFC in both groups, but this effect is most striking in the Sham group (Colour, $F(1,10)=27.67$, $p<0.001$; Colour x Group, $F(1,10)=32.11$,

p<0.001). Moreover, the decrease in Sham coherence did not vary across the frequency band (Colour x Group x Freq[lin], F(1,10)=0.14, p=0.71).

MTT lesions reduced ATN-PFC coherence relative to Sham rats under control orange light conditions (post-hoc orange data only, Group, F(1,10)=85.77, p<0.001).

HPC-PFC post-hoc test (Figure 7.26C): Closed-loop TBS using blue light increases HPC-PFC coherence in both groups but only at lower frequencies (Colour x Freq[lin], F(1,10)=6.60, p=0.03). Although it appears that closed-loop TBS mildly increases global HPC-PFC coherence in both groups, this main effect failed to reach significance (Colour, F(1,10)=4.88, p=0.05).

Overall, HPC-PFC coherence was reduced by MTT lesions compared to Sham rats under control orange light conditions (post-hoc orange data only, Group, F(1,10)=9.66, p=0.01.

7.3.7 Zif268 expression after regular TBS in an open field

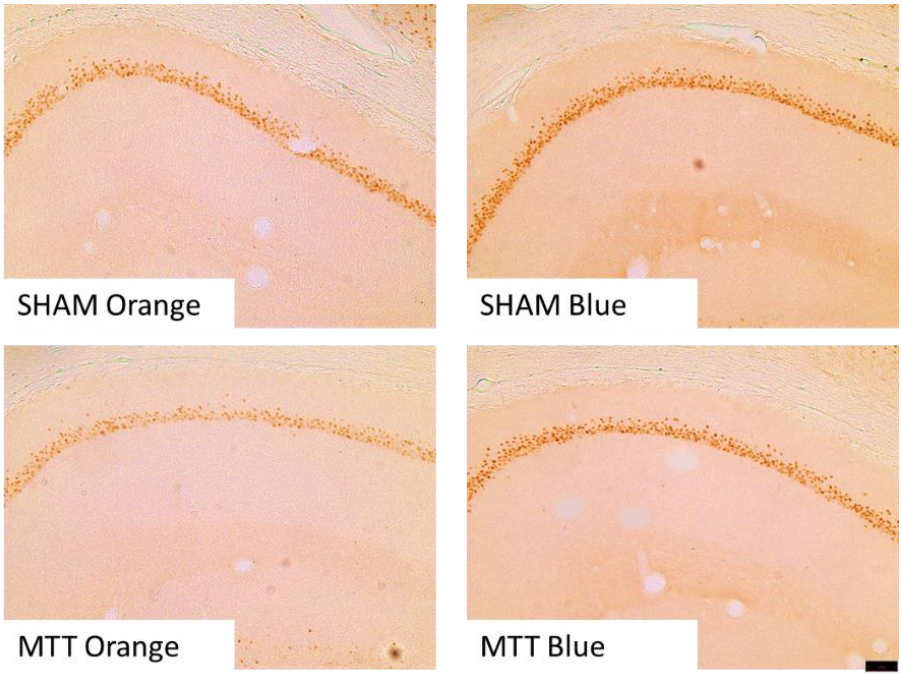

Figure 7.27. Example photographs (10x objective) of Zif268 immunostaining in hippocampal area CA1 of the dorsal hippocampus from a Sham (top) and MTT opsin rat (bottom) showing Zif268 expression following orange (left) and blue (right) stimulation.

At the end of the experiment rats were placed in an open field, allowed to forage for food and given regular TBS at 8.5 Hz. Rats were stimulated with orange light (control) in the ATN in one hemisphere and blue light to activate transduced cells in the contralateral ATN. Zif268 (Figure 7.27) expression was examined across the extended hippocampal system (hippocampus, prefrontal and retrosplenial cortex). Raw cell counts were transformed with a square root transform in order to normalise error variance and make them suitable for analysis with ANOVA.

7.3.7.1 Retrosplenial granular b cortex

Higher Zif268 expression was found in the anterior deep layer of the Rgb (AP x Layer, $F(1,19)=6.42$, $p=0.02$).

MTT lesions reduced Zif268 expression in the Rgb (Group, $F(1,19)=8.44$, $p<0.001$), and this reduction was equivalent across the AP axis (AP x Group, $F(1,19)=1.58$, $p=0.22$) and irrespective of layer (Layer x Group, $F(1,19)=1.24$, $p=0.27$; Figure 7.28A).

Overall, blue light stimulation increased Zif268 activation in the superficial and deep layers of the anterior and posterior Rgb (Colour, $F(1,19)=169.58$, $p<0.001$; Figure 7.28A). Blue light stimulation increased Zif268 expression to a much greater extent in the anterior Rgb compared to the deep Rgb (Colour x AP, $F(1,19)=7.89$, $p=0.01$; anterior sup Rgb, Colour, $F(1,19)=42.25$, $p<0.001$; deep Rgb, Colour, $F(1,19)=40.884$, $p<0.001$; posterior sup Rgb, Colour, $F(1,19)=6.04$, $p<0.02$; deep Rgb ($F(1,19)=9.39$, $p<0.01$). Furthermore, increases in Zif268 expression were greater in the deep layers compared to the superficial layers in both the anterior and posterior Rgb (Layer x Colour, $F(1,19)=8.86$, $p=0.01$; anterior sup Rgb, Colour, $F(1,19)=42.25$, $p<0.001$; deep Rgb, Colour, $F(1,19)=40.884$, $p<0.001$; posterior sup Rgb, Colour, $F(1,19)=6.04$, $p<0.02$; deep Rgb ($F(1,19)=9.39$, $p<0.01$). The effect of blue light stimulation was not dependent on lesion status as it did not differ between MTT and Sham rats (Colour x Group, $F(1,19)=3.19$, $p=0.09$).

7.3.7.2 Retrosplenial dysgranular cortex

MTT lesions did not affect Zif268 expression in the anterior or posterior Rdg (Group, $F(1,19)=0.06$, $p=0.81$; AP x Group, $F(1,19)=3.13$, $p=0.09$; Layer x Group, $F(1,19)=0.26$, $p=0.61$). Unlike the stimulation effect in the Rgb, blue light stimulation did not increase Zif268 immunoreactivity in the Rdg (Colour, $F(1,19)=0.27$, $p=0.60$; AP x Colour, $F(1,19)=0.91$, $p=0.35$; Layer x Colour, $F(1,19)=0.01$, $p=0.91$; Figure 7.28B).

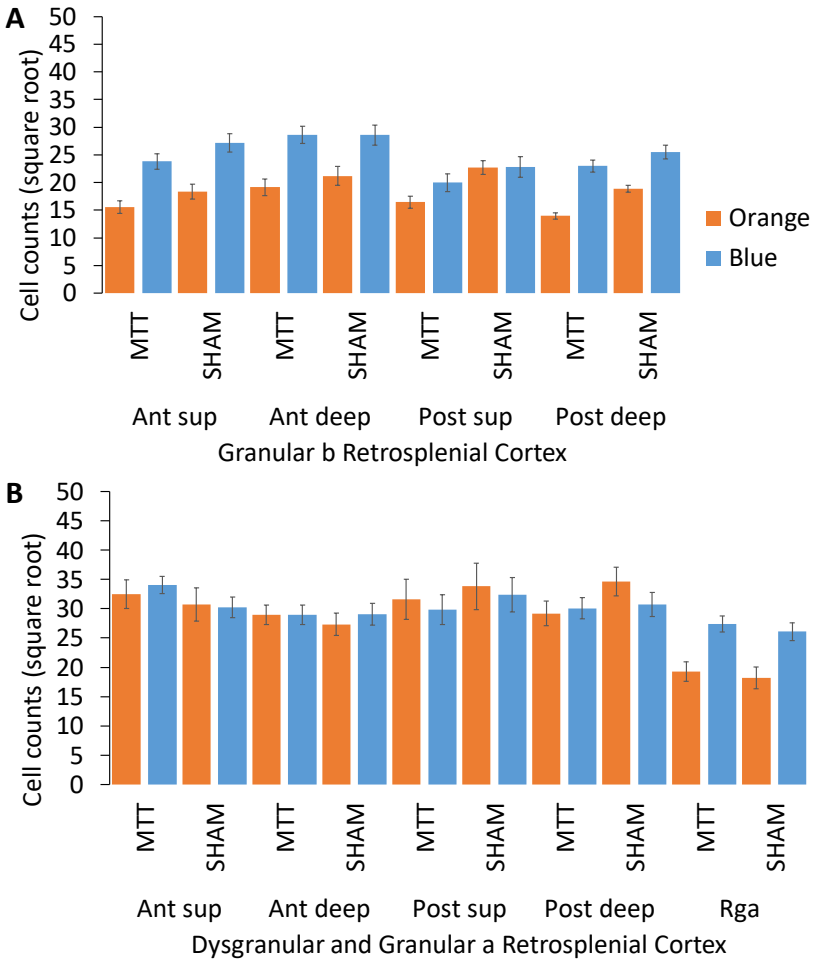

Figure 7.28. Zif268 expression in the retrosplenial cortex. Mean ± SE of square root of Zif268 cell counts for MTT and Sham groups in blue and orange light conditions across the subregions of the anterior and posterior retrosplenial granular b (A) cortex and the retrosplenial granular a and dysgranular cortex (B). Abbreviations: Ant= anterior; Post= posterior; Sup= superficial.

7.3.7.3 Retrosplenial granular a cortex

Blue light stimulation substantially increased Zif268 activity in the Rga (Colour, $F(1,19)=52.18$, $p<0.001$; Figure 7.28B) and this increase was relatively the same in both Sham and MTT rats (Colour x Group, $F(1,19)=0.01$, $p=0.91$). Zif268 expression was relatively similar across both MTT and Sham rats in both conditions (Group, $F(1,19)=0.37$, $p=0.55$).

7.3.7.4 Hippocampus

There were higher Zif268 cell counts in area CA1 compared to all other hippocampal subregions (Region, $F(3,57)=369.79$, $p<0.001$; Figure 7.29A).

Blue light stimulation increased Zif268 cell counts in area CA1 compared to orange light stimulation (Region x Colour, $F(3,57)=13.40$, $p<0.001$; post-hoc area CA1 only, Colour,

F(1,19)=69.75, p<0.001), whilst having a negligible effect in other subregions of the hippocampus (CA3, hilus of the DG and DG all F<1.15, p>0.30). MTT lesions did not affect Zif268 immunoreactivity in the HPC (Group, F(1,19)=0.27, p=0.61; Region x Group, F(3,57)=0.86, p=0.46).

7.3.7.5 Subiculum

As can be seen in Figure 7.29A Zif268 expression was greater in the Sham group compared to the MTT group (Group, F(1,19)=6.75, p=0.02). Blue light stimulation increased Zif268 activation in both MTT and Sham groups (Colour, F(1,19)=128.45, p<0.001). The increase in Zif268 expression following blue light stimulation was similar across both Sham and MTT groups (Colour x Group, F(1,19)=2.54, p=0.12).

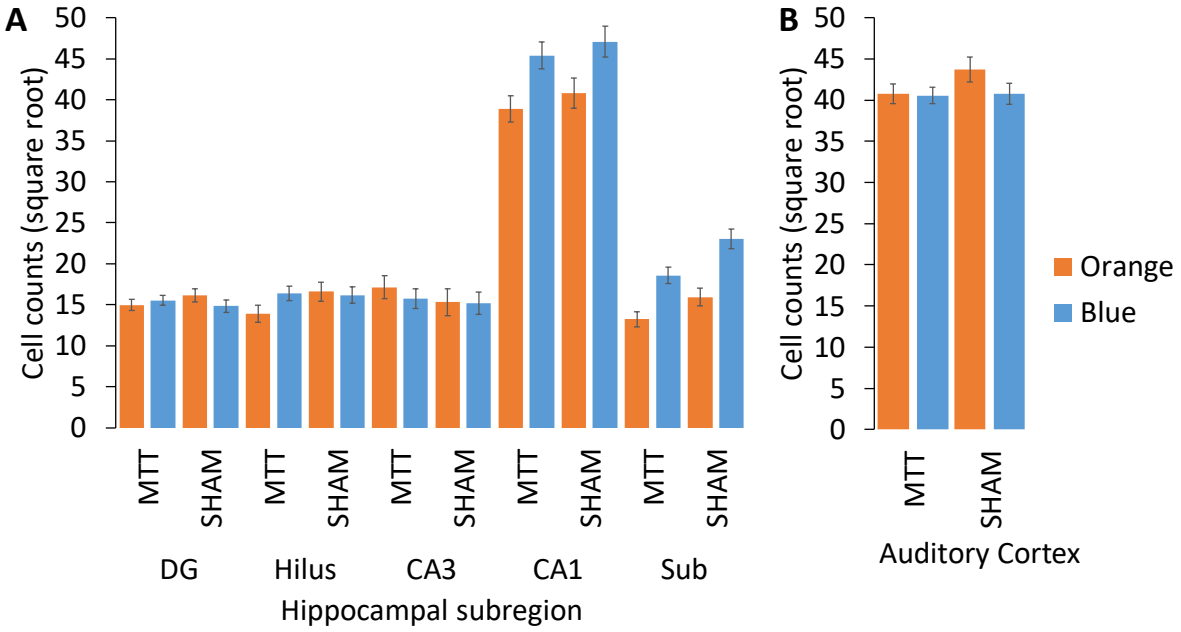

Figure 7.29. Zif268 expression in the hippocampus and auditory cortex. Mean ± SE of square root of Zif268 cell counts for MTT and Sham groups in blue and orange light conditions across the subregions of the hippocampus and the subiculum(A), and auditory cortex (B). Abbreviations: Rga= granular a retrosplenial cortex.

7.3.7.6 Prelimbic

As can be seen in Figure 7.30A, much higher cell counts were observed in Layer 3 of the prelimbic cortex compared to layers II, V and VI (Layer, F(3, 57)=95.87, p<0.001). Blue light stimulation appeared to increase Zif268 immunoreactivity in the deep layers (Layer x Colour, F(3, 57)=6.85, p<0.001; post-hoc Layer V data only, Colour, F(1,19)=119.06, p<0.001; post-hoc Layer VI data only, Colour, (F(1,19)=17.96, p<0.001), but did not have an effect in the

superficial layers (Layer II and III all F<1.00, p>0.30). MTT lesions did not impact Zif268 activity in any of the prelimbic layers (Group, F(1,19)=0.17, p=0.68, Layer x Group, F(3,57)=2.02, p=0.12).

7.3.7.7 Anterior Cingulate

Although blue light stimulation appeared to increase Zif268 expression in Layer VI (Figure 7.30B), this interaction failed to reach significance (Layer x Colour, F(3,57)=1.87, p=0.14). Additionally, no significant effects of Colour or Group were found in any layers of the anterior cingulate (Group, F(1,19)=0.21, p=0.65; Colour, (1,19)=1.48, p=0.24; Layer x Group, F(3,57)=0.23, p=0.87; Colour x Group, F(1,19)=0.43, p=0.52; Layer x Colour x Group, F(3,57)=0.92, p=0.44).

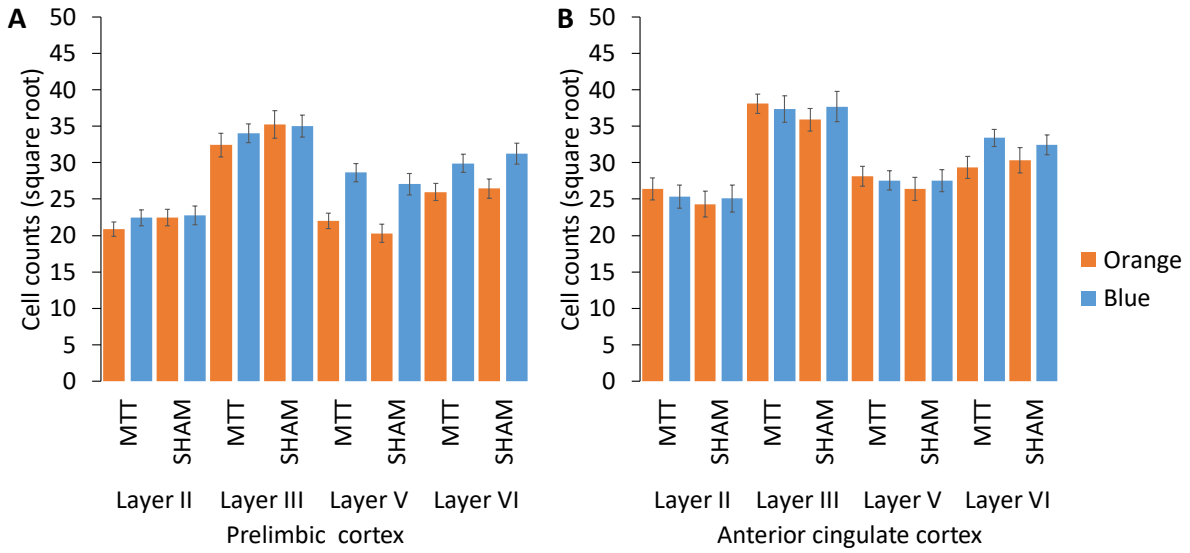

Figure 7.30. Zif268 expression in the prelimbic cortex and anterior cingulate cortex. Mean ± SE of square root of Zif268 cell counts for MTT and Sham groups in blue and orange light conditions across the layers of the prelimbic (A) and anterior cingulate cortices (B).

7.3.7.8 Cingulate cortex

Although the overall pattern of Zif268 activity differed between CG1 and CG2 (Region, F(1,19)=59.96, p<0.001), blue light stimulation increased Zif268 activity in both regions, with the most obvious Zif268 increases found in the deep layers of both CG1 and CG2 (Layer x Colour, F(2,38)=4.56, p=0.02; CG1 Layer 5, F(1,19)=26.41, p<0.001; CG2 Layer 5, F(1,19)=22.12, p<0.001). As can be seen in Figure 7.31A and 7.31B, CG1 Layer II exhibited lower Zif268 cell counts compared to CG2 Layer II (Region x Layer, F(2,38)=8.94, p<0.001).

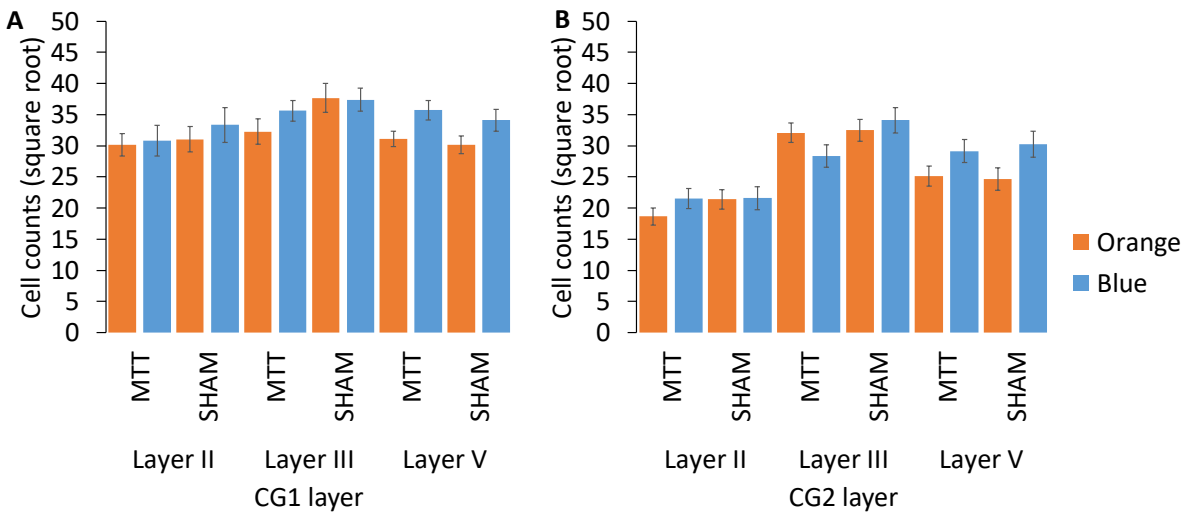

Figure 7.31. Zif268 expression in the cingulate cortex. Mean ± SE of square root of Zif268 cell counts for MTT and Sham groups in blue and orange light conditions across the layers of the cingulate cortex; CG1 (A) and CG2 (B).

7.3.7.9 Auditory Cortex

Zif268 counts were taken in the auditory cortex as a control region (see Figure 7.29B). Neither lesions nor stimulation affected Zif268 immunoreactivity in the control region (Figure 7.25B; Group $F(1,19)=1.88$, $p=0.18$; Colour, $F(1,19)=1.33$, $p=0.26$; Group x Colour $F(1,19)=0.99$, $p=0.33$).

Although the two MTT lesion non-opsin rats were not included in analyses, Zif268 expression was quantified in these rats in order to visualise the effect of blue and orange TBS. Figure 7.32 shows that Zif268 immunoreactivity does not appear to be affected by optogenetic TBS with blue light relative to both Sham and MTT lesion opsin-positive rats in the anterior retrosplenial Rgb cortical region.

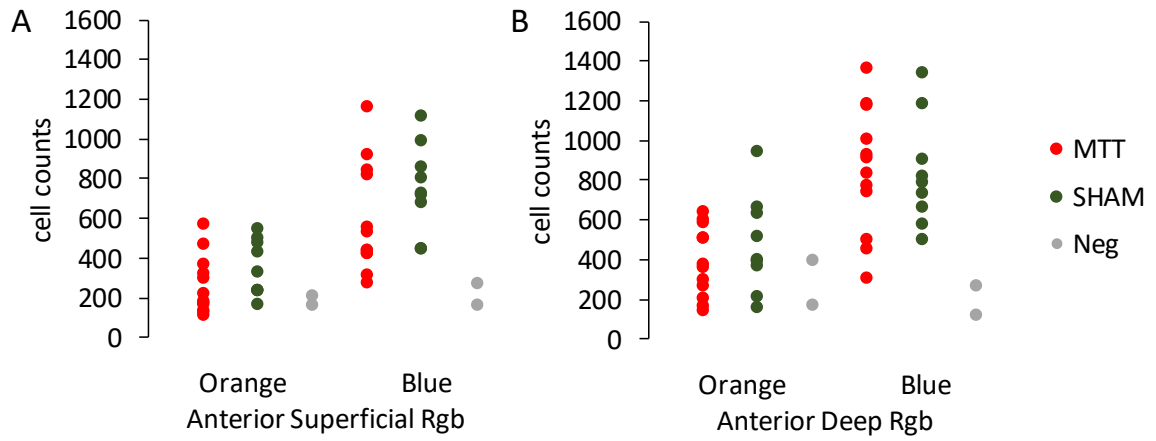

Figure 7.32. Mean Zif268 expression in the anterior superficial (A) and anterior deep (B) Rgb retrosplenial cortical region following optogenetic blue and orange light regular TBS.

7.4 Discussion

The results in the current chapter showed that optogenetic stimulation of the AV using regular, but not closed-loop, TBS parameters can improve spatial memory following MTT lesions in rats, consistent with human evidence showing that electrical stimulation of the AV can improve cognitive performance (Oh et al., 2012). Regular TBS stimulation increased Zif268 immediate early gene activation in a number of structures within the extended hippocampal system, including the HPC, RSC and prelimbic cortex. An increase in global PSD was observed following regular TBS stimulation in the ATN, as well as the HPC and PFC, and a global increase in coherence was found between the ATN-HPC and ATN-PFC, and to a lesser extent between the HPC-PFC. By contrast, closed-loop TBS parameters failed to improve memory performance and resulted in variable electrophysiological effects.

Regular optogenetic TBS stimulation improved spatial working memory performance in the MTT group, and improved performance in both Sham and MTT lesion groups on a reference memory task. The improvement in spatial working memory with regular TBS stimulation was shown to be consistent across Parts 1 and 2. By contrast, closed-loop TBS stimulation did not alter performance in either group. The lack of improvement observed in the Sham group during spatial working memory testing was likely due to a ceiling effect, with most Sham rats making only 1-2 errors per day, leaving little room for improvement. By contrast, rats only received two days of testing on the simultaneous discrimination task prior to receiving stimulation and thus Sham rats were still making enough errors that an improvement in reference memory following stimulation could be detected. These findings suggest that selective AV stimulation using regular theta burst parameters may facilitate memory improvement following permanent damage to the MTT.

Under control conditions, MTT lesions impaired memory function in the 12-arm RAM compared to Sham rats. These results replicated the findings reported in Chapter 6, as well as in previous studies examining the effect of MTT lesions (Vann & Aggleton, 2003; Vann, 2013; Frizzati et al., 2016; Perry et al., 2018). Importantly, MTT lesions impaired spatial working memory on days when regular TBS stimulation was given using orange (620 nm) light both before and after days when rats received TBS with blue (465nm) light. The lack of improvement observed under orange light stimulation demonstrates that the behavioural changes observed were as a result of selective channelrhodopsin activation, as opposed to a

general response to LED light stimulation. Similarly, no behavioural improvements were found following blue light stimulation in those rats that had received non-opsin ATN infusions, again demonstrating that the effect was as a result of channelrhodopsin activation following 465 nm stimulation.

Zif268 immunostaining revealed that optogenetic AV stimulation had general effects across the extended hippocampal network. Regular TBS with blue light led to widespread increases in Zif268 expression. Blue light stimulation increased activation in the cingulate cortices, retrosplenial granular a and b cortices, as well as the dorsal subiculum, which is unsurprising as these structures are directly innervated by the AV (Bubb et al., 2017). The absence of Zif268 effects in the Rdg is unsurprising as the AV has been shown to solely project to the Rgb and Rga, with no evidence of projections to the Rdg (Bubb et al., 2017). In line with this, a preliminary examination of viral expression in the terminals revealed mCherry expression in the anterior and posterior RSC and the subiculum. The expression of mCherry in these terminals implies that AV stimulation would have led to subsequent activation of these structures. However, increased Zif268 expression was also observed in hippocampal area CA1 and the prelimbic cortex. As these regions do not receive direct input from the AV, this suggests that regular TBS stimulation with blue light was able to alter system-wide activity, increasing neuronal activation indirectly in key structures within the extended hippocampal system (Bubb et al., 2017). These novel findings demonstrate that selective stimulation of one structure within an extended neural network can have widespread direct and indirect effects. Moreover these findings show that we achieved our initial aim to alter activity throughout the extended memory circuit, via selective stimulation of the AV. Importantly, stimulation did not increase Zif268 activity in the MTT lesion non-opsin rats.

Although regular TBS at 465 nm increased Zif268 activity, MTT lesions still reduced immediate early gene activation (Vann & Albasser, 2009; Vann, 2013; Frizzati et al., 2016; Perry et al., 2018). However, the number of structures demonstrating a reduction in IEG activation following MTT lesions was reduced relative to previous findings (see Chapter 6; Vann & Albasser, 2009; Vann, 2013; Frizzati et al., 2016; Perry et al., 2018). MTT lesions only reduced activity in the retrosplenial granular b cortex and the subiculum, as opposed to Chapter 6 where MTT lesions reduced expression in the Rgb and Rdg, as well as the

hippocampal areas CA1, CA3 and the DG. The difference in Zif268 expression suggests that blue light stimulation may have returned some MTT lesion effects towards Sham levels on neuronal activation throughout the extended hippocampal system. If the effect of AV regular TBS was constrained by direct AV connections, then we would expect to see clear MTT lesion effects under orange light conditions as AV projections are largely ipsilateral, aside from restricted RSC projections (Mathiasen et al., 2017). However, the reduction in global MTT lesion effects demonstrates a system-wide change, affecting both direct and indirect connections.

Similarly, we found that whilst MTT lesions reduced PSD and coherence within and between the ATN, HPC and PFC, selective AV stimulation appeared to increase oscillatory activity back towards baseline. Specifically, under control conditions MTT lesions reduced spectral power in the ATN, HPC and PFC, as well as ATN-HPC, ATN-PFC and HPC-PFC coherence, consistent with Dillingham et al. (2019) who demonstrated that MTT lesions disrupted rhythmic activity in structures of the extended hippocampal system – attenuating peak theta in the HPC and RSC, and abnormally increasing HPC-RSC coherence (Dillingham et al., 2019). The difference in direction of the coherence changes found by Dillingham et al. (2019; i.e. an increase rather than the decrease found here) in MTT animals compared to controls may be due to differences in tasks used as well as the regions examined. That is, Dillingham et al. (2019) explored the relationship between running speed and theta activity using a bow-tie maze, whereas we examined the relationship between spatial working memory, tested in the 12-arm RAM, and electrophysiological activity. Furthermore, Dillingham et al. (2019) recorded from the HPC and RSC, whilst the current Chapter recorded local field potentials in the ATN, HPC and PFC. Nonetheless, both studies clearly demonstrate the presence of abnormal oscillatory activity following MTT lesions in key structures within the distributed neural network underlying memory function (Aggleton & Brown, 1998).

By contrast, regular TBS with blue light increased spectral power in both groups in all three structures, but did so to the greatest extent in the MTT lesion group. Regular TBS also strikingly increased ATN-HPC and ATN-PFC coherence in the MTT group, but had mild effects in the Sham group. However, increases in HPC-PFC coherence were only found in the MTT group. Overall, the effects of regular TBS stimulation on global oscillatory activity show that

AV stimulation alters activity across the ATN-HPC-PFC axis during correct choice points when cognitive load is high. The results suggest that MTT lesions reduced global PSD and coherence, although the degree of reduction varies as a function of region, whilst ATN stimulation increases both spectral power and coherence in these same structures. Although increases in spectral power and coherence are observed in both groups, the greatest increases are consistently found in the MTT group. The presence of increased PSD in the HPC following regular TBS is consistent with the role of HPC theta in memory function. McNaughton et al. (2006) showed that elimination of HPC theta activity through septal inactivation significantly impaired spatial learning in the Morris Water Maze. Upon reinstatement of theta rhythmicity in the HPC (via a supramammillary bypass circuit), the authors reported restoration of initial learning. These findings are similar to the current Chapter in that they demonstrate an association between reduced HPC theta power and behavioural impairment, and an association between the reinstatement of HPC PSD and mnemonic improvement.

The enhanced ATN-PFC coherence during epochs of successful spatial memory processing and the increase in overall memory performance are consistent with evidence from human studies (Sweeney-Reed et al., 2014; 2015; 2016). Sweeney-Reed et al. (2014) reported that memory of complex stimuli could be predicted by ATN-PFC phase synchrony at theta frequency, as well as by ATN-PFC theta-gamma cross-frequency coupling. Sweeney-Reed et al. (2016) reinforced the importance of the ATN by showing that phase alignment of the medial PFC, ATN and dorsomedial thalamus predicted successful memory encoding.

Increased HPC-PFC coherence at correct choice points and enhanced memory function is also consistent with previous studies (Jones & Wilson, 2005; Hyman et al., 2010; Kim et al., 2011). For example, Jones and Wilson (2005) reported enhanced HPC-PFC coherence during spatial memory testing, as well as HPC-PFC coupling in the theta-frequency range. Similarly, Hyman et al. (2010) demonstrated increased medial PFC entrainment to HPC theta oscillation during correct choice trials, and reduced medial PFC theta entrainment on incorrect trials. Similarly, we reported simultaneous improvements in behavioural performance alongside increased HPC-PFC coherence in MTT lesion rats.

As discussed in Chapter 6, disrupted cholinergic activity may underlie the effect of MTT lesions on oscillatory activity within the extended hippocampal system. MTT lesions

cause dysfunction in the RSC. As the RSC reciprocally innervates the medial septum (Gonzalo-Ruiz & Morte, 2000) and inhibition of cholinergic neurons in the medial septum can block HPC theta rhythmicity, it may be that MTT lesions disrupt cholinergic innervation of the HPC via dysfunction in the RSC (Savage et al., 2012). Our optogenetic AV TBS increased Zif268 activation in the RSC, and so may, at least in part, have restored RSC functionality, helping to reinstate normal cholinergic functioning, and subsequently improving theta activity in the HPC.

Unlike regular TBS, closed-loop TBS had negligible effects on spectral power in the ATN, HPC and PFC compared to orange light stimulation. Closed-loop stimulation mildly increased ATN-HPC and HPC-PFC coherence. However, the most striking effect was the loss of PFC-ATN coherence observed in the Sham group following closed-loop TBS, in contrast to the lack of change found when regular TBS parameters were used. As closed-loop stimulation was associated with negligible behavioural effects, these findings suggest that the marked changes in spectral power associated with regular TBS may contribute more to the improvement in memory function than the observed alterations in ATN-HPC-PFC coherence. The lack of effect of closed-loop stimulation will be discussed later in this section.

The mnemonic effect of ATN stimulation has previously been examined using high frequency stimulation (130 Hz; Hamani et al., 2012). Although the authors reported improved performance on a delayed non-matching to sample task, this was only observed in animals one month after receiving high frequency electrical stimulation. Stimulation also increased hippocampal neurogenesis and therefore the improvement in memory performance was postulated to reflect long-term plastic changes (Hamani et al., 2012). By contrast, the current Chapter observed a relatively instantaneous behavioural improvement following optogenetic stimulation of the ATN, which continued for the duration of stimulation delivery but did not persist in the absence of stimulation. That is, there was no evidence of carry over effects. This pattern of behavioural effects suggests that unlike the findings of Hamani et al. (2012), the improvement in memory function is not attributable to increased neurogenesis or long-term plasticity changes.

TBS stimulation did not appear to *drive* rhythmicity in the ATN, PFC or HPC as there was no discernible peak at the stimulation frequency (8.5 Hz), however there was a clear

broad-band effect with regular TBS stimulation increasing both spectral power and coherence across the ATN-HPC-PFC axis. Further testing would be required to elucidate the exact mechanisms underlying the electrophysiological effects observed here, however we can speculate as to the possible processes at work. The use of theta burst stimulation could have produced either early long-term potentiation (LTP1) or frequency potentiation (FP). LTP1 refers to the first stage of long-term potentiation and describes the strengthening of a synapse occurring when the pre-synaptic cells are active and there is a strong post-synaptic depolarisation. LTP1 occurs 30 min following induction and has a duration of ~4-6 hours (Frey et al., 2001; Lisman, 2017). By contrast, FP is a type of short term potentiation (STP). STP typically refers to the initial large potentiation observed during the induction of long term potentiation, but can be evoked in isolation (i.e. without long term potentiation) through the use of weak stimulation (Lisman, 2017). Moreover, it has been suggested that STP may contribute to working memory performance (Erickson, Maramara & Lisman, 2010; Lisman, 2017). Specifically, FP is the increase in cellular responses during repetitive stimulation and is thought to depend on the transient increase of neurotransmitters due to residual calcium at the presynaptic terminal (Papatheodoropoulos & Kostopoulos, 2000). Note that the effect of this increase is much longer than a theta cycle, and usually builds steadily over the first few pulses of a train. It would therefore produce increased transmission in all frequency bands. As TBS stimulation was given continuously throughout behavioural testing and the amelioration in memory performance appeared almost instantaneous, rather than after 30 min had elapsed, the most likely explanation appears to be FP. In order to test this hypothesis, a future experiment would need to deliver TBS while recording synaptic responses (excitatory post-synaptic potentials) and calculate the FP as the percent value of the Nth response in the train of pulses with respect to the 1st response. If the elicited potential was increasing in magnitude with continuous stimulation, this would suggest the presence of FP (Papatheodoropoulos & Kostopoulos, 2000).

Similarly, future testing is required to better understand the lack of behavioural and electrophysiological effects attributed to closed-loop TBS stimulation. Under closed-loop conditions, the hippocampal signal was filtered online between 8-9 Hz to yield an average frequency of 8.5 Hz, with TBS triggered on the rising phase of hippocampal theta. The lack of effect may have been due to a delay between TBS theoretical triggering and real-time

triggering, or an overall lack of regularity in the pattern of rhythmicity. Closed-loop stimulation techniques inherently involve a delay between receiving input to actual output and this delay can vary in duration across studies from 5-100 ms (Venkatraman et al., 2009; Wu et al., 2015). In the current experiment, the delay was attributed to the time taken to process the LFP data online, send a signal to the Pulse Pal stimulator (NY, USA; Sanders & Kepecs, 2014) and finally trigger the delivery of the theta burst via the Plexbright 4 Channel Optogenetic Controller (Plexon; Tx, USA). Another explanation is that, as detailed in Chapter 6, MTT lesions disrupt oscillatory activity in the HPC. As the signal triggering AV TBS was derived from HPC theta rhythm, it may be that a dysfunctional pattern of TBS was delivered, albeit at an average of 8.5 Hz. Alternatively, common-mode noise such as movement artifacts caused by the rat's running down the arms or AC mains pickup can create false signals in the neural data. The presence of any false signals bandpass filtered between 8-9 Hz may have been included as a trigger for TBS, and therefore resulted in stimulation not occurring as triggered by normal HPC rhythmicity. Although we are unable to determine the reason for the discrepancy in effects between regular and closed-loop TBS, the findings of the current Chapter suggest that a key factor in the significant behavioural improvements observed here were dependent upon the delivery of TBS occurring regularly at 8.5 Hz. This idea is not novel. McNaughton et al. (2006) previously examined the ability to restore rhythmicity using electrical stimulation after blocking HPC theta and found that regular 7.7 Hz stimulation reinstated rhythmicity and improved memory performance, although this effect decreased across trials. By contrast, irregular stimulation with an average frequency of 7.7 Hz produced little rhythmicity and little improvement in learning.

One limitation of the present Chapter is that although we have shown that optogenetic stimulation improves memory performance when regular TBS parameters are used, we only tested the effect of regularity using TBS at a frequency of 8.5 Hz. Consequently the question remains as to whether the beneficial effects of optogenetic TBS is attributable to the regularity of the stimulation pattern used, or to the use of 8.5 Hz as the TBS frequency. Future work could address this issue by comparing the effects of different stimulation frequencies on memory performance. These comparisons should be carried out using the same task, to ensure the behavioural effects are comparable across studies. Further research should also examine whether the improvement in memory function is

unique to TBS stimulation, or whether delivery of single pulses at 8.5 Hz would have similar behavioural effects. In both cases, changes in oscillatory activity associated with each different type of stimulation should be analysed both within and between subjects.

The current chapter shows that selective optogenetic stimulation of the AV, using regular TBS parameters, can substantially improve memory performance in rats following permanent damage to the MTT. Furthermore, AV stimulation alters both oscillatory and IEG activity across key memory structures within the extended hippocampal system. These findings are of clinical importance as they may explain cases of spontaneous recovery observed in neurological conditions such as Korsakoff's syndrome (Kopleman et al., 2009). Most importantly, the current chapter demonstrates that it is possible to recover memory function even in the presence of permanent neuropathology.

Chapter 8:
General discussion

8.1 Overview

This thesis provides novel evidence as to the relative impact of MTT and PCFx lesions on the extended hippocampal system that is thought to underlie episodic memory (Aggleton & Brown, 1999). First, it has shown that MTT and PCFx lesions impaired spatial working memory equally, at least with respect to post-lesion acquisition performance in a 12-arm RAM. In addition, both lesions reduced spectral power across the 2-14 Hz frequency range in the ATN, HPC and PFC, and profoundly reduced ATN-HPC, HPC-PFC and PFC-ATN coherence. The two lesions also reduced IEG Zif268 expression after maze testing in a novel room in the RSC and HPC while increasing expression in layer VI of the prelimbic cortex. Second, optogenetic stimulation of glutamatergic neurons in the ATN led to a striking improvement in memory performance in the MTT lesion group, despite clear evidence of otherwise permanent impairments. PCFx lesions were not tested. This optogenetic stimulation also increased spectral power and coherence across the ATN-HPC-PFC axis in rats with MTT lesions. The same stimulation delivered to rats whilst foraging for chocolate in an open field also increased Zif268 expression across structures within the extended hippocampal system. Together, these new findings suggest that while profound memory deficits are a consequence of subcortical white matter lesions, suitable stimulation can re-instate circuit activity and repair working memory and so may provide a basis for potential treatment strategies.

Although MTT and PCFx lesions led to comparable impairments in spatial working memory, some detailed differences between MTT and PCFx lesions were found. MTT lesions reduced Zif268 expression in both the anterior and posterior RSC, whilst PCFx lesion effects on Zif268 were restricted to the anterior RSC. In the anterior RSC, MTT and PCFx lesions caused an equal reduction in Zif268 expression in the superficial Rgb and the deep Rdg, whereas MTT lesions resulted in a greater reduction in IEG activation in all other RSC subregions. Only MTT lesions reduced Zif268 expression in the dentate gyrus. Both PCFx and MTT lesions equally reduced global spectral power in the ATN and HPC. Only MTT lesions, however, attenuated peak ‘theta’ power in the HPC.

The lesser impact of PCFx lesions on IEG activation and oscillatory activity suggests that removal of the HPC input to the MB cannot entirely account for the widespread effects of MTT lesions. These subtle differences may, therefore, reflect the loss of the additional influence of the brainstem input from the VTNg to the MB. The two major sources of MB innervation are the HPC and VTNg. As loss of HPC input to the MB (PCFx transection) causes equivalent effects elsewhere in the system as removal of the MB input into the ATN (MTT transection), this suggests that the VTNg must be contributing to the signal propagated from the MB to the ATN in those PCFx lesion rats. Therefore, input from the VTNg and HPC may work in conjunction to support normal memory function. However, future work would need to directly address the relative input of VTNg lesions on IEG and oscillatory activity. This will be discussed later in the limitations section of this chapter.

The current evidence of the behavioural, electrophysiological and IEG effects following optogenetic stimulation of the ATN is, to our knowledge, the first of its kind. Optogenetic ATN stimulation using regular TBS led to an improvement in memory performance in every rat in the MTT lesion group. The improvement in spatial working memory in rats with MTT lesions was replicated, but did not appear in the absence of stimulation, that is on subsequent days using either control condition. Impaired performance returned both with no stimulation and with orange light stimulation (which does not activate channelrhodopsin).

Regular optogenetic TBS of the ATN also increased oscillatory activity when spatial working memory was improved; and caused IEG activation of Zif268 throughout the extended hippocampal system, when the rats were stimulated in the open field just prior to sacrifice. Importantly, the increases in Zif268 activation were not restricted to structures directly connected to the ATN. That is, optogenetic ATN stimulation produced both direct and indirect effects throughout the extended memory system. Stimulation increased Zif268 expression in the subiculum, RSC, and cingulate cortex, which are directly innervated by afferents local to the optic fibre (mostly AV); as well as in the prelimbic cortex and area CA1 of the HPC, which would not be directly stimulated. The increase in Zif268 expression was similar across groups in all regions. Regular ATN TBS increased spectral power and coherence within and between the ATN, HPC and PFC in both groups, but with greater increases observed in the MTT lesion group. The greatest increases in spectral power were

observed in the ATN, whilst the greatest increases in coherence were observed between the ATN-HPC and ATN-PFC.

8.2 Experiment 1: Comparing the effects of MTT and PCFx lesions

8.2.1 The effect of MTT and PCFx lesions on spatial working memory.

MTT lesions severely impaired spatial working memory in both experiments. This is consistent with previous studies examining the effect of MTT lesions on memory performance (Vann & Aggleton, 2003; Vann, 2013, Nelson & Vann, 2014; Frizzati et al., 2016; Perry et al., 2018). However, a 12-arm RAM was used in the current study whereas previously an 8-arm RAM has been used. In previous studies, rats with MTT lesions have demonstrated some evidence of improved performance over time (Vann, 2013; Perry et al., 2018). In the present study MTT lesion rats did not show improved memory performance across trials, and this may reflect an increase in task difficulty.

PCFx lesions impaired working memory performance to an equal extent to MTT lesions. This was unexpected because two previous studies using PCFx lesions reported negligible memory effects in the T-maze and 8-arm RAM (Vann et al., 2011; Vann, 2013). The lack of previous spatial working memory impairments reported by Vann et al. (2011) and Vann (2013) may have been due to incomplete lesions, insufficient task difficulty, the age of the rats at the time of behavioural testing, or a combination of all three (discussed below). Nonetheless, the impairment in spatial working memory observed here following PCFx lesions is consistent with human studies implicating the integrity of the PCFx in memory function (Christiansen et al., 2016; Coad et al., 2020).

In the current study, both cresyl violet (a Nissl stain) *and* especially luxol blue (a myelin stain) were used to verify complete transection of the PCFx fibre tract. By contrast, Vann et al. (2011) and Vann (2013) used only cresyl violet. Luxol blue is a myelin stain and therefore directly assesses the loss of MTT fibres; this is more relevant than relying only on the absence of the MTT fibres inferred from Nissl staining to verify lesion extent. However, retrograde tracing by Vann et al. (2011) supported their description that the majority of subicular inputs to the MB had been removed, with minimal evidence of fibre sparing across 8 included and excluded rats. Included rats showed the presence of a very few tracer-labelled cells in the dorsal subiculum following PCFx transection. The sparing of a few subicular input fibres is unlikely to be the sole reason for the discrepancy between the

studies. As in the current study, Vann et al. (2011) and Vann (2013) only trained rats on the RAM task following lesion surgery, so that is also not an explanation.

A more likely reason is that having more arms increases proactive interference, thereby taxing the memory system through increased memory load. Such an increase in task difficulty was suggested by the relatively slower Sham rat acquisition of the task compared to previous studies using an 8-arm RAM (Vann et al., 2011; Vann, 2013; Perry et al., 2018). That said, in the current study, rats with either partial bilateral or unilateral sparing only showed modest impairment, with fewer errors than when there was complete bilateral damage to the PCFx. This suggests that complete PCFx transection was required to produce the especially severe and consistent memory impairment in the current 12-arm RAM study. The current results may depend, then, on both having complete lesions and using a challenging task. Another potential factor is the age of the rats used in the current study. Normal memory function decreases with age in rodents (Barnes, 1979; Geinisman et al., 1986). Our rats were relatively old, between 28 and 30 months at the time of testing, which may have also contributed to the extent of the memory impairment.

8.2.2 The effect of MTT and PCFx lesions on immediate early gene activity.

MTT and PCFx lesions reduced Zif268 expression in subregions of the RSC and HPC in the first experiment. The reduction in Zif268 expression reported here is inconsistent with the lack of PCFx IEG effects reported by Vann (2013). This discrepancy in IEG effects may be due to differences in IEG marker, or the regions of interest that were analysed. In the first experiment, Zif268 reductions following PCFx lesions were reported in the anterior, but not the posterior, RSC, as well as in subregions of the HPC. Vann (2013) only examined c-Fos expression in the posterior RSC and measured global IEG expression in structures of interest rather than analysing individual subregions as was done here. Zif268 was used in the current study due to its reported involvement in spatial memory formation and long-term plasticity. Vann (2013) used c-Fos. Discrepancies between the two markers have been reported previously (Frizzati et al., 2016), although this was tested following MTT lesions only and the authors reported that c-Fos, not Zif268, expression in HPC area CA1 was reduced by MTT lesions (Frizzati et al., 2016). Additionally, in the current study, the survival time following PCFx lesion surgery was relatively long at about ~24 weeks. Previous work has shown that, in rats with ATN lesions, reductions in IEG expression in the RSC become more pronounced

with increased time intervals following lesion surgery (Poirier & Aggleton, 2009). Therefore, the extended time period between lesion and perfusion in the first experiment may have contributed to the extent of IEG hypoactivation.

In sum, the first experiment demonstrated that both MTT and PCFx lesions reduced IEG activation across structures within the extended hippocampal memory system. Although these findings are inconsistent with previous PCFx lesion findings, there are several contributing factors which may explain these discrepancies.

8.2.3 The effect of MTT and PCFx lesions on electrophysiology

Both MTT and PCFx lesions reduced spectral power in the ATN, and HPC. Both PCFx and MTT lesions reduced peak 'theta' power in the ATN at 8.5 Hz. However, only MTT lesions attenuated peak 'theta' power in the HPC. Both lesions also substantially reduced HPC-ATN, ATN-PFC and HPC-PFC coherence. Both MTT and PCFx lesions led to a similar reduction in coherence across all electrode pairs and the greatest reductions were observed at lower frequencies where Sham coherence was highest.

8.2.4 Implications of the effects of MTT and PCFx lesions

PCFx lesions reduced IEG expression in the anterior RSC and HPC, and disrupted normal electrophysiological activity across the ATN-HPC-PFC axis. The presence of dysfunction in structures indirectly connected with the PCFx suggests that the loss of IEG activation does not merely reflect a loss of direct innervation. There is as yet no direct evidence linking reduced IEG activation with behaviour after MTT lesions, but the impairments in spatial working memory following PCFx lesions reported here may also reflect disruption to information processing relevant for memory. Taken together, the loss of Zif268 expression and aberrant rhythmic activity observed following PCFx lesions shows that removal of the HPC input to the MB can disrupt activity in other regions of the extended hippocampal system.

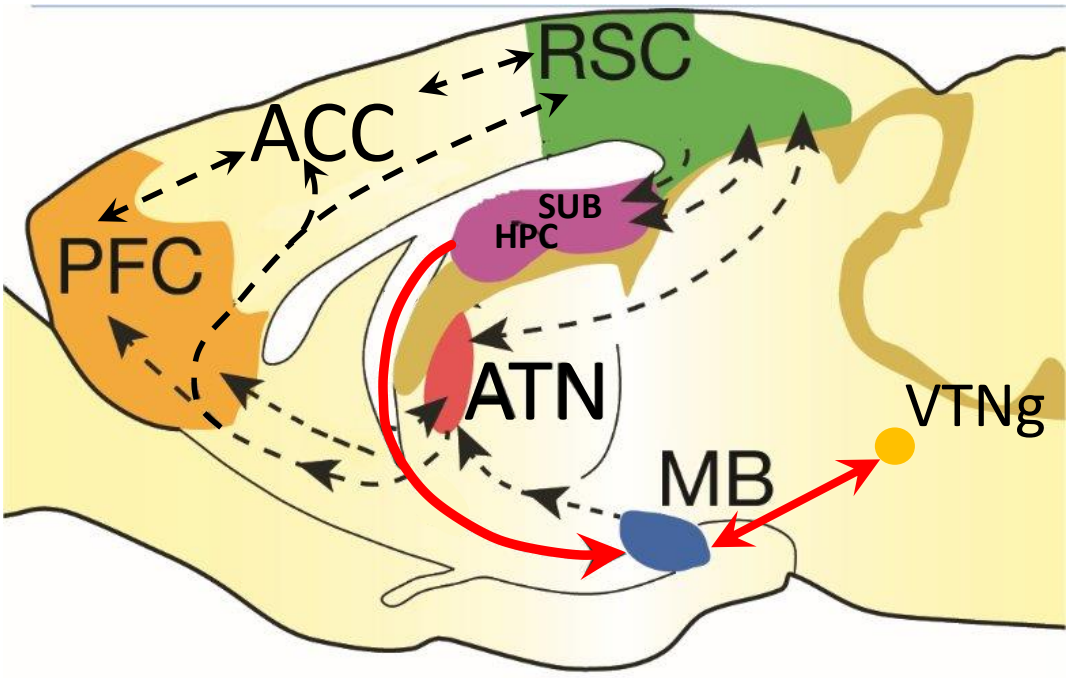

Figure 8.1. Diagrammatic representation of the extended hippocampal system (adapted from Jankowski et al., 2013 and Barnett et al., 2018). Connections of the system are shown in black. The two theories for rhythmic propagation into the MB are shown in red. The first theory suggests that the HPC innervation of the MB, via the subicular projections, is critical for rhythmic propagation throughout the memory system. The second theory emphasises the VTNg and brainstem input into the MB.

The effect of MTT and PCFx lesions on oscillatory activity adds to our current understanding of the propagation of rhythmic slow activity (RSA) throughout the neural network. Both PCFx and MTT lesions attenuated the peak in power across the 2-14 Hz frequency band in the ATN, whilst only MTT lesions attenuated the 8.5 Hz peak in the HPC. There are currently two main theories for the generation and subsequent propagation of rhythmicity throughout the extended hippocampal circuit (see Figure 8.1). Both theories address which of the two mammillary body inputs exerts the most influence on rhythmic activity, the VTNg or the HPC (see Figure 8.1). The first theory is that the septo-hippocampal system is critical for rhythmic activity throughout the diencephalon (Locsis & Vertes, 1994; Kirk et al., 1996; Kirk & Mackay, 2003). That is, the connection of the HPC/subiculum to the diencephalon provides a direct route for rhythmic propagation that originates in the medial septum. Support for this theory has come from studies showing that septal blockade eliminates theta rhythmicity in both the HPC and MB (Kirk et al. 1996; McNaughton et al., 2006). Additionally, MB theta is highly correlated with theta rhythmicity in the HPC,

particularly in area CA1 (Kocsis & Vertes, 1994). Conversely, the other theory is that VTNg rhythmic input into the MB converges with the HPC projections from the subiculum to the MB before ascending to the ATN via the MTT (Bassant & Poindessous-Jazat, 2001; Vann & Aggleton, 2004). The role of the VTNg as a pontine theta generator has stemmed from evidence that the cells of the VTNg discharge in rhythmic bursts at theta frequency. Furthermore, VTNg theta activity precedes HPC theta (Bassant & Poindessous-Jazat, 2001). As both PCFx and MTT lesions disrupted broad band RSA in the HPC, as well as HPC-ATN and HPC-PFC coherence, it is likely that the hippocampal MB input is not redundant in the presence of VTNg-MB innervation. However, only MTT lesions attenuated the RSA peak in the HPC. The lack of attenuation observed in the PCFx group suggests that removal of the HPC projections to the MB cannot account for the loss of peak RSA in the MTT lesion group. Instead, it appears that normal rhythmic propagation from the MB to the ATN and into the wider memory circuit relies on both the hippocampal and brainstem inputs into the MB.

8.3 Experiment 2: Optogenetic stimulation of the ATN following MTT lesions

8.3.1 Effect of optogenetic stimulation on spatial working memory

Regular optogenetic TBS using blue light markedly decreased the number of errors made by MTT lesion rats during spatial memory testing. In the absence of stimulation MTT lesion rats made 8 errors on average. However, under regular TBS conditions, performance in the MTT group improved towards the level of Sham rats, with MTT lesion rats making only around 2.5 errors. By contrast, closed-loop TBS with blue light did not improve memory performance.

Importantly, the beneficial effect of optogenetic stimulation was dependent upon the activation of glutamatergic ATN neurons. First, co-localisation of mCherry and CamKIIα in AV cells showed that channelrhodopsin expression was restricted to glutamatergic neurons. Second, no behavioural improvements or increases in IEG activation were found in non-opsin rats receiving 465 nm (i.e. blue) optogenetic stimulation. Therefore, non-specific effects of viral vector transduction could not explain the current findings. The lack of effect in non-opsin rats shows that improved memory in MTT rats resulted from channelrhodopsin activation only. Third, TBS at a wavelength of 620 nm (i.e. orange) failed to improve memory performance in rats with MTT lesions and expressing channelrhodopsin in the ATN. Taken

together, these three findings show that enhanced memory performance relied on stimulation using the correct activation wavelength for channelrhodopsin (465 nm).

8.3.2 Effect of optogenetic stimulation on immediate early gene activity

Increased Zif268 activity was also observed. Regular TBS was associated with Zif268 upregulation in subregions of the cingulate cortex, dorsal subiculum, HPC, prelimbic cortex and RSC. As area CA1 and the prelimbic cortex are not directly innervated by the AV, the increased IEG expression must be due to indirect (trans-synaptic) effects throughout the extended hippocampal system. Reductions in Zif268 expression were expected in MTT lesion rats following orange light stimulation. However, MTT lesions only reduced expression in the subiculum and Rgb RSC subregion. The lack of MTT lesion effects on Zif268 activity suggests that ATN TBS with blue light increased IEG activation across both hemispheres. As the majority of ATN afferents are unilateral (Bubb et al., 2017), the increase in Zif268 activation suggests that ATN stimulation induced cross-hemispheric effects through activation of other structures within the memory system.

8.3.3 Effect of optogenetic stimulation on electrophysiology

Regular TBS simultaneously increased spectral power and coherence across the ATN-HPC-PFC axis, although this was to a greater extent in MTT lesion rats. Specifically, regular TBS resulted in a global increase in spectral power and coherence across the 2-14 Hz frequency band, rather than driving activity at the 8.5 Hz stimulation frequency. TBS stimulation led to a similar increase in spectral power in the ATN, HPC and PFC. By contrast, increases in coherence were greatest between the ATN-HPC and ATN-PFC, with markedly smaller changes in coherence observed between the HPC-PFC. As discussed in section 7.4, the most likely explanation for the overall increase in excitability is that stimulation induced frequency potentiation at the synapses.

Interestingly, closed-loop TBS did not alter memory performance or spectral power in either group. However, closed-loop TBS mildly increased ATN-HPC and HPC-PFC coherence in MTT rats, as well as strikingly reducing ATN-PFC coherence in Sham rats. As closed-loop TBS did not produce any behavioural effects, this suggests that either increased spectral power across the ATN-HPC-PFC axis was directly connected to memory improvement, or that the mild increases in ATN-HPC and HPC-PFC coherence were insufficient to produce any improvement in memory performance. However, as no

impairment in memory performance was observed in Sham rats during closed-loop TBS, it seems unlikely that ATN-PFC coherence was critically involved in memory. As discussed in section 7.4 a delay between TBS theoretical triggering and real-time triggering, or an overall lack of regularity in the pattern of rhythmicity likely explains the negligible effect of closed-loop TBS on memory performance. The lack of effect of closed-loop TBS suggests that the critically important aspect of TBS for the observed memory improvement was the regularity of 8.5Hz stimulation, rather than the use of the 8.5 Hz frequency per se for stimulation. The importance of regularity in the enhancement of memory function has been suggested by McNaughton et al. (2006). Rats received regular and irregular electrical stimulation of the fornix superior at 7.7 Hz following removal of HPC theta via a septal blockade. Regular stimulation resulted in restoration of rhythmicity and a transient improvement in memory performance. By contrast, irregular stimulation produced little rhythmicity and no improvement in memory (McNaughton et al., 2006). These findings demonstrate that simple activation of neurons at a given average frequency is insufficient to enhance memory performance. Instead, it appears that the regularity of stimulation may play a critical role in memory.

8.3.4 Implications of the effects of ATN stimulation

The fact that improved spatial working memory function appears consistently accompanied by an increase in spectral power and coherence suggests that these electrophysiological changes may contribute to the improvement in memory performance. Further research is required to test the relationship between the altered oscillatory activity and improvement in behaviour. The increase in IEG and oscillatory activity reported here implies that although there is permanent damage to a key diencephalon tract, the 'functional' lesions in the HPC, RSC and PFC may be reversable.

The potential to improve functionality in structures with such functional lesions might also explain instances of spontaneous recovery. For example, an interesting aspect of Korsakoff's syndrome (see Chapter 3) is that approximately 75% of patients show improved memory with abstinence (Kopelman et al., 2009). Importantly, these instances of recovery occur in the presence of considerable and permanent ATN, MB and PFC neuropathology (Kopelman, 2014). Recovery despite enduring pathology likely results from compensatory changes elsewhere in the extended system. Recovery in the presence of permanent damage

has also been observed in the pyrithiamine-induced thiamine deficiency (PTD) rat model of Korsakoff's syndrome (Savage et al., 2012). The PTD model is associated with severely impaired spatial learning and memory, as well as permanent diencephalic lesions and functional abnormalities in the HPC, PFC and RSC. Nonetheless, upregulation of cholinergic activity in the hippocampus, prefrontal cortex or medial septum in PTD rats can improve memory function (Savage et al., 2012).

Similar mechanisms may also explain instances of improved spatial memory in rats with ATN lesions. Environmental enrichment has also been shown to improve memory performance in rodents following permanent damage to the ATN (Loukavenko et al., 2007, 2016; Wolf et al., 2008; Harland et al., 2014; Dalrymple-Alford et al., 2015). Importantly, ATN lesions and environmental enrichment produced opposing functional effects on rhythmic activity (Ulrich et al., 2019). Whereas ATN lesions reduced PFC spectral power, environmental enrichment increased functional connectivity between the PFC and HPC (Ulrich et al., 2019). Together, these findings suggest that recovery of function can occur even in instances of permanent damage. One proposed mechanism of compensation is via enhanced inter-structural communication within the extended hippocampal system (Dalrymple-Alford et al., 2015). The current optogenetic findings with MTT lesions support this idea.

ATN stimulation altered electrophysiological activity and IEG expression across key structures such as the HPC, RSC and PFC. The widespread nature of the effects of ATN stimulation emphasises the interconnected nature of the extended memory system described by Aggleton & Brown (1999). Furthermore, MTT and PCFx lesions both induce electrophysiological and IEG dysfunction, reinforcing the interdependence of the structures located within the neural network (Aggelton et al., 2010).

8.4 Overall implications for the functioning of the extended hippocampal memory system

We found that damage to key fibre tracts within the extended hippocampal system impairs memory function. These memory impairments are accompanied by evidence of neural dysfunction throughout the memory circuit. Selective stimulation of the ATN following damage to the MTT improved memory function and also improved functionality in distally

located structures and their communication. There are clinical implications of the beneficial effects of ATN stimulation.

The effect of ATN stimulation on distally located structures suggests that successful intervention should target nodal structures within the memory system. The interconnected nature of a nodal structure is such that its stimulation is likely to affect multiple regions both directly and indirectly and is therefore capable of enhancing system-wide functionality. The benefit of targeting the ATN in particular applies not only to cases of amnesia but also to impaired memory associated with more disperse dysfunction, such as in Parkinson's disease and especially AD. For example, AD is characterised by widespread but gradually increasing pathology in many structures within the extended hippocampal system (Aggleton et al., 2016). Therefore, successful intervention may benefit from distributed effects, such as those reported in the current study. Perhaps most importantly, our findings show that we can re-activate the extended hippocampal memory system even when there is permanent damage to key structures or pathways.

8.5 Proposed effect of ATN stimulation following MTT lesions

ATN stimulation increased activity across the memory system. ATN stimulation increased IEG activity but also led to a broad band (2-14 Hz) increase in spectral power and coherence. Based on the IEG and electrophysiological evidence in the current thesis, we can suggest some explanations of the observed lesion and optogenetic effects. Two possibilities are discussed below.

It has been suggested that one mechanism by which MTT lesions influence HPC rhythmicity is via disruption of the basal forebrain cholinergic system (Dillingham et al., 2019). Cortical and HPC cholinergic activity is reduced by MB lesions (Beracochea et al., 1995). Although the MTT projection is not cholinergic, it may be capable of modulating cholinergic interactions either via direct innervation of the AV, or via indirect connections with other key structures within the extended hippocampal system (Dillingham et al., 2019). For example, Savage et al. (2011) suggested that the reductions in HPC cholinergic activation observed following ATN lesions may be as a result of a loss of RSC modulation of the medial septum (Gonzalo-Ruiz & Morte, 2000). MTT lesions caused a profound reduction in RSC IEG activation suggesting that the RSC received a functional lesion. By contrast, ATN TBS increased IEG activation, particularly in the anterior RSC. ATN stimulation also enhanced

HPC spectral power and coherence with the ATN and PFC. It may be that MTT lesions impair RSC functioning and thereby alter normal rhythmicity in the HPC (Dillingham et al., 2019) but that regular ATN TBS may improve RSC activity and, as a result, cholinergic function in the medial septum. This cholinergic change in turn may restore HPC oscillatory function. Furthermore, cholinergic changes may explain the broad band nature of AV stimulation, as changes in cholinergic activity do not result in frequency-specific effects. For example, it has been previously demonstrated that cholinergic drugs do not affect theta driving, nor do they alter the frequency of HPC theta (McNaughton et al., 1977; McNaughton & Sedgwick, 1978).

Another possible explanation centres on the effects of MTT lesions and ATN stimulation on activation in HPC area CA1 and the subiculum. MTT lesions reduced IEG activation in area CA1 and the subiculum, whilst ATN TBS increased Zif268 expression in both regions. The subiculum and area CA1 play a critical role in spatial memory (Aggleton & Brown, 1999; Aggleton et al., 2010; Aggleton & Christiansen, 2015). Furthermore, area CA1 sends dense projections to the subiculum, which in turn projects to cortical and subcortical regions (O'Mara, 2005). Thus, the subiculum is the main source of HPC efferents, innervating important structures such as the MB, ATN and RSC (Bubb et al., 2017). MTT lesions reduced activity in the HPC and subiculum, and thus may have disrupted interactions between these two regions, as well as in distal structures receiving subicular innervation. For example, lesions of the ATN, which receives MB input via the MTT, cause a striking loss of spatial-coding by cells in the subiculum (Frost et al., 2020). As the MTT is a major source of ATN innervation, MTT lesions may also impair subicular spatial-coding through induced ATN dysfunction. However, further research would need to examine the effect of MTT lesions on spatial-coding cells in the subiculum in order to properly assess this mechanism.

In Chapter 7, I reported that coherence steadily decreased across electrode pairs, ordered HPC-ATN, then ATN-PFC, then PFC-HPC, which suggests the propagation of a signal from the HPC to the ATN, which is then relayed to the PFC, with signal attenuation at each step, and minimal return signal from the PFC to the HPC. Propagation of the oscillatory signal starting in the HPC is consistent with both of the proposed mechanisms, as both emphasise the restoration of HPC function.

Taken together, the IEG and electrophysiological findings suggest that AV stimulation increases IEG activation in a number of structures, including the RSC, subiculum and area

CA1. It is unclear which structures, or combination of structures, contribute to the improved memory performance observed here; and this should be addressed by future studies. Based on the coherence analysis reported in Chapter 7, increased HPC activity appears to increase oscillatory activity in the ATN and to the on to the PFC. Moreover, it suggests that ATN stimulation increased cellular activations that would otherwise be reduced by MTT lesions and that this increased HPC oscillatory activity back towards baseline levels. As discussed in section 7.4, it seems most likely that ATN stimulation increased activation throughout the extended hippocampal system via frequency potentiation. That is, since stimulation was delivered continuously throughout the behavioural task, this would have caused a substantial and short-term increase in synaptic output, producing increased transmission in all frequency bands (Papatheodoropoulos & Kostopoulos, 2000).

8.6 Conclusions

There were two key proposals in this section. The first is that MTT lesions cause significant dysfunction in the RSC and thereby globally reduce IEG activation, PSD, and coherence in the HPC via disrupted cholinergic signalling. The second is that restored functioning in the HPC and/or subiculum following AV stimulation counteracts the effect of MTT lesions by improving subicular and/or area CA1 spatial-coding, as well as improved HPC electrophysiological activity. Whilst supporting evidence was provided for both mechanisms, the distributed effects of ATN stimulation suggests that the beneficial effect of stimulation result from changes throughout the extended hippocampal memory system. In order to gain a better understanding of the key pathways underlying the effect of ATN stimulation, it is important for future studies to examine effect of stimulation of select AV terminals (this will be discussed in the future directions section below).

8.7 Limitations of the current study

The current study had limitations. Perhaps the greatest limitation is that it has left future work to consider frequencies above the 2-14 Hz frequency range and to look at cross frequency coupling and related measures across the extended system. Another limitation is that memory performance was only tested in the 12-arm RAM. Although the RAM is a useful task for assessing memory performance, inclusion of additional memory tasks may have provided further insight into the severity of the memory impairments observed. Although difficult, it would be useful to increase the number of recording sites. Electrophysiology

from the RSC and MB, in particular, would be valuable considering the impact of the fibre lesions employed. Originally, this study hoped to compare the effects of MTT, PCFx and VTNg lesions on memory and functionality across the extended hippocampal system. However, due to surgery complications, I was unable to include a VTNg lesion group. The following paragraphs discuss these limitations.

Electrophysiology: Due to time constraints, the present study focussed on 'theta' rhythmicity or rhythmic slow activity, due to the implications of this frequency band on memory function. However, given the global effects observed following PCFx and MTT lesions and ATN stimulation, it would be useful for future studies to examine whether these effects extend beyond the frequency range examined here, for example, in the gamma band. The current study analysed spectral power and coherence in order to assess changes in oscillatory activity within and between structures. Nevertheless, future work should aim to examine additional electrophysiological markers such as cross frequency coupling and phase alignment, as these can facilitate better understanding of key interactions during behavioural performance.

Behavioural task: Memory performance was only measured using only one behavioural task, spatial working memory in the 12-arm RAM, although reference memory was also briefly tested in section 7.2.14. As discussed, it would have been informative to also include testing in the 8-arm RAM so as to provide a direct comparison with previous work by Vann et al. (2011) and Vann (2013). It would also have been useful to test reference and spatial working memory using a different apparatus such as the Morris Water Maze. Including an alternative memory task would have allowed us to verify that the PCFx and MTT lesion effects were consistent across tasks, and not restricted to the RAM. Nonetheless, the impact of MTT lesions on memory function has been well-documented (Vann, 2013; Frizzati et al., 2016, Perry et al., 2018) and the overall aim of the current study was to examine not only the mnemonic effects of MTT and PCFx lesions but also their impact on the wider circuit. In this case, the 12-arm RAM was particularly useful as it provided more correct choice data from the MTT group, allowing comparisons in electrophysiological activity to be made between Sham and MTT lesion rats.

Recording sites: Implantation of electrodes in the MB and RSC would have been valuable for the current study. The MB would have been of particular interest as it would

have helped to further partial out the impact of PCFx lesions relative to MTT lesions on electrophysiological activity. The RSC appears especially sensitive to diencephalic damage (Aggleton & Nelson, 2015; Dillingham et al., 2015). Furthermore, functional alterations in the RSC are often observed early in AD progression, with both ATN and RSC suggested to be a critical site of AD pathology (Aggleton et al., 2016). LFP data recorded from the RSC could, therefore, provide critical and clinically relevant insight into the oscillatory dysfunction observed following damage to the extended hippocampal system.

Nonetheless, practical considerations limited the number of electrodes that could be implanted within the rat's brain. This became particularly important when optic fibres were also implanted. The diameter of the optic fibre cannula required that the Open Ephys EIB board be cut so as to allow optic-fibre patch cables and the Open Ephys recording cable to be plugged in simultaneously. One approach might be to use multiple electrode arrays, with contacts spaced along the probe in order to capture multiple regions of interest. However, this technique with standard materials can produce excessive collateral damage. This is a major consideration in regions such as the thalamus, which contains multiple small nuclei, many of which play a role in memory function (Aggleton & Brown, 1999; Aggleton et al., 2010; Mitchell and DA, 2005, 2006). Damage could be minimised through the use of silicon probes (Buzsaki, 2002), some of which can be as small as 10 µm thick and with the capacity to record from up to 64 channels, although these are currently expensive. However, the latter are most commonly used in acute recording experiments, as opposed to the chronic implantation required in this study.

VTNg lesions. The inclusion of a VTNg lesion group would have helped to assess how the two MB inputs (i.e., the HPC input via the PCFx and the VTNg input) work in conjunction. For example, Chapter 6 showed that PCFx lesions lead to a profound reduction in global spectral power but did not cause the same attenuation of the HPC theta peak observed following MTT lesions. It may be that the brainstem input from the VTNg is responsible for driving peak theta in the HPC but has less impact on global spectral power. The initial aim of Chapter 6 was to include all three lesion groups, but issues ascertaining the exact location and size of the lesion meant I ran out of time to establish optimal lesions.

8.8 Future Directions

The present study has demonstrated the efficacy of ATN stimulation in improving memory function. Further research should test the efficacy of a wide range of different parameters. The novel finding that ATN stimulation impacts the wider circuit provides an ideal starting point for future research. An initial study should aim to determine which aspect of TBS was critical for the mnemonic improvement observed. That is, was it the regularity of stimulation or the use of an 8.5 Hz stimulation frequency that was important for memory recovery. However, McNaughton et al. (2006) did not use TBS, instead delivering a single pulse at a frequency of 7.7 Hz. Shirvalkar et al. (2006) have previously shown that continuous 100 Hz stimulation of the central thalamus can improve cognitive performance and increase IEG activation in the neocortex and HPC. In this study, the authors delivered one 50 µsec pulse, as opposed to TBS. Therefore, it may also be worthwhile examining the difference in efficacy of single pulse stimulation compared to TBS. Different optogenetic stimulation parameters could be implemented in the ATN to determine which frequency and pattern of stimulation has the greatest impact. This may help in the design of future interventions in humans following thalamic stroke.

The AV projects to a wide range of structures including the RSC, subiculum, entorhinal cortex, and anterior cingulate (Bubb et al., 2017). In Chapter 7, viral vector infusions and optic fibres were located in the AV. Thus, stimulation potentially activated glutamatergic neurons projecting to all target structures. Although optogenetic stimulation was an effective means of enhancing memory performance, it is unclear whether this was as a result of activation of a particular pathway, or whether this relied on simultaneous stimulation of all target structures. To determine whether there may be one or multiple critical pathways involved, future work should examine the effects on memory of stimulation of select terminals. For example, optic fibres could be placed in the Rgb whilst viral vector infusions were still made in the AV. As a result, optogenetic stimulation would only activate ChR2 expressing AV neuron terminals in the Rgb. Rats could then be tested on the same spatial working memory tasks described in the current study. Adhikari et al. (2015) used a very similar approach and elegantly demonstrated the importance of the mPFC projections to the basomedial amygdala in anxiety. Better understanding of the specific connections underlying the mnemonic effect of AV stimulation increases our understanding

of the neural circuitry involved in memory function. Furthermore, it enables further refinement of a targeted intervention for memory impairment.

PCFx and MTT lesions comparably impaired spatial working memory in the 12-arm RAM. Furthermore, similar electrophysiological and IEG effects were observed following both lesions. It would be of considerable interest to examine whether the memory deficits associated with PCFx damage are also amenable to optogenetic intervention, or whether the effect of ATN stimulation is unique to MTT damage. As both the PCFx and the MTT appear to contribute to the MB-ATN propagation of oscillatory activity, it seems unlikely that optogenetic ATN stimulation would have a negligible effect.

As discussed in Chapter 3, cases of amnesia can arise following pathology in or damage to a range of diencephalic structures, including the MB, ATN and MTT (Harding et al., 2000; Van der Werf et al., 2003; Tsivilis et al., 2008; Carlesimo et al., 2011; Dzieciol et al., 2017). The importance of these structures has been reiterated in the animal literature (Aggleton & Mishkin, 1985; Parker & Gaffan, 1997; Sziklas & Petrides, 1999; Mitchell & Dalrymple-Alford, 2006; Vann, 2013; Perry et al., 2018). Future work could explore the potential to enhance memory deficits associated with damage to or degeneration of different structures within the extended hippocampal system. As optogenetic ATN stimulation clearly improved memory function in rats with MTT transection, ATN stimulation may also be beneficial following damage to the MB, particularly due to the involvement of the medial MB in rhythmic propagation (Kirk & Mackay, 2003). ATN stimulation would clearly be ineffective following ATN lesions. However, it may be that targeting another nodal structure within the extended hippocampal system might produce similar memory improvements. For example, the nucleus reuniens (Re) also maintains a nodal position within the system, with dense interconnections with both the HPC and PFC (Cassel et al., 2013). The presence of Re bifurcating neurons that innervate both the HPC and PFC suggests that the Re may play a modulatory role for HPC-PFC interactions (Hoover & Vertes, 2012). Therefore, future research could examine the ability to achieve recovery of function through selective optogenetic stimulation of other nodal structures, such as the Re, within the distributed memory network.

The current study demonstrates the potential to use optogenetic interventions in rodents. However, there are several technical challenges that need to be overcome before

optogenetic stimulation can be translated for clinical interventions. AAV and LV vectors have been shown to be safe and are tolerated by patients with neurological disorders (Coune et al., 2012; Feigin et al., 2007; Kaplitt et al., 2007; LeWitt et al., 2011; Marks et al., 2008; Olanow et al., 2015; Palfi et al., 2014). In AD patients, for example, the therapeutic benefit of enhanced nerve growth factor production following in vivo transduction of basal forebrain cholinergic neurons using AAV2 awaits the outcome of phase 2 clinical trials (Rafii et al., 2014; Tuszynski et al., 2015). In AD it may be particularly valuable to examine the effects of ATN stimulation. AD pathology is typically widespread, involving key structures within the extended hippocampal system, particularly the RSC and HPC (Aggleton, 2014). As shown by the current study, ATN stimulation enhances activity in the HPC and RSC. However, the further assessment of the safety of long-term expression of viral vector expression is required. Expression of exogenous proteins following injection of AAV are known to remain high in the primate brain for 15 years (Sehara et al., 2017). Nonetheless, considerable testing is required to assess the long-term impact of overexpressing exogenous proteins in mammalian neural tissue. This information is critical for assessing when a gene therapy-based intervention should be conducted to slow memory decline, whilst ensuring that expression remains for the patient's expected life span. Enhanced vector delivery systems need to be developed to ensure that the transduced area is large enough in the human brain for clinical effects. Here, we selectively targeted the ATN in order to successfully circumvent this issue. Finally, implantable optogenetic stimulators will need to produce sufficient light spread to modulate the required target area in the brain. Having a battery storage capacity that only requires recharging once (or less) per day is also important.

8.9 Concluding statements

This thesis has demonstrated two, highly novel pieces of evidence. The effects of both MTT and PCFx both produce major memory impairments, at least when a 12-arm maze is employed. These lesions also resulted in broadly similar aberrant electrophysiological activity across the ATN-HPC-PFC axis. These findings suggest that rhythmic propagation into the MB and onto the ATN is not solely driven by VTNg inputs, but rather relies on both HPC and VTNg innervation. We have reported, for the first time, that optogenetic stimulation of the ATN can improve memory function in rats with MTT lesions. However, the exact

mechanisms underlying this mnemonic enhancement are as yet unclear. ATN stimulation increased spectral ATN, HPC and PFC spectral power and coherence as well as IEG activation across key memory structures in rats with MTT lesions. The electrophysiological and IEG changes were indicative of widespread functional alterations, and reflect direct and indirect effects of stimulation. The lack of mnemonic improvement observed using closed-loop parameters highlights the importance of selecting physiologically relevant stimulation patterns. Even in instances of "permanent" impairments after injury to subcortical tracts associated with memory, the distributed memory network appears amenable to intervention, extending and perhaps pointing to new studies on improved memory performance associated with environmental enrichment after ATN lesions. The functional recovery of key memory structures associated with the beneficial effect of ATN stimulation suggests clinical applications for memory impairment after thalamic stroke. It may also signal treatment prospects for early AD and in patients with Korsakoff's syndrome.

References

Adhikari, A., Lerner, T. N., Finkelstein, J., Pak, S., Jennings, J. H., Davidson, T. J., ... Kim, S. Y. (2015). Basomedial amygdala mediates topdown control of anxiety and fear. *Nature,* 527(7577), 179–185.

Aggleton, J. P., Neave, N., Nagle, S., & Hunt, P. R. (1995). A comparison of the effects of anterior thalamic, mamillary body and fornix lesions on reinforced spatial alternation. *Behavioural brain research*, *68*(1), 91-101.

Aggleton, J. P., Hunt, P. R., Nagle, S., & Neave, N. (1996). The effects of selective lesions within the anterior thalamic nuclei on spatial memory in the rat. *Behavioural brain research*, *81*(1-2), 189-198.

Aggleton, J. P., & Brown, M. W. (1999). Episodic memory, amnesia, and the hippocampal–anterior thalamic axis. *Behavioral and brain sciences*, *22*(3), 425-444.

Aggleton, J. P. (2008). Understanding anterograde amnesia: disconnections and hidden lesions. *The Quarterly Journal of Experimental Psychology*, *61*(10), 1441-1471.

Aggleton, J. P., Poirier, G. L., Aggleton, H. S., Vann, S. D., & Pearce, J. M. (2009). Lesions of the fornix and anterior thalamic nuclei dissociate different aspects of hippocampal-dependent spatial learning: Implications for the neural basis of scene learning. *Behavioral neuroscience*, *123*(3), 504.

Aggleton, J. P., O'Mara, S. M., Vann, S. D., Wright, N. F., Tsanov, M., & Erichsen, J. T. (2010). Hippocampal–anterior thalamic pathways for memory: uncovering a network of direct and indirect actions. *European Journal of Neuroscience*, *31*(12), 2292-2307.

Aggleton, J. P. (2012). Multiple anatomical systems embedded within the primate medial temporal lobe: implications for hippocampal function. *Neuroscience & Biobehavioral Reviews*, *36*(7), 1579-1596.

Aggleton, J. P., & Nelson, A. J. (2015). Why do lesions in the rodent anterior thalamic nuclei cause such severe spatial deficits?. *Neuroscience & Biobehavioral Reviews*, *54*, 131-144.

Aggleton, J. P., Pralus, A., Nelson, A. J., & Hornberger, M. (2016). Thalamic pathology and memory loss in early Alzheimer's disease: moving the focus from the medial temporal lobe to Papez circuit. *Brain*, *139*(7), 1877-1890.

Albo, Z., Di Prisco, G. V., & Vertes, R. (2003). Anterior thalamic unit discharge profiles and coherence with hippocampal theta rhythm. *Thalamus & Related Systems*, *2*(2), 133-144.

Allen, G. V., & Hopkins, D. A. (1989). Mamillary body in the rat: topography and synaptology of projections from the subicular complex, prefrontal cortex, and midbrain tegmentum. *Journal of Comparative Neurology*, *286*(3), 311-336.

Amado, R. G., & Chen, I. S. (1999). Lentiviral vectors--the promise of gene therapy within reach?. *Science*, *285*(5428), 674-676.

Armbruster, B. N., Li, X., Pausch, M. H., Herlitze, S., & Roth, B. L. (2007). Evolving the lock to fit the key to create a family of G proteincoupled receptors potently activated by an inert ligand. *Proceedings of the National Academy of Sciences of the United States of America*, 104(12), 5163–5168.

Aschauer, D. F., Kreuz, S., & Rumpel, S. (2013). Analysis of transduction efficiency, tropism and axonal transport of AAV serotypes 1, 2, 5, 6, 8 and 9 in the mouse brain. *PloS One*, 8(9), e76310.

Atkinson, J. D., Collins, D. L., Bertrand, G., Peters, T. M., Pike, G. B., & Sadikot, A. F. (2002). Optimal location of thalamotomy lesions for tremor associated with Parkinson disease: A probabilistic analysis based on postoperative magnetic resonance imaging and an integrated digital atlas. *Journal of Neurosurgery*, 96(5), 854–866

Baleydier, C., & Mauguiere, F. (1985). Anatomical evidence for medial pulvinar connections with the posterior cingulate cortex, the retrosplenial area, and the posterior parahippocampal gyrus in monkeys. *Journal of Comparative Neurology*, *232*(2), 219-228.

Barnes, C. A. (1979). Memory deficits associated with senescence: a neurophysiological and behavioral study in the rat. *Journal of comparative and physiological psychology*, *93*(1), 74.

Barnett, S. C., Perry, B. A. L., Dalrymple-Alford, J. C., & Parr-Brownlie, L. C. (2018). Optogenetic stimulation: Understanding memory and treating deficits. *Hippocampus*, *28*(7), 457-470.

Barr, M. S., Rajji, T. K., Zomorrodi, R., Radhu, N., George, T. P., Blumberger, D. M., & Daskalakis, Z. J. (2017). Impaired theta-gamma coupling during working memory performance in schizophrenia. *Schizophrenia research*, *189*, 104-110.

Başar, E., Schmiedt-Fehr, C., Mathes, B., Femir, B., Emek-Savaş, D. D., Tülay, E., ... & Yener, G. (2016). What does the broken brain say to the neuroscientist? Oscillations and connectivity in schizophrenia, Alzheimer's disease, and bipolar disorder. *International Journal of Psychophysiology*, *103*, 135-148.

Bassant, M. H., & Poindessous-Jazat, F. (2001). Ventral tegmental nucleus of Gudden: a pontine hippocampal theta generator?. *Hippocampus*, *11*(6), 809-813.

Benabid, A. L., Pollak, P., Hoffmann, D., Gervason, C., Hommel, M., Perret, J. E., ... Gao, D. M. (1991). Long-term suppression of tremor by chronic stimulation of the ventral intermediate thalamic nucleus. *The Lancet*, 337(8738), 403–406.

Benn, A., Barker, G. R., Stuart, S. A., Roloff, E. V. L., Teschemacher, A. G., Warburton, E. C., & Robinson, E. S. (2016). Optogenetic stimulation of prefrontal glutamatergic neurons enhances recognition memory. *Journal of Neuroscience*, *36*(18), 4930-4939.

Berndt, A., Lee, S. Y., Ramakrishnan, C., & Deisseroth, K. (2014). Structure-guided transformation of channelrhodopsin into a light-activated chloride channel. Science, 344(6182), 420–424.

Beuter, A., & Titcombe, M. S. (2003). Modulation of tremor amplitude during deep brain stimulation at different frequencies. Brain and Cognition, 53(2), 190–192.

Binder, S., Dere, E., & Zlomuzica, A. (2015). A critical appraisal of the what-where-when episodic-like memory test in rodents: Achievements, caveats and future directions. *Progress in neurobiology*, *130*, 71-85.

Bisecco, A., Rocca, M. A., Pagani, E., Mancini, L., Enzinger, C., Gallo, A., ... & Fazekas, F. (2015). Connectivity-based parcellation of the thalamus in multiple sclerosis and its implications for cognitive impairment: A multicenter study. *Human brain mapping*, *36*(7), 2809-2825.

Boecker, H., Wills, A. J., Ceballos-Baumann, A., Samuel, M., Thomas, D. G., Marsden, C. D., & Brooks, D. J. (1997). Stereotactic thalamotomy in tremor-dominant Parkinson's disease: An H215O PET motor activation study. *Annals of Neurology*, 41(1), 108–111

Bolkan, S. S., Stujenske, J. M., Parnaudeau, S., Spellman, T. J., Rauffenbart, C., Abbas, A. I., ... Kellendonk, C. (2017). Thalamic projections sustain prefrontal activity during working memory maintenance. *Nature Neuroscience,* 20(7), 987.

Bowden, J. B., Abraham, W. C., & Harris, K. M. (2012). Differential effects of strain, circadian cycle, and stimulation pattern on LTP and concurrent LTD in the dentate gyrus of freely moving rats. *Hippocampus*, 22(6), 1363–1370.

Braak, H., & Braak, E. (1991a). Neuropathological stageing of Alzheimer-related changes. *Acta neuropathologica*, *82*(4), 239-259.

Braak, H., & Braak, E. (1991b). Alzheimer's disease affects limbic nuclei of the thalamus. *Acta neuropathologica*, *81*(3), 261-268.

Brown, M. W., & Aggleton, J. P. (2001). Recognition memory: what are the roles of the perirhinal cortex and hippocampus?. *Nature Reviews Neuroscience*, *2*(1), 51-61.

Bubb, E. J., Kinnavane, L., & Aggleton, J. P. (2017). Hippocampal–diencephalic–cingulate networks for memory and emotion: An anatomical guide. *Brain and Neuroscience Advances*, 1, 239821281772344.

Buckley, M. J., & Mitchell, A. S. (2016). Retrosplenial cortical contributions to anterograde and retrograde memory in the monkey. *Cerebral Cortex*, 26(6), 2905–2918.

Butler, W. N., Smith, K. S., van der Meer, M. A., & Taube, J. S. (2017). The head-direction signal plays a functional role as a neural compass during navigation. *Current Biology*, *27*(9), 1259-1267.

Buzsáki, G. (2002). Theta oscillations in the hippocampus. *Neuron*, *33*(3), 325-340.

Buzsáki, G. (2005). Theta rhythm of navigation: link between path integration and landmark navigation, episodic and semantic memory. *Hippocampus*, *15*(7), 827-840.

Buzsaki, G. (2011). Hippocampus. *Scholarpedia*, *6*(1), 1468.

Buzsáki, G., Anastassiou, C. A., & Koch, C. (2012). The origin of extracellular fields and currents—EEG, ECoG, LFP and spikes. *Nature reviews neuroscience*, *13*(6), 407-420.

Byatt, G., & Dalrymple-Alford, J. C. (1996). Both anteromedial and anteroventral thalamic lesions impair radial-maze learning in rats. *Behavioral neuroscience*, *110*(6), 1335.

Carlesimo, G. A., Serra, L., Fadda, L., Cherubini, A., Bozzali, M., & Caltagirone, C. (2007). Bilateral damage to the mammillo-thalamic tract impairs recollection but not familiarity in the recognition process: a single case investigation. *Neuropsychologia*, *45*(11), 2467-2479.

Carlesimo, G. A., Lombardi, M. G., & Caltagirone, C. (2011). Vascular thalamic amnesia: a reappraisal. *Neuropsychologia*, *49*(5), 777-789.

Carlesimo, G. A., Lombardi, M. G., Caltagirone, C., & Barban, F. (2015). Recollection and familiarity in the human thalamus. *Neuroscience & Biobehavioral Reviews*, 54, 18–28.

Carpenter, F., Burgess, N., & Barry, C. (2017). Modulating medial septal cholinergic activity reduces medial entorhinal theta frequency without affecting speed or grid coding. *Scientific reports*, *7*(1), 1-12.

Carrera, E., & Bogousslavsky, J. (2006). The thalamus and behavior: effects of anatomically distinct strokes. *Neurology*, *66*(12), 1817-1823.

Carter, M. E., & de Lecea, L. (2011). Optogenetic investigation of neural circuits in vivo. Trends in Molecular Medicine, 17(4), 197–206.

Cassel, J. C., De Vasconcelos, A. P., Loureiro, M., Cholvin, T., DalrympleAlford, J. C., & Vertes, R. P. (2013). The reuniens and rhomboid nuclei: Neuroanatomy,

electrophysiological characteristics and behavioral implications. *Progress in Neurobiology*, 111, 34–52.

Cenci, M. A., Whishaw, I. Q., & Schallert, T. (2002). Animal models of neurological deficits: how relevant is the rat?. *Nature Reviews Neuroscience*, *3*(7), 574-579.

Cenquizca, L. A., & Swanson, L. W. (2007). Spatial organization of direct hippocampal field CA1 axonal projections to the rest of the cerebral cortex. *Brain research reviews*, *56*(1), 1-26.

Chaudhuri, A., Zangenehpour, S., Rahbar-Dehgan, F., & Ye, F. (2000). Molecular maps of neural activity and quiescence. *Acta neurobiologiae experimentalis*, *60*(3), 403-410.

Chaturvedi, M., Hatz, F., Gschwandtner, U., Bogaarts, J. G., Meyer, A., Fuhr, P., & Roth, V. (2017). Quantitative EEG (QEEG) measures differentiate Parkinson's disease (PD) patients from healthy controls (HC). *Frontiers in aging neuroscience*, *9*, 3.

Chen, B. T., Yau, H. J., Hatch, C., Kusumoto-Yoshida, I., Cho, S. L., Hopf, F. W., & Bonci, A. (2013). Rescuing cocaine-induced prefrontal cortex hypoactivity prevents compulsive cocaine seeking. *Nature,* 496(7445), 359–362.

Christiansen, K., Aggleton, J. P., Parker, G. D., O'Sullivan, M. J., Vann, S. D., & Metzler-Baddeley, C. (2016). The status of the precommissural and postcommissural fornix in normal ageing and mild cognitive impairment: An MRI tractography study. *NeuroImage*, *130*, 35-47.

Clayton, N. S., & Dickinson, A. (1998). Episodic-like memory during cache recovery by scrub jays. *Nature*, *395*(6699), 272-274.

Coad, B. M., Craig, E., Louch, R., Aggleton, J. P., Vann, S. D., & Metzler-Baddeley, C. (2020). Precommissural and postcommissural fornix microstructure in healthy aging and cognition. *Brain and Neuroscience Advances*, *4*, 2398212819899316.

Coley, E., Farhadi, R., Lewis, S., Whittle, I. R., Coley, E., Farhadi, R., ... Whittle, I. R. (2009). The incidence of seizures following deep brain stimulating electrode

implantation for movement disorders, pain and psychiatric conditions. *British Journal of Neurosurgery*, 23(2), 179–183.

Colgin, L. L. (2011). Oscillations and hippocampal–prefrontal synchrony. *Current opinion in neurobiology*, *21*(3), 467-474.

Colgin, L. L. (2013). Mechanisms and functions of theta rhythms. *Annual review of neuroscience*, *36*, 295-312.

Corkin, S. (2002). What's new with the amnesic patient HM?. *Nature reviews neuroscience*, *3*(2), 153-160.

Corkin, S. (2013). *Permanent present tense: The man with no memory, and what he taught the world*. Penguin UK.

Coune, P. G., Schneider, B. L., & Aebischer, P. (2012). Parkinson's disease: Gene therapies. *Cold Spring Harbor Perspectives in Medicine*, 2 (4), a009431.

Cozac, V. V., Chaturvedi, M., Hatz, F., Meyer, A., Fuhr, P., & Gschwandtner, U. (2016). Increase of EEG spectral theta power indicates higher risk of the development of severe cognitive decline in Parkinson's disease after 3 years. *Frontiers in aging neuroscience*, *8*, 284.

Cruce, J. A. (1977). An autoradiographic study of the descending connections of the mammillary nuclei of the rat. *Journal of Comparative Neurology*, *176*(4), 631-644.

Czajkowski, R., Jayaprakash, B., Wiltgen, B., Rogerson, T., Guzman-Karlsson, M. C., Barth, A. L., ... & Silva, A. J. (2014). Encoding and storage of spatial information in the retrosplenial cortex. *Proceedings of the National Academy of Sciences*, *111*(23), 8661-8666.

Dalrymple-Alford, J. C., Harland, B., Loukavenko, E. A., Perry, B., Mercer, S., Collings, D. A., ... & Wolff, M. (2015). Anterior thalamic nuclei lesions and recovery of function: Relevance to cognitive thalamus. *Neuroscience & Biobehavioral Reviews*, *54*, 145-160.

Danet, L., Barbeau, E. J., Eustache, P., Planton, M., Raposo, N., Sibon, I., ... & Pariente, J. (2015). Thalamic amnesia after infarct: the role of the mammillothalamic tract and mediodorsal nucleus. *Neurology*, *85*(24), 2107-2115.

Davis, S., Bozon, B., & Laroche, S. (2003). How necessary is the activation of the immediate early gene zif268 in synaptic plasticity and learning?. *Behavioural brain research*, *142*(1-2), 17-30.

de Jong, L. W., van der Hiele, K., Veer, I. M., Houwing, J. J., Westendorp, R. G. J., Bollen, E. L. E. M., ... & van der Grond, J. (2008). Strongly reduced volumes of putamen and thalamus in Alzheimer's disease: an MRI study. *Brain*, *131*(12), 3277-3285.

Delacourte, A., David, J. P., Sergeant, N., Buee, L., Wattez, A., Vermersch, P., ... & Petit, H. (1999). The biochemical pathway of neurofibrillary degeneration in aging and Alzheimer's disease. *Neurology*, *52*(6), 1158-1158.

Delay, J., & Brion, S. (1969). *Le syndrome de Korsakoff*. Masson.

Delli Pizzi, S., Franciotti, R., Taylor, J. P., Thomas, A., Tartaro, A., Onofrj, M., & Bonanni, L. (2015). Thalamic involvement in fluctuating cognition in dementia with Lewy bodies: magnetic resonance evidences. *Cerebral Cortex*, *25*(10), 3682-3689.

Deng, W., Aimone, J. B., & Gage, F. H. (2010). New neurons and new memories: How does adult hippocampal neurogenesis affect learning and memory? *Nature Reviews Neuroscience*, 11(5), 339–350.

Deng, W., Goldys, E. M., Farnham, M. M. J., & Pilowsky, P. M. (2014). Optogenetics, the intersection between physics and neuroscience: light stimulation of neurons in physiological conditions. *American Journal of Physiology - Regulatory Integrative and Comparative Physiology*, 307, R1292–R1302.

Denyer, R., & Douglas, M. R. (2012). Gene therapy for Parkinson's disease. *Parkinson's Disease*, 2012, 1

de Sousa, A. F., Cowansage, K. K., Zutshi, I., Cardozo, L. M., Yoo, E. J., Leutgeb, S., & Mayford, M. (2019). Optogenetic reactivation of memory ensembles in the retrosplenial

cortex induces systems consolidation. *Proceedings of the National Academy of Sciences*, *116*(17), 8576-8581.

Dezawa, M., Takano, M., Negishi, H., Mo, X., Oshitari, T., & Sawada, H. (2002). Gene transfer into retinal ganglion cells by in vivo electroporation: A new approach. *Micron* (Oxford, England : 1993), 33(1), 1–6.

Diester, I., Kaufman, M. T., Mogri, M., Pashaie, R., Goo, W., Yizhar, O., ... Shenoy, K. V. (2011). An optogenetic toolbox designed for primates. *Nature Neuroscience*, 14(3), 387–397.

Dillingham, C. M., Frizzati, A., Nelson, A. J., & Vann, S. D. (2015). How do mammillary body inputs contribute to anterior thalamic function?. *Neuroscience & Biobehavioral Reviews*, *54*, 108-119.

Dillingham, C. M., Milczarek, M. M., Perry, J. C., Frost, B. E., Parker, G. D., Assaf, Y., ... & Vann, S. D. (2019). Mammillothalamic Disconnection Alters Hippocampocortical Oscillatory Activity and Microstructure: Implications for Diencephalic Amnesia. *Journal of Neuroscience*, *39*(34), 6696-6713.

Dimidschstein, J., Chen, Q., Tremblay, R., Rogers, S. L., Saldi, G.-A., Guo, L., ... Fishell, G. (2017). A viral strategy for targeting and manipulating interneurons across vertebrate species. *Nature Neuroscience*, 20(7), 1033.

Drapeau, E., Mayo, W., Aurousseau, C., Le Moal, M., Piazza, P. V., & Abrous, D. N. (2003). Spatial memory performances of aged rats in the water maze predict levels of hippocampal neurogenesis. *Proceedings of the National Academy of Sciences*, 100(24), 14385–14390.

Duan, A. R., Varela, C., Zhang, Y., Shen, Y., Xiong, L., Wilson, M. A., & Lisman, J. (2015). Delta frequency optogenetic stimulation of the thalamic nucleus reuniens is sufficient to produce working memory deficits: Relevance to schizophrenia. *Biological Psychiatry*, 77(12), 1098–1107.

Dumont, J. R., Amin, E., Poirier, G. L., Albasser, M. M., & Aggleton, J. P. (2012). Anterior thalamic nuclei lesions in rats disrupt markers of neural plasticity in distal limbic brain regions. *Neuroscience*, *224*, 81-101.

Dumont, J. R., & Aggleton, J. P. (2013). Dissociation of recognition and recency memory judgments after anterior thalamic nuclei lesions in rats. *Behavioral neuroscience*, *127*(3), 415.

Dumont, J. R., Amin, E., & Aggleton, J. P. (2014). Selective importance of the rat anterior thalamic nuclei for configural learning involving distal spatial cues. *European Journal of Neuroscience*, *39*(2), 241-256.

Dupire, A., Kant, P., Mons, N., Marchand, A. R., Coutureau, E., Dalrymple-Alford, J., & Wolff, M. (2013). A role for anterior thalamic nuclei in affective cognition: interaction with environmental conditions. *Hippocampus*, *23*(5), 392-404.

Dusoir, H., Kapur, N., Byrnes, D. P., McKinstry, S., & Hoare, R. D. (1990). The role of diencephalic pathology in human memory disorder: evidence from a penetrating paranasal brain injury. *Brain*, *113*(6), 1695-1706.

Duval, C., Panisset, M., Strafella, A. P., & Sadikot, A. F. (2006). The impact of ventrolateral thalamotomy on tremor and voluntary motor behavior in patients with Parkinson's disease. *Experimental Brain Research*, 170(2), 160–171.

Dzieciol, A. M., Bachevalier, J., Saleem, K. S., Gadian, D. G., Saunders, R., Chong, W. K., ... & Vargha-Khadem, F. (2017). Hippocampal and diencephalic pathology in developmental amnesia. *Cortex*, *86*, 33-44.

Eichenbaum, H. (2017). Prefrontal–hippocampal interactions in episodic memory. *Nature Reviews Neuroscience*, *18*(9), 547.

Eichenbaum, H. (2017). Memory: organization and control. *Annual review of psychology*, *68*, 19-45.

Erickson, M. A., Maramara, L. A., & Lisman, J. (2010). A single brief burst induces GluR1-dependent associative short-term potentiation: a potential mechanism for short-term memory. *Journal of cognitive neuroscience*, *22*(11), 2530-2540.

Falkner, A. L., Grosenick, L., Davidson, T. J., Deisseroth, K., & Lin, D. (2016). Hypothalamic control of male aggression-seeking behavior. *Nature Neuroscience*, 19(4), 596–604.

Farina, F. R., & Commins, S. (2016). Differential expression of immediate early genes Zif268 and c-Fos in the hippocampus and prefrontal cortex following spatial learning and glutamate receptor antagonism. *Behavioural brain research*, *307*, 194-198.

Feigin, A., Kaplitt, M. G., Tang, C., Lin, T., Mattis, P., Dhawan, V., ... Eidelberg, D. (2007). Modulation of metabolic brain networks after subthalamic gene therapy for Parkinson's disease. *Proceedings of the National Academy of Sciences*, 104(49), 19559–19564.

Fell, J., Klaver, P., Elfadil, H., Schaller, C., Elger, C. E., & Fernández, G. (2003). Rhinal–hippocampal theta coherence during declarative memory formation: interaction with gamma synchronization?. *European Journal of Neuroscience*, *17*(5), 1082-1088.

Fell, J., & Axmacher, N. (2011). The role of phase synchronization in memory processes. *Nature reviews neuroscience*, *12*(2), 105-118.

Fenno, L., Yizhar, O., & Deisseroth, K. (2011). The development and application of optogenetics. *Annual Review of Neuroscience*, 34(1), 389.

Field, T. D., Rosenstock, J., King, E. C., & Greene, E. (1978). Behavioral role of the mammillary efferent system. *Brain research bulletin*, *3*(5), 451-456.

Frey, S., Bergado-Rosado, J., Seidenbecher, T., Pape, H. C., & Frey, J. U. (2001). Reinforcement of early long-term potentiation (early-LTP) in dentate gyrus by stimulation of the basolateral amygdala: heterosynaptic induction mechanisms of late-LTP. *Journal of Neuroscience*, *21*(10), 3697-3703.

Frizzati, A., Milczarek, M. M., Sengpiel, F., Thomas, K. L., Dillingham, C. M., & Vann, S. D. (2016). Comparable reduction in Zif268 levels and cytochrome oxidase activity in the retrosplenial cortex following mammillothalamic tract lesions. *Neuroscience*, *330*, 39-49.

Frost, B., Cafalchio, M., Martin, S. K., Islam, M. N., Aggleton, J., & O'Mara, S. M. (2020). Spatial Coding in the Subiculum Requires Anterior Thalamic Inputs. *CURRENT-BIOLOGY-D-20-00365*.

Fuster, J. M. (1995). Memory and planning: Two temporal perspectives of frontal lobe function.

Gallo, F. T., Katche, C., Morici, J. F., Medina, J. H., & Weisstaub, N. V. (2018). Immediate early genes, memory and psychiatric disorders: focus on c-Fos, Egr1 and Arc. *Frontiers in behavioral neuroscience*, *12*, 79.

Galvan, A., Hu, X., Smith, Y., & Wichmann, T. (2016). Effects of optogenetic activation of corticothalamic terminals in the motor thalamus of awake monkeys. *Journal of Neuroscience*, 36(12), 3519–3530.

Gomez, J. L., Bonaventura, J., Lesniak, W., Mathews, W. B., Sysa-Shah, P., Rodriguez, L. A., ... Pomper, M. G. (2017). Chemogenetics revealed: DREADD occupancy and activation via converted clozapine. *Science*, 357(6350), 503–507.

Gonzalo-Ruiz, A., Alonso, A., Sanz, J. M., & Llinas, R. R. (1992). Afferent projections to the mammillary complex of the rat, with special reference to those from surrounding hypothalamic regions. *Journal of Comparative Neurology*, *321*(2), 277-299.

Gonzalo-Ruiz, A., & Morte, L. (2000). Localization of amino acids, neuropeptides and cholinergic markers in neurons of the septum-diagonal band complex projecting to the retrosplenial granular cortex of the rat. *Brain research bulletin*, *52*(6), 499-510.

Goutagny, R., Gu, N., Cavanagh, C., Jackson, J., Chabot, J. G., Quirion, R., ... & Williams, S. (2013). Alterations in hippocampal network oscillations and theta–gamma coupling arise before Aβ overproduction in a mouse model of Alzheimer's disease. *European Journal of Neuroscience*, *37*(12), 1896-1902.

Gradinaru, V., Mogri, M., Thompson, K. R., Henderson, J. M., & Deisseroth, K. (2009). Optical deconstruction of parkinsonian neural circuitry. *Science,* 324(5925), 354–359.

Gu, Y., Arruda-Carvalho, M., Wang, J., Janoschka, S. R., Josselyn, S. A., Frankland, P. W., & Ge, S. (2012). Optical controlling reveals timedependent roles for adult-born dentate granule cells. *Nature Neuroscience*, 15(12), 1700–1706.

Gudden, H. (1896). Klinische und anatomische Beiträge zur Kenntniss der multiplen Alkoholneuritis nebst Bemerkungen über die Regenerationsvorgänge im peripheren Nervensystem. *Archiv für Psychiatrie und Nervenkrankheiten*, *28*(3), 643-741.

Guillery, R. W. (1956). Degeneration in the post-commissural fornix and the mamillary peduncle of the rat. *Journal of anatomy*, *90*(Pt 3), 350.

Gunaydin, L. A., Yizhar, O., Berndt, A., Sohal, V. S., Deisseroth, K., & Hegemann, P. (2010). Ultrafast optogenetic control. *Nature Neuroscience*, 13(3), 387–392.

Guzowski, J. F., Setlow, B., Wagner, E. K., & McGaugh, J. L. (2001). Experience-dependent gene expression in the rat hippocampus after spatial learning: a comparison of the immediate-early genesArc, c-fos, and zif268. *Journal of Neuroscience*, *21*(14), 5089-5098.

Hadaczek, P., Stanek, L., Ciesielska, A., Sudhakar, V., Samaranch, L., Pivirotto, P., ... Forsayeth, J. (2016). Widespread AAV1-and AAV2-mediated transgene expression in the nonhuman primate brain: Implications for Huntington's disease. *Molecular Therapy—Methods & Clinical Development*, 3, 16037.

Hamani, C., Stone, S. S., Garten, A., Lozano, A. M., & Winocur, G. (2011). Memory rescue and enhanced neurogenesis following electrical stimulation of the anterior thalamus in rats treated with corticosterone. *Experimental Neurology*, 232(1), 100–104.

Han, W., Tellez, L. A., Rangel Jr, M. J., Motta, S. C., Zhang, X., Perez, I. O., ... & de Araujo, I. E. (2017). Integrated control of predatory hunting by the central nucleus of the amygdala. *Cell*, *168*(1-2), 311-324.

Harding, A., Halliday, G., Caine, D., & Kril, J. (2000). Degeneration of anterior thalamic nuclei differentiates alcoholics with amnesia. *Brain*, *123*(1), 141-154.

Harland, B. C., Collings, D. A., McNaughton, N., Abraham, W. C., & Dalrymple-Alford, J. C. (2014). Anterior thalamic lesions reduce spine density in both hippocampal CA1 and retrosplenial cortex, but enrichment rescues CA1 spines only. *Hippocampus*, *24*(10), 1232-1247.

Hayakawa, T., & Zyo, K. (1984). Comparative anatomical study of the tegmentomammillary projections in some mammals: a horseradish peroxidase study. *Brain research*, *300*(2), 335-349.

He, X., Zhang, Y., Chen, J., Xie, C., Gan, R., Wang, L., & Wang, L. (2017). Changes in theta activities in the left posterior temporal region, left occipital region and right frontal region related to mild cognitive impairment in Parkinson's disease patients. *International Journal of Neuroscience*, *127*(1), 66-72.

Henry, J., Petrides, M., St-Laurent, M., & Sziklas, V. (2004). Spatial conditional associative learning: effects of thalamo-hippocampal disconnection in rats. *Neuroreport*, *15*(15), 2427-2431.

Herrmann, C. S., & Demiralp, T. (2005). Human EEG gamma oscillations in neuropsychiatric disorders. *Clinical neurophysiology*, *116*(12), 2719-2733.

Honda, Y., & Ishizuka, N. (2015). Topographic distribution of cortical projection cells in the rat subiculum. *Neuroscience Research*, *92*, 1-20.

Hoover, W. B., & Vertes, R. P. (2007). Anatomical analysis of afferent projections to the medial prefrontal cortex in the rat. *Brain Structure and Function*, *212*(2), 149-179.

Houtchens, M. K., Benedict, R. H. B., Killiany, R., Sharma, J., Jaisani, Z., Singh, B., ... & Bakshi, R. (2007). Thalamic atrophy and cognition in multiple sclerosis. *Neurology*, *69*(12), 1213-1223.

Hoy, K. E., Bailey, N., Michael, M., Fitzgibbon, B., Rogasch, N. C., Saeki, T., & Fitzgerald, P. B. (2016). Enhancement of working memory and task-related oscillatory activity following intermittent theta burst stimulation in healthy controls. *Cerebral cortex*, *26*(12), 4563-4573.

Hurley, K. M., Herbert, H., Moga, M. M., & Saper, C. B. (1991). Efferent projections of the infralimbic cortex of the rat. *The Journal of Comparative Neurology*, 308(2), 249–276.

Hyman, J. M., Zilli, E. A., Paley, A. M., & Hasselmo, M. E. (2010). Working memory performance correlates with prefrontal-hippocampal theta interactions but not with prefrontal neuron firing rates. *Frontiers in integrative neuroscience*, *4*, 2.

Jankowski, M. M., Ronnqvist, K. C., Tsanov, M., Vann, S. D., Wright, N. F., Erichsen, J. T., ... O'Mara, S. M. (2013). The anterior thalamus provides a subcortical circuit supporting memory and spatial navigation. *Frontiers in Systems Neuroscience*, 7.

Janvin, C. C., Larsen, J. P., Salmon, D. P., Galasko, D., Hugdahl, K., & Aarsland, D. (2006). Cognitive profiles of individual patients with Parkinson's disease and dementia: comparison with dementia with lewy bodies and Alzheimer's disease. *Movement Disorders*, *21*(3), 337-342.

Jelic, V., Johansson, S. E., Almkvist, O., Shigeta, M., Julin, P., Nordberg, A., ... & Wahlund, L. O. (2000). Quantitative electroencephalography in mild cognitive impairment: longitudinal changes and possible prediction of Alzheimer's disease. *Neurobiology of aging*, *21*(4), 533-540.

Jenkins, T. A., Dias, R., Amin, E., & Aggleton, J. P. (2002). Changes in Fos expression in the rat brain after unilateral lesions of the anterior thalamic nuclei. *European Journal of Neuroscience*, *16*(8), 1425-1432.

Jenkins, T. A., Vann, S. D., Amin, E., & Aggleton, J. P. (2004). Anterior thalamic lesions stop immediate early gene activation in selective laminae of the retrosplenial cortex: evidence of covert pathology in rats?. *European Journal of Neuroscience*, *19*(12), 3291-3304.

Johkura, K., & Naito, M. (2008). Wernicke's encephalopathy-like lesions in global cerebral hypoxia. *Journal of Clinical Neuroscience*, *15*(3), 318-319.

Jones, M. W., Errington, M. L., French, P. J., Fine, A., Bliss, T. V. P., Garel, S., ... & Davis, S. (2001). A requirement for the immediate early gene Zif268 in the expression of late LTP and long-term memories. *Nature neuroscience*, *4*(3), 289-296.

Jones, M. W., & Wilson, M. A. (2005). Theta rhythms coordinate hippocampal–prefrontal interactions in a spatial memory task. *PLoS biology*, *3*(12).

Jyoti, A., Plano, A., Riedel, G., & Platt, B. (2010). EEG, activity, and sleep architecture in a transgenic AβPPswe/PSEN1A246E Alzheimer's disease mouse. *Journal of Alzheimer's Disease*, *22*(3), 873-887.

Kantarci, K. (2014). Fractional anisotropy of the fornix and hippocampal atrophy in Alzheimer's disease. *Frontiers in aging neuroscience*, *6*, 316.

Kaplitt, M. G., Feigin, A., Tang, C., Fitzsimons, H. L., Mattis, P., Lawlor, P. A., ... During, M. J. (2007). Safety and tolerabillity of gene therapy with an adeno-associated virus (AAV) borne GAD gene for Parkinson's disease: An open label, phase 1 trial. *Lancet*, 369(9579), 2097– 2105

Ketz, N. A., Jensen, O., & O'Reilly, R. C. (2015). Thalamic pathways underlying prefrontal cortex–medial temporal lobe oscillatory interactions. *Trends in neurosciences*, *38*(1), 3-12.

Khan, U. A., Liu, L., Provenzano, F. A., Berman, D. E., Profaci, C. P., Sloan, R., ... Small, S. A. (2014). Molecular drivers and cortical spread of lateral entorhinal cortex dysfunction in preclinical Alzheimer's disease. *Nature Neuroscience*, 17(2), 304–311

Kim, E., Ku, J., Namkoong, K., Lee, W., Lee, K. S., Park, J. Y., ... & Jung, Y. C. (2009). Mammillothalamic functional connectivity and memory function in Wernicke's encephalopathy. *Brain*, *132*(2), 369-376.

Kim, J., Delcasso, S., & Lee, I. (2011). Neural correlates of object-in-place learning in hippocampus and prefrontal cortex. *Journal of Neuroscience*, *31*(47), 16991-17006.

Kim, C. K., Adhikari, A., & Deisseroth, K. (2017). Integration of optogenetics with complementary methodologies in systems neuroscience. *Nature Reviews Neuroscience*, 18(4), 222–235.

Kirk, I. J., & Mackay, J. C. (2003). The role of theta-range oscillations in synchronising and integrating activity in distributed mnemonic networks. *Cortex*, *39*(4-5), 993-1008.

Klein, J. C., Barbe, M. T., Seifried, C., Baudrexel, S., Runge, M., Maarouf, M., ... Timmermann, L. (2012). The tremor network targeted by successful VIM deep brain stimulation in humans. *Neurology*, 78(11), 787–795.

Kocsis, B., & Vertes, R. P. (1994). Characterization of neurons of the supramammillary nucleus and mammillary body that discharge rhythmically with the hippocampal theta rhythm in the rat. *Journal of Neuroscience*, *14*(11), 7040-7052.

Kocsis, B., Di Prisco, G. V., & Vertes, R. P. (2001). Theta synchronization in the limbic system: the role of Gudden's tegmental nuclei. *European Journal of Neuroscience*, *13*(2), 381-388.

Kopelman, M. D. (1995). The korsakoff syndrome. *The British Journal of Psychiatry*, *166*(2), 154-173.

Kopelman, M. D. (2002). Disorders of memory. *Brain*, *125*(10), 2152-2190.

Kopelman, M. D., Thomson, A. D., Guerrini, I., & Marshall, E. J. (2009). The Korsakoff syndrome: clinical aspects, psychology and treatment. *Alcohol and alcoholism*, *44*(2), 148-154.

Kopelman, M. D. (2015). What does a comparison of the alcoholic Korsakoff syndrome and thalamic infarction tell us about thalamic amnesia?. *Neuroscience & Biobehavioral Reviews*, *54*, 46-56.

Korsakoff, S. S. (1887). Disturbance of psychic function in alcoholic paralysis and its relation to the disturbance of the psychic sphere in multiple neuritis of non-alcoholic origin. *Vestnik Psichiatrii*, *4*(2), 1-102.

Korsakoff, S. S. (1889). A few cases of peculiar cerebropathy in the course of multiple neuritis. *Ejenedelnaja Klinicheskaja Gazeta*, *5*(6), 7.

Krieckhaus, E. E., & Randall, D. (1968). Lesions of mammillothalamic tract in rat produce no decrements in recent memory. *Brain*, *91*(2), 369-378.

Krook-Magnuson, E., Armstrong, C., Oijala, M., & Soltesz, I. (2013). Ondemand optogenetic control of spontaneous seizures in temporal lobe epilepsy. *Nature Communications*, 4, 1376.

Kumar, R., Birrer, B. V., Macey, P. M., Woo, M. A., Gupta, R. K., Yan-Go, F. L., & Harper, R. M. (2008). Reduced mammillary body volume in patients with obstructive sleep apnea. *Neuroscience letters*, *438*(3), 330-334.

Laxton, A. W., Tang-Wai, D. F., McAndrews, M. P., Zumsteg, D., Wennberg, R., Keren, R., ... Lozano, A. M. (2010). A phase I trial of deep brain stimulation of memory circuits in Alzheimer's disease. *Annals of Neurology*, 68(4), 521–534.

Lerchner, W., Corgiat, B., Der Minassian, V., Saunders, R. C., & Richmond, B. J. (2014). Injection parameters and virus dependent on choice of promoters to improve neuron targeting in the nonhuman primate brain. *Gene Therapy*, 21(3), 233–241.

LeWitt, P. A., Rezai, A. R., Leehey, M. A., Ojemann, S. G., Flaherty, A. W., Eskandar, E. N., ... Feigin, A. (2011). AAV2-GAD gene therapy for advanced Parkinson's disease: A double-blind, sham-surgery controlled, randomised trial. *Lancet Neurology*, 10(4), 309–319.

Li, S. F., Wang, R. Z., Meng, Q. H., Li, G. L., Hu, G. J., Dou, W. C., ... Zhang, Z. X. (2006). Intra-ventricular infusion of rAAV1-EGFP resulted in transduction in multiple regions of adult rat brain: A comparative study with rAAV2 and rAAV5 vectors. *Brain Research*, 1122 (1), 1–9.

Li, S., Arbuthnott, G. W., Jutras, M. J., Goldberg, J. A., & Jaeger, D. (2007). Resonant antidromic cortical circuit activation as a consequence of high frequency subthalamic deep-brain stimulation. *Journal of Neurophysiology*, 98(6), 3525–3537.

Li, Q., Ke, Y., Chan, D. C. W., Qian, Z. -M., Yung, K. K. L., Ko, H., ... Yung, W.-H. (2012). Therpeutic deep brain stimulation in parkinsonian rats directly influences motor cortex. *Neuron*, 76(5), 1030–1041.

Li, J., & Zhang, Y. (2014). Relationship between promoter sequence and its strength in gene expression. *The European Physical Journal* E, 37 (9), 86

Lisman, J. (2017). Glutamatergic synapses are structurally and biochemically complex because of multiple plasticity processes: long-term potentiation, long-term

depression, short-term potentiation and scaling. *Philosophical Transactions of the Royal Society B: Biological Sciences*, *372*(1715), 20160260.

Liu, Y., Paajanen, T., Zhang, Y., Westman, E., Wahlund, L. O., Simmons, A., ... & Vellas, B. (2011). Combination analysis of neuropsychological tests and structural MRI measures in differentiating AD, MCI and control groups—the AddNeuroMed study. *Neurobiology of Aging*, *32*(7), 1198-1206.

Loukavenko, E. A., Ottley, M. C., Moran, J. P., Wolff, M., & Dalrymple-Alford, J. C. (2007). Towards therapy to relieve memory impairment after anterior thalamic lesions: improved spatial working memory after immediate and delayed postoperative enrichment. *European Journal of Neuroscience*, *26*(11), 3267-3276.

Loukavenko, E. A., Wolff, M., Poirier, G. L., & Dalrymple-Alford, J. C. (2016). Impaired spatial working memory after anterior thalamic lesions: recovery with cerebrolysin and enrichment. *Brain Structure and Function*, *221*(4), 1955-1970.

Loureiro, M., Cholvin, T., Lopez, J., Merienne, N., Latreche, A., Cosquer, B., ... Pereira de Vasconcelos, A. (2012). The ventral midline thalamus (reuniens and rhomboid nuclei) contributes to the persistence of spatial memory in rats. *Journal of Neuroscience*, 32(29), 9947–9959.

Lux, S., Bindrich, V. N., Markowitsch, H. J., & Fink, G. R. (2015). Medial temporal lobe activation during autobiographical context memory retrieval of time and place and its dependency upon recency. *Neurocase*, 21(1), 23–32.

Marks, W. J., Jr., Ostrem, J. L., Verhagen, L., Starr, P. A., Larson, P. S., Bakay, R. A., ... Bartus, R. T. (2008). Safety and tolerability of intraputaminal delivery of CERE-120 (adeno-associated virus serotype 2- neurturin) to patients with idiopathic Parkinson's disease: An openlabel, phase I trial. *Lancet Neurology*, 7(5), 400–408

Mayes, A. R., Meudell, P. R., Mann, D., & Pickering, A. (1988). Location of lesions in Korsakoff's syndrome: neuropsychological and neuropathological data on two patients. *Cortex*, *24*(3), 367-388.

Mair, W. G., Warrington, E. K., & Weiskrantz, L. (1979). Memory disorder in Korsakoff's psychosis: a neuropathological and neuropsychological investigation of two cases. *Brain: a journal of neurology*, *102*(4), 749-783.

Mair, R. G., Burk, J. A., & Porter, M. C. (2003). Impairment of radial maze delayed nonmatching after lesions of anterior thalamus and parahippocampal cortex. *Behavioral neuroscience*, *117*(3), 596.

Maisson, D. J. N., Gemzik, Z. M., & Griffin, A. L. (2018). Optogenetic suppression of the nucleus reuniens selectively impairs encoding during spatial working memory. *Neurobiology of learning and memory*, *155*, 78-85.

Mathiasen, M. L., Dillingham, C. M., Kinnavane, L., Powell, A. L., & Aggleton, J. P. (2017). Asymmetric cross-hemispheric connections link the rat anterior thalamic nuclei with the cortex and hippocampal formation. *Neuroscience,* 349, 128–143.

Matthaei, K. I. (2007). Genetically manipulated mice: A powerful tool with unsuspected caveats. *The Journal of Physiology*, 582(Pt 2), 481–488.

McNaughton, N., James, D. T. D., Stewart, J., Gray, J. A., Valero, I., & Drewnowski, A. (1977). Septal driving of hippocampal theta rhythm as a function of frequency in the male rat: Effects of drugs. *Neuroscience*, *2*(6), 1019-1027.

McNaughton, N., & Sedgwick, E. M. (1978). Reticular stimulation and hippocampal theta rhythm in rats: effects of drugs. *Neuroscience*, *3*(7), 629-632.

Mendez-Lopez, M., Arias, J. L., Bontempi, B., & Wolff, M. (2013). Reduced cytochrome oxidase activity in the retrosplenial cortex after lesions to the anterior thalamic nuclei. *Behavioural brain research*, *250*, 264-273.

Merrill, D. R., Bikson, M., & Jefferys, J. G. (2005). Electrical stimulation of excitable tissue: Design of efficacious and safe protocols. *Journal of Neuroscience Methods*, 141(2), 171–198.

Mielke, M. M., Okonkwo, O. C., Oishi, K., Mori, S., Tighe, S., Miller, M. I., ... & Lyketsos, C. G. (2012). Fornix integrity and hippocampal volume predict memory decline and progression to Alzheimer's disease. *Alzheimer's & Dementia*, *8*(2), 105-113.

Mitchell, A. S., Dalrymple-Alford, J. C., & Christie, M. A. (2002). Spatial working memory and the brainstem cholinergic innervation to the anterior thalamus. *Journal of Neuroscience*, *22*(5), 1922-1928.

Mitchell, A. S., & Dalrymple-Alford, J. C. (2006). Lateral and anterior thalamic lesions impair independent memory systems. *Learning & Memory*, *13*(3), 388-396.

Mitchell, D. J., McNaughton, N., Flanagan, D., & Kirk, I. J. (2008). Frontal-midline theta from the perspective of hippocampal "theta". *Progress in neurobiology*, *86*(3), 156-185.

Mitchell, A. S., Czajkowski, R., Zhang, N., Jeffery, K., & Nelson, A. J. (2018). Retrosplenial cortex and its role in spatial cognition. *Brain and neuroscience advances*, *2*, 2398212818757098.

Miyashita, T., & Rockland, K. S. (2007). GABAergic projections from the hippocampus to the retrosplenial cortex in the rat. *European Journal of Neuroscience*, *26*(5), 1193-1204.

McNaughton, N., Ruan, M., & Woodnorth, M. A. (2006). Restoring theta-like rhythmicity in rats restores initial learning in the Morris water maze. *Hippocampus*, *16*(12), 1102-1110.

Mölle, M., Marshall, L., Fehm, H. L., & Born, J. (2002). EEG theta synchronization conjoined with alpha desynchronization indicate intentional encoding. *European Journal of Neuroscience*, *15*(5), 923-928.

Mormann, F., Fell, J., Axmacher, N., Weber, B., Lehnertz, K., Elger, C. E., & Fernández, G. (2005). Phase/amplitude reset and theta–gamma interaction in the human medial temporal lobe during a continuous word recognition memory task. *Hippocampus*, *15*(7), 890-900.

Morris, R. G. M. (1983). An attempt to dissociate" spatial-mapping and working-memory" theories of hippocampal function. *Neurobiology of the hippocampus*, 405-432.

Nathanson, J. L., Yanagawa, Y., Obata, K., & Callaway, E. M. (2009). Preferential labeling of inhibitory and excitatory cortical neurons by endogenous tropism of adeno-associated virus and lentivirus vectors. *Neuroscience*, 161(2), 441–450.

Nauta, W. J. (1958). Hippocampal projections and related neural pathways to the mid-brain in the cat. *Brain*, *81*(3), 319-340.

Nelson, A. J., & Vann, S. D. (2014). Mammilliothalamic tract lesions disrupt tests of visuo-spatial memory. *Behavioral neuroscience*, *128*(4), 494.

Nelson, A. J., & Vann, S. D. (2017). The importance of mammillary body efferents for recency memory: towards a better understanding of diencephalic amnesia. *Brain Structure and Function*, *222*(5), 2143-2156.

Nestor, P. J., Fryer, T. D., Ikeda, M., & Hodges, J. R. (2003). Retrosplenial cortex (BA 29/30) hypometabolism in mild cognitive impairment (prodromal Alzheimer's disease). *European Journal of Neuroscience*, *18*(9), 2663-2667.

Neves, G., Cooke, S. F., & Bliss, T. V. (2008). Synaptic plasticity, memory and the hippocampus: A neural network approach to causality. *Nature Reviews Neuroscience*, 9(1), 65–75.

Nimmrich, V., Draguhn, A., & Axmacher, N. (2015). Neuronal network oscillations in neurodegenerative diseases. *Neuromolecular medicine*, *17*(3), 270-284.

Nyhus, E., & Curran, T. (2010). Functional role of gamma and theta oscillations in episodic memory. *Neuroscience & Biobehavioral Reviews*, *34*(7), 1023-1035.

Oesterhelt, D., & Stoeckenius, W. (1971). Rhodopsin-like protein from the purple membrane of Halobacterium halobium. *Nature: New Biology*, 233(39), 149–152.

Oishi, K., & Lyketsos, C. G. (2014). Alzheimer's disease and the fornix. *Frontiers in aging neuroscience*, *6*, 241.

Oh, Y. S., Kim, H. J., Lee, K. J., Kim, Y. I., Lim, S. C., & Shon, Y. M. (2012). Cognitive improvement after long-term electrical stimulation of bilateral anterior thalamic nucleus in refractory epilepsy patients. *Seizure*, 21(3), 183–187

Okun, M. S., & Vitek, J. L. (2004). Lesion therapy for Parkinson's disease and other movement disorders: Update and controversies. *Movement Disorders*, 19(4), 375–389.

Olanow, W. C., Bartus, R. T., Baumann, T. L., Factor, S., Boulis, N., Stacy, M., ... Lang, A. E. (2015). Gene delivery of neurturin to putamen and substantia nigra in Parkinson disease: A double-blind, randomized, controlled trial. *Annals of Neurology*, 78(2), 248–257.

Olson, E. J., & Tabor, J. J. (2014). Optogenetic characterization methods overcome key challenges in synthetic and systems biology. *Nature Chemical Biology*, 10(7), 502–511.

O'Mara S. (2005). The subiculum: what it does, what it might do, and what neuroanatomy has yet to tell us. *Journal of anatomy*, *207*(3), 271–282. https://doi.org/10.1111/j.1469-7580.2005.00446.x

O'Neill, P. K., Gordon, J. A., & Sigurdsson, T. (2013). Theta oscillations in the medial prefrontal cortex are modulated by spatial working memory and synchronize with the hippocampus through its ventral subregion. *Journal of Neuroscience*, *33*(35), 14211-14224.

Öngür, D., & Price, J. L. (2000). The organization of networks within the orbital and medial prefrontal cortex of rats, monkeys and humans. *Cerebral cortex*, *10*(3), 206-219.

Palfi, S., Gurruchaga, J. M., Ralph, G. S., Lepetit, H., Lavisse, S., Buttery, P. C., ... Mitrophanous, K. A. (2014). Long-term safety and tolerability of ProSavin, a lentiviral vector-based gene therapy for Parkinson's disease: A dose escalation, open label, phase 1/2 trial. *Lancet*, 383 (9923), 1138–1146.

Parr-Brownlie, L. C., Bosch-Bouju, C., Schoderboeck, L., Sizemore, R. J., Abraham, W. C., & Hughes, S. M. (2015). Lentiviral vectors as tools to understand central nervous system biology in mammalian model organisms. *Frontiers in Molecular Neuroscience*, 8.

Palop, J. J., & Mucke, L. (2016). Network abnormalities and interneuron dysfunction in Alzheimer disease. *Nature Reviews Neuroscience*, *17*(12), 777.

Pan, W. X., & McNaughton, N. (1997). The medial supramammillary nucleus, spatial learning and the frequency of hippocampal theta activity. *Brain research*, *764*(1-2), 101-108.

Papatheodoropoulos, C., & Kostopoulos, G. (2000). Decreased ability of rat temporal hippocampal CA1 region to produce long-term potentiation. *Neuroscience letters*, *279*(3), 177-180.

Papez, J. W. (1937). A proposed mechanism of emotion. *Archives of Neurology & Psychiatry*, *38*(4), 725-743.

Pause, B. M., Zlomuzica, A., Kinugawa, K., Mariani, J., Pietrowsky, R., & Dere, E. (2013). Perspectives on episodic-like and episodic memory. *Frontiers in behavioral neuroscience*, *7*, 33.

Paxinos, G. & Watson, C. (2014). Paxinos and Watson's *The Rat Brain in Stereotaxic Coordinates*, 7th Edition. Elsevier Academic Press, San Diego.

Paz, J. T., Davidson, T. J., Frechette, E. S., Delord, B., Parada, I., Peng, K., ... Huguenard, J. R. (2013). Closed-loop optogenetic control of thalamus as a tool for interrupting seizures after cortical injury. *Nature Neuroscience*, 16(1), 64–70.

Penke, Z., Morice, E., Veyrac, A., Gros, A., Chagneau, C., LeBlanc, P., ... & Laroche, S. (2014). Zif268/Egr1 gain of function facilitates hippocampal synaptic plasticity and long-term spatial recognition memory. *Philosophical Transactions of the Royal Society B: Biological Sciences*, *369*(1633), 20130159.

Perry, B. A., Mercer, S. A., Barnett, S. C., Lee, J., & Dalrymple-Alford, J. C. (2018). Anterior thalamic nuclei lesions have a greater impact than mammillothalamic tract lesions on the extended hippocampal system. *Hippocampus*, *28*(2), 121-135.

Pitel, A. L., Chételat, G., Le Berre, A. P., Desgranges, B., Eustache, F., & Beaunieux, H. (2012). Macrostructural abnormalities in Korsakoff syndrome compared with uncomplicated alcoholism. *Neurology*, *78*(17), 1330-1333.

Poirier, G. L., Amin, E., & Aggleton, J. P. (2008). Qualitatively different hippocampal subfield engagement emerges with mastery of a spatial memory task by rats. *Journal of Neuroscience*, *28*(5), 1034-1045.

Poirier, G. L., & Aggleton, J. P. (2009). Post-surgical interval and lesion location within the limbic thalamus determine extent of retrosplenial cortex immediate-early gene hypoactivity. *Neuroscience*, *160*(2), 452-469.

Poletti, C. E., & Creswell, G. (1977). Fornix system efferent projections in the squirrel monkey: an experimental degeneration study. *Journal of Comparative Neurology*, *175*(1), 101-127.

Postle, B. R. (2016). The hippocampus, memory, and consciousness. In *The Neurology of Conciousness* (pp. 349-363). Academic Press.

Powell, T. P. S., Guillery, R. W., & Cowan, W. M. (1957). A quantitative study of the fornixmamillo-thalamic system. *Journal of anatomy*, *91*(Pt 4), 419.

Powell, A. L., Hindley, E., Nelson, A. J., Davies, M., Amin, E., Aggleton, J. P., & Vann, S. D. (2018). Lesions of retrosplenial cortex spare immediate-early gene activity in related limbic regions in the rat. *Brain and Neuroscience Advances*, *2*, 2398212818811235.

Preston, A. R., & Eichenbaum, H. (2013). Interplay of hippocampus and prefrontal cortex in memory. *Current Biology*, 23(17), R764–R773

Rafii, M. S., Baumann, T. L., Bakay, R. A. E., Ostrove, J. M., Siffert, J., Fleisher, A. S., ... Bartus, R. R. (2014). A phase1 study of stereotactic gene delivery of AAV2-NGF for Alzheimer's disease. *Alzheimer's and Dementia*, 10(5), 571–581.

Ramirez, S., Liu, X., Lin, P. A., Suh, J., Pignatelli, M., Redondo, R. L., ... Tonegawa, S. (2013). Creating a false memory in the hippocampus. *Science,* 341(6144), 387–391.

Reed, L. J., Lasserson, D., Marsden, P., Stanhope, N., Stevens, T., Bello, F., ... & Kopelman, M. D. (2003). FDG-PET findings in the Wernicke-Korsakoff syndrome. *Cortex*, *39*(4-5), 1027-1045.

Rein, M. L., & Deussing, J. M. (2012). The optogenetic (r) evolution. *Molecular Genetics and Genomics*, 287(2), 95–109.

Roy, D. S., Arons, A., Mitchell, T. I., Pignatelli, M., Ryan, T. J., & Tonegawa, S. (2016). Memory retrieval by activating engram cells in mouse models of early Alzheimer's disease. *Nature*, 531(7595), 508–512.

Rüb, U., Del Tredici, K., Schultz, C., Ghebremedhin, E., De Vos, R. A. I., Steur, E. J., & Braak, H. (2002). Parkinson's disease: the thalamic components of the limbic loop are severely impaired by α-synuclein immunopositive inclusion body pathology. *Neurobiology of aging*, *23*(2), 245-254.

Ryan, T. J., Roy, D. S., Pignatelli, M., Arons, A., & Tonegawa, S. (2015). Engram cells retain memory under retrograde amnesia. *Science*, 348 (6238), 1007–1013.

Salegio, E. A., Samaranch, L., Kells, A. P., Mittermeyer, G., San Sebastian, W., Zhou, S., ... Bankiewicz, K. S. (2013). Axonal transport of adenoassociated viral vectors is serotype-dependent. *Gene Therapy*, 20(3), 348–352.

Sanders, J. I., & Kepecs, A. (2014). A low-cost programmable pulse generator for physiology and behavior. *Frontiers in neuroengineering*, *7*, 43.

Savage, L. M., Hall, J. M., & Vetreno, R. P. (2011). Anterior thalamic lesions alter both hippocampal-dependent behavior and hippocampal acetylcholine release in the rat. *Learning & Memory*, 18(12), 751–758.

Savage, L. M., Hall, J. M., & Resende, L. S. (2012). Translational rodent models of Korsakoff syndrome reveal the critical neuroanatomical substrates of memory dysfunction and recovery. *Neuropsychology review*, *22*(2), 195-209.

Schmidt-Kastner, R., & Freund, T. F. (1991). Selective vulnerability of the hippocampus in brain ischemia. *Neuroscience*, *40*(3), 599-636.

Schmitt, L. I., Wimmer, R. D., Nakajima, M., Happ, M., Mofakham, S., & Halassa, M. M. (2017). Thalamic amplification of cortical connectivity sustains attentional control. *Nature*, 545(7653), 219–223

Schoonheim, M. M., Hulst, H. E., Brandt, R. B., Strik, M., Wink, A. M., Uitdehaag, B. M., ... & Geurts, J. J. (2015). Thalamus structure and function determine severity of cognitive impairment in multiple sclerosis. *Neurology*, *84*(8), 776-783.

Scott, L., Feng, J., Kiss, T., Needle, E., Atchison, K., Kawabe, T. T., ... & Hajós, M. (2012). Age-dependent disruption in hippocampal theta oscillation in amyloid-β overproducing transgenic mice. *Neurobiology of aging*, *33*(7), 1481-e13.

Scoville, W. B., & Milner, B. (1957). Loss of recent memory after bilateral hippocampal lesions. *Journal of neurology, neurosurgery, and psychiatry*, *20*(1), 11.

Sechi, G., & Serra, A. (2007). Wernicke's encephalopathy: new clinical settings and recent advances in diagnosis and management. *The Lancet Neurology*, *6*(5), 442-455.

Senkowski, D., & Gallinat, J. (2015). Dysfunctional prefrontal gamma-band oscillations reflect working memory and other cognitive deficits in schizophrenia. *Biological psychiatry*, *77*(12), 1010-1019.

Sesack, S. R., Deutch, A. Y., Roth, R. H., & Bunney, B. S. (1989). Topographical organization of the efferent projections of the medial prefrontal cortex in the rat: An anterograde tract-tracing study with Phaseolus vulgaris leucoagglutinin. *The Journal of Comparative Neurology*, 290(2), 213–242

Sie, L. T. L., Van der Knaap, M. S., Oosting, J., De Vries, L. S., Lafeber, H. N., & Valk, J. (2000). MR patterns of hypoxic-ischemic brain damage after prenatal, perinatal or postnatal asphyxia. *Neuropediatrics*, *31*(03), 128-136.

Siegle, J. H., & Wilson, M. A. (2014). Enhancement of encoding and retrieval functions through theta phase-specific manipulation of hippocampus. *eLife*, 3, e03061.

Sikes, R. W., & Vogt, B. A. (1987). Afferent connections of anterior thalamus in rats: sources and association with muscarinic acetylcholine receptors. *Journal of Comparative Neurology*, *256*(4), 538-551.

Sizemore, R. J., Seeger-Armbruster, S., Hughes, S. M., & Parr-Brownlie, L. C. (2016). Viral vector-based tools advance knowledge of basal ganglia anatomy and physiology. *Journal of Neurophysiology*, 115(4), 2124–2146.

Shirvalkar, P., Seth, M., Schiff, N. D., & Herrera, D. G. (2006). Cognitive enhancement with central thalamic electrical stimulation. *Proceedings of the National Academy of Sciences*, *103*(45), 17007-17012.

Shibata, H., & Naito, J. (2005). Organization of anterior cingulate and frontal cortical projections to the anterior and laterodorsal thalamic nuclei in the rat. *Brain research*, *1059*(1), 93-103.

Shibata, H., Honda, Y., Sasaki, H., & Naito, J. (2009). Organization of intrinsic connections of the retrosplenial cortex in the rat. *Anatomical science international*, *84*(4), 280.

Shipton, O. A., El-Gaby, M., Apergis-Schoute, J., Deisseroth, K., Bannerman, D. M., Paulsen, O., & Kohl, M. M. (2014). Left–right dissociation of hippocampal memory processes in mice. *Proceedings of the National Academy of Sciences*, 111(42), 15238–15243.

Spellman, T., Rigotti, M., Ahmari, S. E., Fusi, S., Gogos, J. A., & Gordon, J. A. (2015). Hippocampal-prefrontal input supports spatial encoding in working memory. *Nature*, 522(7556), 309–314.

Spiers, H. J., Maguire, E. A., & Burgess, N. (2001). Hippocampal amnesia. *Neurocase*, *7*(5), 357-382.

Squire, L. R., Amaral, D. G., Zola-Morgan, S., Kritchevsky, M., & Press, G. (1989). Description of brain injury in the amnesic patient NA based on magnetic resonance imaging. *Experimental neurology*, *105*(1), 23-35.

Squire, L. R., Stark, C. E., & Clark, R. E. (2004). The medial temporal lobe. *Annu. Rev. Neurosci.*, *27*, 279-306.

Squire, L. R. (2009). Memory and brain systems: 1969–2009. *Journal of Neuroscience*, 29(41), 12711-12716.

Squire, L. R., & Wixted, J. T. (2011). The cognitive neuroscience of human memory since HM. *Annual review of neuroscience*, *34*, 259-288.

Stuber, G. D., Sparta, D. R., Stamatakis, A. M., Van Leeuwen, W. A., Hardjoprajitno, J. E., Cho, S., ... Bonci, A. (2011). Excitatory transmission from the amygdala to nucleus accumbens facilitates reward seeking. *Nature*, 475(7356), 377–380.

Stujenske, J. M., Spellman, T. & Gordon, J. A. (2015). Modeling the spatiotemporal dynamics of light and heat propagation for in vivo optogenetics. *Cell Reports*, 12(3), 525–534

Suthana, N., & Fried, I. (2014). Deep brain stimulation for enhancement of learning and memory. *Neuroimage*, 85, 996–1002.

Sweeney-Reed, C. M., Zaehle, T., Voges, J., Schmitt, F. C., Buentjen, L., Kopitzki, K., ... & Richardson-Klavehn, A. (2014). Corticothalamic phase synchrony and cross-frequency coupling predict human memory formation. *Elife*, *3*, e05352.

Sweeney-Reed, C. M., Zaehle, T., Voges, J., Schmitt, F. C., Buentjen, L., Kopitzki, K., ... & Richardson-Klavehn, A. (2015). Thalamic theta phase alignment predicts human memory formation and anterior thalamic cross-frequency coupling. *Elife*, *4*, e07578.

Sweeney-Reed, C. M., Zaehle, T., Voges, J., Schmitt, F. C., Buentjen, L., Kopitzki, K., ... & Rugg, M. D. (2016). Pre-stimulus thalamic theta power predicts human memory formation. *Neuroimage*, *138*, 100-108.

Sweet, J. A., Eakin, K. C., Munyon, C. N., & Miller, J. P. (2014). Improved learning and memory with theta-burst stimulation of the fornix in rat model of traumatic brain injury. *Hippocampus*, *24*(12), 1592-1600.

Sziklas, V., & Petrides, M. (1999). The effects of lesions to the anterior thalamic nuclei on object–place associations in rats. *European Journal of Neuroscience*, *11*(2), 559-566.

Sziklas, V., & Petrides, M. (2007). Contribution of the anterior thalamic nuclei to conditional learning in rats. *Hippocampus*, *17*(6), 456-461.

Taniguchi, Y., Young-Pearse, T., Sawa, A., & Kamiya, A. (2012). In utero electroporation as a tool for genetic manipulation in order to study psychiatric disorders: From genes to circuits and behaviors. *Neuroscientist,* 18, 169–179.

Thayyil, S., Chandrasekaran, M., Taylor, A., Bainbridge, A., Cady, E. B., Chong, W. K., ... & Robertson, N. J. (2010). Cerebral magnetic resonance biomarkers in neonatal encephalopathy: a meta-analysis. *Pediatrics*, *125*(2), e382-e395.

Thomas, G. J., & Gash, D. M. (1985). Mammillothalamic tracts and representational memory. *Behavioral neuroscience*, *99*(4), 621.

Thomsen, S. (1991). Pathologic analysis of photothermal and photomechanical effects of laser-tissue interactions. *Photochemistry and Photobiology*, 53(6), 825–835.

Ting, J. T., & Feng, G. (2014). Recombineering strategies for developing next generation BAC transgenic tools for optogenetics and beyond. *Frontiers in Behavioral Neuroscience*, 8, 111.

Tonkiss, J., Feldon, J., & Rawlins, J. N. P. (1990). Section of the descending columns of the fornix produces delay-and interference-dependent working memory deficits. *Behavioural brain research*, *36*(1-2), 113-126.

Tsanov, M. (2015). Septo-hippocampal signal processing: Breaking the code. *Progress in Brain Research*, 219, 103–120.

Tsivilis, D., Vann, S. D., Denby, C., Roberts, N., Mayes, A. R., Montaldi, D., & Aggleton, J. P. (2008). A disproportionate role for the fornix and mammillary bodies in recall versus recognition memory. *Nature neuroscience*, *11*(7), 834.

Tulving, E. (2002). Episodic memory: From mind to brain. *Annual review of psychology*, *53*(1), 1-25.

Tuszynski, M. H., Yang, J. H., Barba, D., Hoi-Sang, U., Bakay, R. A. E., Pay, M. M., ... Nagahara, A. H. (2015). Nerve growth factor therapy. Activation of neuronal responses in Alzheimer's disease. *JAMA Neurology*, 72(10), 1139–1147.

Tye, K. M., Prakash, R., Kim, S. Y., Fenno, L. E., Grosenick, L., Zarabi, H., ... Deisseroth, K. (2011). Amygdala circuitry mediating reversible and bidirectional control of anxiety. *Nature*, 471(7338), 358–362.

Tye, K. M., & Deisseroth, K. (2012). Optogenetic investigation of neural circuits underlying brain disease in animal models. *Nature Reviews Neuroscience*, 13(4), 251

Ulrich, K., Aitken, P. N., Abraham, W. C., Dalrymple-Alford, J. C., & McNaughton, N. (2014). Effects of thalamic lesions on repeated relearning of a spatial working memory task. *Behavioural brain research*, *261*, 56-59.

Ulrich, K., Spriggs, M. J., Abraham, W. C., Dalrymple-Alford, J. C., & McNaughton, N. (2019). Environmental enrichment increases prefrontal EEG power and synchrony with the hippocampus in rats with anterior thalamus lesions. *Hippocampus*, *29*(2), 128-140.

Urban, D. J., & Roth, B. L. (2015). DREADDs (designer receptors exclusively activated by designer drugs): Chemogenetic tools with therapeutic utility. *Annual Review of Pharmacology and Toxicology*, 55(1), 399–417.

Van Der Werf, Y. D., Jolles, J., Witter, M. P., & Uylings, H. B. (2003). Contributions of thalamic nuclei to declarative memory functioning. *Cortex*, *39*(4-5), 1047-1062.

van Duuren, E., van der Plasse, G., van der Blom, R., Joosten, R. N. J. M. A., Mulder, A. B., Pennartz, C. M., & Feenstra, M. G. (2007). Pharmacological manipulation of neuronal ensemble activity by reverse microdialysis in freely moving rats: A comparative study of the effects of tetrodotoxin, lidocaine, and muscimol. *Journal of Pharmacology and Experimental Therapeutics*, 323(1), 61–69.

van Groen, T., Kadish, I., & Wyss, J. M. (2002). Role of the anterodorsal and anteroventral nuclei of the thalamus in spatial memory in the rat. *Behavioural brain research*, *132*(1), 19-28.

Vann, S. D., & Aggleton, J. P. (2003). Evidence of a spatial encoding deficit in rats with lesions of the mammillary bodies or mammillothalamic tract. *Journal of Neuroscience*, *23*(8), 3506-3514.

Vann, S. D., Honey, R. C., & Aggleton, J. P. (2003). Lesions of the mammillothalamic tract impair the acquisition of spatial but not nonspatial contextual conditional discriminations. *European Journal of Neuroscience*, *18*(8), 2413-2416.

Vann, S. D., & Aggleton, J. P. (2004). The mammillary bodies: two memory systems in one?. *Nature Reviews Neuroscience*, *5*(1), 35-44.

Vann, S. D., Denby, C., Love, S., Montaldi, D., Renowden, S., & Coakham, H. B. (2008). Memory loss resulting from fornix and septal damage: impaired supra-span recall but preserved recognition over a 24-hour delay. *Neuropsychology*, *22*(5), 658.

Vann, S. D., Aggleton, J. P., & Maguire, E. A. (2009). What does the retrosplenial cortex do?. *Nature reviews neuroscience*, *10*(11), 792-802.

Vann, S. D., & Albasser, M. M. (2009). Hippocampal, retrosplenial, and prefrontal hypoactivity in a model of diencephalic amnesia: Evidence towards an interdependent subcortical-cortical memory network. *Hippocampus*, *19*(11), 1090-1102.

Vann, S. D. (2010). Re-evaluating the role of the mammillary bodies in memory. *Neuropsychologia*, *48*(8), 2316-2327.

Vann, S. D., Erichsen, J. T., O'Mara, S. M., & Aggleton, J. P. (2011). Selective disconnection of the hippocampal formation projections to the mammillary bodies produces only mild deficits on spatial memory tasks: implications for fornix function. *Hippocampus*, *21*(9), 945-957.

Vann, S. D. (2013). Dismantling the Papez circuit for memory in rats. *Elife*, *2*, e00736.

Vann, S. D., & Nelson, A. J. (2015). The mammillary bodies and memory: more than a hippocampal relay. In *Progress in brain research* (Vol. 219, pp. 163-185). Elsevier.

Van Someren, E. J. W., Van Gool, W. A., Vonk, B. F. M., Mirmiran, M., Speelman, J. D., Bosch, D. A., & Swaab, D. F. (1993). Ambulatory monitoring of tremor and other movements before and after thalamotomy: A new quantitative technique. *Journal of the Neurological Sciences*, 117(1–2), 16–23.

Venkatraman, V., Payne, J. W., Bettman, J. R., Luce, M. F., & Huettel, S. A. (2009). Separate neural mechanisms underlie choices and strategic preferences in risky decision making. *Neuron*, *62*(4), 593-602.

Vertes, R. P., Albo, Z., & Di Prisco, G. V. (2001). Theta-rhythmically firing neurons in the anterior thalamus: implications for mnemonic functions of Papez's circuit. *Neuroscience*, *104*(3), 619-625.

Vertes, R. P., Hoover, W. B., & Di Prisco, G. V. (2004). Theta rhythm of the hippocampus: subcortical control and functional significance. *Behavioral and cognitive neuroscience reviews*, *3*(3), 173-200.

Vertes, R. P. (2015). Major diencephalic inputs to the hippocampus: Supramammillary nucleus and nucleus reuniens. Circuitry and function. *Progress in Brain Research*, 219, 121–144.

Victor, M., Adams, R. D., & Collins, G. H. (1971). The Wernicke-Korsakoff syndrome. A clinical and pathological study of 245 patients, 82 with post-mortem examinations. *Contemporary neurology series*, *7*, 1.

Von Cramon, D. Y., Hebel, N., & Schuri, U. (1985). A contribution to the anatomical basis of thalamic amnesia. *Brain*, *108*(4), 993-1008.

Wang, B., Gonzalo-Ruiz, A., Sanz, J. M., Campbell, G., & Lieberman, A. R. (1999). Immunoelectron microscopic study of γ-aminobutyric acid inputs to identified thalamocortical projection neurons in the anterior thalamus of the rat. *Experimental brain research*, *126*(3), 369-382.

Warburton, E. C., Baird, A. L., & Aggleton, J. P. (1997). Assessing the magnitude of the allocentric spatial deficit associated with complete loss of the anterior thalamic nuclei in rats. *Behavioural brain research*, *87*(2), 223-232.

Warburton, E. C., & Aggleton, J. P. (1998). Differential deficits in the Morris water maze following cytotoxic lesions of the anterior thalamus and fornix transection. *Behavioural brain research*, *98*(1), 27-38.

Warburton, E. C., Morgan, A., Baird, A. L., Muir, J. L., & Aggleton, J. P. (1999). Does pretraining spare the spatial deficit associated with anterior thalamic damage in rats?. *Behavioral neuroscience*, *113*(5), 956.

Warburton, E. C., Baird, A., Morgan, A., Muir, J. L., & Aggleton, J. P. (2001). The conjoint importance of the hippocampus and anterior thalamic nuclei for allocentric spatial learning: evidence from a disconnection study in the rat. *Journal of Neuroscience*, *21*(18), 7323-7330.

Weiss, S., Müller, H. M., & Rappelsberger, P. (2000). Theta synchronization predicts efficient memory encoding of concrete and abstract nouns. *NeuroReport*, *11*(11), 2357-2361.

Weiss, S., Müller, H. M., & Rappelsberger, P. (2000). Theta synchronization predicts efficient memory encoding of concrete and abstract nouns. *NeuroReport*, *11*(11), 2357-2361.

Wietek, J., Beltramo, R., Scanziani, M., Hegemann, P., Oertner, T. G., & Wiegert, J. S. (2015). An improved chloride-conducting channelrhodopsin for light-induced inhibition of neuronal activity in vivo. *Scientific Reports*, 5(1), 14807.

Wells, J., Kao, C., Mariappan, K., Albea, J., Jansen, E. D., Konrad, P., & Mahadevan-Jansen, A. (2005). Optical stimulation of neural tissue in vivo. *Optics letters*, *30*(5), 504-506.

Winter, S. S., Wagner, S. J., McMillin, J. L., & Wallace, D. G. (2011). Mammillothalamic tract lesions disrupt dead reckoning in the rat. *European Journal of Neuroscience*, *33*(2), 371-381.

Wolff, M., Loukavenko, E. A., Will, B. E., & Dalrymple-Alford, J. C. (2008a). The extended hippocampal-diencephalic memory system: Enriched housing promotes recovery of the flexible use of spatial representations after anterior thalamic lesions. *Hippocampus*, *18*(10), 996-1007.

Wolff, M., Gibb, S. J., Cassel, J. C., & Dalrymple-Alford, J. C. (2008b). Anterior but not intralaminar thalamic nuclei support allocentric spatial memory. *Neurobiology of learning and memory*, *90*(1), 71-80.

Wu, H., Ghekiere, H., Beeckmans, D., Tambuyzer, T., Van Kuyck, K., Aerts, J. M., & Nuttin, B. (2015). Conceptualization and validation of an open-source closed-loop deep brain stimulation system in rat. *Scientific reports*, *5*, 9921.

Yang, X., Yao, C., Tian, T., Li, X., Yan, H., Wu, J., ... Zhu, L. Q. (2016). A novel mechanism of memory loss in Alzheimer's disease mice via the degeneration of entorhinal–CA1 synapses. *Molecular Psychiatry*, 23, 199–210.

Ye, L., Allen, W. E., Thompson, K. R., Tian, Q., Hsueh, B., Ramakrishnan, C., ... & Witten, I. B. (2016). Wiring and molecular features of prefrontal ensembles representing distinct experiences. *Cell*, *165*(7), 1776-1788.

Yizhar, O., Fenno, L. E., Davidson, T. J., Mogri, M., & Deisseroth, K. (2011). Optogenetics in neural systems. *Neuron*, 71(1), 9–34

Young, C. K., & McNaughton, N. (2009). Coupling of theta oscillations between anterior and posterior midline cortex and with the hippocampus in freely behaving rats. *Cerebral Cortex*, *19*(1), 24-40.

Żakowski, W. (2017). Neurochemistry of the anterior thalamic nuclei. *Molecular neurobiology*, *54*(7), 5248-5263.

Zhang, F., Wang, L. P., Brauner, M., Liewald, J. F., Kay, K., Watzke, N., ... Deisseroth, K. (2007). Multimodal fast optical interrogation of neural circuitry. *Nature*, 446(7136), 633–639.

Zhang, F., Gradinaru, V., Adamantidis, A. R., Durand, R., Airan, R. D., De Lecea, L., & Deisseroth, K. (2010). Optogenetic interrogation of neural circuits: Technology for probing mammalian brain structures. *Nature Protocols*, 5(3), 439–456.

Zhang, Y., Schuff, N., Camacho, M., Chao, L. L., Fletcher, T. P., Yaffe, K., ... & Weiner, M. W. (2013). MRI markers for mild cognitive impairment: comparisons between white matter integrity and gray matter volume measurements. *PloS one*, *8*(6).

Zhuang, L., Sachdev, P. S., Trollor, J. N., Kochan, N. A., Reppermund, S., Brodaty, H., & Wen, W. (2012). Microstructural white matter changes in cognitively normal individuals at risk of amnestic MCI. *Neurology*, *79*(8), 748-754.

Zhuang, L., Sachdev, P. S., Trollor, J. N., Reppermund, S., Kochan, N. A., Brodaty, H., & Wen, W. (2013). Microstructural white matter changes, not hippocampal atrophy, detect early amnestic mild cognitive impairment. *PloS one*, *8*(3).